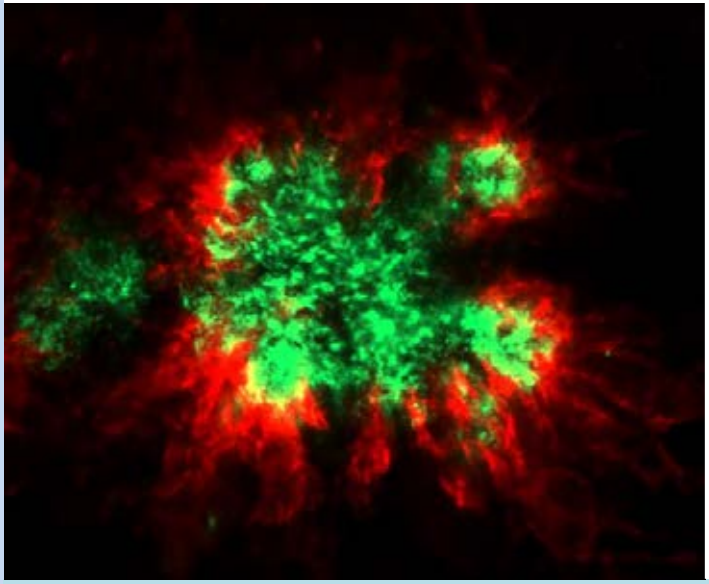

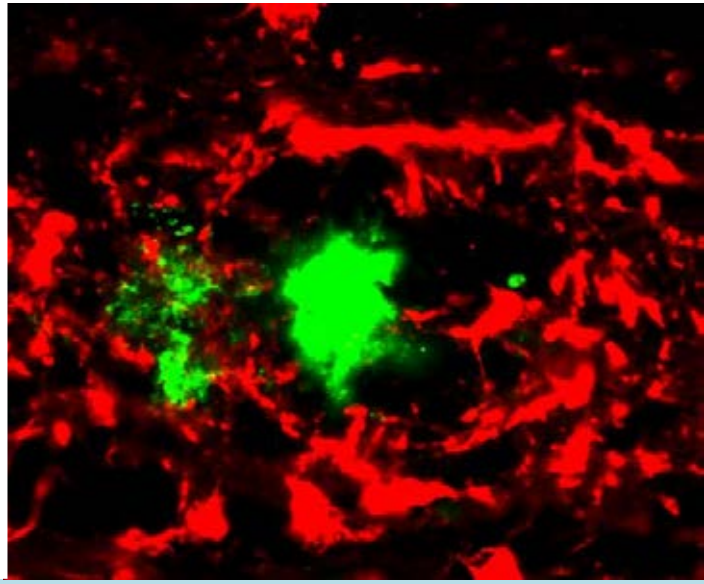

PhD THESIS

CONFORMATIONAL Aβ STRAINS AND CROSS-SEEDING MECHANISM IN ALZHEIMER'S DISEASE PATHOGENESIS: *IN VIVO* STUDIES IN TRANSGENIC ANIMAL MODELS

Rubén Gómez Gutiérrez

Directors:
Dr. Antonia Gutiérrez
Dr. Rodrigo Morales

PhD in Cellular and Molecular Biology

Department of Cell Biology, Genetics and Physiology
Cell Biology Area. Faculty of Sciences

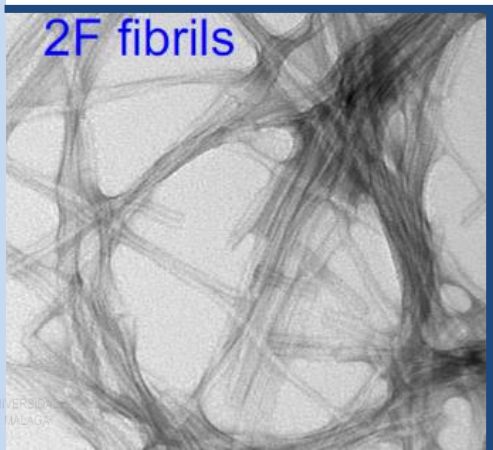

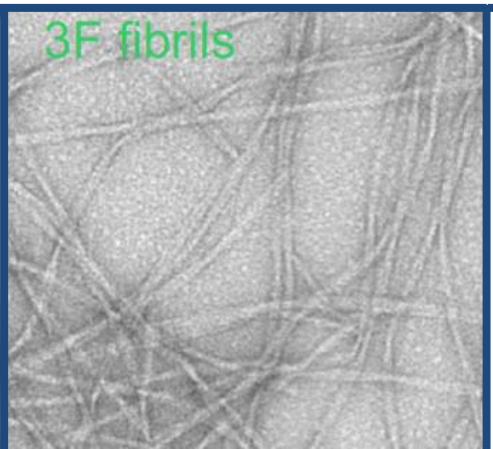

UNIVERSIDAD DE MÁLAGA

MÁLAGA 2021

Department of Cell Biology, Genetics and Physiology

Cell Biology Area. Faculty of Sciences

University of Málaga

PhD Thesis

CONFORMATIONAL Aβ STRAINS AND CROSS-SEEDING MECHANISM IN ALZHEIMER'S DISEASE PATHOGENESIS: *IN VIVO* STUDIES IN TRANSGENIC ANIMAL MODELS

Thesis manuscript presented by Mr. Rubén Gómez Gutiérrez in order to obtain a PhD degree from the University of Malaga

Directors: Dr. Antonia Gutiérrez
Dr. Rodrigo Morales

PhD in Cellular and Molecular Biology

Málaga, November 2021

UNIVERSIDAD
DE MÁLAGA

AUTOR: Rubén Gómez Gutiérrez

https://orcid.org/0000-0001-9134-4375

EDITA: Publicaciones y Divulgación Científica. Universidad de Málaga

DECLARACIÓN DE AUTORÍA Y ORIGINALIDAD DE LA TESIS PRESENTADA PARA OBTENER EL TÍTULO DE DOCTOR

D./Dña RUBEN GOMEZ GUTIERREZ
Estudiante del programa de doctorado EN BIOLOGIA CELULAR Y MOLECULAR de la Universidad de Málaga, autor/a de la tesis, presentada para la obtención del título de doctor por la Universidad de Málaga, titulada: CONFORMATIONAL AB STRAINS AND CROSS-SEEDING MECHANISM IN ALZHEIMER'S DISEASE PATHOGENESIS: IN VIVO STUDIES IN TRANSGENIC ANIMAL MODELS

Realizada bajo la tutorización de LA DRA. ANTONIA GUTIERREZ y dirección de EL DR. RODRIGO MORALES Y LA DRA. ANTONIA GUTIERREZ (si tuviera varios directores deberá hacer constar el nombre de todos)

DECLARO QUE:

La tesis presentada es una obra original que no infringe los derechos de propiedad intelectual ni los derechos de propiedad industrial u otros, conforme al ordenamiento jurídico vigente (Real Decreto Legislativo 1/1996, de 12 de abril, por el que se aprueba el texto refundido de la Ley de Propiedad Intelectual, regularizando, aclarando y armonizando las disposiciones legales vigentes sobre la materia), modificado por la Ley 2/2019, de 1 de marzo.

Igualmente asumo, ante a la Universidad de Málaga y ante cualquier otra instancia, la responsabilidad que pudiera derivarse en caso de plagio de contenidos en la tesis presentada, conforme al ordenamiento jurídico vigente.

En Málaga, a 15 de NOVIEMBRE de 2021

Fdo.: RUBEN GOMEZ GUTIERREZ Doctorando/a	Fdo.: DRA. ANTONIA GUTIERREZ Tutor/a

Fdo.: DR. RODRIGO MORALES
Director/es de tesis

UNIVERSIDAD DE MÁLAGA

Facultad de Ciencias
Departamento de Biología Celular, Genética y Fisiología
Área de Biología Celular

Dra. Antonia Gutiérrez Pérez, Catedrática de Biología Celular del Departamento de Biología Celular,Genética y Fisiología de la Facultad de Ciencias de la Universidad de Málaga,

Dr. Rodrigo Morales, Profesor Asociado en el Departamento de Neurología de la escuela de medicina de la University of Texas Health Science Center (UTHealth) en Houston

INFORMAN

Que **D. Rubén Gómez Gutiérrez** ha realizado bajo su dirección el trabajo experimental que ha llevado a la redacción de la presente memoria de Tesis Doctoral, titulada "**Conformational Aβ strains and cross-seeding mechanism in Alzheimer's disease pathogenesis: *In vivo* studies in transgenic animal models**". Considerando que constituye Trabajo de Tesis Doctoral, autorizamos su presentación para optar al Grado de Doctor por la Universidad de Málaga.

Y para que así conste y surta los efectos oportunos, firmamos el presente documento en Málaga a 15 de Noviembre de 2021.

Fdo. Antonia Gutiérrez Pérez

Fdo. Rodrigo Morales

Proyectos

El presente Trabajo de Tesis Doctoral se ha financiado con los siguientes **Proyectos de Investigación:**

Characterization of natural and synthetic Aβ "conformational strains". Entidad Financiera: Alzheimer's Association. Ref. AARGD-18-566576. IP: Dr. Rodrigo Morales. Duración 2018-2022.

Isolation, characterization and pathogenic role of self-propagating conformational amyloid-beta strains. Entidad Financiera: NIH/NIA. Ref. R56AG061878-01. IP: Dr. Rodrigo Morales. Duración 2018-2020.

Start-Up Funds. Entidad Financiera: The University of Texas Health Science Center at Houston. IP: Dr. Rodrigo Morales. Duración 2017-2025.

Evaluando la disfunción microglial y astroglial como parte del proceso neurodegenerativo yla demencia en la enfermedad de Alzheimer: nuevas aproximaciones terapéuticas. Entidad financiera: Instituto de Salud Carlos III. Ministerio de Economía y Competitividad. Ref. PI15/00796. IP: Dra. Antonia Gutiérrez Pérez. Duración: 2016-2018.

Descifrando la diversidad funcional de la respuesta microglial y astroglial en la enfermedad de Alzheimer: potencial patológico y terapéutico. Entidad financiera: Instituto de Salud Carlos III. Ministerio de Economía y Competitividad. Ref. PI18/01557. IP: Dra. Antonia Gutiérrez Pérez. Duración: 2019-2021.

Astrogliopatía como mecanismo patogénico en la enfermedad de Alzheimer: nuevas opciones terapéuticas. Entidad Financiera: Junta de Andalucía. Proyecto Excelencia modalidad RETOS Consolidado. Ref. PI18-RT-2233. IP: Dr. Antonia Gutiérrez Pérez. Duración 2020-2022.

Publicaciones

1. **Gomez-Gutierrez R,** Morales R. *The prion-like phenomenon in Alzheimer's disease: evidence of pathology transmission in humans.* ***PLoS Pathogens*** 2020. *16(10): e1009004.* DOI: 10.1371/journal.ppat.1009004. Índice de impacto: 6,823

2. Kramm C, **Gomez-Gutierrez R**, Soto C, Telling G, Nichols T, Morales R. *In Vitro detection of Chronic Wasting Disease (CWD) prions in semen and reproductive tissues of white tailed deer bucks (Odocoileus virginianus).* ***PLoS ONE*** 2019. *14(12): e0226560.* DOI: 10.1371/journal.pone.0226560. Índice de impacto: 3,24

3. Loureiro JA, Goderis L, Andrade S, **Gomez-Gutierrez R**, Soto C, Morales R, Pereira MDC. *(De)stabilization of alpha-synuclein fibrillary aggregation by 2 charged and uncharged surfactants.* ***International Journal of Molecular Sciences*** 2021. Índice de impacto: 5,924

4. **Gomez-Gutierrez R,** Morales R. *Molecular basis of Alzheimer's Disease: New research perspectives.* ***NRC Newsletter*** 2019. *2:1-10.* Índice de impacto: Articulo de divulgación

En revisión actualmente

5. **Gomez-Gutierrez R**, Ghosh U, Do K, Yau WM, Kramm C, Schulz J, Gutierrez A, Nilsson P, Tycko R, Soto C, Morales R. *Structure-defined Aβ polymorphs promote specific pathological outcomes in susceptible mice.*

6. Wirianto M, Wang CY, Kim E, Koike N, **Gomez-Gutierrez R**, Nohara K, Escobedo Jr. G, Choi JM, Han C, Yagita K, Jung SY, Soto C, Lee HK, Morales R, Yoo SH, Chen Z. *The clock modulator Nobiletin mitigates astrogliosis-associated neuroinflammation and disease hallmarks in an Alzheimer's disease model.*

Agradecimientos

"*Es de bien nacido ser agradecido*" y por ello, me encantaría dedicar estas palabras a todos aquellos que de una manera u otra han colaborado en este trabajo y me han ayudado a llegar a donde estoy y a ser la persona que soy.

En primer lugar, dar las gracias a los directores de este trabajo la Dra. Antonia Gutiérrez y el Dr. Rodrigo Morales. A Antonia por haberme acogido en su grupo de investigación desde los primeros años de carrera y por haberme dado tantos consejos y tanta ayuda como he necesitado, hasta el día de hoy. Sobre todo, por supuesto por su gran ayuda en este trabajo de tesis doctoral. De verdad siento que hay momentos que, si no fuera por tu ayuda, no hubiera completado esta tesis doctoral. A Rodrigo, por haber dirigido este gran proyecto que hemos completado y por haberme dado la oportunidad de cruzar el charco y conocer la manera de trabajar en un laboratorio de Estados Unidos. He aprendido mucho de ti en estos años y de no haber estado en tu laboratorio y bajo tu dirección estoy seguro de que no habría aprendido ni la mitad de los conocimientos que tengo hoy en día. De nuevo, gracias mis directores por haberme dedicado tanto tiempo, sin vosotros esta Tesis Doctoral no habría sido posible. En segundo lugar, me gustaría agradecer a Inés. Aunque no te guste cuando lo digo, para mi has sido y eres como una madre científica que me ha ayudado muchísimo a estar donde estoy. Me has enseñado muchísimo en estos años, me abriste las puertas de mi futuro como investigador y me acogiste en Houston como si de un hijo se tratara. A ti, a Juan, a Lucas y a Mateo, muchísimas gracias de corazón.

Muchas gracias por supuesto a todos los integrantes del grupo NeuroAD, ya que, aunque estemos últimamente más a la distancia, vosotros sois los que me ayudasteis a iniciar este camino y me hicisteis amar la ciencia, porque la hicisteis mucho más divertida en el día a día. No sabéis lo mucho que os he echado de menos. Especial mención en este grupo a José Carlos y Raquel, por todo lo que me enseñasteis tras dirigirme tanto mi TFG como el TFM, ya que toda esa enseñanza ha sido esencial para poder escribir esta Tesis Doctoral. Por supuesto agradecer también a Eli, por todo lo que me enseñaste científicamente cuando no sabía nada y sobre todo por tus "escribe y no pienses" cuando he estado muy agobiado con la tesis. Aun en la distancia tanto tu como Raquel, habéis sabido animarme en mis peores momentos y me habéis enseñado mucho sobre la vida. A Ángela, Juanjo, Mercedes y Cristina por todas las enseñanzas que también me habéis aportado y por todos los buenos momentos vividos, en especial con Juanjo por Houston. A Laura por haberme enseñado tantísimas cosas cuando aún coincidíamos en Málaga y por su invitación a Irvine, me alegro mucho de que hayas tenido la oportunidad de volver a tu casa, te la mereces. A David, por todas tus charlas en cada congreso que hemos coincidido, porque con ellas has acabado pegándome aún más tu gran pasión por la neurociencia (y por el Jamón Ibérico y las comidas de los congresos). Ojalá algún día podamos coincidir trabajando codo con codo, porque la verdad es uno de mis sueños como científico y estoy seguro de que pronto se dará.

Gracias también a todos los compañeros del Mitchell Center en Houston. En especial a Carlos, porque ha sido mi mejor amigo en todo el tiempo pasado en Houston y porque me hizo sentir como en casa en el laboratorio de Rodrigo. También gracias a Adam, quien ha sido mi compañero de aventuras durante muchos años y a Nazaret, por traer un poco de sabor de Málaga al laboratorio de Houston, cuando más falta hacía. Tanto en congresos, como en el día a día, he disfrutado muchísimo con los tres. También dar las gracias al Dr. Claudio Soto, por su acogida y enseñanzas en esta estancia en Houston. He aprendido muchísimo en el día a día contigo. Muchas gracias también al Dr. Javier Vitorica, por brindarme la oportunidad hace años de aprender muchas técnicas moleculares en su laboratorio, que han sido de gran ayuda y empleadas en este trabajo. Gracias por acogerme tan bien en los meses de estancia en Sevilla, cuando todavía era un completo inexperto.

Muchas gracias a mi familia, sobre todo a mis padres, porque sin vuestro apoyo diario nunca habría llegado donde he llegado, de eso no hay duda. Especialmente, quiero agradecer a mi madre

Agradecimientos

por todo lo que ha hecho por mí siempre y sobre todo en estos últimos años, solo tú sabes por lo que he pasado hasta llegar a este momento. Han sido momentos muy duros y en algunos, los más duros de ellos, tú has sido mi único apoyo. Nunca habrá suficientes palabras para agradecerte lo que has hecho desde la distancia por mí. También agradecer a mi padre el estar día a día ahí para mí, incluso llegando a descargarse toda esa "tecnología" que no te gusta, para así poder seguir hablando conmigo. Se que haces todo lo que está dentro de tus posibilidades para ayudarme en todo y sé que tanto tu como abuelita, siempre estáis pendiente de mi este donde este. Por supuesto, agradecer a "mami", por toda su ayuda, porque gracias a ti he podido hacer posible todos mis sueños y me he criado como me he criado. Sabes que eres una madre para mí y que siempre estaré aquí para ti. Gracias infinitas a mis tíos por hacerme amar la neurociencia. Ver vuestro ejemplo a diario me hizo decantarme por tomar esta carrera. Gracias a mi hermano, porque pese a tantas peleas, me has enseñado cosas de la vida que nadie más me ha enseñado. Gracias al resto de la familia, porque no solo los citados aquí me han apoyado durante toda mi vida, sois muchos los que me habéis animado a estudiar y me habéis enseñado cosas únicas. Por último, respecto a mi familia me gustaría hacer mención especial a mi abuelo, que en paz descanse, porque fuiste el abuelo que todo nieto soñó y porque me enseñaste muchísimos valores como la humildad, la educación y la paciencia que me hacen ser la persona que soy hoy. Eres el único capaz de hacerme soltar unas lágrimas al escribir estos agradecimientos. Esta tesis y todo lo que haga en mi vida, va por ti.

Muchísimas gracias también a todos mis amigos que me han apoyado toda mi vida, pero que además han creído incondicionalmente en mí durante todos estos años. Mención especial a mis grandes amigos Bush, Quesada, Edu, Jorge y Marco porque, aunque estemos cada uno en una parte del mundo, vuestros ánimos siempre son especiales y nuestras vivencias en el pasado y las que ocurrirán en el futuro me hacen ser muy feliz. También agradecer a mi amigo Juan, por su incondicional amistad y por hacerme vivir mis mejores momentos tanto en el instituto como en la facultad. Eres el amigo que toda persona querría y que ojalá yo tenga toda mi vida. Eres muy grande.

También darle las gracias a Erika, mi pareja. Gracias por apoyarme, acompañarme y entenderme en esos momentos en los que peor lo he pasado y sobre todo gracias por aguantarme cuando mi estado anímico no ha sido el mejor. Has estado a mi lado en los mejores y en los peores momentos de mi vida, y la verdad has sido la mejor persona que he podido encontrar. En muchos momentos, ha sido mi único apoyo y no he podido tener mejor apoyo que a ti. Por ello espero pasar toda una vida a tu lado. Eres única y espero que nunca cambies y por siempre sigas dándome ese amor que solo tú me das y me hace el más feliz.

Y por supuesto, finalmente me gustaría dar las gracias a mis bebes, mis hijas perrunas (Coco y Maya). Aunque no podáis leer esto, quiero agradeceros todo el amor que me dais. No sabéis la alegría que es llegar de trabajar y teneros ahí esperándome. Nuestros paseos diarios de una hora han sido mi única escapada del estrés de escribir este trabajo y me habéis hecho muy feliz en momentos muy difíciles. Especialmente a ti Coco, muchos momentos has sido mi única salvación y compañía, y no puedo estar más agradecido que al día en el cual te encontré en el *shelter* y decidí adoptarte. Coco y Maya, siempre estaré aquí para vosotras.

Espero no haberme olvidado a nadie. Por si acaso, gracias a todo los que leáis esta Tesis Doctoral.

A todos, **GRACIAS.**

"Toda obra grande es el fruto de la paciencia y de la perseverancia, combinadas con una atención orientada tenazmente durante meses y aún años hacia un objeto particular"

Santiago Ramón y Cajal

Aβ: β-amyloid peptide
$Aβ_{40}$: β-amyloid peptide of 40 aminoacids
$Aβ_{42}$: β-amyloid peptide of 42 aminoacids
Aβ(pE3): Pyroglutamate-modified (pE3) form of the β-amyloid peptide.
ABCA7: ATP Binding Cassette, subfamily A, member 7
ACTH: Adrenocorticotropic Hormone
AD: Alzheimer's disease
ADAM: A Disintegrin And Metalloprotease
AICD: APP Intracellular Domain
ALS: Amyotrophic Lateral Sclerosis
Alv: Alveus
AMP: Antimicrobial Peptide
ApoE: Apolipoprotein E
APP: Amyloid Precursor Protein
a.u: arbitrary units
BACE: Beta-site APP Cleaving Enzyme
BBB: Blood Brain Barrier
BDNF: Brain Derived Neurotrophic Factor
BFA: Bacterial Functional Amyloids
BIN1: Bridging Integrator 1
C83: C-terminal fragment of 83 aminoacids
C99: C-terminal fragment of 99 aminoacids
CA: *Cornu Ammonis*
CAA: Cerebral Amyloid Angiopathy
CCL: CC chemokine ligands
CD33: Cluster of Differentiation 33
CDI: Conformation Dependent Immunoassay
CLU: Clusterin
CMV: Cytomegalovirus
CNS: Central Nervous System
COVID-19: Coronavirus disease 2019
CR1: Complement Receptor 1
Cryo-EM: Cryo-Electron Microscopy
CSF: Cerebrospinal Fluid
CSF1R: Colony Stimulating Factor 1
CTF: C-terminal Fragment
CTSB: Cathepsin B
CytD: Cytosolic C-terminal Domain
DAB: 3-3'-diaminobenzidine tetrahydrochloride
DAA: Disease Associated Astrocytes
DAM: Disease Associated Microglia
DAPI: 4′,6-diamidino-2-phenylindole
DG: Dentate Gyrus
DMSO: Dimethylsulfoxide
dpi: days post-injection
DPX: Dibutylphthalate Polystyrene Xylene
DSS: 4,4-dimethyl-4-silapentane-1-sulfonic acid
DTT: Dithiothreitol
ECE: Endotelin Converting Enzymes
EDTA: Ethylenediaminetetraacetic Acid
EM: Electron Microscopy
EOAD: Early-onset Alzheimer's disease
ER: Endoplasmic Reticulum
EtOH: Ethanol
FA: Formic acid
FAD: Familial Alzheimer's Disease
FDA: Food and Drug Administration
FDG-PET: Fluorodeoxyglucose-Positron Emission Tomography
FFPE: Formalin-fixed paraffin-embedded
FTIR: Fourier transform infrared
g: granule cell layer of the dentate gyrus
GdnHCl: Guanidine hydrochloride
GFAP: Glial Fibrillary Acidic Protein
GVB: Granulovacuolar Degeneration Bodies
h: Hilus
HAM: Human AD-associated Microglia
HAVCR2: Hepatitis A Virus Cellular Receptor 2

HLA-DRB1: Human Leukocyte Antigen DRB1
HP: Hippocampus Proper
HRP: Horseradish peroxidase
HSV-1: Herpes Simplex Virus 1
IAPP: Islet Amyloid Polypeptide or amylin
Iba-1: Ionized calcium Binding Adapter molecule 1
i.c: Intracerebrally injected
IDE: Insulin-Degrading Enzyme
IFN-γ: Interferon gamma
IgG: Immunoglobin G
IHC: Immunohistochemistry or Immunohistochemical
IL: Interleukin
IQCK: IQ Motif Containing K
INPP5D: Inositol Polyphosphate-5-Phosphatase D
IPTG: isopropyl-β-D-thiogalactoside
kDa: Kilodaltons
kHz: Kilohertz
KPi: Potassium phosphate buffer
LB: Luria-Bertani medium
LCOs: Luminescent Conjugated Oligothiophenes
LILRB2: Leukocyte Immunoglobulin Like Receptor B2
LOAD: Late-onset Alzheimer's disease
LV: Lateral ventricle
LPS: Lipopolysaccharides
m: *Stratum moleculare* or molecular layer
MAM: Mitochondrial-Associated endoplasmic reticulum Membranes
MCI: Mild Cognitive Impairment
M1: Classical/Cytotoxic Microglia
M2: Alternative/Neuroprotective Microglia
Mcc: Microcin E492
MPL: Mass-per-length
MS4A: Membrane-Spanning 4-domains subfamily A
MSA: Multiple System Atrophy
MT5-MMP: Membrane-Type-5-Matrix Metalloproteinases
MW: Molecular Weight
N-APP: N-terminal fragment generated from sAPPβ
NaCl: Sodium chloride
NaOH: Sodium hydroxide
NEP: Neprilysin
NFL: Neurofilamente light
NFTs: Neurofibrillary tangles
NH_4OH: Ammonium hydroxide
N.S.: Nonsignificant result
PBS: Phosphate-Buffered Saline
PCA-AD: Posterior cortical atrophy variant of AD
PD: Parkinson's Disease
PET: Positron Emission Tomography
PHF: Paired Helical Filaments
PiB: Pittsburgh compound B
PICALM: Phospatidyl Inositol-binding Clathrin Assembly protein
PIPES: piperazine-N,N′-bis (2-ethanesulfonic acid) buffer
PK: Proteinase K
PLCG2: Phospholipase C Gamma 2
PMCA: Protein Misfolding Cyclic Amplification
PMD: Protein Misfolding Disorders
Pmel17: Premelanosome protein 17
PMSF: Paramethylsulfoxide
PNS: Peripheral Nervous System
PrP: Prion Protein
PrP^{Sc}: Disease-associated conformation of the Prion Protein
PrP^{C}: Normally folded Prion Protein

PS: Presenilins
PSEN1 or PS1: Presenilin 1
PSEN2 or PS2: Presenilin 2
pTau: Phosphorylated tau protein
r-AD: Rapidly-progressive form of AD
rf: Radio-frequency
RIP1: Receptor Interacting Serine/Threonine Kinase 1
RIP3: Receptor Interacting Serine/Threonine Kinase 3
RT: Room Temperature
SAD: Sporadic Alzheimer's Disease
SCFAs: Short-chain Fatty Acids
SA-PE: Streptavidin-phycoerythrin
sAPPα: Soluble APP alpha fragment
sAPPβ: Soluble APP beta fragment
sAPPη: Soluble APP Eta fragment
SD: Standard Deviation
SDS: Sodium Dodecyl Sulfate
SERPINA3N: Serpin Family A Member 3
SEM: Standard error of the mean
slm: *Stratum lacunosum-moleculare*
so: *Stratum oriens*
SORL1: Sortilin Related Receptor 1
sp: *Stratum pyramidale*
SPI1: Spi-1 Proto-Oncogene
sr: *Stratum radiatum*
ssNMR: solid state Nuclear Magnetic Resonance
sub: Subiculum
SVZ: Subventricular zone
T: Temperature
TAAD: Tangle-associated Amyloid Deposits
t-AD: Typical prolonged-duration form of AD
TDP-43: TAR DNA-binding protein 43
TEM: Transmission Electron Microscopy
Th: T helper lymphocyte
ThS or Thio-S: Thioflavin S
ThT: Thioflavin T
TLR: Toll Like Receptor
TMAO: Trimethylamine N-oxide
TMD: Transmembrane domain
TMEM106B: Transmembrane Protein 106B
TNF-α: Tumor Necrosis Factor α
TNIP1: TNFAIP3 Interacting Protein 1
TREM2: Triggering Receptor Expressed on Myeloid cells 2
Tris-HCl: Tris (hydroxymethyl) aminomethane hydrochloride
v/v: volume/volume
w/v: weight/volume
WT: Wild Type (non transgenic)

Indexes

Index

Index

Index

Figures and tables Index

Tables

Figures

Figures and tables Index

1. Introduction

1. 1. ALZHEIMER'S DISEASE

Alzheimer's disease (AD), the most common cause of dementia in people over 65 years old, is a neurodegenerative proteinopathy characterized by a gradual and unrelenting decline in memory and cognitive functions. This disease occurs along a continuum process starting with a long asymptomatic phase, that is characterized by pathophysiological changes that start decades before symptoms arise. This long preclinical phase is followed by the symptomatic AD phase which is first characterized by a prodromal stage also referred to as mild cognitive impairment (MCI) that progresses to mild, moderate, and finally severe dementia (Alzheimer Association Report 2020). The dementia phase, usually lasting 8-10 years, is characterized by substantial memory loss and other functional impairments that affect a person's ability to function in daily life including reasoning capacity, language/speech (aphasia), executive function (apraxia), complex attention (agnosia) as well as visuospatial processing, social and behavioral deficits. These alterations are consequence of a selective damage of brain regions (associative regions of the cerebral cortex and medial temporal lobe) implicated in these processes, such as the hippocampus, the entorhinal cortex, the amygdala, and the basal ganglia (basal forebrain). Specifically, these regions suffer a progressive and irreversible loss of synaptic/neuronal functions which are thought to be caused by specific neuropathological hallmarks such as extracellular deposits of β-amyloid (Aβ) peptide (senile plaques), intraneuronal accumulation of aggregated hyperphosphorylated tau protein (neurofibrillary tangles or NFTs), and glial (microglial and astroglial) activation (Scheltens et al., 2021)(See **Figure 1.1**).

Despite the great advances made in biomedical research, there are not effective disease-modifying therapies at this time that could prevent, slow or ideally revert the progression of AD. Currently, drugs available for AD only ameliorate the symptoms and none is completely effective (Cummings et al., 2021; Scheltens et al., 2021). The lack of an effective treatment is due, at least in part, by the scarcity of novel drug targets and a poor understanding of disease biology. In addition, a successful treatment at late stages (dementia) when the integrity of the nervous tissue is highly compromised is very unlikely to be effective. Recently, Biogen's drug, aducanumab, was the first disease-modifying drug to be approved for AD and the only drug to be approved for AD in the past 18 years. This drug, a monoclonal antibody targeting Aβ, was approved under the FDA's accelerated approval pathway. Even though this treatment successfully proved that it

decreases brain Aβ levels, its weakness in efficacy regarding cognitive improvement resulted in huge controversy within the scientific community and thus it is still not considered a clear therapy for AD (Fillit and Green, 2021; Hooker, 2021; Tampi et al., 2021).

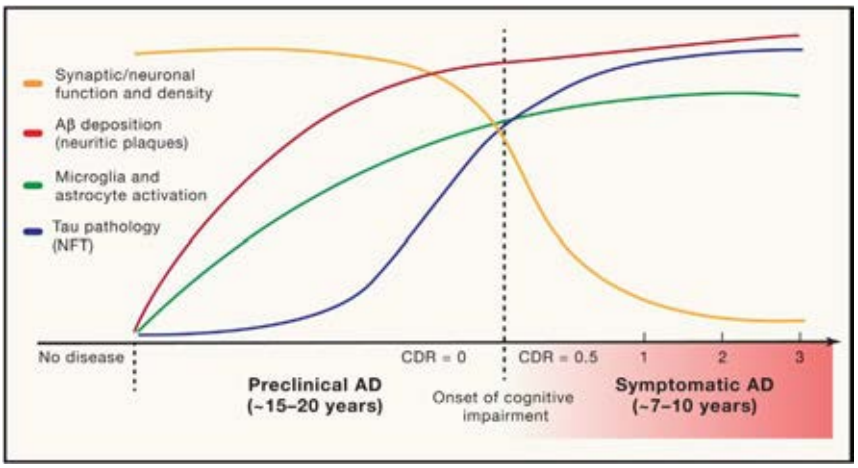

Figure 1.1. AD neuropathological hallmarks and clinical course. Early and presymptomatic stages of AD are characterized by an increase in levels of Aβ deposition and microgliosis detected by PET imaging. This is followed by accumulation of tau pathology (NFT) which correlates with loss of synaptic and neuronal function and density and thus onset of clinical symptoms of AD. Figure adapted from Long and Holtzman (2019).

Another limitation found in the field of AD research is in regard to diagnosis (World Alzheimer's Report 2021). In fact, AD is diagnosed according to a clinical framework based on the presence of cognitive and behavioral symptoms. Even though several AD biomarkers, such as neurofilament light (NFL) and pTau217, have been recently found to effectively predict AD in early presymptomatic stages of the disease (Barthélemy et al., 2020; Palmqvist et al., 2020; Preische et al., 2019; Zetterberg and Schott, 2019), a definitive diagnose is only possible by a neuropathological *postmortem* analysis. However, the development and optimization of clinically useful assays to detect serum levels of pTau217 and NFL, as well as the discovery of novel PET imaging tracers, will potentially allow for the detection of pre-symptomatic AD and will be critical for clinical care of this devastating disease before cognitive symptoms develop (Ashton et al., 2020; Hansson, 2021; Zetterberg and Bendlin, 2021; Zetterberg and Blennow, 2021).

The National Institute of Aging (USA) and the Alzheimer's Association (NIA-AA) recently proposed a biological framework for defining the **AD continuum** (Jack et al., 2018). This new framework is based upon the key AD biomarkers, amyloid-beta (**A**),

pathologic tau (**T**), and neurodegeneration (**N**) instead of clinical symptoms. This **[AT(N)]** classification system is based in imaging and biofluids biomarkers in living people. Evidence of amyloid deposition with a normal pathologic tau indicates "Alzheimer's pathologic change". Therefore, evidence of Aβ accumulation is essential to be considered within the AD continuum. The term "Alzheimer's disease" applies if both Aβ and pathologic tau biomarkers are present. Neurodegeneration biomarkers and cognitive symptoms are used only to stage AD severity. The disease process begins long before symptoms, therefore AD is now regarded as a continuum rather than a clinically defined entity. Moreover, this AT(N) system is now evolving towards an **ATX(N)** system where **X** could be a novel candidate biomarker for other pathophysiological mechanisms involved in AD such as innate immune dysregulation, vascular dysfunction or synaptic dysfunction (Hampel et al., 2021a).

1.1.1. Epidemiology

Currently, AD is the most common form of dementia (50-75%; See **Figure 1.2**) and the major cause of disability and dependency among older adults. Earlier than age 65, termed early-onset AD (EOAD), the prevalence of AD is below 5%, increasing exponentially with advancing age. Indeed, 13.5% of people age 75 to 84 have AD dementia and population older than 85 years old shows an incidence of 34.6% in Europe and North America, reaching an incidence of 63.9% in people older than 90 (Prince et al., 2013; Rajan et al., 2021). The increase of elderly population, due to the rise in life expectancy, makes AD one of the most severe health problems in developed countries (only behind cardiovascular accidents and cancer). Even though, life expectancy has decreased due to the current coronavirus disease 2019 (COVID-19) pandemic, studies have shown that AD might have been even exacerbated by this pandemic (Li et al., 2020; Zhou et al., 2021). In fact, recent findings support a link between genetic risk for AD and susceptibility to severe COVID-19 (Magusali et al., 2021).

From the approximately 47 million affected people worldwide estimated by the World Health Organization (www.who.int/news-room/fact-sheets/detail/dementia), 7 million are in Europe and almost one million in Spain (www.alzheimer-europe.org/). It is predicted that there will be 131 million individuals afflicted by AD in the world by the year 2050. Countries like the United States, which currently has 6.1 million people older than 65 that live with AD, are projected to have 13.8 million people older than 65 living with AD dementia by 2060 (Rajan et al., 2021).

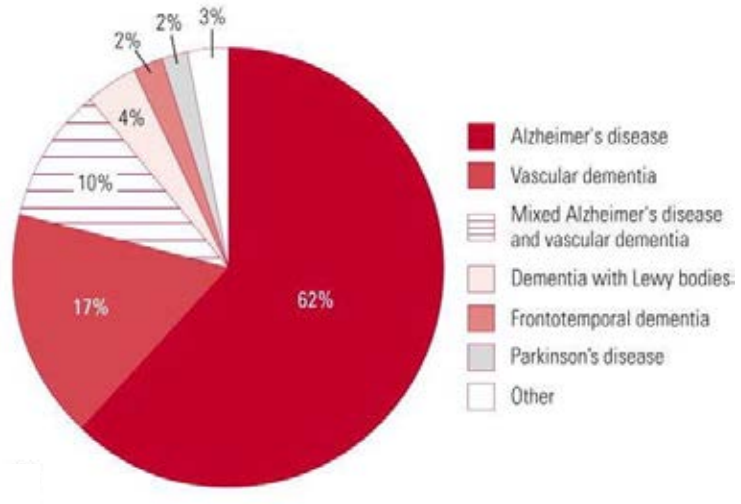

Figure 1.2. Distribution of the different types of dementia. Epidemiological studies have revealed that AD is the most common form of dementia occurring in later life (62% of total types of late-onset dementia). Diagram adapted from Jefferies and Agrawal (2009).

1.1.2. Alzheimer's disease classification

AD is mostly classified in two main types depending on the cause, the age of onset and its incidence. Both forms exhibit the same symptomatology and histopathological features (Ayodele et al., 2021; Ballard et al., 2011; Bateman et al., 2011; Reitz et al., 2020; Ryan et al., 2016):

- **Late-onset form of AD (LOAD)**: Appearing in people aged over 60-65 years, it constitutes the vast majority of cases (>95%). It has a multifactorial origin with advanced age as the main risk factor along with certain genetic polymorphisms (*APOE4* is the most important genetic risk factor for sporadic AD; reviewed in Serrano-Pozo et al., 2021), in fact, LOAD has a strong genetic component (heritability of 70%-80%) and it has been described as polygenic (Andrews et al., 2020; Neuner et al., 2020; Scheltens et al., 2021; Sims et al., 2020). In recent years, genome-wide association studies (GWAS) have identified, in addition to APOE4, over 40 polymorphisms in certain genes associated with increased risk of developing LOAD, such as *CLU, CR1, PICALM, HLA-DRB1, TREM2, ABCA7, SORL1, BIN1, ADAM10, IQCK, TNIP1, HAVCR2, LILRB2, TMEM106B* and others (Ando et al., 2020; Chen et al., 2021; Efthymiou and Goate, 2017; Harold et al., 2009; Kunkle et al., 2019; Lambert et al., 2009; Shi and Holtzman,

2018; Wightman et al., 2021). These genetic data implicate immune networks as being enriched in LOAD. Many of these genes (*CR1, TREM2, ABCA7, MS4A4A/MS4A6A, PLCG2, SPI1, CD33, INPP5D, TNIP1, LILRB2, and others*) are expressed by microglia, the resident immune cells of the brain (Efthymiou and Goate, 2017; Griciuc and Tanzi, 2021; Hansen et al., 2018; Hodges et al., 2021). In addition, sex, diet, physical activity, smoking, sleep deprivation and some comorbidities such as vascular diseases, type 2 diabetes, traumatic brain injury, epilepsy and depression are also risk factors of LOAD (Edwards III et al., 2019).

- **Early-onset form of AD (EOAD)**: Symptoms begin in people younger than 60-65 years, even as early as 35-40 years. EOAD cases make up to 5% of AD cases but only 10–15% of these cases are due to dominantly inherited mutations in presenilin 1 (*PSEN1*), presenilin 2 (*PSEN2*) and amyloid precursor protein (*APP*) genes. In total, around 330 mutations in these genes haven been reported (alzforum.org/alzgene). These mendelian EOAD forms are fully penetrant with an autosomal dominant inheritance pattern and are also refer as Familial AD forms (FAD) Interestingly, individuals with PSEN1-related mutations appears to have an earlier age of onset of AD than those with APP mutations (Ballard et al., 2011; Kim et al., 2014; Ryan et al., 2016). A significant portion of unexplained EOAD cases do not show a mendelian pattern of inheritance, and therefore, there are other genetic variations (e.g. APOE4 the most important genetic risk factor) and mechanisms at play (Efthymiou and Goate, 2017).

1. 1. 3. Neuropathology

Alzheimer's disease is characterized by both macroscopic and microscopic distinctive features (Deture and Dickson, 2019; Selkoe and Hardy, 2016; Serrano-Pozo et al., 2011). At the macroscopic level, brains from AD patients exhibits different morphological alterations, such as regional atrophy in the medial temporal brain region, decrease in hippocampal volume (hippocampal atrophy) and weight loss (Boccardi et al., 2015; Zhang et al., 2021a), reduced cortical thickness in the posterior cingulate gyrus (Lehmann et al., 2010) together with bigger and dilated ventricles and sulci (**Figure 1.3**).

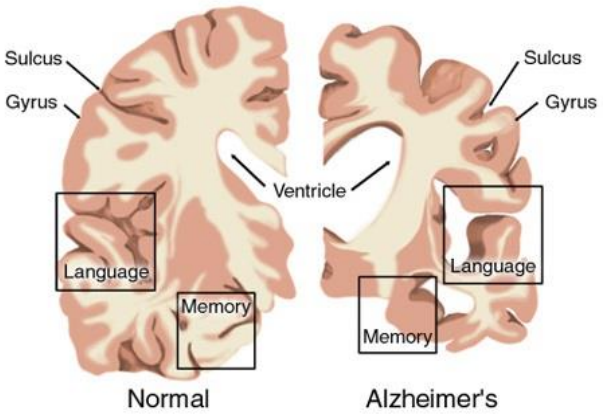

Figure 1.3. Differences between normal adult (left hemisphere) and AD patient (right hemisphere) brains. AD brains exhibit cortical atrophy, gyri reduction and dilation of sulci and ventricles. The brain regions affected are related memory and language task. Image taken from www.brightfocus.org.

At the microscopic level, the main histopathological lesions are (Knopman et al., 2021; Long and Holtzman, 2019; Selkoe and Hardy, 2016):

- Amyloid or senile plaques. Extracellular accumulation of Aβ peptides within the brain parenchyma. These deposits are found in two main forms: diffuse plaques and fibrillar neuritic plaques. Fibrillar plaques are spherical structures surrounded by dystrophic neurites and activated microglial and astroglial cells, and they are used in the pathological diagnosis of AD. However, diffuse plaques are normal structures in cognitively intact aged brains and not considered pathognomonic for AD. How they arise and how they are related to each other is unclear. In AD brains these extracellular deposits are found in a widespread distribution throughout the hippocampus and cerebral cortex. For more details see **section 1. 2. 3. 3.**
- Cerebral amyloid angiopathy (CAA). Aβ aggregates found in the perivascular space of brain blood vessels. This type of aggregates can damage the vessel wall and lead to microhemorrhages.
- Neurofibrillary tangles (NFTs). Intracellular aggregates of hyperphosphorylated tau protein. Specifically, tau is known to aggregate as paired helical filaments (PHFs) intraneuronally forming both NFTs and within dystrophic neurites as neuropil threads. This lesion is also found in many other neurodegenerative diseases known as primary tauopathies such as frontotemporal dementia, Pick disease, progressive supranuclear palsy and corticobasal degeneration. Tau

pathology usually appear first within the perirhinal and entorhinal cortex and then, extend to the hippocampus. At later stages, neocortical brain regions are also affected (Braak and Braak, 1991) giving rise to memory and learning deficits.

- Glial activation and neuroinflammation. Multiple lines of research found that activation of innate immune cell mediators play a central role on AD pathology (Heneka et al., 2015; Heppner et al., 2015; Leng and Edison, 2021; Newcombe et al., 2018; Scuderi et al., 2020). These neuroimmune activation is mostly triggered by reactive astrocytes and activated microglial cells in the brain parenchyma mainly surrounding neuritic amyloid plaques (Fakhoury, 2018; Kaur et al., 2019; Lier et al., 2021). The activation of these two cell types have become one of the most prominent pathological features found in AD brains and several genetic risk factors for AD have been shown to be associated these cells supporting a gliocentric view of AD pathology, though their roles (protective/toxic) in AD initiation and progression are unclear and highly debated. Activated microglia can exhibit a protective, neurotoxic and/or dystrophic/dysfunctional phenotype depending on their environment and disease stage (Gutierrez and Vitorica, 2018; Navarro et al., 2018; Onuska, 2020; Sanchez-Mejias et al., 2016; Shahidehpour et al., 2021; Streit et al., 2020). Single-cell transcriptomic studies have proliferated in the literature trying to decipher microglial phenotypes and the molecular pathways involved in AD. Different microglia subpopulations with unique transcriptomic profile might co-exist at a given physiological or pathological stage (Boche and Gordon, 2021; Butovsky and Weiner, 2018; Olah et al., 2020; Stratoulias et al., 2019; Tan et al., 2020). In this sense, a microglial subset named "disease-associated microglia" (DAM), that accumulate around amyloid plaques, is characterized by the upregulation of genes involved in lysosomal, phagocytic, and lipid metabolism pathways, including AD risk genes such as *ApoE* and *Trem2* (Deczkowska et al., 2018; Keren-Shaul et al., 2017). However, human AD microglia (named HAM) showed an enhanced human aging profile supporting microglial activation impairment and, similar to DAM, present *ApoE* upregulation as well as genes involved in lipid/lysosomal biology (Srinivasan et al., 2020). Numerous findings support microglia dysfunction as a central mechanism in AD etiology (Baik et al., 2019; Chatila and Bradshaw, 2021; Marschallinger et al., 2020; Swanson et al., 2020). However, the inflammatory response is an extremely complex phenomenon that can change over the disease's progression and brain

area. On the other hand, reactive astrocytes are also a key feature of AD brains (Perez-Nievas and Serrano-Pozo, 2018; Preman et al., 2021). However, it is not clear whether this response exacerbates or attenuates AD pathology, or it is a consequence of the disease with little pathological bearing. Using single-nucleus RNA sequencing a population of disease-associated astrocytes (DAA phenotype) has recently been identified in an AD transgenic model (Habib et al., 2020). These are enriched in *Gfap, Serpina3n, Ctsb, Apoe and Clu* among other genes. Since controversies regarding these cells abound, a recent consensus paper on the features of reactive astrocytes and their impact on CNS disease has been published (Escartin et al., 2021) as future unifying research guidelines. Recent accumulating evidence supports the idea that reactive astrocytes in AD acquire neurotoxic properties, likely due to both a gain of toxic function and a loss of their neurotrophic effects. In addition, the contribution of these glial cells in amyloid/tau pathology and propagation is beginning to be recognized (Fleeman and Proctor, 2021; Huang et al., 2021; Pascoal et al., 2021). The key role of glial cells in the AD pathological mechanisms has become extremely important for clinical diagnosis and the development of novel therapeutic strategies (Hemonnot et al., 2019; Lewcock et al., 2020; Qiao et al., 2021; Zhang et al., 2021b).

- Neuronal and synaptic loss. The loss of neurons and the loss of synaptic homeostasis is one of the main histopathological hallmarks of AD. In fact, it has been reported that synaptic and neuronal loss in the entorhinal cortex of AD patients correlates with the onset of cognitive impairment (Olajide et al., 2021). A similar phenomenon has been found in AD transgenic mice (Sanchez-Mejias et al., 2020). Furthermore, the presence of dystrophic neurites, which are mainly swollen axons and presynaptic terminals near amyloid plaques, is a common phenomenon in brains from AD patients and transgenic mice (Sanchez-Varo et al., 2012; Sharoar et al., 2019). These plaque-associated abnormal swellings of neuronal processes represent the first indicator of disease development and might compromise neuronal integrity and synaptic function at early ages. This neuronal and synaptic loss are known to affect the neuronal network integrity which usually occurs in vulnerable brain regions related to information and memory processing, such as the CA1 region of the hippocampus.
- Others: α-synuclein accumulation (Twohig and Nielsen, 2019), Hirano bodies, granulovacuolar degeneration bodies (GVB) (Wiersma et al., 2020),

mitochondrial dysfunction (Wong et al., 2020), autophagy (Tran and Reddy, 2021) and oxidative stress (Butterfield and Halliwell, 2019).

1. 1. 4. Diagnosis

To this date, the definitive way to diagnose AD is only possible by performing a *postmortem* analysis of the brain to find out whether the main histopathological lesions such as amyloid plaques, neurofibrillary tangles and inflammatory response are present in the tissue. In the case of sporadic AD, it has been historically difficult to perform an early diagnosis since AD was undetectable until the first symptoms of cognitive failure arise. At this stage, the brain is already extensively damaged so the discovery of reliable biomarkers to diagnose AD in the preclinical phase is extremely important for both the recruitment of AD patients for clinical trials at early-stages of the disease and to treat and prevent further cognitive decline in AD patients. *Antemortem* diagnosis of AD neuropathology can be made now with reasonable validity thanks to the use of Positron emission tomography (PET) and the use of cerebrospinal fluid (CSF) and blood-based biomarkers (Knopman et al., 2021). PET is an *in vivo* diagnostic method for AD when combined to Pittsburgh compound B (PiB) (Mathis et al., 2003). Since PiB binds selectively to the Aβ peptide and is tagged with C^{11}. It allows the imaging of amyloid plaques within the brain (Klunk et al., 2004). Moreover, three other Aβ-PET tracers (florbetapir, florbetaben and flutemetamol) have also been approved by the FDA and are commercially available. These PET imaging tracers are often run together with fluorodeoxyglucose (FDG)-PET tracer. This tracer measures cerebral metabolism, which is thought to match neuronal activity. Thus, in AD patients' brains is normal to find decreased FDG-PET signal as a sign of hypometabolism. Usually, temporal-parietal and hippocampal volume loss, which is highly characteristic of AD, is preceded by hypometabolism in these brain regions (Chételat et al., 2020; Laforce et al., 2014). Furthermore, several PET ligands for tau protein have also been developed. One of them, ^{18}F-flortaucipir, has been already approved by the FDA and is being used in the clinic (Harada et al., 2016; Jeong et al., 2020). This tracer is not specific for AD since it will also detect tau in other tauopathies but its binding to specific regions of the brain match the regional patterns of different AD clinical subtypes and strongly correlate with cognitive performance (see **Figure 1.4**. Aschenbrenner et al., 2018). In regards to CSF biomarkers, Tau/$A\beta_{42}$ ratio has been proven as another high-accuracy method (Hansson et al., 2006; Harari et al., 2014). Currently is widely accepted that in AD there is a

decrease in CSF $A\beta_{42}$ (or $A\beta_{42}/A\beta_{40}$ ratio), a decrease in total tau and an increase in pTau181 (Molinuevo et al., 2018). Furthermore other AD biomarkers such as Neurofilament Light (NFL), pTau217 and pTau231 have been recently found to effectively predict AD in early pre-symptomatic stages of the disease (Barthélemy et al., 2020; Kern et al., 2019; Palmqvist et al., 2020; Preische et al., 2019; Suárez-Calvet et al., 2020; Zetterberg and Schott, 2019). However, these biomarkers are not yet available for clinical practice as additional validation is needed. Furthermore, blood-based biomarkers are being developed for $A\beta_{42}$ (Schindler et al., 2019), pTau181 (Karikari et al., 2020) , pTau217 (Palmqvist et al., 2020), pTau231 (Ashton et al., 2021) and NFL (de Wolf et al., 2020). Nevertheless, these are still not as sensitive as CSF-based biomarkers. In 2020, the European Union and USA approved a blood-based assay that measure $A\beta_{42}/A\beta_{40}$ ratio. This assay was found to correlate well with the status of Aβ-PET imaging (Schindler et al., 2019). Regarding other blood-based biomarkers, a simple, fast, non-invasive and cheap diagnostic method, based on the lipidic profile**,** was discovered and predicts the cognitive deficits 2-3 years before the onset of symptoms with 90% accuracy (Mapstone et al., 2014). The development and optimization of clinically useful assays to detect serum levels of Aβ42, pTau181, pTau217, pTau231 and NFL, as well as the discovery of novel PET imaging tracers, will potentially allow for definitive detection of asymptomatic AD and will be critical for clinical care of this devastating disease before the onset of cognitive symptoms (Castellani et al., 2010; Khachaturian, 1985; Knopman et al., 2021; Lilly S.A., 2012; Long and Holtzman, 2019; Masters et al., 2015; Ryan et al., 2015; Webster et al., 2014).

In this sense, the development of both neuroimaging biomarkers and highly accurate fluid biomarkers gave rise to a new unbiased biological classification system to define AD as a continuum as previously described. By this classification AD patients are differentated from non-AD patients by three biomarkers: Aβ (A), tau (T) and neurodegeneration (N). Aβ is measured by either amyloid-PET or $A\beta_{42}$ in CSF, Tau pathology is measured either by tau-PET or pTau markers in CSF, and neurodegenerations is measured by either structural MRI or FDG-PET.

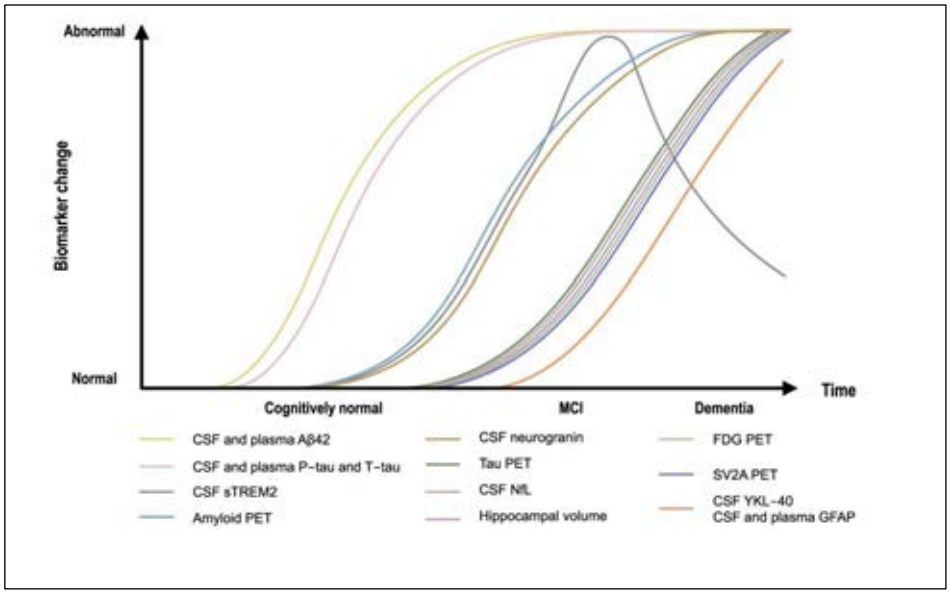

Figure 1.4. Temporal staging of AD biomarkers along the AD continuum. It has been proven that the first biomarkers to change are CSF and plasma $A\beta_{42}/A\beta_{40}$ ratio followed by increase in tau. Later, at the MCI stage, there is an increase of soluble TREM2 released by microglial cells, CSF neurogranin and amyloid PET positivity. Finally, at the end of the MCI stage and in the dementia stage there is an increase in tau PET positivity, NFL levels in CSF and plasma and change in hippocampal volume and FDG-PET. Studies have shown that astrocytic biomarkers (YKL-40 and GFAP) change late in disease. Figure adapted from Zetterberg and Bendlin, (2021).

Aβ accumulation in the brain is the first pathological lesion in AD and is characterized by distinct clinical and neuropathological phenotypes (Ferreira et al., 2017, 2020). In fact, recent studies revealed that Aβ assemblies might have structural differences among AD brains and may explain the distinct disease phenotypes (Di Fede et al., 2018; Ghosh et al., 2021; Qiang et al., 2017). However, the molecular basis of these phenotypic variations is largely unknown. This Thesis is focused on this topic and, therefore, an overview about Aβ pathology is provided below.

1. 2. AMYLOID-β PEPTIDE AND AMYLOID PLAQUES

One of the main pathological hallmarks of AD, along with NFTs, is the extracellular deposition of amyloid-β (Aβ) peptides. These deposits give rise to what are known as amyloid plaques. The Aβ peptide is a 4 to 4.5 kDa fragment that is generated by the proteolytic processing of its precursor, the amyloid precursor protein (APP) in neurons,

astrocytes, and vascular cells. This peptide is the result of the sequential cleavage of APP by the β-secretase (β-APP-cleaving enzyme-1 or BACE1) and γ-secretase enzymes (Haass et al., 2012; Hampel et al., 2021b; Selkoe and Hardy, 2016). APP is a type-1 transmembrane glycoprotein with a large extracellular region or ectodomain containing the amino-terminal domain, a single transmembrane domain (TMD) and a short cytosolic tail containing the carboxyl terminus (**Figure 1.5**) (Dyrks et al., 1988; Kang et al., 1987). Specifically, BACE1 cleaves at the ectodomain and γ-secretase cleaves at the transmembrane domain, thus the Aβ sequence contains part of both the APP transmembrane domain and ectodomain. This peptide structure, due to its amphipathic nature, is highly prone to aggregation within the brain parenchyma (Evin and Weidemann, 2002). High expression levels of APP are found in the nervous tissue, both in the endomembrane system (lysosomes, endoplasmic reticulum (ER) and Golgi apparatus) and in the plasma membrane of nervous cells (Plácido et al., 2014). Recent findings suggest that mitochondrial-associated endoplasmic reticulum (ER) membranes (MAMs) plays a critical role on regulating the transport of APP to the cell surface and hence Aβ generation (Bhattacharyya et al., 2021).

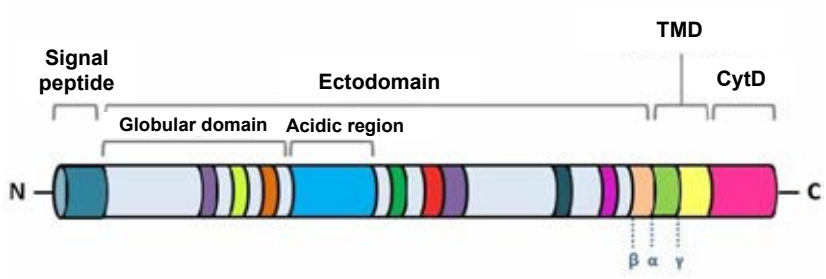

Figure 1.5. Structure of the amyloid precursor protein (APP). This protein exhibits a short cytosolic C-terminal domain (CytD), a transmembrane domain (TMD) and a long N-terminal ectodomain with binding sites for extracellular matrix molecules such as heparine and collagen and metals such as zinc and copper. Three main proteolytic cleavages occur in the vicinity of the transmembrane domain and the C-site of the ectordomain. β- and γ-secretase cleavages release, respectively, the N- and C-termini of Aβ. Modified from Evin and Weidemann (2002).

1. 2. 1. Presenilins 1 and 2

Presenilin 1 and 2 were discovered as key elements in AD pathology, and specifically in Aβ pathology, by large-scale genetic studies that found autosomal dominant mutations in the *PSEN1* and *PSEN2* genes associated to early-onset AD. Presenilin 1 (PS1) and presenilin 2 (PS2) proteins constitutes the catalytic elements of the intramembrane-cleaving γ-secretase enzymatic complex, an aspartyl-type protease tetrameric complex that mediates the Notch receptor signaling pathway and the production of Aβ (De Strooper et al., 2010). PS1 and PS2 are homologous type IV transmembrane proteins (>65% sequence homology). Presenilins have a nine-transmembrane domain topology, with a cytosolic amino terminus and a luminal carboxyl terminus. Specifically, these proteins are found in the plasma membrane and in the membrane of many organelles (endoplasmic reticulum, Golgi apparatus, lysosomes, mitochondria, phagosomes and endosomes) and its activity have been found to be associated with the different Braak senile plaque stages (Kakuda et al., 2020). Interestingly, PS2 is less efficient than PS1 regarding APP cleavage and Aβ generation. Missense mutations in these enzymes result in significant increases in the production of Aβ peptides and are the most common cause of early-onset AD. Therefore, γ-secretase could be one of the main targets for therapeutic intervention. However, presenilins play a key role on cellular homeostasis. Presenilins substrates such as Notch receptors and other 90 type I transmembrane proteins involved in protein degradation, lysosomal activity, intracellular vesicle trafficking and autophagy, raise concerns about side-effects and toxicity of targeting these enzymes (Li et al., 2009; Nixon, 2017; Selkoe and Hardy, 2016; De Strooper, 2010).

1. 2. 2. Proteolytic processing of APP: amyloidogenic and non-amyloidogenic pathways

There are three main proteolytic proteases involved in the processing of APP: α-, β- and γ-secretases. Cleavage by these enzymes give rise to two main APP proteolytic processing pathways, which results in protein fragments such as the Aβ peptide, soluble APPα and the APP intracellular domain A or AICD (**Figure 1.6**). These APP proteolytic processing pathways are described as follow (Hampel et al., 2021b):

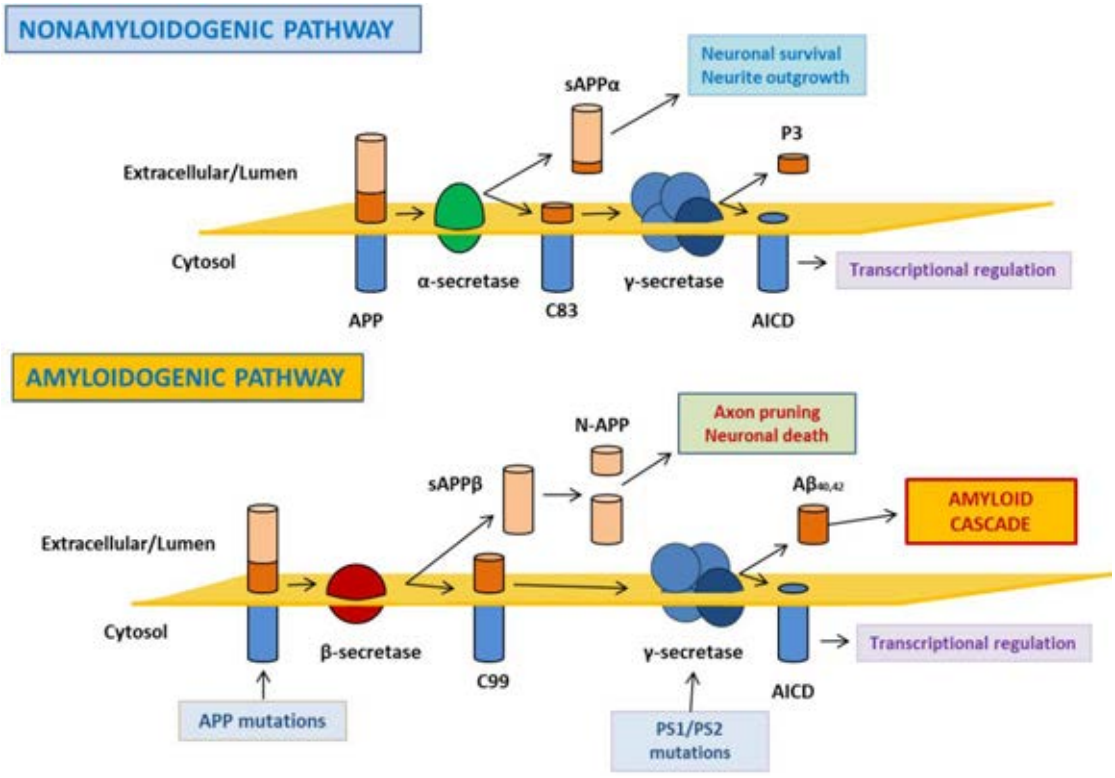

Figure 1.6. Proteolytic processing of APP. Through the non-amyloidogenic pathway, APP is sequentially cleaved by α- and γ- secretases, generating the sAPPα, P3 and AICD fragments. On the other hand, through the amyloidogenic pathway, the sequential cleavage of APP by β- (BACE) and γ-secretase results in the generation of a range of Aβ peptides ranging from 38 to 43 aminoacids, being the ones of 42 and 40 aminoacids the most common. Modified from Kim and Tsai (2009).

- Non-amyloidogenic pathway: This is the main pathway for the proteolytic processing of APP. The cleavage of APP by this route is performed sequentially by the enzymes α- and γ-secretase. More than 90% of total APP is processed through this pathway, which mostly takes place in the plasma membrane. In this proteolytic pathway APP is cleaved in the middle of what would be the Aβ sequence, hence avoiding its formation. Specifically, APP is fragmented by the α-secretase proteolytic enzyme, which as other secretases is a membrane-bound protein, resulting in a soluble fragment (sAPPα) with neuroprotective functions released into the vesicular lumen or the extracellular space. The C-terminal resultant fragment, named C83 (83 aminoacids), remains bound to the membrane and is later processed by γ-secretase (Plácido et al., 2014; Zhao et al., 2020) generating the p3 and AICD (APP intracellular domain, also known as p7) peptides. The latter, is a

cytosolic peptide that might play a role in transcriptional regulation (Jiang et al., 2020). Recent research points towards ADAM10 as the major α-secretase responsible for APP cleavage in the brain (Vassar, 2013). Alternatively, in this non-amyloidogenic pathway APP might be cleaved by η-secretase releasing a soluble fragment (sAPPη) and forming carboxyl-terminal fragments (CTFη), which are mostly found in dystrophic neurites (Willem et al., 2015). This process is mostly mediated by membrane-bound matrix metalloproteinases, such as MT5-MMP, that have η-secretase activity. CTFη fragments are further processed by α- (ADAM10) and β- (BACE1) secretases resulting the release of short peptides known as Aη-α and Aη-β. It is now known that Aη-α peptides are inhibitors of hippocampal neuronal activity. Interestingly, BACE1 inhibition induce the activation of the η-secretase pathway, causing an increase in CTFη fragments and Aη-α peptides, and hence lowers neuronal activity. This raised concerns on BACE1 inhibitors as an approach to treat AD (Willem et al., 2015).

- Amyloidogenic pathway: Minor proteolytic pathway, except in neurons. However, this proteolytic cleavage is the has huge pathophysiological implications in AD. This pathway mainly takes place in the endomembrane system. Specifically, the β-secretase (β-APP-cleaving enzyme-1 or BACE1) cleaves the extracellular region of APP at the N-terminal end of the Aβ region. This leads to the generation and release of the sAPPβ soluble fragment and formation of the C99 peptide (C-terminal fragment of 99 aminoacids, also known as CTFβ). The latter fragment remains bound to the membrane and is cleaved by the γ-secretase enzyme generating Aβ and AICD peptides. Aβ is released to the extracellular space or lumen, while AICD peptides are released into the cytoplasm (Hampel et al., 2021b; Li et al., 2009; Plácido et al., 2014; Selkoe and Hardy, 2016; De Strooper, 2010). Moreover, an N-terminal fragment (N-APP) generated from the sAPPβ might trigger axon pruning and neuron death (Lee et al., 2020). As mentioned above, the catalytic elements of the γ-secretase complex are the aspartyl-type proteases presenilin 1 and 2. The generation of Aβ is a **physiological process**, and normal concentrations of this peptide might have beneficial effects such as enhancement of learning and memory, dendritic tree branches and increased neuronal survival (Morley and Farr, 2014). In fact, Aβ monomers generated from the proteolytic cleavage of APP, can trigger intracellular signaling that is essential for neurotransmission, such as excitation/inhibition balance and synaptic vesicle trafficking regulation (Abramov

et al., 2009; Lee et al., 2020). Furthermore, Aβ monomers can mediate the transcription of the brain-derived neurotrophic factor (BDNF) which is known to be involved in hippocampal neurogenesis and hence adult synaptic plasticity (Moreno-Jiménez et al., 2019; Zimbone et al., 2018). Aβ, at the synaptic cleft, might also have critical role in sustaining a proper synaptic activity (Giuffrida et al., 2015). However, in AD, the amyloidogenic proteolytic pathway is exacerbated inducing a pathological cascade that results in cognitive impairment and dementia (Hampel et al., 2021b; Ryan et al., 2015). Most Aβ peptides ends in Val40 in its C-terminal end ($A\beta_{1\text{-}40}$ or $A\beta_{40}$), however some (10%) ends in Ala42 ($A\beta_{1\text{-}42}$ or $A\beta_{42}$). The $A\beta_{42}$ form is more hydrophobic and toxic due to its tendency to aggregate as oligomers and fibrils and is therefore the main component of Aβ parenchymal deposits. During AD, the $A\beta_{42}/A\beta_{40}$ ratio usually increases in the brain of patients. In the case of FAD, all autosomic dominant mutations occur either in the substrate (APP) or the proteases (presenilins) of the reaction that generates Aβ, resulting in increased APP cleavage through the amyloidogenic pathway and thus exacerbated $A\beta_{42}$ generation (Hampel et al., 2021b; Selkoe and Hardy, 2016; Socher et al., 2014). Moreover, there are some N-terminally truncated species of Aβ, being $A\beta_{4\text{-}42}$ the most abundant (Lewis et al., 2006) and also modified species of Aβ, such as the pyroglutamate-modified Aβ, also known as Aβ(pE3), which are highly abundant in the AD brain and had gained attention in the field due to their high aggregation propensity, stability and impact on synaptic dysfunction (Grochowska et al., 2017; Jawhar et al., 2011; Wittnam et al., 2012).

1. 2. 3. Extracellular aggregation of Aβ: from monomers to amyloid

After APP cleavage, Aβ peptide is released in its soluble monomeric form. Later, Aβ goes through different intermediate aggregation states such as dimers, trimers, soluble oligomers and protofibrils to end up forming amyloid fibrils, which indeed will precipitate and accumulate, generating the main neuropathological hallmark of AD, the extracellular amyloid plaques (Hampel et al., 2021b). In this section of the thesis introduction, the formation of Aβ plaques from the soluble monomers and the different type and conformations acquired by the amyloid plaques will be reviewed.

1. 2. 3. 1. Aβ monomers

As mentioned above, Aβ monomers are involved in a wide range of physiological conditions such as vesicle trafficking, synaptic activity homeostasis and hippocampal neurogenesis. Specifically, there are two main forms of Aβ monomers: $Aβ_{42}$, which is more prone to aggregation, and $Aβ_{40}$ (Knowles et al., 2014). Furthermore, modifications such as glycosylations, N-terminal truncations and pyroglutamate additions are known to increase insolubility and propensity to aggregate of the Aβ peptide (Nussbaum et al., 2012; Vitek et al., 1994; Wildburger et al., 2017). In AD, monomeric Aβ peptides misfold and usually follow a seeding-nucleation mechanism in which, after a long and thermodynamically unfavorable phase (nucleation or lag phase), they will undergo the formation of stable aggregates or seeds that will then rapidly elongate (elongation phase) forming polymerized oligomers and protofibrils that will then grow by incorporating more Aβ monomers to the polymer (Jarrett and Lansbury, 1993). Interestingly, recent work has shown that for tau protein, the protein that forms intraneuronal aggregates in AD brains, there are two different structural forms of the monomeric protein. One that is seed-competent and other that is inert (Mirbaha et al., 2018). Therefore, the pathogenic seed for tau is a single molecule and conversion of tau from the inert form to the seed competent form might be the rate-limiting step for fibrils formation. However, a similar scenario has not been proven yet for Aβ.

1. 2. 3. 2. Soluble oligomeric Aβ forms

Soluble Aβ oligomers are described as non-fibrillar, water-soluble and neurotoxic structure. Biochemically, these structures has been defined as assemblies of Aβ found in physiological fluids that are not pelleted upon high-speed ultracentrifugation (Kulenkampff et al., 2021). A great variety of Aβ oligomeric forms have been described, being these populations highly dynamic and existing in equilibrium with the monomeric and fibrillar forms of Aβ (Soto and Pritzkow, 2018). Specifically, oligomeric species have been found to be formed by two different pathways. On one hand, they could be **on-pathway** intermediates, which means they will end up forming fibrillar Aβ forms and are purely intermediates of the fibrilization process. On the other hand, **off-pathway** oligomers do not lead to the formation of Aβ fibrils and will stay as oligomers unless they are disassembled back to monomers (Breydo and Uversky, 2015; Lesné, 2014). Interestingly, it has been reported that most of the $Aβ_{42}$ oligomers do not convert into amyloid fibrils, instead the vast majority of these oligomers dissociate into their

monomeric state without forming new fibrils (Michaels et al., 2020). Currently, soluble oligomeric forms are thought to be the most toxic amyloid derivative, instead of amyloid plaques, and are considered the main mediator of the synaptic and neuronal pathology (NFTs, synaptic and neuron loss) (Lesné, 2014; Li and Selkoe, 2020). Specifically, it has been shown that Aβ oligomers affect synaptic plasticity and neurite integrity, induce a decrease in spine density, decrease membrane expression of some memory-related receptors and promote synaptotoxicity (Hong et al., 2018; Lacor et al., 2007; Li and Selkoe, 2020; Selkoe, 2008; Townsend et al., 2006; Walsh et al., 2002; Yang et al., 2017). Importantly, some studies have shown evidences that soluble Aβ oligomers might be released from amyloid plaques (Koffie et al., 2011; Krafft and Klein, 2010) establishing an important connection between both amyloid forms and further supporting the highly dynamic and equilibrium existing between the different Aβ species. The levels of soluble Aβ have been demonstrated to correlate better with cognitive dysfunction than amyloid plaques in both AD and transgenic mouse models (Tomic et al., 2009).

1. 2. 3. 3. Insoluble deposits of Aβ. Types of parenchymal (amyloid plaques) and vascular (CAA) deposits.

As commented above, Aβ peptides are able to aggregate in the extracellular space giving rise to amyloid or senile plaques and also deposit in the walls of leptomeningeal and intracortical (parenchymal) arteries, arterioles, capillaries and veins, pathology known as cerebral amyloid angiopathy (CAA) (Allen et al., 2014; Hampel et al., 2021b).

In AD, anatomical-temporal distribution pattern of the amyloid deposition is observed with pathology usually starting in neocortical regions of the brain and then expanding to allocortical areas and finally into the rest of the brain. Specifically, this anatomical-temporal distribution of amyloid plaques occurs as follows: 1) neocortex, 2) allocortical regions such as entorhinal cortex, subiculum, hippocampus (CA1 and dentate gyrus) and cingulate gyrus, 3) hypothalamaus, thalamus, striatum and basal forebrain, 4) midbrain and medulla oblongata and 5) cerebellum and pons (See **Figure 1.7**) (van der Kant et al., 2020; Thal et al., 2015).

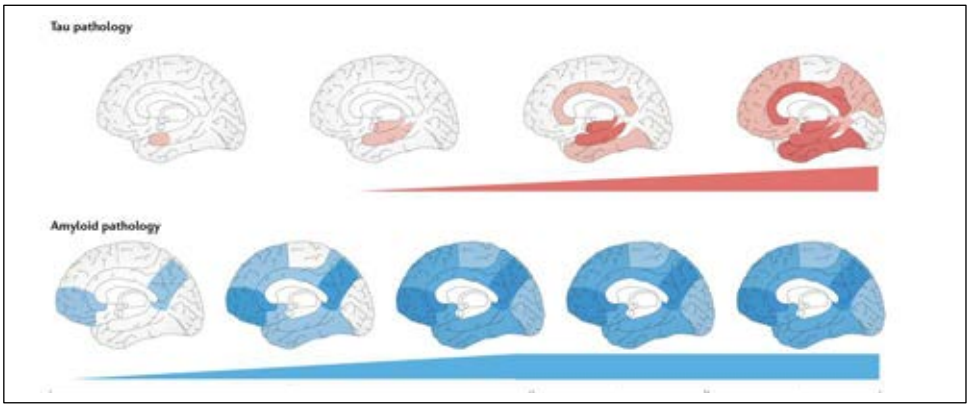

Figure 1.7. Spatiotemporal progression of Aβ and tau pathology in AD. Areas affected by tau (red) and Aβ (blue) are shown. In the case of tau pathology (Top), it starts in the entorhinal cortex and spreads to limbic areas. Aβ (Bottom) starts in neocortex and association cortices from where this pathology spreads to the allocortex. Aβ pathology is observed in individuals before development of AD symptoms, while tau pathology develops later in time, at symptomatic stages. Modified from van der Kant (2020).

Intriguingly, amyloid plaques have been shown to appear in different arrangements or type of plaques (Calderon-Garcidueñas and Duyckaerts, 2018; Duran-Aniotz et al., 2021; Duyckaerts et al., 2009; Lau et al., 2021; Thal et al., 2015). These are classified in two main groups:

- **Neuritic or dense-core plaques:** fibrillar plaques, containing both $A\beta_{40}$ and $A\beta_{42}$. This type of plaques display a spherical core with tightly packed Aβ, which is reactive to Congo red and thioflavin S, and a "corona" of dystrophic neurites, glial cells and less dense Aβ deposits (Thal et al., 2000, 2015). These plaques are thought to be the most relevant in AD pathology (Castellani et al., 2010; Selkoe and Hardy, 2016), due to the involvement of dystrophic neurites and glial cells. The former are aberrant neuronal projections containing many mitochondria, big lysosomes and paired helical filaments (PHFs). In fact, there are two main types of neuritic plaques (Selkoe, 2001): Classical or mature, which exhibit a spherical and compact nucleus surrounded by Aβ oligomers, and primitive or immature plaques, which are spherical but lacks a compact nucleus.
- **Diffuse plaques:** non-fibrillar amorphous plaques containing loosely-packed Aβ. Mostly contain $A\beta_{42}$ with little or none amounts of $A\beta_{40}$. In contrast to neuritic

plaques, these deposits are not reactive to fibrillar amyloid-binding dyes (Congo red and Thioflavin S) and lack both dystrophic neurites and reactive glia around them (Calderon-Garcidueñas and Duyckaerts, 2018). Interestingly, these deposits acquire also different morphologies in different brain regions appearing as lake-like deposits in the presubiculum and as fleecy deposits in the internal layers of the enthorhinal cortex. It is worth noting that diffuse deposits have been found in aged brains from individual without cognitive deficits. However, patients suffering from AD exhibit both neuritic and diffuse plaques (Braak et al., 2013).

Besides these two main types of parenchymal deposits, a few other types have been described as well. These includes the plaques known as **"Cotton-wool plaques"**. These are extracellular, diffuse-like deposits of Aβ that are round, homogeneous, and eosinophilic. In contrast to diffuse plaques, cotton-wool plaques display clear limits and contain sparse glial components with tau-positive processes crossing them, however these deposits do not show a corona as the dense-core plaques. Similar to diffuse plaques, they are made mostly of $A\beta_{42}$ and do not react to amyloid-binding dyes (Calderon-Garcidueñas and Duyckaerts, 2018). Cotton-wool plaques are rarely associated to sporadic cases of AD and are mostly found in familial cases caused by the deletion of the exon 9 of the Presenilin 1 gene (Le et al., 2001). The most prominent Aβ species found in cotton-wool plaque are N-truncated Aβ (Miravalle et al., 2005). Another parenchymal deposit found in AD patients are the **tangle-associated amyloid deposits** or TAAD. There are amyloid plaques that also contain extracellular tangles (ghost tangle). These tangles are also reactive to Aβ.

As mentioned above, Aβ deposition also occurs in the walls of vessels such as arteries, capillaries and even veins. This type of pathology receives the name of **Cerebral Amyloid Angiopathy** or CAA. In contrast to dense-core amyloid plaques, these deposits are mostly made of $A\beta_{40}$. Two main types of CAA have been described: **Type 1**, which involves capillaries (microangiopathy), correlate well with the parenchymal lesions, and is frequently associated to ApoE ε4 allele-bearing patients, and **type 2** which is mostly associated with cortical vessels (macroangiopathy) and is found in higher frequency in patients with ε2 allele of ApoE. Both of these types of CAA have in common the deposition of Aβ deposits in the leptomeningeal vessels (Thal et al., 2002). It is worth noting that severe CAA pathology can lead to microscopic infarcts and microhemorrhages, further worsening cognitive deficits in AD patients (Thal et al., 2003).

1. 2. 4. Intracellular accumulation of Aβ

Emerging evidence from AD patients and transgenic AD mice indicates that Aβ can also accumulate inside neurons, contributing to disease progression. Intracellular Aβ seems to be an early even in the disease and hence could be the source for extracellular amyloid plaques (Hampel et al., 2021b; LaFerla et al., 2007). Aβ found in the intracellular space can be the result of Aβ produced within the cells or might be related to neuronal cells taking up and internalizing the extracellular Aβ by receptor binding mechanisms in order undergo Aβ clearance mechanisms (Iwata et al., 2001; Schützmann et al., 2021). The latter, results in accumulation of Aβ within endosomes, lysosomes, and endoplasmic reticulum. Aβ oligomers may be produced within the cells and thus might be causing neuronal dysfunction before being released to the extracellular space (Lord et al., 2006). Intracellular Aβ aggregates before paired helical filaments (PHFs), therefore this might be one of the earliest events in AD and in transgenic mice it has been associated to tau phosphorylation, neuronal loss, synaptic dysfunction, and cognitive deficits (Billings et al., 2005; Tseng et al., 2008). Interestingly, the Arctic mutation in APP have been shown to increase the formation of intraneuronal Aβ species, which preceded the accumulation of parenchymal deposits and correlated with cognitive performance in transgenic mice (Lord et al., 2006, 2009; Sahlin et al., 2007). Further research on whether these types of deposits might be unique strains of Aβ could elucidate the biological mechanisms behind Aβ fibril's structure and AD phenotypes.

1. 2. 5. Aβ degradation

The process of Aβ degradation avoids the accumulation/deposition of this peptide, and hence the formation of amyloid plaques. In AD, the build-up and aggregation of Aβ peptides as amyloid plaques within the brain parenchyma, occurs due to an altered balance in biogenesis/clearance of Aβ amyloid peptides. Currently, many mechanisms are known to be involved in the process of elimination/clearance of Aβ: endosomal-lysosomal pathways such as autophagy, endothelin converting enzymes (ECE), which degrade the peptide that is produced within the endosomal/lysosomal pathway and autophagosomes, and non-lysosomal pathways such as the proteasome, proteolytic enzymes, i.e. neprilysin (NEP) and insulin degrading enzyme (IDE), and chaperones such as ApoE (Crews and Masliah, 2010; Pacheco-Quinto and Eckman, 2013; Ryan et al.,

2015). It has been proved that during aging, the levels of NEP and IDE are reduced, decreasing the rate of Aβ degradation (De Strooper, 2010).

1. 2. 6. Amyloid cascade hypothesis

The amyloid cascade hypothesis, postulated by Hardy and Higgins, posits that accumulation of Aβ is the causative agent in AD (Hardy and Higgins, 1992). This theory postulates that accumulation of Aβ peptides, due to both an altered balance in biogenesis/clearance and aberrant folding of Aβ in the brain, leads to a chronic inflammatory response (activation of microglial and astroglial cells), hyperphosphorylation of tau, neurofibrillary tangles (NFTs) onset, disruption of axonal transport, emergence of dystrophic neurites, synaptic loss, and neuronal death (See **Figure 1.8**). All these pathological events result in progressive cognitive decline in patients (Selkoe and Hardy, 2016).

This hypothesis is the predominant framework for AD research and drug development; however, it is also a source of controversy. Several concerns have been counterpoised to the amyloid hypothesis (Herrup, 2015; Musiek and Holtzman, 2015):

- Amyloid plaque burden does not correlate, as much as NFTs do, with cognitive deficits.
- Many non-demented patients show abundant deposits of Aβ at death.
- Some studies suggest that NFTs might precede amyloid plaques.
- Clinical trials centered on anti-amyloid compounds have not been successful.

Nonetheless, soluble Aβ oligomers correlate well with degree of cognitive impairment. Thus, the original amyloid hypothesis have been reviewed considering the important role of these toxic soluble forms of Aβ on synaptic loss and cognitive decline (Selkoe and Hardy, 2016).

1. 2. 7. Prion like transmission of Aβ

AD pathogenic features, such as presence of misfolded protein aggregates and progressive neuronal loss in specific areas of the Central Nervous System (CNS), are shared with other neurodegenerative diseases, such as Prion diseases, Parkinson's disease (PD) and amyotrophic lateral sclerosis (ALS) (Vaquer-Alicea and Diamond, 2019). First described by Nobel Prize awardee Stanley B. Prusiner in 1982, the prion protein (PrP)

was the first disease-causing "proteinaceous infectious agent" ever described (Prusiner, 1982).

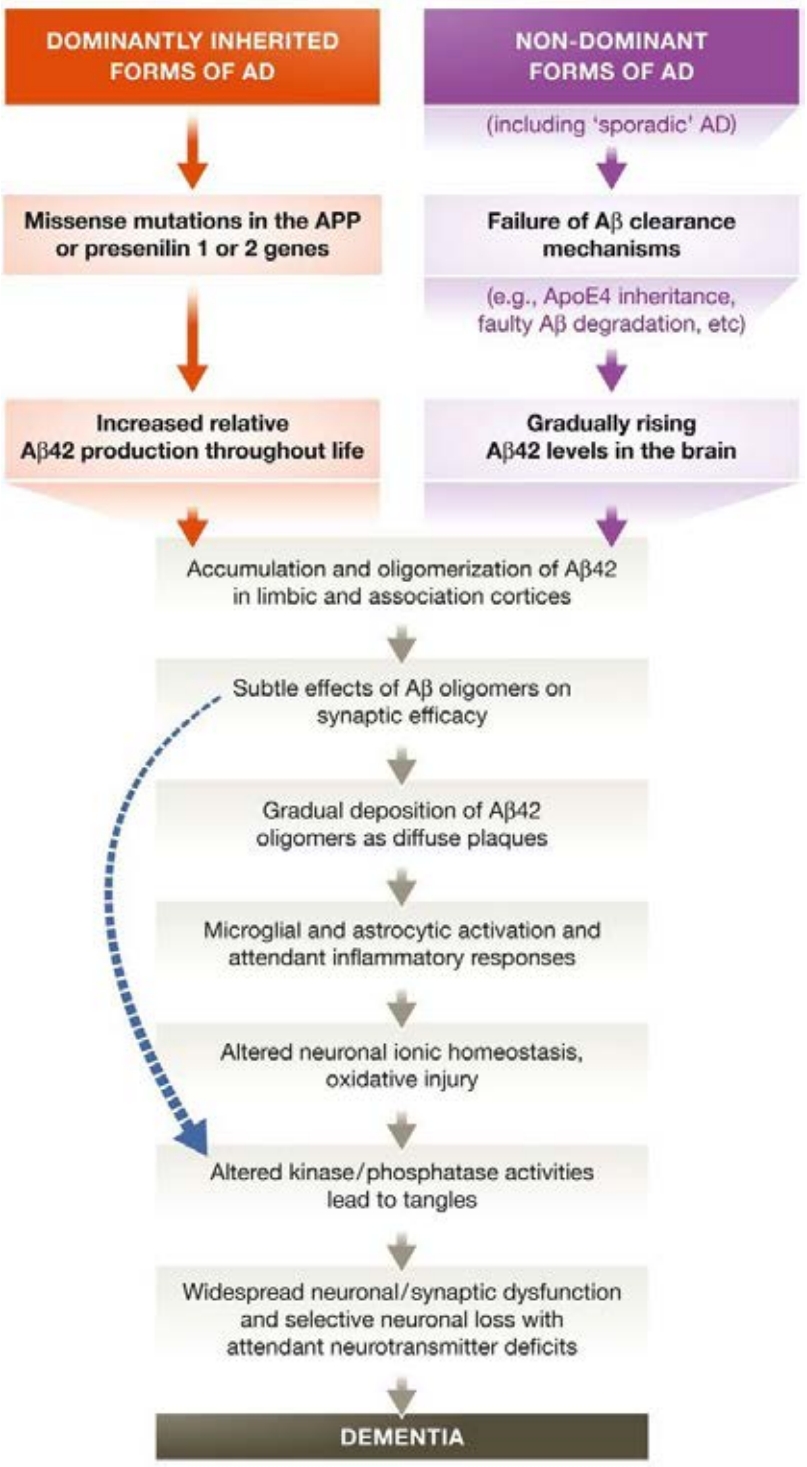

Figure 1.8. Amyloid cascade hypothesis (Reviewed). As postulated by this hypothesis, a sequence of gradual pathogenic events leads to AD onset, being Aβ the main player in this cascade. This reviewed version of the amyloid hypothesis includes Aβ oligomers, which may activate glial response or directly injure the synapses and neurites (blue arrow). Adapted from Selkoe and Hardy (2016).

Although prion diseases differ in the clinical and neuropathological features with the aforementioned proteinopathies, these diseases consistently share a strikingly similar pathogenic mechanism which is the ability of their disease-associated proteins (Aβ, tau, prions, α-synuclein and TDP-43) to misfold, aggregate and self-propagate (Jucker and Walker, 2018). These pathogenic proteins also share structural, biological, and biochemical features with prions such as insolubility, toxicity, resistance to proteolytic degradation and reactivity to amyloid specific dyes such as Congo red and Thioflavin (Lau et al., 2021). The prion protein has the ability to self-replicate its disease-associated conformation (PrP^{Sc}) from the normally folded prion protein (PrP^{C}). The prion infectious isoform is demonstrated to have the ability to be transmitted from cell-to-cell, between individuals and even from surfaces, partially contributing to the etiology of a group of fatal neurodegenerative disease known as Transmissible Spongiform Encephalopathies (TSEs). Due to the strikingly biochemical and biological similarities between PrP^{Sc} and other neurodegenerative disease-associated amyloids, pathological aspects of diseases such as AD, PD and ALS are hypothesized to be transmissible through **prion-like propagation mechanisms**. In the case of Alzheimer's disease, Aβ and tau protein have shown to propagate both *in vitro* and *in vivo* in different laboratory settings, further supporting the possibility of this disease being transmissible in a prion-like manner (Gomez-Gutierrez and Morales, 2020; Iba et al., 2013; Meyer-Luehmann et al., 2006; Morales et al., 2012a). Remarkably, there are growing evidence for human iatrogenic transmission of Aβ pathology that highlight the potential issue of inter-individual transmission of AD-like neuropathology (Banerjee et al., 2019; Cali et al., 2018; Frontzek et al., 2016; Gomez-Gutierrez and Morales, 2020; Hamaguchi et al., 2016; Hervé et al., 2018; Jaunmuktane et al., 2015, 2018; Kovacs et al., 2016; Purro et al., 2018; Ritchie et al., 2017).

The first proteinopathy, other than prion diseases, demonstrated to propagate in a prion-like manner was Alzheimer's disease. **Amyloid-β** was found to self-propagate *in vitro* decades ago (Jarrett and Lansbury, 1993). At the same time, it was confirmed that this phenomenon could occur *in vivo* when marmosets displayed robust Aβ pathology 6-7 years after receiving intracerebral injections of brain extracts from AD patients (Baker et al., 1993). At the beginning of this century, *in vivo* self-propagation of Aβ was further confirmed when AD transgenic animals displayed robust Aβ pathology 5 months after being intracerebrally injected with brain extracts from AD patients (Kane et al., 2000). However, the idea of Aβ as the sole source of amyloidosis induction was not confirmed

until experiments showed that Aβ-depleted brain extracts were not able to self-propagate the Aβ misfolded conformation in AD transgenic mice (Duran-Aniotz et al., 2014; Meyer-Luehmann et al., 2006). These results were well complemented with experiments that revealed that intracerebral injections of purified, brain-derived, Aβ aggregates and synthetic aggregates accelerated AD pathology in transgenic mice (Stöhr et al., 2012). All mice-related experiments previously mentioned were performed in animals that normally develops AD-like neuropathology as a result of overexpression of mutated human APP. Therefore, these experiments demonstrated an acceleration of an already occurring pathology. Importantly, these results were accompanied with experiments that revealed that Aβ propagation could occur *de novo* in transgenic animals that would not normally develop Aβ deposition in their lifespan, further confirming the ability of Aβ aggregates to propagate in a prion-like manner (Morales et al., 2012a; Rosen et al., 2012). Most of these aforementioned experiments entails direct intracerebral injection, however, prion-like propagation of Aβ aggregates were also achieved by intraperitoneal inoculation (Eisele et al., 2010), blood stream inoculation (Burwinkel et al., 2018; Morales et al., 2020) and by exposed surfaces (Eisele et al., 2009), but not by other peripheral routes, further confirming similarities between infectious prions and Aβ.

1. 2. 8. The concept of strains: Aβ strains

Similar to prion diseases, Aβ is not only able to self-propagate but it is also believed to exist as different **strains**. This means that misfolded Aβ aggregates can adopt several structural or conformational variants (Lau et al., 2021). The concept of protein strains was originally acquired from the prion field. Prion protein strains are defined as unique conformational arrangements of PrP protein that are able to cause unique pathological and clinical outcomes in diseased animals. This unique conformation is stable and self-propagate both *in vitro* and *in vivo* (Cali et al., 2006; Ironside and Head, 2004; Noble et al., 2015; Safar et al., 2015; Telling et al., 1996). Several biochemical and biological techniques have strongly suggested that different PrP strains lies in the diverse conformation that the misfolded version of this protein can acquire (**Figure 1.9**). This has been recently confirmed by high-resolution studies that have elucidated the structure of different prion strains (Kraus et al., 2021), **Biochemically**, prion strains are defined by several techniques such as their electrophoretic mobility in western blots after proteinase K (PK) digestion, glycosylation pattern and conformational stability assays. The latter distinguish between prion strains by measuring their susceptibility to degradation or

denaturation after exposure to increasing concentrations of PK or chaotropic agents such as guanidine hydrochloride (GdnHCl) (Lau et al., 2021; Morales, 2017). **Biologically,** the most-used technique to differentiate PrP strains have been the analysis of the clinical signs and incubation periods developed by mice after infection with several PrP strains. Moreover, the patterns and regional specificity of the spongiform degeneration (lesion profile) developed in the brain by these mice is also widely used and might explain the heterogeneity of clinical signs developed by mice challenged with different strains (See **Figure 1.9**) (Bessen and Marsh, 1992; Fraser and Dickinson, 1968).

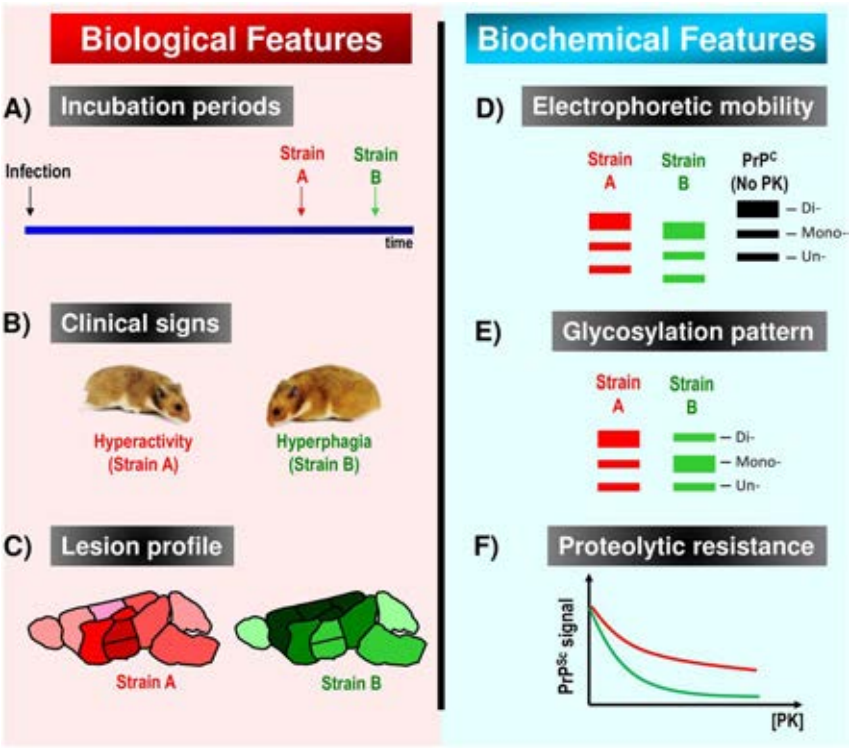

Figure 1.9. Biological and biochemical properties used to define prion strains. A) The main biological feature used to distinguish two prion strains is the incubation period. This is the time between prion inoculation and development of symptoms. **B)** Mice also display distinctive clinical signs such as hyperactivity or hyperphagia. **C)** Strain-specific brains tropism is also observed with different strains. Biochemically, distinct PrP strains show unique electrophoretic mobilities after proteolytic degradation **(D)**, different glycosylation patterns **(E)** and distinct resistance to proteolytic degradation with the exposure to increasing concentrations to proteases or chaotropic agents. Figure adapted from Morales R. (2017).

In the case of **Aβ aggregates**, it has been proven that they exhibit two key properties that define strains: unique conformational arrangements and ability to self-propagate these unique structures both *in vivo* and *in vitro*. However, the ability of these conformational variants or morphotypes to cause distinct disease phenotypes, both pathologically and clinically, still needs further research (Heilbronner et al., 2013; Petkova et al., 2005). Clinical heterogeneity and neuropathological heterogeneity are observed in AD patients, however the link between each conformational variant of Aβ and its biological significance has not been elucidated.

By conformational stability assay, a technique similar to the one explained above for prions, the more stable the strains the higher concentrations of denaturant that it requires to be fully solubilized (Lau et al., 2018). In this sense, it has been demonstrated that samples from patients displayed differential susceptibility to increasing concentrations of GdnHCl (**Figure 1.10A**) confirming conformationally-distinct strains between FAD patients harboring the Swedish mutation and patients with the Arctic mutation (Watts et al., 2014). Moreover, PK digestion or fractionation by particle size has also been proven to be useful to distinguish Aβ strains (Cohen et al., 2015; Di Fede et al., 2018). Chemical probes, such as Thioflavin T (ThT), Congo Red and their derivatives, are amyloid-binding dyes that recognize β-sheet-rich structures within amyloid protein aggregates. These amyloid-binding dyes have been proven useful in deciphering the structure of Aβ aggregates (**Figure 1.10B**) (Condello et al., 2018; Reinke and Gestwicki, 2011).

Specifically, the affinity of these dyes for a given Aβ aggregate can inform on conformation and distinguish Aβ strains (Cloe et al., 2011). A new class of amyloid-binding dyes to distinguish conformational variants of Aβ have been developed by the research group of Dr. Peter R. Nilsson. These dyes are luminescent conjugated oligothiophenes (LCOs) that, due to their flexible backbones, are able to display conformation-dependent emission spectrum and thus distinguish between distinct Aβ strains. This new generation of dyes have been proven useful on distinguishing Aβ conformational variants *in vitro* as well as *in vivo*, in both AD patients and AD transgenic mice (Åslund et al., 2009; Heilbronner et al., 2013; Nilsson et al., 2007; Rasmussen et al., 2017). Other amyloid-binding dye, such as the Congo red derivative FSB, BF-188 and curcumin, have successfully distinguish specific conformations of Aβ in the brain of patients suffering from different AD subtypes (Condello et al., 2018). Moreover, electron microscopy (EM) has been also useful on distinguishing Aβ strains. By using this

technique, it has been found that Aβ conformational variants display differential ultrastructural properties and exhibit variable morphologies (Kodali et al., 2010; Meinhardt et al., 2009; Petkova et al., 2005; Tycko, 2014, 2015). Interestingly, conformation-specific antibodies have been also developed to detect Aβ strains in the AD brain (Cohen et al., 2015; Hatami et al., 2014). Recently, techniques with higher resolution, such as solid-state Nuclear Magnetic Resonance (ssNMR) spectroscopy and cryo-EM have definitively elucidated structural variations in Aβ fibrils (Bertini et al., 2011; Cendrowska et al., 2020; Colvin et al., 2016; Gremer et al., 2017; Lührs et al., 2005; Makowski, 2020; Paravastu et al., 2008; Petkova et al., 2006; Qiang et al., 2013; Sachse et al., 2008; Schmidt et al., 2009, 2015; Wälti et al., 2016; Xiao et al., 2015; Zhang et al., 2009).

In addition, the existence of distinct Aβ strains have also been proven by *in vivo* seeding studies (Stöhr et al., 2012, 2014; Watts et al., 2014). As mentioned before, one of the key features to define an Aβ strain is the ability of these structures to self-propagate their unique conformational arrangements by templating monomeric Aβ with their unique conformation. To fulfill the criteria of self-propagating strains, these conformations should not only spread from one region of the brain to another but also should demonstrate distinct disease phenotype, such brain region-specific tropism of the aggregates, distinctive seeding activities, different types of aggregates (Vascular vs parenchymal) or morphological (dense-core vs diffuse plaques) differences between the Aβ aggregates induced by *in vivo* seeding (**Figure 1.10C**). Aβ strains have been observed to maintain some of their biochemical, structural, and pathological features after *in vivo* seeding, via intracerebral inoculation, in AD transgenic animals (Stöhr et al., 2012, 2014; Watts et al., 2014). Specifically, this phenomenon has been observed by using inocula derived from both synthetic Aβ strains and brain extracts from the different subtypes of AD patients (Stöhr et al., 2014; Watts et al., 2014). Indeed, different plaque morphologies, region-specific tropism and seeding efficiency have been observed in transgenic mice when seeded with brain homogenates from patients that displayed distinctive pathological features (Duran-Aniotz et al., 2021; Di Fede et al., 2018).

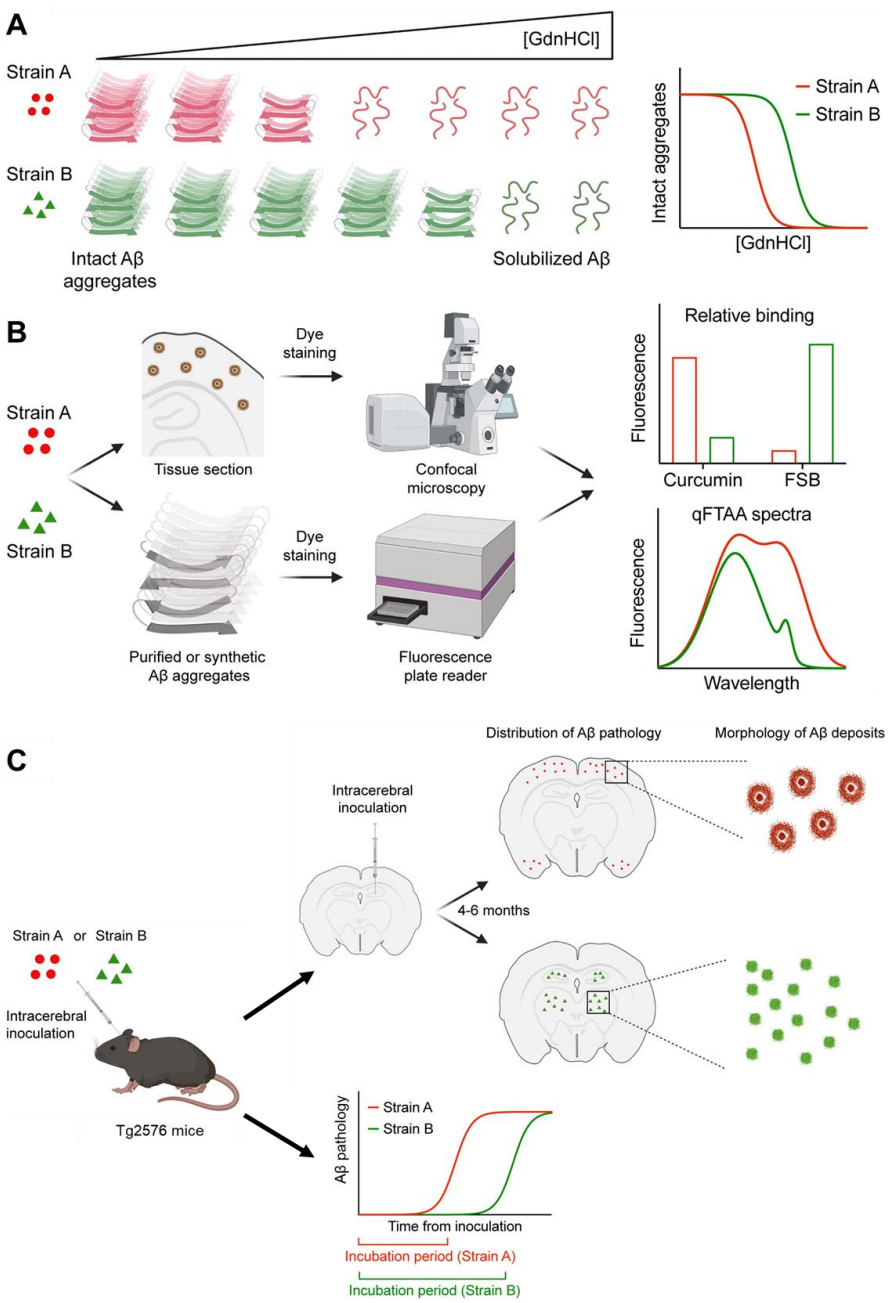

Figure 1.10. Biochemical and biological techniques used to define Aβ strains. A) Conformational stability assays using chaotropic agents or proteinase K are used to differentiate Aβ strains. Aggregates are exposed to increased concentrations of these agents and its resistance determine the stability of the different strains. **B)** Staining of Aβ, either in brain or *in vitro*, with conformation-specific dyes can discriminate between several Aβ strains. Differences on binding affinity and unique emission spectra are the result of distinct Aβ strains. **C)** *In vivo* seeding experiments can result in distinct pathological phenotypes, indicative of different Aβ strains in the inocula. Distinct Aβ strains can induce differential brain tropism of the aggregates and specific type of plaques (**C**, Top). Also, Aβ strains can result in longer vs shorter incubation periods (**C**, bottom). Figure modified and adapted from Lau *et al.* (2021).

1. 2. 8. 1. Synthetic Aβ40 strains used in this study: 2F vs 3F fibrils

As reported above, there is increasing evidence of the existence of Aβ strains in Aβ fibrils made from either synthetic Aβ or brain extracts from AD patients. Perhaps, one of the most extensively characterized synthetic Aβ40 fibrils are the two morphologically distinct fibrils generated *in vitro* in the lab of Professor Robert Tycko (Petkova et al., 2005). This lab extensively characterized the structure of these two strains by transmission electron microscopy (TEM) and solid-state NMR (ssNMR). Specifically, these two Aβ40 synthetic strains were produced by either incubating monomeric Aβ40 under **agitating** (shaking) or **quiescence** (non-shaking) conditions. By TEM, these two distinct fibrils demonstrated different morphological features with fibrils prepared under agitation not showing a clear twist and smaller width, and fibrils prepared un quiescent conditions exhibiting a pronounced twist and larger width (**Figure 1.11A**). As expected, both strains displayed a structure in parallel β sheets, however when analyzed by scanning TEM, histograms of fibril mass-per-length (MPL) for **agitated fibrils** showed mode values of 21.4 kDa/nm, while **quiescent fibrils** had mode values of 30.3 kDa/nm (**Figure 1.11B**). Given that in an ideal cross β structure the space between peptides should be 0.48 nm, one layer (1 nm) of Aβ40 (4.3 kDa) would have a MPL of 9.1 kDa/nm. Therefore, these data suggested that protofilaments from the agitated fibrils contain two molecular layers and quiescent fibrils three molecular layers, indicating that these structures have approximate 2-fold and 3-fold rotational symmetry about the fibril growth axis (**Figure 1.11C**). Thus, these fibrils were named **2F** and **3F** respectively. 2F fibrils are also known as "striated ribbon" fibrils and 3F fibrils are also known as "slowly twisting" fibrils (Tycko, 2014, 2015).

Interestingly, both Aβ40 strains also display different mechanical properties. In fact, 2F fibrils were shown to be more susceptible to fragmentation than 3F fibrils when solutions containing these fibrils were stirred (Qiang et al., 2013). Moreover, morphological features, such as twist period and width, of these fibrils and the molecular structure of their protofilaments are self-propagating (**Figure 1.11A**). This means that 2F and 3F fibrils transmitted their distinctive structural properties into naïve monomeric Aβ40 by seeding. Finally, these 2F and 3F fibrils also displayed distinct toxicity in primary rat hippocampal neurons culture. Both fibrils were toxic, however 3F fibrils were significantly more toxic than 2F fibrils (**Figure 1.11D**) (Petkova et al., 2005).

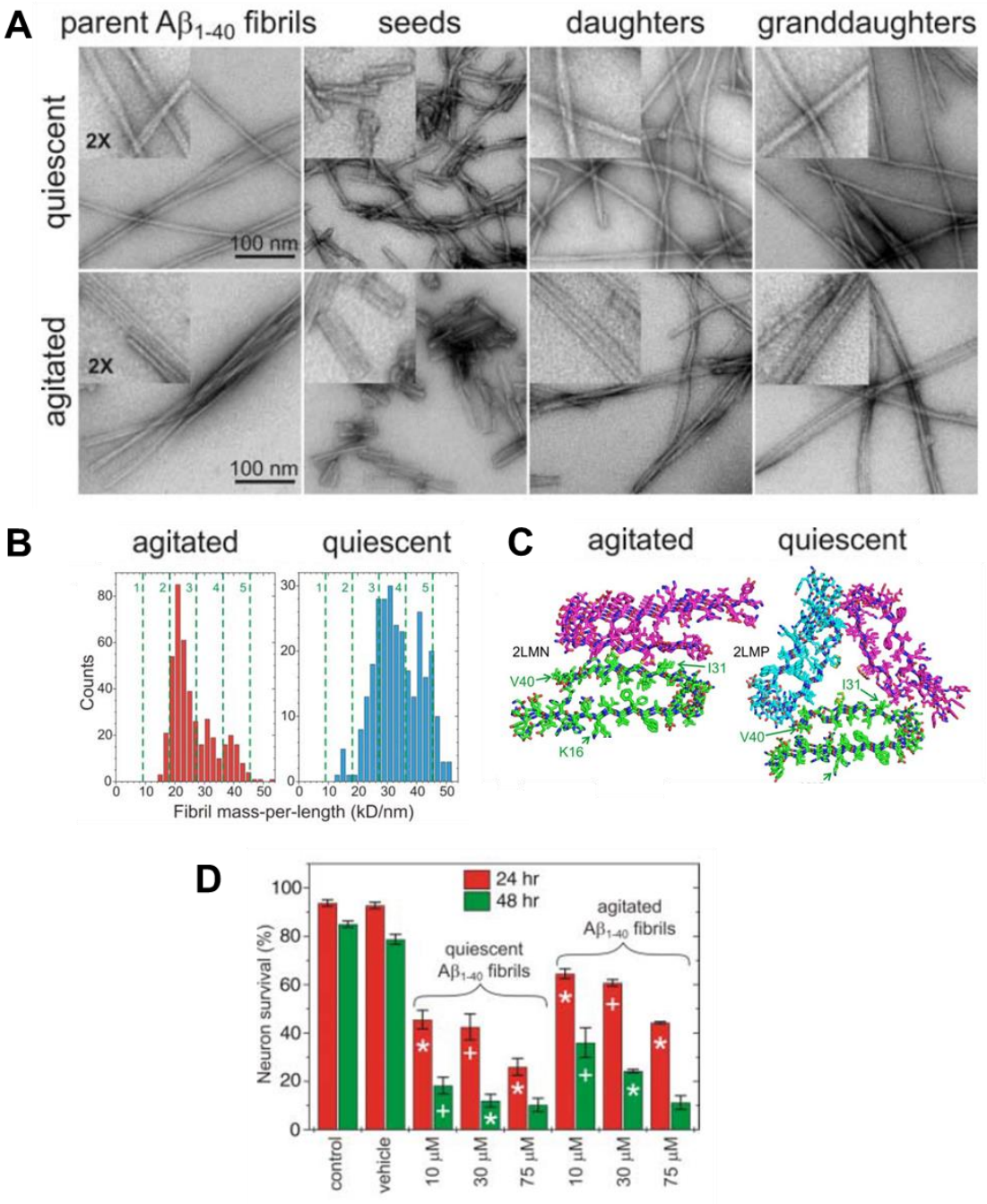

Figure 1.11. Unique structural and morphological properties of 2F and 3F fibrils. A) 2F (agitated) and 3F (quiescent) fibrils display different morphological features. 2F fibrils do not show a clear twist and smaller width while 3F fibrils exhibit a pronounced twist and larger width. These morphological features are transmitted to daughter and granddaughter fibrils. **B)** Histograms of fibril mass-per-length (MPL). 2F fibrils showed mode values of 21.4 kDa/nm and 3F fibrils mode values of 30.3 kDa/nm. **C)** Structural models for $A\beta_{40}$ fibrils based on data from ssNMR and TEM. Agitated fibrils display a model with 2-fold symmetry (2F), while quiescent fibrils show approximate a 3-fold symmetry (3F). **D)** Toxicity of $A\beta_{40}$ strains fibrils in cultures of primary rat hippocampal neurons after 24- and 48-hours of exposure. Clearly, 3F fibrils show significantly higher toxicity. Figure modified and adapted from Petkova *et al*. (2005) and Tycko R. (2014).

1. 2. 8. 2. *In vivo* Aβ strains using ssNMR

Several studies have highlighted the presence of distinct Aβ conformational strains in AD patients, which might occur in a brain region-dependent manner and could explain the heterogeneity seen across these patients (Cohen et al., 2016, 2015; Condello and Stöehr, 2018; Condello et al., 2018; Lau et al., 2021; Liu et al., 2021; Watts et al., 2014). However, the analysis of structure of these Aβ conformational strains were performed with low-resolution techniques such as conformation-dependent immunoassay (CDI) and exposure to conformation-specific amyloid binding dyes. In an attempt to study the heterogeneity of the aggregates in AD patients with **high resolution**, the laboratory of professor Robert Tycko at NIH seeded the growth synthetic Aβ fibrils with brain extracts from the cortex of AD patients, templating the formation of disease-specific Aβ structures and then measuring these fibrils by ssNMR (Qiang et al., 2017). This study revealed that AD-seeded fibrils are distinct from those obtained by spontaneous polymerization of synthetic Aβ and demonstrated that patients with the rapidly-progressive form of AD (r-AD) display an Aβ fibril structure with greater structural variability and completely different that those found in patients with either typical prolonged-duration form of AD (t-AD) or posterior cortical atrophy variant of AD (PCA-AD). Therefore, for the first time with **high-resolution**, this study revealed conformational heterogeneity between brains of AD patients with different clinical subtypes, further supporting the existence of Aβ strains (Qiang et al., 2017). Recently, the structure of Aβ fibrils purified from meningeal AD brain tissue (CAA) has also been determined using cryo-EM (Kollmer et al., 2019). Both of these results highlight the **importance of using high-resolution** techniques when interrogating the presence of Aβ strains in the brain of AD patients and also demonstrate that the Aβ fibrils strains derived from brain tissue, either from human patients or mice after *in vivo* seeding, will be more informative in deciphering the biological significance of the Aβ strains than using pure synthetic *in vitro* strains.

1. 2. 9. Cross-seeding: a common mechanism between amyloid proteins

Amyloid proteins found in neurodegenerative diseases such as AD and PD are not only able to self-propagate the morphology and the molecular structure of their fibrils in a prion-like manner but also share an interesting common mechanism known as **cross-seeding**. This mechanism, also known as heterologous seeding, occurs when oligomers or fibrils of one misfolded protein promote the polymerization of a different amyloid protein (Morales et al., 2013). The cross-seeding mechanism also follows a seeding-

nucleation polymerization model; however, the addition of heterologous seeds (cross-seeding) seems to result in a lower seeding efficiency and longer lag phase, hence resulting in slower aggregation than the addition of homologous seeds (**Figure 1.12A**). As a result of the cross-seeding mechanism, amyloid fibrils formed by the two heterologous seed might form giving rise to fibrils that simultaneously contain two or more different misfolded proteins (**Figure 1.12B**). This mechanism might explain why in some proteinopathies there is presence of more than one misfolded protein and might be reason why some proteinopathies are risk factors and exacerbates the clinical futures of other proteionopathies (Morales et al., 2013). Interestingly, many proteins acquire an amyloid structure as part of their normal function (functional amyloids) and thus cross-seeding might play a key role in either exacerbating some pathologies or affecting the normal function of these functional amyloids (Soto, 2012).

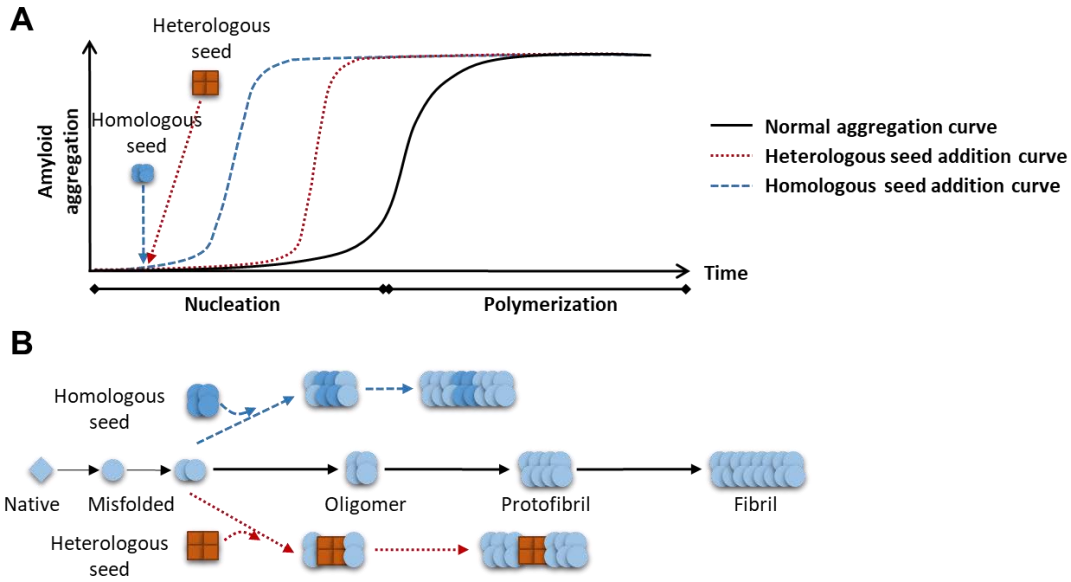

Figure 1.12. Seeding nucleation model of the cross-seeding mechanism. A) Amyloid fibrils are formed by a seeding-nucleation polymerization model with 2 clear phases: nucleation or lag phase, in which there is not aggregate formation, and an elongation or polymerization phase, in which there is in an exponential growth of amyloid fibrils. This process can be accelerated by the addition of preformed fibrils (seeds) from homologous or heterologous amyloid proteins (dashed lines). **B)** Fibrils that result from this seeding mechanism can result in the formation of homologous fibrils (blue fibrils) or heterologous/cross-seeded fibrils (orange and blue fibrils). Figure modified and adapted from Morales *et al*. (2013).

The cross-seeding mechanism have been reported for several amyloidogenic proteins both *in vitro* and *in vivo* (Clinton et al., 2010; Daskalov et al., 2020; Guo et al., 2006; Ivanova et al., 2021; Krebs et al., 2004; Mandal et al., 2006; Montalbano et al., 2020; Morales et al., 2010; Moreno-Gonzalez et al., 2017; Mukherjee et al., 2017; O'Nuallain et al., 2004; Tsigelny et al., 2008; Vaneyck et al., 2021; Yan et al., 2007). Interestingly, one of the most studied cross-seeding mechanisms have been the ones involving Aβ due to its importance in AD pathogenesis. This peptide has been found to interact with many other neurodegeneration-associated misfolded proteins such as tau, α-synuclein and PrP (Clinton et al., 2010; Guo et al., 2006; Morales et al., 2010) further supporting the idea of molecular and pathological crosstalk between different neurodegenerative diseases at the protein misfolding level. Most of the cross-seeding mechanisms seem to be bidirectional, however in some cases such as Aβ with IAPP *in vitro* and Aβ with tau *in vivo* seem to be unidirectional cross-seeding mechanism in which Aβ induced the aggregation of IAPP or tau but these proteins do not induce the aggregation of Aβ *in vitro* and *in vivo*, respectively (Gotz et al., 2001; Lewis et al., 2001; O'Nuallain et al., 2004).

Differences found between cross-seeding mechanism *in vitro* and *in vivo* raise the *in vitro* findings may not be directly extrapolated to *in vivo* settings. For this reason, *in vivo* seeding studies using various transgenic mice are critical to decipher the cross-seeding mechanisms between amyloidogenic proteins. The best examples of *in vivo* cross-seeding of Aβ are the cross-talk at the molecular level of prion and AD pathologies (Morales et al., 2010), the potentiation of AD pathology by aggregates of IAPP (an amyloid protein that accumulate in pancreatic islets in type-2 diabetes (Moreno-Gonzalez et al., 2017)) and the interaction between Aβ and tau and α-synuclein (Clinton et al., 2010; Masliah et al., 2001). Cross-talk between different proteinopathies have also been found in human studies. Specifically, there is increasing evidence of interactions between type 2 diabetes and AD (Biessels and Kappelle, 2005; Sims-Robinson et al., 2010), prion diseases and AD (Debatin et al., 2008; Ferrer et al., 2001; Miyazono et al., 1992; Tsuchiya et al., 2004), dementia with Lewy-bodies and AD (Hamilton, 2000; Mandal et al., 2006), PD and AD (Twohig and Nielsen, 2019) and AD and TDP-43 pathology (Nelson et al., 2019).

All these experimental evidence for cross-seeding, together with the prion-like mechanism of Aβ and the existence of strains (See **1.2.7** and **1.2.8**), demonstrates a clear cross-talk between prion protein and Aβ in regard to their mechanisms of propagation.

1.3. FUNCTIONAL AMYLOIDS

Similar to amyloid-β, there are several proteins that can acquire an amyloid structure. An amyloid structure is a distinct β-sheet-rich fibrillary structure. Specifically, this structure consists in β-sheets that are aligned in parallel to each other and in perpendicular position respect to the fibril axis. All amyloids share distinguishing biophysical and structural properties, which have been defined by high resolution techniques such as X-ray fiber diffraction CD spectroscopy, FTIR and solid-state nuclear magnetic resonance spectroscopy (ssNMR). These structures also display birefringence to polarized light, their resistance to protease digestion, binding to amyloid-specific dyes such as Congo red and Thioflavin T and binding to conformation specific antibodies (Knowles et al., 2014).

1. 3. 1. Functional amyloids in mammals

Historically, the amyloid structure of proteins has been associated with debilitating and chronic human diseases, known as proteinopathies or protein misfolding disorders (PMD). Traditional examples of such diseases are AD (Aβ and tau), PD/Lewy Body dementia (α-synuclein), bovine spongiform encephalopathy (prion protein) and Huntington's disease (Huntingtin). PMDs are not only associated to neurodegenerative diseases, systemic amyloidoses such as Amyloid A amyloidosis (serum amyloid A) and senile systemic amyloidosis (transthyretin), and also localized amyloidosis such as type 2 diabetes (IAPP) and injection-localized amyloidosis (insulin) are also examples of diseases associated to amyloid proteins. However, the concept of amyloid structure has evolved and nowadays is widely accepted that these structural arrangements can fulfill important physiological functions, rising the term of **functional amyloids** (Loquet et al., 2018; Otzen and Riek, 2019).

Functional amyloids have been described in both eukaryotes and prokaryotes organisms (Kosolapova et al., 2020; Sergeeva and Galkin, 2020). Some of the functions that these amyloids serve are signaling, structure formation, storage, and protein function regulation (Brown and Török, 2021). The best examples of functional amyloids found in mammals are **Pmel17**, which template the synthesis of melanin and thus is involved in skin pigmentation (Fowler et al., 2006; Watt et al., 2013), **RIP1/RIP3**, which are kinases that forms a signaling complex with an amyloid structure that play a central role in programmed necrosis (Li et al., 2012), and certain **hormones**, such as oxytocin,

vasopressin β-endorphin, ACTH, prolactin, and growth hormone, are sorted and stored in an amyloid structure in secretory granules and this amyloid state actually control their release from these granules (Maji et al., 2009).

1. 3. 2. Functional amyloids in bacteria

In the case of Bacteria, functional amyloids were described two decades ago (Chapman et al., 2002). In these organisms, proteins with these conformational arrangements are really well understood and found in abundance. Specifically, functional amyloids in bacteria have been shown to be involved in the formation and stabilization of biofilms, adhesion to surfaces, cell-to cell adhesion, epigenetic control, antimicrobial activity and cytotoxicity (Levkovich et al., 2021). The best studied bacterial amyloid protein, made by *Escherichia coli* and *Salmonella spp*, is **curli** (Barnhart and Chapman, 2006; Chapman et al., 2002). Other example of an amyloidogenic protein found in bacteria is the bacteriocin **microcin E492**, produced by *Klebsiella pneumoniae*. Besides these amyloids produced by Gram-negative bacteria, Gram-positive bacteria, such as *Bacillus subtilis* and *Bacillus cereus*, also form amyloid proteins (**TasA** and CalY) that are critical for biofilms formation (Branda et al., 2006; Caro-Astorga et al., 2015; Romero et al., 2010). These are only three examples of the more than 30 functional amyloids that have been found in microorganisms. Since these three functional amyloids were used in this thesis, further information about them is provided below:

- Curli: This protein constitute one of the major component of the biofilms made by enterobacteria (*Escherichia coli* and *Salmonella* spp.) and was discovered to have amyloidogenic, structural and biophysical properties (Chapman et al., 2002). Biofilms are communities of bacteria that adhere to each other and to surfaces in order to increase their adaptation to the environment by providing higher resistance to nutritional, physical, and chemical stresses. The formation of biofilms also increases their competitive fitness and aid these bacterial communities with colonization and host invasion (Levkovich et al., 2021). Biofilms are mostly composed of proteins and polysaccharides, being curli the major proteinaceous component of the biofilms formed by enterobacteria such as *Escherichia coli* and *Salmonella enterica* (Barnhart and Chapman, 2006). Curli fibers (See **Figure 1.13**) are produced by a complex machinery that follows a nucleation-precipitation coordinated mechanism. This machinery is encoded by the operons csgBAC and csgDEFG, which are responsible

of generating the structural and assembly components respectively. The main subunits that form the curli fibrils are the CsgA and CsgB subunits, being CsgB a nucleator protein that induce the polymerization of CsgA intro fibrils (Hammer et al., 2007). Specifically, **CsgA** is the **major structural subunit** of the curli fiber. Intriguingly, purified CsgA is able to assemble into curli-like fibers upon pure incubation *in vitro* (Barnhart and Chapman, 2006; Dueholm et al., 2011; Van Gerven et al., 2015; Jain and Chapman, 2019; Wang et al., 2006). Since CsgA is able to self-polymerize *in vitro* into amyloid fibrils similar to the ones produced *in vivo* (Sleutel et al., 2017), we decided to work with pure amyloid fibrils from CsgA, a 17.5 kDa protein, in this thesis. It is worth mentioning that these fibrils were provided by the lab of Professor Mathew Chapman, one of the top experts in the biology of curli fibrils.

- Microcin E492 (Mcc): This protein is produced by the gram-negative bacteria *Klebsiella pneumoniae*. Microcin E492 is a known bacteriocin that kills other competing bacteria through the formation of pores in their cytoplasmic membranes, thus serving as an amyloid with cytotoxic properties that increase the competitive fitness of the bacteria that produce it providing an adaptive self-benefit (Destoumieux-Garzón et al., 2003; Levkovich et al., 2021). Interestingly, it has been shown that this protein is active in its soluble oligomeric state and upon formation of amyloid fibrils it loses its function. Therefore, in the case of microcin E492, the amyloid arrangement serves a loss-of-function mechanism (Arranz et al., 2012; Bieler et al., 2005; Shahnawaz and Soto, 2012). As in the case of the CsgA subunit of curli, purified microcin E492 is also capable of forming amyloid fibrils *in vitro* with prion-like activity (See **Figure 1.13**). Specifically, these Mcc fibrils showed to be resistant to proteinase K digestion and displayed specific binding to amyloid-specific dyes such as Thioflavin T and Congo red (Shahnawaz et al., 2017a). Thus, we also decided to work with pure Mcc fibrils in this thesis.
- TasA: Similar to curli fibrils in *Escherichia coli*, the major proteinaceous component in biofilms formed by the gram-positive bacteria *Bacillus subtilis* and *Bacillus cereus* is the protein TasA (Branda et al., 2006). The production of this protein is encoded by the *tapA-sipW-tasA* operon and similar to curli, TasA was found to form amyloid fibrils (See **Figure 1.13**) that serve as structural scaffold for the biofilm matrix of *Bacillus subtilis* and *Bacillus cereus* biofilms (Álvarez-Mena et al., 2020; Romero et al., 2010). TasA amyloid fibrils are also composed of accessory proteins, which enhance the assembly and polymerization of these fibrils, such as TapA, in *Bacillus*

subtilis and CalY in *Bacillus cereus* (Caro-Astorga et al., 2015; Romero et al., 2011). Interestingly, purified TasA is able to form amyloid fibrils *in vitro* and maintain its biological activity, as shown in rescue experiments with *tasA* mutants (Romero et al., 2010). Recently, biophysical and structural studies, such as ssNMR, TEM, X-ray diffraction, Fourier transform infrared (FTIR) and dynamic light scattering, have confirmed the amyloid arrangement acquired by TasA and also pointed to the lack of C-terminal end in TasA from *Bacillus cereus*, which did not affect the ability of the protein to form amyloid fibrils (Diehl et al., 2018; Mammeri et al., 2019). Importantly, it has been shown that besides its role in biofilm formation, TasA also plays a key role in maintaining cell membrane stability to prevent cell death upon bacterial growth, and as a signal for promoting motility (Cámara-Almirón et al., 2020; Steinberg et al., 2020). Since TasA forms amyloid fibrils *in vitro*, we decided to work with amyloid fibrils from purified TasA. Indeed, these fibrils were provided by the lab of Professor Diego Romero, one of the top experts in the biology of TasA.

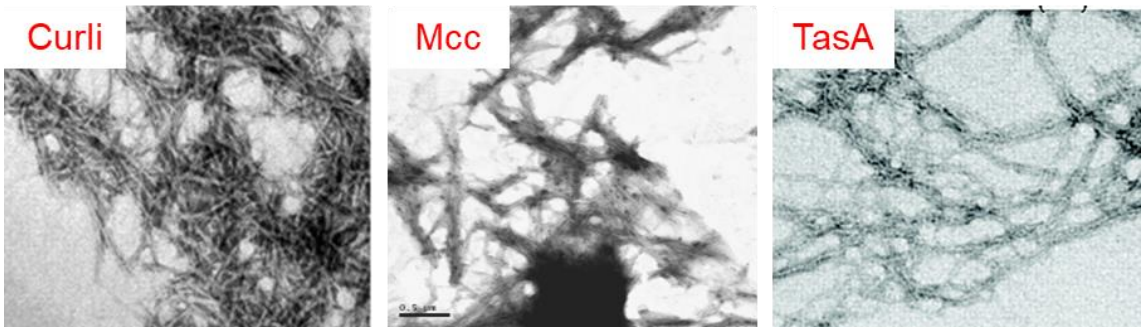

Figure 1.13. Transmission Electron Microscope micrographs of curli, microcin E492 and TasA. Negative staining electron micrographs from *in vitro* prepared curli (Left), microcin E492 (Middle) and TasA (Right) fibrils are shown. These micrographs clearly show the amyloid fibrils generated by these bacterial functional amyloids. Figures adapted from Chapman *et al.* (2002), Shahnawaz *et al.* (2017a) and Romero *et al.* (2010).

1. 3. 3. The role of microbes in neurodegeneration

For the last decade, several studies have demonstrated a link between brain function and our microbiota (Friedland and Chapman, 2017; Sharon et al., 2016). There are trillions of microbes such as bacteria, viruses, fungi, and parasites that resides inside and on the surface of the human body, which are together known as the microbiome

(Turnbaugh et al., 2007). The microbiome is known to influence physiological functions of the human body such as digestion, immunity, protection to pathogens and even our metabolism (Ubeda et al., 2017; Zeng et al., 2016). There is growing evidence on the involvement of the microbiome on brain function, with high amount of research focusing on the new concept of gut-brain axis, which is a bidirectional communication between gut microbes and the brain serving as a communication link between the central nervous system and the enteric nervous system in humans (Rutsch et al., 2020; Vuong et al., 2017). Specifically, the microbiome plays a fundamental role in modulating key functions in the brain such as **neuronal communication**, by releasing neuroactive metabolites such as short-chain fatty acids (SCFAs) (Cryan and Dinan, 2012), **inflammation**, by modulation microglial cells activation (Erny et al., 2015), **myelination** (Boukhvalova et al., 2019; Hoban et al., 2016) and **neurogenesis** (Ogbonnaya et al., 2015). Since they play an essential role in these important brain homeostatic functions, alterations on the normal gut microbiome, or dysbiosis, and defective gut-brain communication, have been associated to several pathological brain conditions such as anxiety, stress, sickness behavior, memory impairment, depression, and Parkinson's disease (Hasan Mohajeri et al., 2018). Several mechanisms that are influenced by gut bacteria could be at the center of the role of microbes in neurodegeneration. Mechanisms such as modulation of immunological response in the central nervous system, oxidative stress, metabolites production and balance microbial populations in the gut, are known to be critical for homeostatic brain function in humans. Since our microbiome is able to modulate all these mechanisms, their involvement in human brain pathology is of great interest for the scientific community (reviewed in Friedland and Chapman, 2017). Alternative mechanisms, such as cross-seeding between bacterial amyloids and human pathogenic amyloids, should be explored as well.

1. 3. 4. The role of microbes in Alzheimer's disease pathology

There is increasing evidence of microbe's involvement in neurodegenerative diseases and specifically, in the case of Alzheimer's disease, an **infection hypothesis** has been proposed. This hypothesis posits that a pathogen, such as a bacterium, virus, prion, etc. is the main causative agent of AD (Seaks and Wilcock, 2020). This hypothesis has been supported by scientific research that found microbes such as viruses, bacteria, and fungi in AD patients. However, the specific mechanisms by which these pathogens induce the pathological hallmarks of AD have not been elucidated yet (Bulgart et al., 2020).

Plausible mechanisms are the direct toxicity to neuronal cells, the induction of an inflammatory environment that could lead to the aggregation of amyloid proteins and tissue damage, oxidative stress and even the direct induction of Aβ aggregation, which could be serving as an antimicrobial peptide by sequestering these microbes in the CNS. The latter led to the proposal of the antimicrobial protection hypothesis of AD (Moir et al., 2018).

1. 3. 4. 1. Viruses

This view of an infection hypothesis for AD was first suggested by Alois Alzheimer but was later refused by the field (Fulop et al., 2018). This hypothesis resurged with the findings, by Itzhaki's group, that amyloid plaques from AD patients contains herpes simplex virus 1 (HSV-1) DNA (Itzhaki, 2016; Itzhaki et al., 1997, 2016). HSV-1 is known to be a neurotropic virus that enter in the neural system by inhibiting autophagy. Autophagy is a critical mechanism by which the brain is able to clear cellular debris and protein aggregates, thus the inhibition of this mechanism by HSV-1 of this mechanism might have detrimental consequences in the brain (Orvedahl et al., 2007). Further research in mice have shown that HSV-1 infection induces AD neuropathological hallmarks such as Aβ deposition and cognitive deficits (De Chiara et al., 2019). Another virus from the Herpesviridae family, cytomegalovirus or CMV, was also found to be involved in AD pathogenesis (Lövheim et al., 2018). This same group suggested that the more microbes found in the periphery, the more probability to develop AD, suggesting that it might not be a single microbe but a community of them being the plausible trigger for AD (Carter, 2017; Lövheim et al., 2018). Interestingly, the current coronavirus disease 2019 (COVID-19) pandemic has brought into play, once again, the potential implication of viruses in cognition. It has been observed that COVID-19 patients develop neurological manifestations such as consciousness impairment, stroke and PNS diseases (Pezzini and Padovani, 2020). This, together with evidence of this virus being found in neurons of COVID-19 patients and the higher likelihood of severe outcomes of COVID-19 in patients with dementia (Atkins et al., 2020; Paniz-Mondolfi et al., 2020), have resulted in speculation that the SARS-CoV-2 (COVID-19) virus might increase the risk to develop AD (Miners et al., 2020). Therefore, viruses seem to play an important role in AD pathogenesis (Sait et al., 2021).

1. 3. 4. 2. Bacteria

More than a decade ago, two different groups observed that bacteria have a role in AD. Balin *et al*. demonstrated that a Gram-negative bacterium, *Chlamydophila pneumonia*, was somehow related to AD. This group made 3 main observations: presence of *C. pneumonia* in *post-mortem* AD brains (90% of people with LOAD had this infection compared to 5% in healthy people), AD occurrence is positively correlated with systemic infection by this bacterium and increased anti-*C. pneumonia* antibody in blood of AD patients (Balin et al., 1998, 2008; Hammond et al., 2010). These findings were later corroborated by another group (Gérard et al., 2006). On the other hand, Miklossy *et al.*, discovered that the spirochete *Borrelia burgdorferi*, the causative agent of Lyme disease, was present in brains of AD patients. Interestingly, this group demonstrated that amyloid plaques in AD patients were built by biofilms from these organisms (Miklossy, 2011). The possible biological explanation for these biofilms formation by *B. burgdorferi*, is the protection of these organisms against host defense in order to survive within human brains (Miklossy, 2016). Recently, periodontal microbes such as *Porphyromonas gingivalis* have been associated with AD neuropathology. Periodontal diseases have been linked to increased amyloid deposition in healthy elderly patients and with increased risk to develop AD pathology (Kamer et al., 2015; Sparks Stein et al., 2012). Specifically, in the case of *Porphyromonas gingivalis,* it was recently demonstrated that infecting mouse with this pathogen leads to brain colonization, increased formation of amyloid plaques and increased inflammation, and exacerbated neurotoxicity. This was found to be mediated by gingipain production from this bacterium. Gingipains are toxic proteases that in this study were also found in the brain of AD patients and whose inhibition was able to rescue Aβ pathology, neuroinflammation and neuronal toxicity (Dominy et al., 2019). Bacterial infections have become such a hot topic that gingipain inhibitors (small molecules) are now in clinical trials by the company Cortexyme. Other bacteria, such as *Escherichia coli*, *Shigella*, *Eubacterium rectale*, *Eubacterium nodatum*, *Treponema* species, etc., have also been associated to AD pathology (Bulgart et al., 2020). Since many bacteria present in the human microbiome, such as members from the *Streptococcus*, *Klebsiella*, *Bacillus*, *Staphylococcus*, *Salmonella* and *Citrobacter* genus, are able to produce bacterial functional amyloids, alternative mechanisms such as cross-seeding should be explored as this could be at the center of all the links found between bacteria and AD.

1. 3. 4. 3. Others

Other organisms, such as protozoa and fungi might be linked to AD. For example, *Toxoplasma gondii*, which is a parasite (protozoa) that is common in humans, have been associated to neurodegeneration and AD-like pathology in both humans and mouse models (Nayeri Chegeni et al., 2019; Torres et al., 2018). In regards to fungi, *Candida glabrata* infection was observed in human AD brains (Pisa et al., 2015b, 2015a). Further studies found that the fungal proteins, enolase and β-Tubulin, and the polysaccharide chitin were the specific fungal structures found in the brains of AD patients and these were mostly localized inside neuronal cells and in corpora amylacea (Pisa et al., 2016b, 2016a). Proteomic analysis confirmed these findings and the presence of bacterial polypeptides in corpora amylacea of AD patients (Pisa et al., 2018). Studies using human cerebrospinal fluid from AD patients also confirmed the presence of fungal proteins and DNA from species such as *Cryptococcus*, *Candida albicans* and *Sacharomyces cerevisae* (Alonso et al., 2015). Interestingly, intravenous injection of *Candida albicans* cells (Candidemia) induced a localized cerebritis with Aβ pathology in wild-type mice, increased pro-inflammatory cytokines such as IL-1β, IL-6 and TNF-α and resulted in recruitment of activated microglial and astroglial cells around the fungi aggregates. This study also showed memory impairment in mice with candidemia, further supporting the role of fungi infections in cognitive impairment (Wu et al., 2019).

1. 3. 5. The antimicrobial protection hypothesis of Alzheimer's disease

Historically, Aβ pathology has been seen as a trigger for NFT formation, and inducer of inflammatory and cytotoxic mechanisms in AD. However, increased amount of research about microbes influence in AD and Aβ deposition have found that Aβ might play a beneficial role and serve as antimicrobial peptide (AMP) that protects the brain from microbial infection. These findings gave rise to what is currently known as Antimicrobial Protection Hypothesis of Alzheimer's Disease (Moir et al., 2018).

Initially, Tanzi and Moir groups demonstrated Aβ activity as AMP by *in vitro* experiments with pure Aβ and brains from AD patients. These studies showed antimicrobial activities against 8 clinically relevant microbes with the same potency or even greater than a common human AMP, the peptide LL-37 (Soscia et al., 2010). Later studies by this group demonstrated that Aβ also displays AMP activity *in vivo* by using mice infected with fungi and bacteria. Specifically, infection with *Salmonella Typhimurium* resulted in increased Aβ pathology and colocalization of Aβ with these

microbes mediating their agglutination and entrapment (Kumar et al., 2016). This antimicrobial activity was further supported by other groups (Golde, 2016; Spitzer et al., 2016). Other studies have also shown the AMP activity of Aβ against viral infectivity from influenza A virus and HSV-1 virus (Bourgade et al., 2015, 2016; Powell-Doherty et al., 2020; White et al., 2014). Interestingly, it has been shown that Aβ share structural similarities with antimicrobial peptides and some viral fusion domains (Pastore et al., 2020). This supports the idea that Aβ mechanism of action as an AMP might be similar to those of classical AMPs, such as providing microbes agglutination and entrapment (Moir et al., 2018). Others have shown that Aβ oligomers have the ability to form pores in cellular membranes, supporting the idea that Aβ might kill bacteria, viruses, and other organisms by acting as a bacteriocin (Bode et al., 2017). However, recent studies have shown that in fungi Aβ does not have a direct antifungal activity but instead it prime microglial cells to respond to fungal infection with *C. albicans* (Wu et al., 2019). Definitive mechanism for Aβ as an AMP has not been elucidated and mechanisms such as Aβ acting as an anti-prion or by cross-seeding amyloid proteins from bacteria, thus affecting their biofilm formation should be explored.

In summary, the antimicrobial protection hypothesis serves as a link between the amyloid cascade hypothesis and the infection hypothesis, in which an infection by microbes such as bacteria, viruses and fungi would induce Aβ deposition. This deposition of Aβ would act as an innate immune response to protects against microbial infection in the human brain with chronic Aβ deposition and AMP response leading to NFT formation, chronic inflammation, and neuronal loss, thus leading to cognitive deficits in AD patients (Bulgart et al., 2020; Fulop et al., 2018).

1. 4. HYPOTHESIS AND OBJECTIVES

Even though many labs have reported the existence of distinct Aβ strains in both *in vitro* and *in vivo* experiments, the association between the different Aβ morphotypes and differential biological response to these aggregates have not been elucidated. The fact that many clinical subtypes have been described in AD and that different Aβ arrangements have been found in distinct AD subtypes, we can deduce that there is a link between the conformation of Aβ aggregates and the heterogeneity in clinical symptoms. Thus, a definitive association between Aβ strains and biological significance should be explored

and would be critical for the development of better treatments for patients, hence leading to personalized medicine for each of the different subtypes of AD.

On the other hand, bacterial infections have also been associated to AD pathology. As we discussed in this introduction, bacteria are able to produce different functional amyloids. This fact, together with the known ability of amyloid proteins to cross-seed and induce the aggregation of other amyloidogenic proteins, lead us to think that bacterial-induced aggregation of Aβ in AD brains might be caused by a cross-seeding mechanism between bacterial amyloids and Aβ.

In summary, the biological significance of Aβ strains in AD and the involvement and mechanisms of bacterial-induced AD pathology are unexplored. In this sense, we **hypothesize** that different conformers or "strains" of Aβ are responsible for pathological progression including toxicity, tissue and cell tropism, prion-like rate of propagation and neuroinflammation, leading to clinical variants of AD. Moreover, we also **hypothesize** that protein misfolding associated with Alzheimer's disease might be induced by functional bacterial amyloids (e.g., pathogenic to humans or from gut microbiota) through a cross-seeding mechanism. If proven, both of our hypotheses will elucidate new pathological mechanisms associated with many neurodegenerative diseases and thus could be critical for future therapeutic approaches aiming to prevent and treat these devastating illnesses.

The **main aim** of this work is *to associate specific Aβ strains with the induction of different pathological outcomes in susceptible mice exposed to polymorphic Aβ fibrils*. In the same manner, we aim to *demonstrate and characterize, by in vitro and in vivo assays, the interaction between bacterial functional amyloids (BFA) and Aβ.*

The specific aims for this thesis work are the following:

Specific Aim 1. Pathological relevance of Aβ morphotypes in Alzheimer's disease.

SA1.1. Analysis of the *in vitro* interaction between previously characterized *in vitro* Aβ conformers or "strains" and wild type Aβ. By using an *in vitro* aggregation assay we aim to assess the seeding potency of two different Aβ conformers over soluble forms of wild type Aβ. These Aβ conformers will be further characterized by using a set of conformation-specific dyes and PK resistance assays.

SA1.2. Determine *in vivo* seeding of two Aβ conformers in a mouse model of AD. In short, acceleration of AD pathological features (Aβ pathology, microglial and astroglial responses) will be assessed by conventional methods (immunohistochemistry and Luminex Bead-based Multiplex Assays) in brains of AD transgenic mice receiving intra-cerebral injections of two conformationally distinct aggregates, mouse derived Aβ aggregates and monomeric/soluble Aβ. The conformation of the aggregates induced in treated mice will be analyzed by conformation-specific dyes and by solid-state NMR, in collaboration with Dr. Robert Tycko (NIH, USA).

Specific Aim 2. Interaction between mammalian and bacterial amyloidogenic proteins.

SA2.1. Analysis of the *in vitro* interaction between mammalian (Aβ) and bacterial amyloids (CsgA subunit from curli, Tas A and microcin E492). By using an *in vitro* aggregation assays we aim to assess the cross-seeding potential of bacterial amyloids over soluble forms of Aβ. Source of bacterial amyloid seeds include purified proteins

SA2.1. Determine the *in vivo* interaction between bacterial amyloidogenic proteins and mammalian amyloids in mouse models of AD. In this work, the acceleration of Aβ pathology will be assessed by conventional methods (immunohistochemistry and Luminex Bead-based Multiplex Assays) in brains of AD animal models that are intra-cerebrally treated with aggregates made from bacterial amyloids (CsgA, TasA and microcin E492). Markers of inflammation are also assessed on treated animals by Luminex Bead-based Multiplex Assays.

All the experiments have the approval of the corresponding Ethic Committees of Animal Research.

2. Materials and methods

2.1. ANIMALS AND INOCULATION

2.1.1. Transgenic Tg2576 APP (695-S) mice:

The Tg2576 transgenic mouse strain, expressing a familial AD-causing mutation, was used for this work (https://www.alzforum.org/research-models/tg2576). This strain is commercially supplied by *Taconic, Stock #1349*. Specifically, these mice overexpress a mutant isoform (695 aminoacids isoform) of the human APP harboring the Swedish mutation (KM670/671NL, where the Lys-Met at positions 670-671 are replaced by Asn-Leu; see **Figure 2.1**). The expression of this transgene is under the controls of the hamster prion protein promoter and thus enriched towards the CNS. These mice were bred in a B6;SJL genetic background. These mice start developing cerebral Aβ deposits at approximately 8 months of age and show numerous parenchymal Aβ plaques by 15 months (Hsiao et al., 1996; Irizarry et al., 1997).

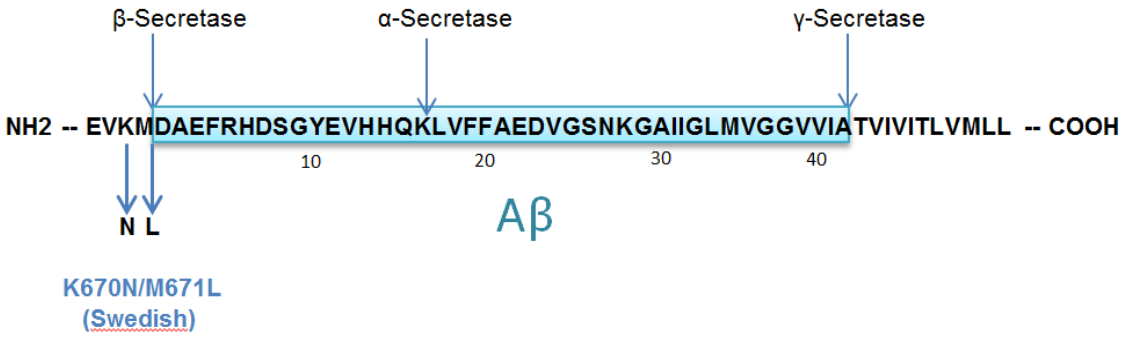

Figure 2.1. Representation of the Swedish mutation location in the human APP transgene. The Swedish mutation is the only one described immediately adjacent to the β-secretase cleavage site in the APP. It is actually a double mutation, resulting in a substitution of two amino acids, lysine (K) and methionine (M) to asparagine (N) and leucine (L). Aβ sequence is colored in blue.

To test our hypothesis, brains of Tg2576 mice were stereotaxically injected with either 2F or 3F synthetic $A\beta_{40}$ fibrils (n=7, for each fibril). Additionally, age-matched Tg2576 mice were treated with either brain homogenate from an aged (15-month-old) Tg2576 mouse (n=5) or monomeric synthetic $A\beta_{40}$ (n=4) as positive and negative control groups, respectively (See 2.1.2.). For cross-seeding experiments, Tg2576 mice were challenged with CsgA- (n=12), Mcc- (n=8) or TasA-fibrils (n=10). All animals were housed in standard conditions (22°C, 12 h dark/light cycles, food and water *ad libitum*) as groups of no more than 5 animals per cage (*vide infra*). All animal procedures described in this work were done in agreement with the regulations of the Institutional

Animal Care and Use Committee of The University of Texas Health Science Center at Houston (UTHealth) and approved by the local Animal Welfare Committee.

All experimental designs described in this thesis were included in a collaborative research project from the National Institute of Health (NIH) and granted to the group of UTHealth (PI Dr. Rodrigo Morales) and NIH (PI Dr. Robert Tycko). Additionally, several experiments (immunolabeling and image analysis) were performed with the collaboration of the group of University of Malaga (PI Dr. A. Gutiérrez). The number of animals was reduced as much as possible, according to the three R's principle (Replacement, Reduction and Refinement).

2.1.2. Preparation of inocula

For the positive control, a brain from an aged (15 months old) Tg2576 mouse (frontal cortex) was homogenized at 10% w/v using a glass homogenizer in phosphate buffer saline (HyClone™ Dulbecco's phosphate buffered saline, without calcium or magnesium, GE Healthcare Life Sciences, USA) supplemented with a cocktail of protease inhibitors (Roche Diagnostics, Switzerland). As negative control, monomeric synthetic $A\beta_{40}$ (Biomatik, USA) was dissolved in PBS at 1 mg/mL right before inoculation to avoid self-aggregation. For the experimental groups, 2F and 3F fibrils, provided by Dr. Robert Tycko, and fibrils from all three bacterial functional amyloids (BFA), were pelleted by ultracentrifugation at 100,000 x g using an Optima L-100K ultracentrifuge (Beckman-Coulter, USA) and resuspended in PBS at 1 mg/mL. The resulting inocula, both from brains and from the synthetic and BFA fibrils, was stored at -80°C until used for animal injection. Prior to use, inocula (Synthetic 2F/3F Fibrils, BFAs and brain homogenates) were sonicated for 30 seconds in an ice-cold water bath.

2.1.3. Animal procedures

50 days old Tg2576 mice were intracerebrally (i.c.) injected with a 10% w/v brain homogenate from an aged Tg2576 mouse, synthetic Aβ (2F or 3F fibrils, or monomeric protein) or fibrils from all three bacterial functional amyloids (**Figure 2.2**). Injections were performed stereotaxically in the hippocampus of both brain hemispheres in anesthetized animals using the following coordinates from bregma: anteroposterior: -1.8 mm; medio-lateral: ±1.8 mm; dorso-ventral: -1.8 mm. 10 µL of the brain homogenate, synthetic $A\beta_{40}$ or BFA (1 mg/mL) were administered per injection using a Hamilton 1700 Series Syringe (Hamilton company, USA). All animal procedures described in this work

were done in agreement with the regulations of the Center of Laboratory Animal Medicine and Care (CLAMC) at UTHealth and approved by the local Animal Welfare Committee (AWC).

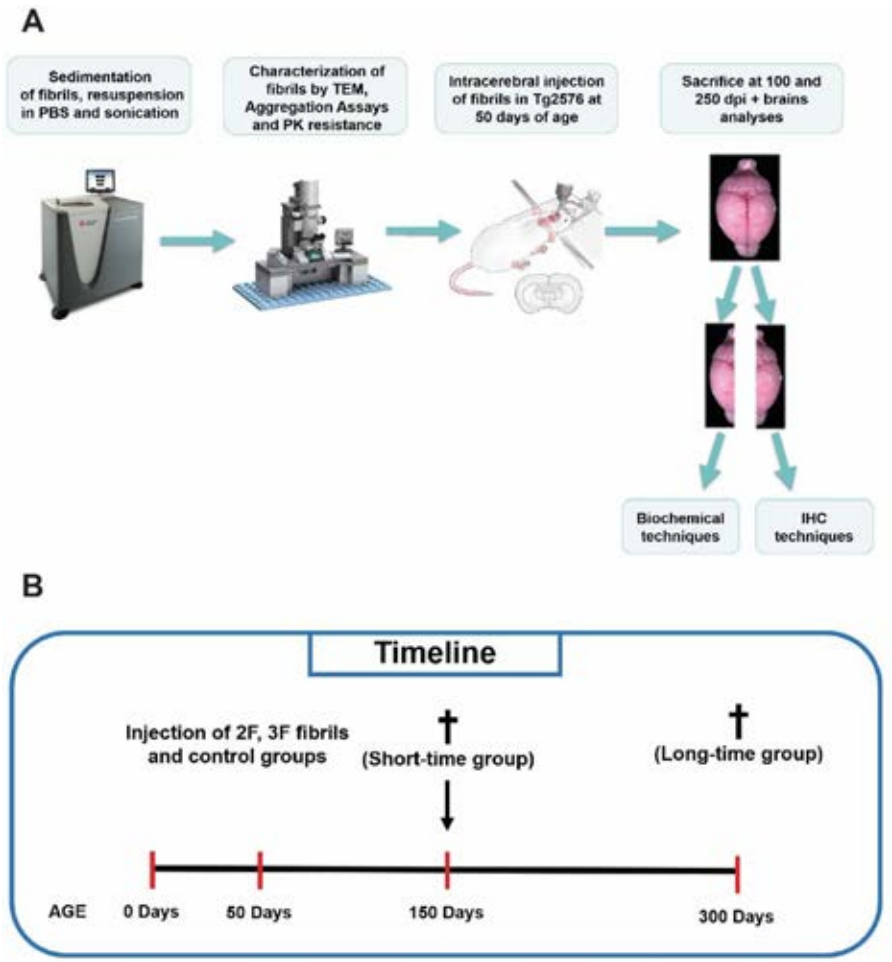

Figure 2.2. Project workflow from 2F and 3F samples to analysis. (A) For this project, both 2F and 3F fibrils, provided by Dr. Robert Tycko, were pelleted by ultracentrifugation at 100,000 x g and resuspended in PBS at 1 mg/mL concentration. These fibrils were later characterized by Transmission Electron Microscopy (TEM), *in vitro* aggregation assays, pK resistance and LCOs co-incubation and spectra analysis. The resulting inocula, both from brains and from the synthetic fibrils, was stored at -80°C until used for animal injection. Prior to use, inocula were sonicated for 30 seconds in an ice-cold water bath and stereologically injected in both hippocampi of Tg2576 animals at 50 days of age. 100- or 250-days post-injection (dpi) animals were euthanized, and mouse brains were quickly removed and hemidissected. Left brain halves were frozen to be analyzed by protein-based multiplex immunoassay for both $A\beta_{40}/A\beta_{42}$, and Cytokines levels using commercially available kits. Opposite brain halves were fixed by immersion in formalin and saved for further immunohistochemical (IHC) studies. **(B)** Timeline of this study as described in **(A)**.

2.2. EXPERIMENTAL PROCEDURES

2.2.1. Preparation of synthetic $A\beta_{40}$ aggregates

In order to prepare both the 2F and 3F synthetic $A\beta_{40}$ fibrils, 3-5 mg of lyophilized synthetic $A\beta_{40}$ was first dissolved in DMSO at approximately 5 mM. Aliquots of DMSO-solubilized peptide were then diluted rapidly into 10 mM sodium phosphate buffer (pH 7.4), containing 0.1% w/v of sodium azide to produce final $A\beta_{40}$ concentrations of 100 µM. Peptide-containing solutions were then incubated at room temperature in 15 mL or 50 mL polypropylene tubes, either quiescently to produce 3F fibrils or with orbital mixing (approximately 60 rotations/minute) to produce 2F fibrils (Petkova et al., 2005). Seeds of previously prepared 2F or 3F fibrils (i.e., sonicated fibril fragments with typical lengths of 50-150 nm, approximate 1:30 ratio of $A\beta_{40}$ seeds to DMSO-solubilized $A\beta_{40}$) were added to the solutions before incubation, to accelerate fibril growth and ensure formation of the desired polymorphs. Solutions were incubated for several days. Fibril formation was verified by negative-stain TEM. (**Figure 3.1**).

2.2.2. Measurement of the relative resistance to proteolysis of synthetic $A\beta_{40}$ aggregates

The structural features of the two synthetic $A\beta_{40}$ fibrils (2F and 3F) used in this study have been previously characterized by our collaborator Dr. Robert Tycko (Petkova et al., 2005) (See **Figure 1.11** in Introduction). Additional structural characterization was performed for this work. First, these two synthetic $A\beta_{40}$ aggregates were challenged with proteinase K enzyme. Proteins resistant to proteinase K are rare due to the potency, wide optimum pH and low peptide bond specificity of this enzyme. In general, amyloid proteins show some degree of resistance to this enzyme and the proteinase K resistance assay serves as an indirect measurement/characterization of the biochemical structure of the proteins. For this assay, both fibril preparations (2F and 3F), at 0.1 mg/mL, were treated with different concentrations of proteinase K (PK, 100 µg/mL, 50 µg/mL, 25 µg/mL and 12.5 µg/mL) for 1 hour at 37°C with gentle agitation (600 rpm in a thermomixer (Eppendorf, Germany)). Digestion products were analyzed by silver staining after separation in NuPage Bis-Tris 12% gels (Invitrogen). The monomeric band of $A\beta_{40}$ was analyzed using the WCIF ImageJ software (National Institutes of Health, Bethesda, MD, USA). This experiment was independently repeated three times.

2.2.3. Ultrastructural characterization of synthetic $A\beta_{40}$ aggregates by Transmission Electron Microscopy

Further structural characterization was performed by Transmission Electron Microscopy (TEM). TEM images of 2F and 3F fibrils and fibrils grown from brain homogenates were obtained with an FEI Morgagni microscope, operating at 80 keV, equipped with an Advantage HR camera (Advanced Microscopy Techniques). Each fibril sample was diluted by 5-10 times in deionized water and applied as a 10 µL aliquot to a glow-discharged grid (carbon film supported by lacey carbon on 300 mesh copper), allowed to adsorb for approximately 2 minutes, blotted, rinsed twice with deionized water, blotted, stained with a 10 µL aliquot of 2% w/v uranyl acetate for 15-30 seconds, blotted, and dried in air.

2.2.4. Structural characterization of 2F and 3F fibrils with Luminescent Conjugated Thiophenes (LCOs)

The structural features of the two synthetic $A\beta_{40}$ fibrils used in this study were further evaluated by using a battery of luminescent conjugated oligothiophenes (LCOs) provided by Dr. K. Peter R. Nilsson (Linköping University, Denmark). LCOs have great affinities with amyloids and have been previously shown to discriminate between α-synuclein strains (Shahnawaz et al., 2020) and different conformation of misfolded Aβ and tau deposits (Klingstedt et al., 2011, 2013; Nilsson et al., 2007). Here, we tested 9 different LCOs (See **Table 2.1**). In short, 2F and 3F fibrils, provided by Dr. Robert Tycko were resuspended at 1 mg/mL (**See 2.1.2** preparation of Inocula) and diluted to 100 µM in PBS. These fibrils were further diluted at a 1:10 ratio (10 µM) in PBS in a 96-well microtiter plate. Stock solutions of luminescent conjugated oligothiophenes (LCOs) at 1.5 mM, were diluted in distilled water to 15 µM and added to the wells, containing the 2F and 3F fibrils, to a final concentration of 0.3 µM. The samples were incubated at 37°C and the emission spectrum of each probe was collected after 30 minutes by exciting the samples at the excitation wavelength shown in **Table 2.1** for each probe.

LCO	Concentration (nM)	Excitation (nm)
p-FTAA	300	450
h-FTAA	300	465
HS-68	300	440
HS-167	300	370 or 525
HS-169	300	370 or 535
HS-194	300	535
HS-199	300	545
HS-208	300	535
HS-212	300	535

Table 2.1. Luminescent Conjugated Oligothiophenes (LCOs) used in this study. All LCOs were tested at a final concentration of 300 nM and each LCO was excited at the wavelength (nm) shown in the right column of this table.

2.2.5. Preparation of Bacterial Functional Amyloids (BFA) aggregates

2.2.5.1. Purification of curli subunit CsgA and preparation of CsgA-derived fibrils

Curli CsgA subunit was purified from *E. coli* cells (NEB C2566, a New England Biolabs Inc. T7 expression strain) containing the pNH11 plasmid. Specifically, this plasmid, donated by Professor Matthew R. Chapman (University of Michigan, USA), was made by cloning C-terminal 6× His tagged CsgA without the Sec- signal sequence into the pET11d vector. These cells produce the CsgA curli subunit without Sec- signal sequences and thus are expressed in the cytoplasm. Then, the cytoplasmic CsgA can be purified via a denaturation method (Zhou et al., 2013). For simplicity, we refer to C-terminal 6× His tagged CsgA protein as CsgA in this method. CsgA, trapped in the cytoplasm, can be purified from the bacterial lysate. In brief, *Escherichia coli* cells harboring the pNH11 plasmid were grown overnight in 10 mL Luria-Bertani (LB) medium, supplemented with 100 µg/mL ampicillin and 25 µg/mL chloramphenicol, at 37 °C, with shaking. This culture was later diluted in 1L of antibiotics supplemented LB and cells were grown with shaking to an absorbance of 0.8-0.9 at 600 nm. Then, expression was induced by adding 0.5 mM isopropyl-β-D-thiogalactoside (IPTG) and incubating at 37 °C with shaking. After 1 hour, the 1L culture was divided in four 250 mL cultures and cells were harvested by pelleting down the culture centrifugating at 5,000 x g for 20 minutes. At this step, pellets can be stored at −80 °C until used. These pellets were resuspended in 25 mL of 8M Gdn-HCl (50mM KPi, pH 7.3) and incubated at room temperature (RT) for 24 hours. The suspension was spun down at 10,000 × g for 20

minutes at 4°C and supernatant was collected. Supernatant was sonicated with a probe sonicator, at power 3, for three 20 seconds burst at RT. At this step, 1 mL of fresh Ni-NTA (HisPur™ Ni-NTA Resin, Thermo Scientific™, Cat. No: 88221) was added to the supernatant and incubated in a rocker for 1 hour at RT. This mixture was loaded onto a disposable polypropylene column and washed with 10 mL of 50mM KPi, pH 7.3 (KPi buffer). The column was further washed with 3 mL of 12.5 mM imidazole in KPi buffer and finally eluted with 3 mL of 125 mM imidazole in KPi buffer and collected in microfuge tubes. Fractions containing most of the protein, measured by change in refractive index, were pooled and filtered through a 30 kDa cut-off filter (Amicon Ultra Centrifugal Filter Units, Millipore, Cat No: UFC503096, USA) at 7,000 x g for 10 min to remove large aggregates. To remove the imidazole from the filtrated protein, spin desalting columns (Zeba™ Spin Desalting Columns, Thermo Scientific™, Cat. No: 0089894, USA) were used. In short, the spin desalt column was washed with KPi buffer two times. Filtrated protein was loaded onto the prewashed spin desalting column and centrifuged at 1,000 × g for 2 minutes at 4°C. At the end, protein concentration was measured by Pierce Micro BCA™ Protein Assay Kit (Thermo Scientific™, Cat No: 23235, USA) and saved on ice until further use.

Freshly purified CsgA self-polymerize into amyloid fibers in a nucleation dependent pattern. In order to prepare CsgA-derived amyloid fibrils, freshly purified, soluble CsgA protein, was incubated at a concentration of 1 mg/mL in KPi buffer for 24 h at 37 °C with shaking. Fibril formation was characterized by Thioflavin T (ThT) binding assay and turbidity, as previously described (Hartman et al., 2013). Before both *in vitro* and *in vivo* experiments, fibrils were prepared as stated above (**See 2.1.2.** Preparation of Inocula). In brief, CsgA fibrils were pelleted by ultracentrifugation at 100,000 x g and resuspended in PBS at 1 mg/mL concentration

2.2.5.2. Purification of Microcin E492 (Mcc) and preparation of Mcc-derived fibrils

Microcin E492 was purified from culture supernatants. In brief, *Escherichia coli* VCS257 cells containing the pJEM15 plasmid were grown at 37 °C with shaking to an absorbance of 1.2 at 600 nm in M9 minimal medium containing 0.2% glucose, 0.2% sodium citrate, 1 g/liter casamino acid, 1 mg/liter thiamine, and 100 mg/liter ampicillin. Bacterial cell debris was removed by centrifugation at 4,000 RPM for 10 min. The resultant supernatant was passed through a Sep-Pak C18 cartridge (Waters corporation, USA). The cartridge was sequentially washed with 3 mL of 65% methanol and 3 mL of

25% acetonitrile. Finally, the bound Microcin E492 was eluted with 3 mL of 50% acetonitrile and lyophilized. Lyophilized powder of Mcc was stored at −20 °C until used. Under these conditions, the preparation contains highly purified Mcc (>90%).

The powder containing lyophilized Mcc was dissolved in sterile 10 mM NaOH solution and, to remove aggregates, this solution was filtered through a 30-kDa cutoff filter. Then, the protein concentration in this filtrate (monomers) was estimated by using the Pierce Micro BCA™ Protein Assay Kit (Thermo Scientific™, Cat No: 23235, USA) and used immediately or stored frozen at −80 °C. In order to prepare Mcc-derived amyloid fibrils, soluble Mcc protein was incubated at a concentration of 400 µg/mL in aggregation buffer (50 mM PIPES-NaOH, pH 6.5, 0.5M NaCl) for 24 h at 37 °C with shaking. Fibril formation was characterized by Thioflavin T (ThT) binding assay and turbidity, as previously described (Shahnawaz et al., 2017a).

2.2.5.3. Purification of *Bacillus subtilis*-derived TasA and preparation of TasA-derived fibrils

TasA was purified and kindly donated by the lab of Dr. Diego Romero (University of Malaga, Spain). TasA was purified from *E. coli* BL21 (DE3) cells containing the pDFR6 plasmid (pET22b-*tasA*). This plasmid contains the open reading frame of the *tasA* gene from *Bacillus subtilis* NCIB3610 without the signal peptide or the stop codon and was constructed by Dr. Romero as previously described (Romero et al., 2011). *E. coli* BL21 (DE3) cells containing the pDFR6 plasmid were grown, as previously described (Cámara-Almirón et al., 2020; Mammeri et al., 2019), in 10 mL of Luria-Bertani (LB) medium supplemented with ampicillin (100 µg/mL) and incubated overnight at 37° C with shaking. This pre-culture was then used to inoculate 500 mL of LB medium, supplemented with ampicillin, and grown at 37°C with shaking to an absorbance of 0.7-0.8 at 600 nm. Then, TasA expression was induced by adding 1 mM isopropyl-β-D-thiogalactoside (IPTG) and incubating at 30 °C, with shaking, for 20 hours. Cells were harvested by centrifugation (JLA 8.1 rotor; Beckman Coulter, USA) at 5,000 x g for 10 minutes at 4° C, resuspended in buffer A (50 mM Tris, 150 mM NaCl, pH 8), and centrifuged again. Pellets were frozen and kept at -80°C until purification.

After thawing the pellets, cells were resuspended in buffer A again, sonicated (3 × 45 s, 60% amplitude) on ice and centrifuged at 15,000 x g for 60 minutes at 4° C. Pellets containing the inclusion bodies were resuspended in buffer A supplemented with 2% Triton X-100, incubated 20 minutes at 37°C with shaking and centrifuged at 15,000

x g for 10 minutes at 4° C. The pellet was extensively washed with buffer A, centrifuged at 15,000 x g for 10 minutes at 4° C, resuspended in denaturing buffer (50 mM Tris, 0.5 M NaCl, 6M Gdn-HCl) and incubated at 60 °C overnight until complete solubilization. Lysates were clarified by sonication on ice (3 × 45 s, 60% amplitude) followed by centrifugation at 15,000 x g for 1 hour at 16° C and passed through a 0.45-µm filter prior to affinity chromatography. Protein was purified using an AKTA Start FPLC system (GE Healthcare, USA). Solubilized inclusion bodies were loaded in 5 mL HisTrap HP columns (GE Healthcare, USA) that were previously equilibrated with binding buffer (50 mM Tris, 0.5 M NaCl, 20 mM imidazole, 8M urea, pH 8). Proteins were eluted from the column with elution buffer (50 mM Tris, 0.5 M NaCl, 500 mM imidazole, 8M urea, pH 8). To remove the imidazole from the purified protein, desalting columns (HiPrep 26/10, GE Healthcare, USA) were used, and the buffer was exchanged to 20 mM Tris, 50 mM NaCl to perform the aggregation.

In order to prepare TasA-derived amyloid fibrils, freshly purified, soluble TasA protein, was incubated at a concentration above 1 mg/mL in 20 mM Tris, 50 mM NaCl buffer for 5 days at 28 °C with shaking. Fibril formation was characterized by Thioflavin T (ThT) binding assay and turbidity. Before both *in vitro* and *in vivo* experiments, fibrils were prepared as stated above (**See 2.1.2.** Preparation of Inocula). In brief, TasA fibrils were pelleted by ultracentrifugation at 100,000 x g and resuspended in PBS at 1 mg/mL concentration.

2.2.6. *In vitro* $A\beta_{40}$ aggregation assay by Protein Misfolding Cyclic Amplification (PMCA)

2.2.6.1. Purification of recombinant $A\beta_{40}$

E. coli cells (BL21 (DE3) pLysS Competent Cells) containing the pET28 GroES-Ub-$A\beta_{40}$ plasmid were grown in Luria-Bertani (LB) medium supplemented with kanamycin (50 µg/mL) at 37° C, and expression was induced with 0.4 mM isopropyl-β-D-thiogalactoside (IPTG). After 6 hours, cells were harvested and lysed with lysis buffer (50 mM Tris-HCl, (pH 8.0), 150 mM NaCl, 5 mM EDTA, 0.5% triton X-100, 1mM dithiothreitol (DTT) and 0.1 mM paramethylsulfoxide (PMSF)). After 30 min on ice, lysozyme (1 mg/mL) was added to the re-suspended pellet and incubated for 20 min at room temperature. After incubation, the re-suspended pellet was sonicated and centrifuged at 15,000 x g for 30 minutes. Pellet was resuspended in lysis buffer, sonicated,

and centrifuged twice. After 4 washing steps (3 with washing buffer I (50 mM Tris-HCl, pH 8.0, 150 mM NaCl, 5 mM EDTA, 0.5% triton X-100 and 1mM DTT) and 1 with washing buffer II (50 mM Tris-HCl, pH 8.0, 150 mM NaCl, 5 mM EDTA and 1mM DTT)), inclusion bodies were obtained by centrifugation at 15,000 x g for 30 minutes. Inclusion bodies were re-suspended in a specific solubilization buffer (50 mM Tris-HCl, pH 8.0, 150 mM NaCl, 1 mM DTT and 8 M urea). Insoluble proteins were removed by centrifugation at 30,000 x g for 30 minutes. The supernatant containing GroES-Ub-Aβ$_{40}$ fusion protein was collected and purified through a Ni-NTA column. To cleave off Aβ$_{40}$, fusion proteins were diluted 3-fold with resuspension buffer (50 mM Tris-HCl, pH 8.0, 150 mM NaCl and 3 M urea) and digested with recombinant de-ubiquinating enzyme (Usp2cc) in a 1:100 enzyme to substrate molar ratio at 37° C for 2 hours. After digestion, samples were sonicated and centrifuged at 30,000 x g for 30 minutes. Supernatant was then loaded on a PRP-3 Reversed-Phase column (21.5 mm×250 mm, Hamilton Company, USA). Aβ$_{40}$ was purified with a solvent system buffer 1 (10 mM ammonium acetate, pH 10, 2% acetonitrile) and buffer 2 (70% acetonitrile) at a flow rate 10 mL/min using a 0-20% linear gradient of buffer 2 over 5 minutes, then 20%-40% linear gradient for 30 minutes and finally 40%-100% for 30 minutes. Purified Aβ$_{40}$ was lyophilized and stored at −80° C, until use.

2.2.6.2. Preparation of aggregate-free Aβ$_{40}$

Lyophilized Aβ$_{40}$ was dissolved at 1 mg/mL concentration in 500 µL of 0.1% ammonium hydroxide (NH_4OH) on ice and filtered through a 30 KDa cut-off filter (Amicon Ultra Centrifugal Filter Units, Millipore, Cat No: UFC503096, USA) at 14,000 x g for 12 min to remove large aggregates. Filtrated protein concentration was measured by Pierce Micro BCA™ Protein Assay Kit (Thermo Scientific™, Cat No: 23235, USA) and saved at −80° C, until further use.

2.2.6.3. *In vitro* aggregation assay

Homologous seeding: 2F and 3F synthetic Aβ aggregates were further characterized for their seeding potential *in vitro* using the Aβ version of the Protein Misfolding Cyclic Amplification (PMCA) technique previously developed by our collaborator's lab (Salvadores et al., 2014). In summary, purified, aggregate-free Aβ$_{40}$ (1 µM) was incubated in 100 mM Tris-HCl buffer, pH 7.4 and 5 µM ThT, at 20°C in opaque 96-well

microtiter plates with cycles of 1-minute cyclic agitation (500 rpm) every 30 minutes. Wells containing aggregate-free Aβ40 were incubated in the presence of 100 pM of either 2F or 3F fibrils. Protein aggregation was monitored by ThT fluorescence measured at 485 nm after excitation at 435 nm using a plate spectrofluorometer (SpectraMax® iD3 Multi-Mode Microplate Reader, Molecular Devices, USA) and fitted using Boltzmann equation. It is worth mentioning that during this thesis the Aβ PMCA assay has been further developed and characterized in order to increase the replicability of our results.

Heterologous seeding: Bacteria-derived functional amyloids were tested for their ability to cross-seed monomeric Aβ40. Similar that in homologous seeding (*vide supra*), aggregate-free Aβ40 (1 µM) was incubated in the presence of 10 nM or 100 pM of CsgA, microcin or TasA-derived fibrils. Protein aggregation kinetics was monitored by measuring ThT fluorescence at 485 nm and cross-seeding was confirmed when acceleration of monomeric Aβ40 aggregation was observed.

Calculation of T20, T50 and T90: The average time ± standard error at which fluorescence is 20% (T20), 50% (T50) or 90% (T90) of the maximum fluorescence was calculated by performing a nonlinear regression (curve fit) using the following formula in the GraphPad Prism 9.1.0 software:

$$logEC50 = logECF - \left(\frac{1}{HillSlope}\right) * \log\left(\frac{F}{100 - F}\right)$$

$$Y = Bottom + \frac{Top - Bottom}{(1 + 10^{(LogEC50 - X) * HillSlope})}$$

Where F=20 for T20, F=50 for T50 and F=90 for T90.

2.2.7. Preparation of brain homogenates and extraction of aqueous insoluble Aβ and soluble cytokines

Brain homogenates were prepared by homogenizing each left-brain hemisphere at 10% w/v in Phosphate Buffer Saline (HyClone™ Dulbecco's phosphate buffered saline, without calcium or magnesium, GE Healthcare Life Sciences, USA) containing a cocktail of protease inhibitors (Roche Diagnostics, Switzerland) using a glass dounce homogenizer. For the extraction of the different fractions (soluble and insoluble) 200 µL of 10% w/v brain homogenates were ultra-centrifuged at 100,000 x g for 1 h at 4°C using

a Optima L-100K ultracentrifuge (Beckman-Coulter, USA). Supernatant (S1) was snap frozen in liquid nitrogen and the pellets (P) were resuspended in 200 µL of 70% v/v formic acid. Samples were sonicated and centrifuged again, in the same conditions, for 30 minutes. Supernatants (S2) were diluted 25 times in 1 M Tris base buffer (pH 11), in order to stabilize the pH to 7.4, and snap frozen in liquid nitrogen (See **Figure 2.3**). Resulting samples were stored at -80°C until used (next day).

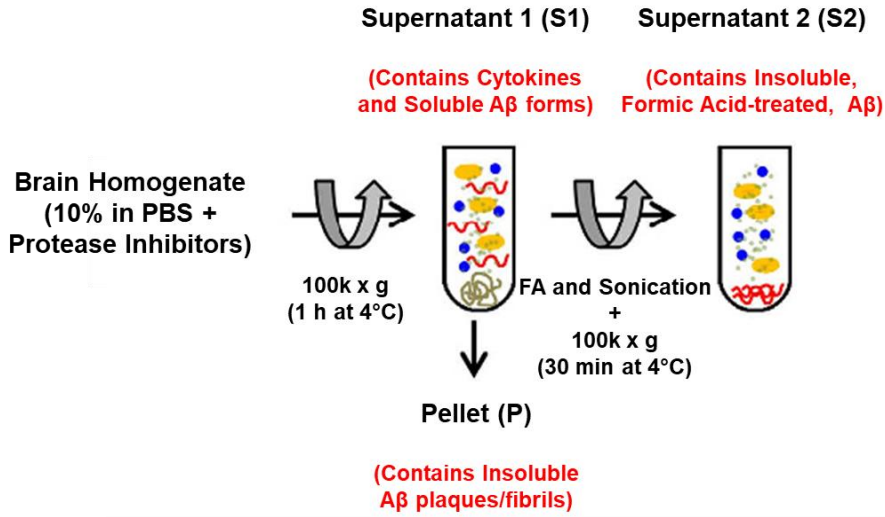

Figure 2.3. Method for isolating soluble cytokines and soluble/insoluble Aβ species from mouse AD brain. Brain hemisphere was dounce homogenized in PBS containing protease inhibitors. Soluble forms of Aβ and soluble cytokines (S1) were isolated by differential ultracentrifugation. Then, insoluble Aβ aggregates were purified by treating the pellet (P) with formic acid (FA), sonicating and another step of ultracentrifugation. Specifically, insoluble FA-treated Aβ was recovered from the second supernatant (S2). Figure adapted from (Esparza et al., 2016).

2.2.8. Protein-based multiplex immunoassay measurement of aqueous insoluble Aβ and soluble cytokines

In order to measure insoluble Aβ and soluble Cytokines, we took advantage of the multiplex immunoassay system that use Luminex xMAP technology (Austin, TX). This assay principle is similar to a sandwich ELISA with the difference that the immunoassay is formatted on magnetic microspheres/beads (See **Figure 2.4**).

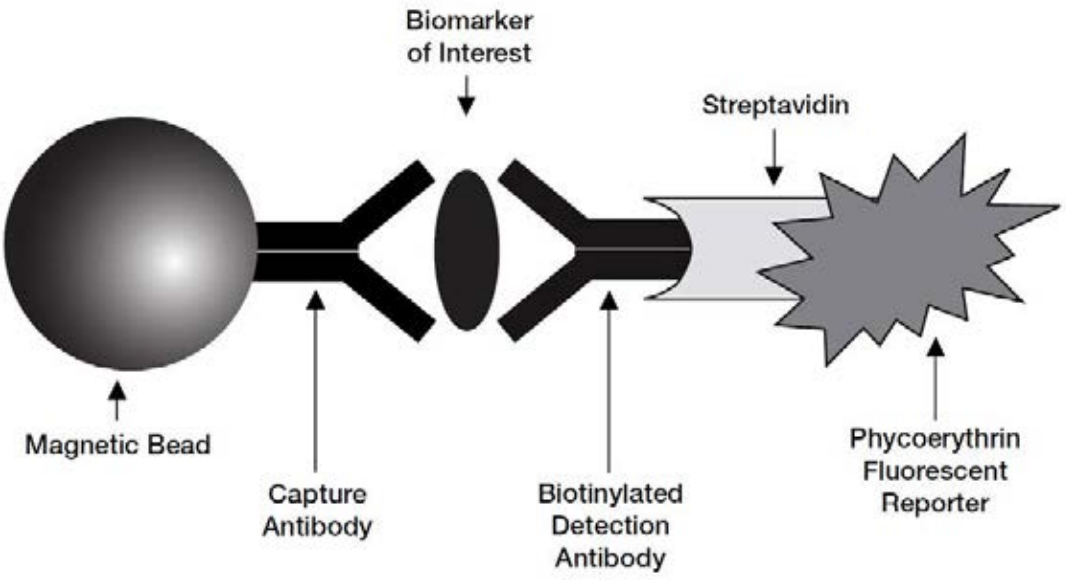

Figure 2.4. Multiplex Immunoassay Magnetic Bead. Each set of beads, for each analyte, is fluorescently dyed. These beads contain covalently bound capture antibodies directed against the desired analyte. Beads then react with the sample, in our case S1 or S2 supernatants, containing the biomarker of interest (Aβ/cytokines). Then, a biotinylated detection antibody is added to the reaction, binds to the biomarker of interest, and creates a sandwich complex. The final step involves the addition of streptavidin-phycoerythrin (SA-PE) conjugate, which will form the final detection complex. This complex, due to the PE, serves as a fluorescent reporter that will be read by the Bio-Plex 200 system. Figure adapted from Bio-Rad website.

Specifically, the xMAP technology uses different sets of magnetic beads in a liquid suspension. Each bead set is fluorescently dyed with a distinct color code or "address" that permits to discriminate between individual beads in a multiplex suspension. This allows for simultaneous detection of up to 100 different molecules. These beads, containing covalently bound capture antibodies directed against the desired analyte, react with the sample containing the biomarker of interest (Aβ/cytokines). After several washes, a biotinylated detection antibody is added to the reaction, binds to the biomarker of interest, and creates a sandwich complex. In the final step, a streptavidin-phycoerythrin (SA-PE) conjugate is added and the final detection complex is formed. This complex, due to the PE, serves as a fluorescent reporter that will be read by the Bio-Plex 200 system (Bio-Rad, USA). The Bio-Plex® 200 system is a dedicated flow cytometer with two lasers: the red classification laser/LED (635 nm), which excite the fluorescent dye of the bead and thus classify the bead by their spectral signature, and the green reporter laser/LED (525–532 nm) that recognizes the fluorescent reporter (PE) bound to the

captured analyte on the bead surface. These two sets of lasers and associated optics of the Bio-Plex® 200 system allow to measure the different molecules bound to the surface of the beads, classify the beads according to the analyte it binds to (multiplex) and thus quantify the amount of a given analyte in a sample. This classification/quantification capability, together with the high-speed digital signal processor, allows for efficient measurement of up to 100 analytes from a single sample. Since these assays are usually performed in 96-well plates, these multiplex systems allow to quantify many analytes from 96 samples simultaneously.

For measuring $A\beta_{40}/A\beta_{42}$ concentrations, a specific protein-based multiplex immunoassay kit (MILLIPLEX MAP Human Amyloid Beta Magnetic Bead Panel, Millipore, Cat. No: HNDG4MAG-36K, USA) was used. Specifically, S2 samples diluted in Tris Buffer (See **Figure 2.3**) were used to measure the different Aβ species. Before starting this experiment, the protein concentration in each sample was estimated by using the Pierce Micro BCA™ Protein Assay Kit (Thermo Scientific™, Cat No: 23235, USA), and then the protocol provided by the kit's manufacturers was followed. In brief, these samples were diluted 1 to 50 in Assay Buffer (included in the kit) and the plate wells were prewet with 200 µL of Assay Buffer. After shaking for 10 minutes, the Assay Buffer was decanted and 25 µL of each Standard/Control or sample was added to the wells. In this step, 25 µL of Aβ Detection Antibody (Cat# HNDG4-ABETA) and 25 µL of Mixed Beads were also added to each well. The plate was then sealed and incubated overnight at 4°C with agitation on a plate shaker. Next day, we used a handheld magnet to allow complete settling of magnetic beads at the bottom of the plate. Then, the well contents were discarded, and plate was washed three times with 200 µL of Wash Buffer. After completing the washes, 25 µL of streptavidin-phycoerythrin (SA-PE) was added to the wells, incubated for 30 minutes at RT with shaking, discarded and plate was washed three times with 200 µL of Wash Buffer to finish resuspending the beads in 100 µL of Sheath Fluid. Finally, plates were read on the Bio-Plex® 200 system with the settings set a 50 events per bead and 50 µL per well. Data acquisition and analysis was performed with the Bio-Plex Manager™ software obtaining data in pg/mL. Extractions and Multiplex measurements were performed in duplicates.

Additionally, the concentration of a panel of 23 cytokines was measured by using another protein-based multiplex immunoassay kit (Bio-Plex® Pro Mouse Cytokine 23-plex Assay, Bio-Rad, Cat. No: M60009RDPD, USA). This multiplex assay detects the following cytokines:

- Eotaxin
- G-CSF
- GM-CSF
- IFN-γ
- IL-1α
- IL-1β
- IL-2
- IL-3
- IL-4
- IL-5
- IL-6
- IL-9
- IL-10
- IL-12 (p40)
- IL-12 (p70)
- IL-13
- IL-17A
- KC
- MCP-1 (MCAF)
- MIP-1α
- MIP-1β
- RANTES
- TNF-α

Specifically, S1 samples (See **Figure 2.3**) were used to measure the different cytokines species. Before starting this experiment, the protein concentration in each sample was estimated by using the Pierce Micro BCA™ Protein Assay Kit (Thermo Scientific™, Cat No: 23235, USA), and then the protocol provided by the kit's manufacturers was followed. In short, these samples were diluted 1 to 2 in Bio-Plex® sample diluent buffer (included in the kit) and the plate wells were prewet with 100 µL of Assay Buffer. After shaking for 10 minutes, the Assay Buffer was decanted and 50 µL of 1x coupled beads was added to the wells. Then, by using a handheld magnet to settle the magnetic beads, and the plate containing the beads was washed two times with 100 µL of Bio-Plex® wash Buffer. At this step, 50 µL of diluted standard/control or sample was added to the wells. The plate was sealed and incubated for 1 hour at RT with agitation (850 RPM) on a plate shaker. Next, well contents were discarded, and plate was washed three times with 100 µL of wash Buffer. After completing the washes, 25 µL of detection antibodies was added to the wells and plate was sealed and incubated again for 30 minutes at RT with shaking. Again, the well contents were discarded, and plate was washed three times with 100 µL of wash Buffer. After washes, 50 µL of streptavidin-phycoerythrin (SA-PE) was added to the wells, incubated for 10 minutes at RT with shaking, discarded and plate was washed three times with 100 µL of wash Buffer to finish by resuspending the beads in 125 µL of assay buffer. Finally, plates were agitated for 30 seconds and read on the Bio-Plex® 200 system with the settings set a 50 events per bead and 50 µL per well. Data acquisition and analysis was performed with the Bio-Plex Manager™ software obtaining data in pg/mL. Again, extractions and Multiplex measurements were performed in duplicates as explained above.

2.2.9. Tissue preparation

All animals were deeply anesthetized by CO_2 inhalation at either 100- or 250-days post injection (dpi) (See **Figure 2.2B**). Then, mouse brains were quickly removed and divided through the middle line. Left brain halves were frozen to be analyzed by protein-based multiplex immunoassay for both $A\beta_{40}/A\beta_{42}$, and cytokines levels using commercially available kits (Milliplex from Millipore for $A\beta_{40}$ and $A\beta_{42}$, and Bio-Plex Pro Mouse Cytokine 23-plex Assay from Bio-Rad, USA). Opposite brain halves were fixed by immersion in 10% neutral buffered formalin (Fisher HealthCare™ PROTOCOL™ Color-Coded Prefilled Formalin Containers, Thermo Scientific™, Cat. No: 23-032059, USA) and saved for further immunohistochemical (IHC) studies. Fixed hemibrains were inserted in tissue cassettes (Epredia™ Cassette, Thermo Scientific™, Cat. No: 10-009-61, USA) and dehydrated in graded ethanol and xylene for embedding in paraffin (Fisherbrand™ Histoplast PE Paraffin Wax, Thermo Scientific™, Cat. No: 22-900-700, USA) as follows:

- Overnight incubation in 70% EtOH
- Serial incubations of 2 hours each in 80% EtOH, 90% EtOH, 95% EtOH I and 95% EtOH II, followed by an overnight incubation in 95% EtOH III.
- Serial incubations of 2 hours each in 100% EtOH I, 100% EtOH II, 100% EtOH III, 100% Xylene I and 100% Xylene II, followed by an overnight incubation in 100% Xylene III.
- Serial incubations of 2 hours each in 100% Paraffin I and 100% Paraffin II, followed by an overnight incubation in 100% Paraffin III.
- Next day, brains were taken from the paraffin jar and included in molds (Epredia™ Shandon™ Disposable Base Molds, Thermo Scientific™, Cat. No: 41-744, USA) with paraffin and dried overnight.

After inclusion in paraffin, brains were sectioned at 10 µm thickness in the sagittal plane on a microtome (Leica, RM2235 Manual Rotary Microtome, Germany) and serially collected in microscope glass slides (Fisherbrand, USA).

2.2.10. Anatomical delimitation of the hippocampus

The hippocampus is a large, complex and layered sausage-shaped allocortical structure, located from Bregma -0.94 to -4.04 mm in the mouse brain atlas (Paxinos and

Franklin, 2008) (See **Figure 2.5**). It lays above the dorsal thalamus and underneath the corpus callosum and is dorsally and laterally bordered by the parietal cortex (Cassel et al., 1997).

In this work we focused on the hippocampal formation and the alveus (see **Figures 2.5 and 2.6**), which are located within the medial temporal lobe and is part of the limbic system. These regions are involved in memory (maintenance of the acquired information) and learning (new information acquisition), specifically in declarative/explicit (memory about events and facts, which are recalled consciously) long-term memory (acquired during long periods of time) memory. Hence, hippocampal neurodegeneration explains the main cognitive symptoms observed in AD patients (van Strien et al., 2009).

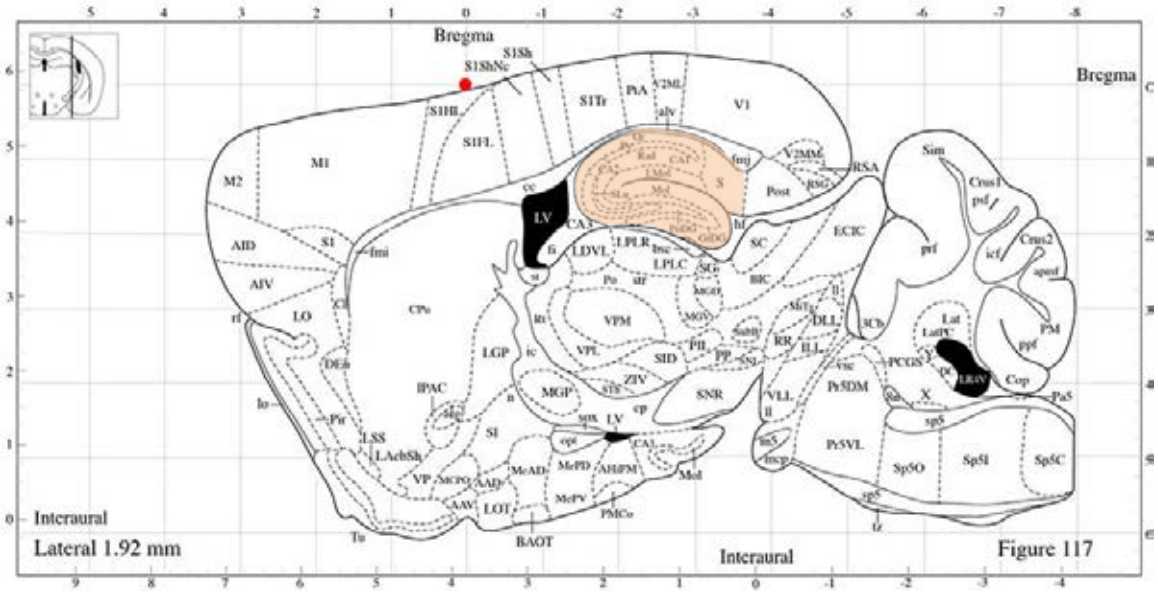

Figure 2.5. Schematic mediolateral representation of the mouse brain hippocampus. Level 117 (Lateral 1.92 mm) is depicted. In this image the hippocampus is highlighted in orange. Figure from Paxinos and Franklin mouse brain atlas (Paxinos and Franklin, 2008)

The hippocampal formation is divided in 3 grey matter regions (**Figure 2.6**): dentate gyrus (DG), hippocampus proper (HP) and subiculum, and 4 white matter regions: alveus (alv), fimbria, perforant pathway and Schaffer collaterals. The hippocampus proper, also known as Ammon's horn, is divided in 4 CA (*Cornu Ammonis*) subregions, CA1 to CA4 (CA4 is almost indistinguishable in the mouse brain). Moreover, in the hippocampus proper, we are able to distinguish several layers: the *stratum oriens* (so), the *stratum pyramidale* (sp, where glutamatergic principal neuron somata are concentrated), *strata*

radiatum (sr) and *lacunosum-moleculare* (slm). In this sense, the DG also exhibits 3 layers: the hilus (h), the granule cell layer (g, which is equivalent to sp) and the *stratum moleculare* (m) (van Strien et al., 2009). Important for this work is the alveus, a white matter tract that contains myelinated afferent and efferent axons and connect fibers from CA Pyramidal neurons, DG, and subiculum with the temporal hippocampus (fimbira/fornix), as well as contralateral/ipsilateral entorhinal neurons that project to CA1.

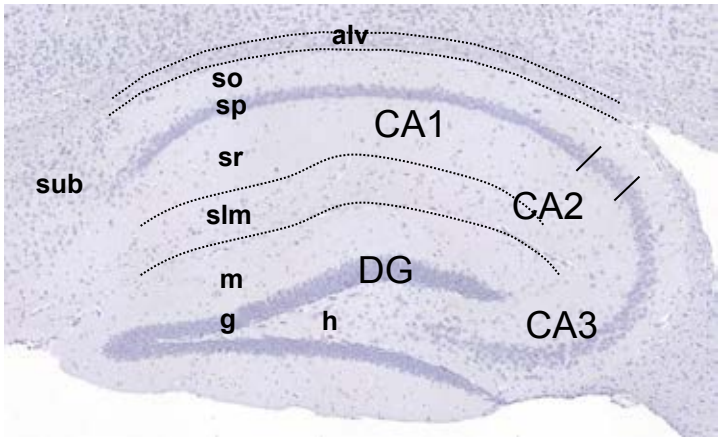

Figure 2.6. Hematoxylin-stained sagittal section of the mouse hippocampus. The different layers of both the hippocampus proper and the dentate gyrus are indicated. *CA1-3: Cornu Ammonis Area 1-3, DG: dentate gyrus, so: stratum oriens, sp: stratum pyramidale, sr: stratum radiatum, slm: stratum lacunosum-moleculare, m: stratum moleculare, g: granule cell layer, h: hilus. Subiculum (sub)* and *alveus (alv)* are also labeled.

2.2.11. Light microscopy immunohistochemistry

The immunohistochemical (IHC) technique is based on the intrinsic capability of antibodies to specifically interact with an antigen, allowing the detection of a target molecule in a cell/tissue. In this work, 10 µm thickness paraffin-embedded brain sagittal sections that represented 1/10th of the hippocampus from control (uninjected or monomeric $A\beta_{40}$), BFA- or synthetic-fibrils injected Tg2576 mice were assayed for light microscopy immunostaining. This technique was specifically performed to study the area covered by amyloid plaques and glial cells, and also for analyzing cerebral amyloid angiopathy (CAA). The information about the markers, primary and secondary antibodies are specified in **tables 2.2-2.4**, and the IHC protocol was performed as follows:

Protocol

Before starting the IHC protocol, paraffin was removed from the samples by incubating the tissue slices for 2 hours at 65°C and rinsing them (3 x 10 minutes) in Xylene (Fisherbrand™, HistoPrep™, Cat. No: HC-700-1GAL, USA). Then samples were sequentially rehydrated by incubating them in graded ethanol (100%, 95%, 90%, 80% and 70%) for 5 minutes each and twice in the case of 100% ethanol (Fisherbrand™, HistoPrep™, Cat. No: HC-800-1GAL, USA). Finally, slides were rinsed with water and washed 3 times for 10 minutes with PBS (HyClone™ Dulbecco's Phosphate Buffered Saline, Thomas Scientific, Cat. No: C838R12, USA).

A formic acid (FA) pretreatment was used when studying amyloid plaques with the 4G8 marker. In brief, after 3 x 10 minutes rinsing steps with PBS, sections were treated with 85% FA (prepared from FA 88% (Certified ACS), Fisher Chemical™, Cat. No: A118P-100, USA) for 5 minutes at room temperature. Also, a heating pretreatment was performed to induce the antigen retrieval in order to improve the quality of staining when needed (anti-Iba-1 straining). Specifically, after 3 x 10 minutes rinsing steps with PBS, sections were treated with antigen retrieval buffer (sodium citrate 50mM, pH 6) in a commercial microwave making the samples to reach 80ºC for 30 minutes. Then, sections were cooled to room temperature for 15 minutes and the general IHC protocol was performed as follows:

- Rinsing sections (3 x 10 minutes) with PBS to remove any EtOH/H_2O or antigen retrieval buffer from the tissue.
- On-slide sections treatment with 3% H_2O_2 (Hydrogen Peroxide, 30% (Certified ACS), Fisher Chemical, Cat. No: 7722-84-1, USA) and 10% methanol in PBS for 20 minutes. This step suppresses endogenous peroxidase activity to reduce background staining.
- Rinsing sections (3 x 10 minutes) with PBS to remove any H_2O_2/methanol traces.
- Incubation overnight with the appropriate primary antibody diluted in PBS with 0.2% Triton X-100 (See dilutions and conditions in **Table 2.3**).
- Rinsing sections (3 x 10 minutes) with PBS.
- Incubation for 1 hour and 30 minutes with the corresponding HRP-conjugated secondary antibody diluted in PBS with 0.2% Triton X-100 (see dilutions and conditions in **Table 2.4**).
- Rinsing sections (3 x 10 minutes) with PBS.

- Visualization/developing of the peroxidase reaction incubating in a solution with 3-3'-diaminobenzidine tetrahydrochloride (DAB) with Peroxidase (HRP) Substrate DAB Kit with Nickel (Vector Labs, Cat. No: SK-4100, USA). The incubation time is monitored on the microscope (0–10 min), stopping the reaction once the specific staining is clear enough, avoiding unspecific background at the same time. All sections are incubated for the same time.
- Rinsing sections (3 x 10 min) with PBS.
- Dehydration of the slides in ascendant graded ethanol (70%, 80%, 90%, 95% and 100%, for 10 min each), cleared in xylene for 15 minutes and coverslipped with DPX mounting medium (Electron Microscopy Science DPX Mountant, Thermo Scientific™, Cat. No: 50-980-370, USA).

Every rinsing step was carried out with constant gentle shaking. For each experiment, immunostaining was performed simultaneously and using same batches of solutions for every section to minimize variability in labeling conditions. Specificity of the immune reactions was controlled in additional tissues slices subjected to the same procedures explained above but omitting the primary antibody addition step.

MARKER	DESCRIPTION
4G8	Reacts to amino acid residues 17 to 24 of Aβ. The epitope lies within amino acids 18 to 22 of Aβ (VFFAE). Thus, this marker reacts to both abnormally processed Aβ isoforms and precursor forms.
Aβ40	β-amyloid peptide of 40 aminoacids, generated after the amyloid precursor protein (APP) cleavage. $A\beta_{40}$ is the most abundant Aβ isoform in the brain and is thought to be less prone to aggregation and to form fibrils than $A\beta_{42}$. It is mainly found in diffuse amyloid plaques and vessels (CAA), as well as in extracellular dense-core amyloid plaques.
Aβ42	β-amyloid peptide of 42 aminoacids, generated after the amyloid precursor protein (APP) cleavage. Aβ42 is highly prone to aggregation and to form fibrils. Therefore, it is the main component of extracellular amyloid plaques.
GFAP	Glial fibrillary acidic protein that forms the astroglial intermediate filaments. Commonly used as a specific marker of astrocytes.
Iba-1	Ionized calcium binding adapter molecule 1 expressed specifically by microglial cells and peripheral macrophages. This marker is commonly used to detect microglial cells in the brain.

Table 2.2. List of markers studied by immunohistochemistry.

Primary antibody	Manufacturer (reference)	Animal	Dilution	Incubation time	Incubation Temp.
Anti- 4G8	Biolegend (800708)	Mouse	1/1,000	24 h	R.T.
Anti- Aβ40	Millipore (AB5074P)	Rabbit	1/1,000	24 h	R.T.
Anti-Aβ42	Biolegend (805509)	Mouse	1/1,000	24 h	R.T.
Anti-GFAP	Abcam (ab7260)	Rabbit	1/1,000	24 h	R.T.
Anti-Iba1	FUJIFILM Wako (019-19741)	Rabbit	1/1,000	24 h	R.T.

Table 2.3. List of primary antibodies used for immunohistochemistry. Temp: Temperature. R.T.: Room Temperature.

Primary antibody	Manufacturer (reference)	Animal	Dilution	Incubation time	Incubation Temp.
Anti-Rabbit IgG	GE Healthcare (LNA934V/AG)	Donkey	1/500	1 h 30 min	R.T.
Anti-Rabbit IgG	Vector Labs (BA-1000)	Goat	1/500	1 h 30 min	R.T.
Anti-Mouse IgG	Vector Labs (BA-9200)	Goat	1/500	1 h 30 min	R.T.

Table 2.4. List of secondary antibodies used for immunohistochemistry. Temp: Temperature. R.T.: Room Temperature.

2.2.12. Immunofluorescence

This technique is similar to light microscopy but instead of being based on a peroxidase reaction (HRP-conjugated secondary antibody), a secondary antibody that has a photostable fluorescent dye attached is used. Stained samples are imaged by exciting them at a certain wavelength depending on the fluorescent dye used. The main advantage of this technique is the possibility to co-label two or more markers with different fluorescence colors (i.e., microglia in red, astrocytes in green and cells nuclei in blue) and analyze several markers in the same section to see whether these markers colocalize. This technique was specifically performed for our qualitative analysis of microglial and astroglial cells, as well as for our colocalization studies. The fluorescence IHC in our formalin-fixed paraffin-embedded (FFPE) brain slices was performed as follows:

- Rinsing sections (3 x 10 minutes) with PBS to remove any EtOH/H_2O or antigen retrieval buffer from the tissue.
- Incubation overnight with the appropriate primary antibody diluted in PBS with 0.2% Triton X-100 (See dilutions and conditions in **table 2.3**).
- Rinsing sections (3 x 10 minutes) with PBS.
- Incubation for 1 hour and 30 minutes with the corresponding Alexa Fluor®-conjugated secondary antibody diluted in PBS (See dilutions and conditions in **table 2.5**).
- Rinsing sections (3 x 10 minutes) with PBS.
- Coverslip slides with VECTASHIELD® Antifade Mounting Medium with DAPI (Vector Labs, Cat. No: H-1200-10, USA).

All rinsing steps were carried out with constant gentle shaking and always in complete darkness to avoid fading of the fluorescent dye. When double immunostaining was performed, both primary antibodies were incubated in separate by incubating them overnight with the first primary antibody, washing them 3 times for 10 minutes with PBS and incubating them with the second primary antibody overnight. In these co-labeling experiments, incubation in secondary antibodies was done simultaneously adding both secondary antibodies in the same step and following the protocol as stated above.

Primary antibody	Manufacturer (reference)	Animal	Dilution	Incubation time	Incubation Temp.
Alexa Fluor® 594-Anti-Rabbit IgG	Invitrogen (A-11037)	Goat	1/500	1 h 30 min	R.T.
Alexa Fluor® 488-Anti-Mouse IgG	Invitrogen (A-11001)	Goat	1/500	1 h 30 min	R.T.

Table 2.5. List of secondary antibodies used for fluorescent immunohistochemistry. Temp: Temperature. R.T.: Room Temperature.

2.2.13. Thioflavin S staining

Thioflavin S (ThS) is fluorescent dye that binds to crossed β-pleated sheet structures and therefore stains fibrillar amyloid deposits (Bussière et al., 2004). In this sense, Thio-S is also able to bind to β-sheets of the neurofibrillary tangles. This dye was used to stain

dense-core amyloid plaques with the aim of observing differences in the structure/nature of the amyloid plaques formed after injection with the different inocula. To perform this staining, we carried out the following protocol:

- Rinsing sections (3 x 10 minutes) with PBS to remove any EtOH/H_2O from the tissue.
- Incubation for 10 minutes with 0.025% Thio-S (Millipore Sigma, Cat. No: T1892, USA) in 50% EtOH. In order to prepare this solution, powdered Thio-S was diluted in 50% EtOH and filtered through Whatman® grade filter paper.
- Rinsing sections (2 x 5 minutes) with 50% EtOH to wash the excess of Thio-S.
- Rinsing sections (3 x 10 min) with PBS to remove excess of ethanol.
- Dehydration of the slides in ascendant graded ethanol (70%, 80%, 90%, 95% and 100%, for 10 min each), cleared in xylene for 15 minutes and coverslipped with DPX mounting medium (Electron Microscopy Science DPX Mountant, Thermo Scientific™, Cat. No: 50-980-369, USA).

All rinsing steps were carried out with constant gentle shaking and always in complete darkness to avoid fading of the fluorescent dye.

2.2.14. Luminescent Conjugated Thiophenes (LCOs) staining of brain slices

The structural features of the amyloid plaques formed in the brain of Tg2576 animals injected with the two synthetic $A\beta_{40}$ fibrils (2F and 3F Fibrils), as wells as the deposits developed in animals injected with the Aged Tg2576 brain homogenate, were further evaluated by using a battery of luminescent conjugated oligothiophenes (LCOs) provided by Dr. K. Peter R. Nilsson. LCOs have great affinities with amyloids and have been previously shown to discriminate between α-synuclein strains (Shahnawaz et al., 2020) and different conformation of misfolded Aβ and tau deposits (Klingstedt et al., 2011, 2013; Nilsson et al., 2007). Here, based on our *in vitro* results with the 2F and 3F fibrils, we tested 2 different LCOs (HS-68 and HS-194, See **Table 2.1**). Stock solutions of luminescent conjugated oligothiophenes (LCOs) at 1.5 mM, were diluted in PBS to 15 µM and once again diluted in PBS to a final concentration of 300 nM. To perform this staining, we carried out the following protocol:

- Rinsing sections (3 x 10 min) with PBS to eliminate the excess of EtOH/H_2O from the tissue.
- Stain section with a combination of HS-68 and HS-194 LCOs at 300 nM diluted in PBS for 30 minutes at room temperature
- Rinsing sections (2 x 10 minutes) with PBS to remove any excess of dye
- Coverslip slides with VECTASHIELD® Antifade Mounting Medium with DAPI (Vector Labs, Cat. No: H-1200-10, USA).

All rinsing steps were carried out with constant gentle shaking and always in complete darkness to avoid fading of the LCOs fluorescence.

2.2.15. Preparation of brain-seeded fibrils for solid state nuclear magnetic resonance (ssNMR)

Aβ-containing extracts were prepared from mouse brain homogenates by following a protocol developed previously for ssNMR studies (Lu et al., 2013). Briefly, homogenates were thawed, added to 5 mL of buffer A (10 mM Tris-HCl, pH 7.5, 0.25M sucrose, 3 mM EDTA, 0.1% w/v NaN_3) with Complete Protease Inhibitor (Roche Diagnostics, Switzerland), then rotated end-over-end overnight at 4°C. After increasing the sucrose concentration to 1.2M, the mixtures were centrifuged at 220,000 x g for 60 minutes at 4°C. The resulting pellets were resuspended in 11 mL of buffer B (10 mM Tris-HCl, pH 7.5, 1.9M sucrose, 3 mM EDTA, 0.1% w/v NaN_3) and centrifuged again with the same conditions. Top layers were resuspended in 10 mL of Tris-HCl buffer (50 mM, pH 8.0) and centrifuged at 11,000 x g for 15 minutes at 4°C. Pellets were resuspended in 10 mL of Tris-HCl buffer with 2 mM $CaCl_2$ and 10 µg/mL of DNAse I, then incubated at room temperature for 60 minutes with orbital mixing. After pelleting again, pellets were resuspended in 4.5 mL of buffer C (10 mM Tris-HCl, pH 7.5, 1.3M sucrose, 3 mM EDTA, 0.1% w/v NaN_3, 1% w/v SDS), then centrifuged at 350,000 x g for 30 minutes at 4°C. Pellets were washed twice by resuspension in deionized water followed by centrifugation.

Fibrils for ssNMR measurements were then prepared by resuspending the pelleted extracts from mouse brain homogenates in 0.5 mL of 10 mM sodium phosphate buffer, pH 7.4, containing 0.1% w/v NaN_3. Suspensions were sonicated vigorously for 20 minutes (Branson S-259A sonifier with tapered 1/8" microtip horn, lowest power, 10% duty factor) to break amyloid into short fragments. Aliquots of isotopically labeled $Aβ_{40}$,

solubilized in DMSO and containing 0.22 mg of the peptide to produce $A\beta_{40}$ at 100 µM, were then added to the sonicated suspensions and mixed by vortexing. TEM images were recorded after 4 h of quiescent incubation at room temperature. Observation of abundant long fibrils confirmed seeded fibril growth, as control experiments without brain extract produced no detectable fibrils after 4 h incubation. Sample volumes were then increased to 2.5 mL by addition of the same buffer and DMSO-solubilized, isotopically labeled $A\beta_{40}$ was added to restore the total peptide concentration to 100 µM (1.1 mg total peptide). Samples were then incubated at room temperature for an additional 4-5 days, after which TEM images were recorded again. To maximize conversion of monomeric $A\beta_{40}$ to fibrils, samples were given a 10 s burst of sonication once every hour for the first 24 hours (Qsonica model Q55 sonifier, 1/8" horn, power level 20, controlled by an Omega PTC-16 timer). Aside from these brief sonication bursts, incubation was quiescent.

Finally, fibrils were pelleted, resuspended in deionized water, pelleted again, and lyophilized. Lyophilized material (containing ≤ 1 mg of isotopically labeled fibrils in a larger quantity of non-fibrillar material from the brain tissue) was then packed into 1.8 mm-diameter magic-angle spinning (MAS) rotors for ssNMR measurements and fully rehydrated by addition of 10 mM sodium phosphate buffer to the rotor.

2.2.16. Solid state nuclear magnetic resonance (ssNMR)

ssNMR spectra were acquired at 17.5 T (187.5 MHz ^{13}C NMR frequency, 75.6 MHz ^{15}N NMR frequency), using a Varian InfinityPlus spectrometer and a 1.8 mm magic-angle spinning (MAS) probe obtained from the laboratory of Dr. Ago Samoson (Tallinn University of Technology, Estonia). MAS frequencies were 17.00 kHz. Sample temperatures were 25°C ± 1°C. All measurements used standard cross-polarization techniques for ^{1}H-^{13}C, ^{1}H-^{15}N, and ^{15}N-^{13}C polarization transfers, and two-pulse phase-modulated ^{1}H decoupling with a 100 kHz radio-frequency (rf) field amplitude (Bennett et al., 1995). 2D ^{15}N-^{13}C spectra were obtained in 2.0-3.5 days, using maximum t_1 values of 7.35 ms, t_1 increments of 49.0 µs, and 1.0 s recycle delays. Similar conditions were used to obtain 2D spectra of synthetic 2F and 3F fibrils (grown *in vitro*, not seeded with brain extract), which were used for the comparisons.

Data were processed with NMRPipe software (Delaglio et al., 1995). Pure Gaussian apodization functions were used, corresponding to 0.8 ppm and 1.3 ppm line-broadening in ^{13}C and ^{15}N dimensions, respectively, without artificial resolution enhancement. ^{13}C and ^{15}N chemical shifts are relative to 4,4-dimethyl-4-silapentane-1-

sulfonic acid (DSS) and liquid ammonia, respectively, based on an external standard of 1-^{13}C-L-alanine powder at 179.65 ppm relative to DSS. Contour levels in plots of 2D ^{13}C-^{13}C and 2D ^{15}N-^{13}C spectra increase by successive factors of 1.4 and 1.2, respectively.

It is worth mentioning that both the preparation of brain-seeded fibrils for solid state nuclear magnetic resonance (ssNMR) (**Section 2.2.15**) and the ssNMR experiment itself (**Section 2.2.16**) was performed by the lab of Dr. Robert Tycko.

2.2.17. Image captures

2.2.17.1. Immunolabeling and other stainings

Immunostained sections, as well as those stained with Thio-S and LCOs, were visualized in a dual (bright field and fluorescence) microscope (DMI6000B microscope from Leica Microsystems, Germany) connected to a computer with the Leica Application Suite (LAS) software from Leica Microsystems (Germany). Photomicrographs of samples were taken with a digital camera (DFC310 FX Leica, Germany). The camera settings were adjusted at the beginning of the experiment and maintained for uniformity. All images were captured with a 2560x1920 size in .tiff format.

2.2.17.2. Image processing

All images were processed using the software Adobe PhotoShop 22.4.1 version (2021), modifying size and bright/contrast in the complete image when needed. Images from the same experiment were modified in the same manner. Then, figures were prepared using the Adobe Illustrator, version 25.2.3 (2021), software.

2.2.18. Image analysis and quantification

2.2.18.1. Loading analysis: amyloid plaques, microglia and astrocytes

Digital images (6 sections/animal), obtained with the digital camera (DFC310 FX Leica, Germany) of the microscope (DMI6000B, Leica Microsystems, Germany), were analyzed using the ImageJ software (National Institutes of Health). The areas specifically labelled for amyloid plaques or glial cells (microglia and astrocytes), were selected in 8 bit gray-scale images by dark-level threshold, which was maintained throughout the experiment for uniformity. Then, the areas positive for that threshold (red in **Figure 2.7D**) within the selected regions (yellow in **Figure 2.7C**) were calculated. The dentate gyrus,

hippocampus, hippocampal formation, alveus or subiculum were manually outlined in each 5x (or 10x) image (yellow in **Figure 2.7C**) and area of the selected region was calculated. In order to calculate the percentage of the area occupied by the immunolabeled structure (optical density of the immunostained structures) or dye-labeled plaques, we divided the area with positive threshold in the binary image (red in **Figure 2.7D**) by the whole dentate gyrus, hippocampus, hippocampal formation, alveus or subiculum surfaces area (see **Figure 2.7**). Finally, data were expressed as mean and SEM. Quantitative comparisons were performed on sections processed at the same time.

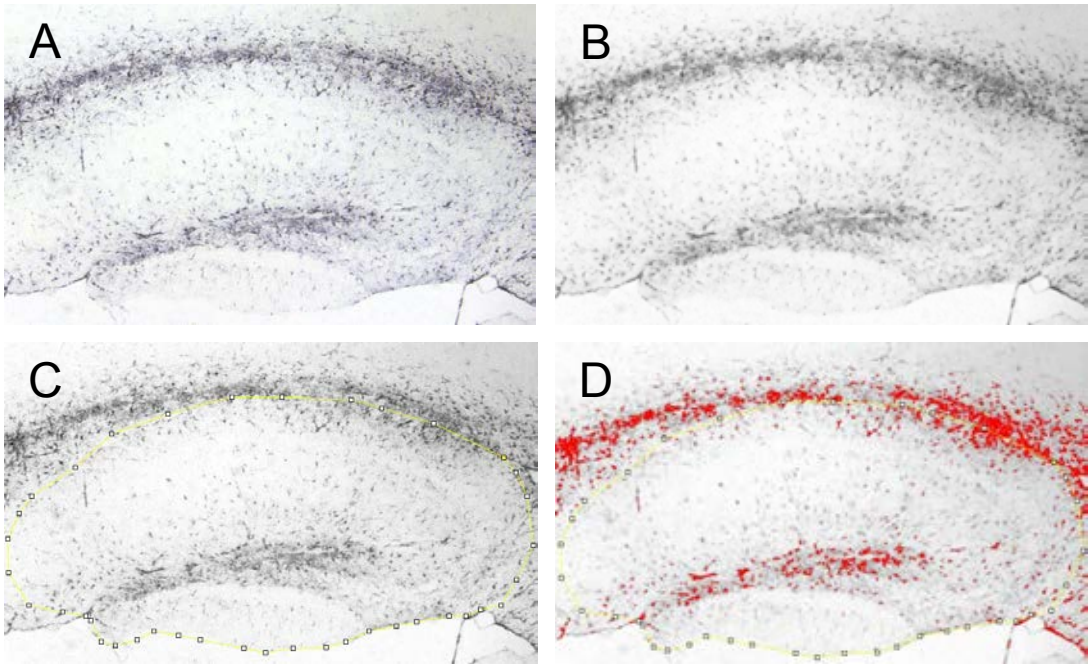

Figure 2.7. Loading analysis with ImageJ (National Institutes of Health, USA). In order to perform this analysis, we followed these steps: 1) Conversion of the immunostaining (with anti-GFAP in this case) picture to an 8-bit gray-scale picture **(A to B)**. 2) Manual outlining of the studied region (**C**, in yellow, Hippocampal formation). 3) Manual setting of the dark-level threshold (**D**, in red, GFAP-positive area) to quantify immunolabeled-positive Area. 4) Automatic quantification with the ImageJ software of the area of the outlined (inside yellow line) surface and the area occupied by immunolabeled-positive cells (in red) inside the outlined area. In order to calculate the area occupied by the immunolabelled structures, we divided the immunolabeled-positive area (in red, **D**) by the total area of the outlined (yellow line) surface.

2.2.18.2. Cerebral amyloid angiopathy (CAA) analysis

Analysis of blood vessels containing amyloid deposits, also known as cerebral amyloid angiopathy (CAA), was perform by manually counting the total amount of meningeal vessels and the number of 4G8-positive meningeal vessels. The total percentage of CAA-positive vessels was calculated following this formula:

$$\%\ 4G8+\ vessels\ =\ \frac{Total\ \#\ 4G8+\ vessels}{Total\ \#\ of\ vessels}$$

2.2.18.3. Lateral Ventricles Visual Score analysis

Quantification in the lateral ventricle was performed by analyzing plaques that surround the lateral ventricles and giving a visual score ranging from 0 (no plaques) to 10 (plaques found in the tissue with more plaques). Given the subjectivity of this measurement, this was performed blinded by 2 independent researchers (Ruben Gomez-Gutierrez and Katherine Do) and data was compared and analyzed together.

2.2.19. Statistical analyses

Every *in vitro* experiment of this work was carried out at least twice, and the data were expressed as mean ± SEM. In the case of the *in vitro* aggregation assays, the reactions were always performed in quintuplicates (5 replicates for the same condition). The comparison between mice groups in the first part of this thesis (monomeric $A\beta_{40}$, aged Tg2576 brain homogenate, 2F- and 3F-fibrils injected mice), both for histology and molecular measurements, was done by One-way ANOVA and Tukey as *post-hoc* test using the GraphPad Prism 9 software (GraphPad Software Inc, USA). The comparison between mice groups in the second part of this thesis (uninjected, CsgA-, Mcc- and TasA-fibrils injected mice), both for histology and molecular measurements, was also analyzed by One-way ANOVA and Tukey as *post-hoc* test using the GraphPad Prism 9 software. For all analysis, the significance was set at 95% of confidence and thus p values of less than 0.05 (*), 0.01 (**), and 0.001 (***) were considered statistically significant. p values higher than 0.05 were considered nonsignificant (N.S.).

3. Results

3.1. THE 2F AND 3F SYNTHETIC Aβ$_{40}$ FIBRILS SHOW DISTINCT STRUCTURAL AND BIOCHEMICAL FEATURES

3.1.1. 2F and 3F aggregates are polymorphic at the molecular structural level.

To test our hypothesis and study the pathological features of conformational variants of misfolded Aβ, we used the previously described 2F and 3F synthetic Aβ$_{40}$ fibrils (Petkova et al., 2005). Importantly, it has been previously shown by the research group of Dr. Robert Tycko (NIH, Bethesda, USA) using transmission electron microscopy (TEM) that these particular Aβ morphotypes show distinct morphological (width and twist period of the fibrils) and molecular (i.e. distinctive Mass per length, MPL) features (Petkova et al., 2005). Since additional 2F and 3F fibrils were synthetized by Dr. Tycko lab for this work, our initial approach was to show that these unique morphological and molecular features are retained in the newly synthesized fibrils. First, we visualized these aggregates by TEM and observed that the two polymorphs show morphological differences in their width and twist (**Figure 3.1A and B**) that correlated well with the differences found in structure at the molecular level (data not shown, observed by Dr. Tycko).

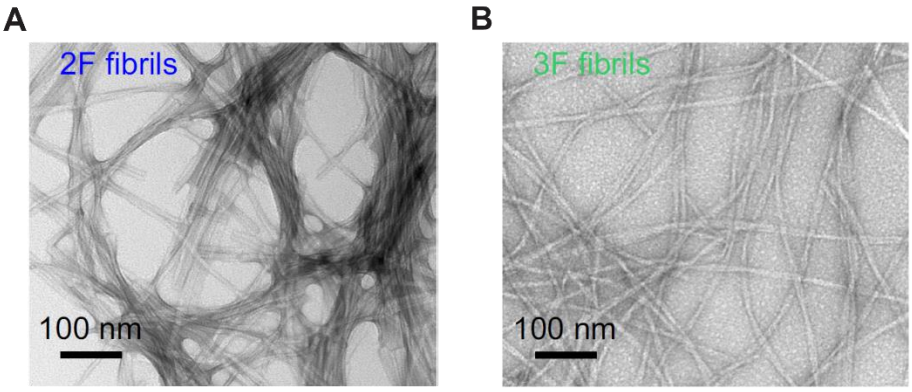

Figure 3.1. Ultrastructural properties of 2F and 3F fibrils. Electron micrographs of 2F **(A)** and 3F **(B)** fibrils provided by professor Dr. Robert Tycko (NIH, Bethesda, USA).

3.1.2. Biochemical characterization of 2F and 3F fibrils demonstrates their distinct prion-like properties.

In order to analyze the biochemical properties of the 2F and 3F aggregates, we employed tools similar to those used to characterize prion strains (Morales, 2017; Shahnawaz et al., 2017b, 2020). Specifically, the aggregates were tested for their specific

resistance to proteolytic degradation using increasing concentrations of proteinase K (PK). Our results show that 2F and 3F fibrils were clearly distinguishable by their biochemical properties, with 2F fibrils displaying a significant higher resistance to proteolytic digestion compared to 3F fibrils (**Figure 3.2A and B**).

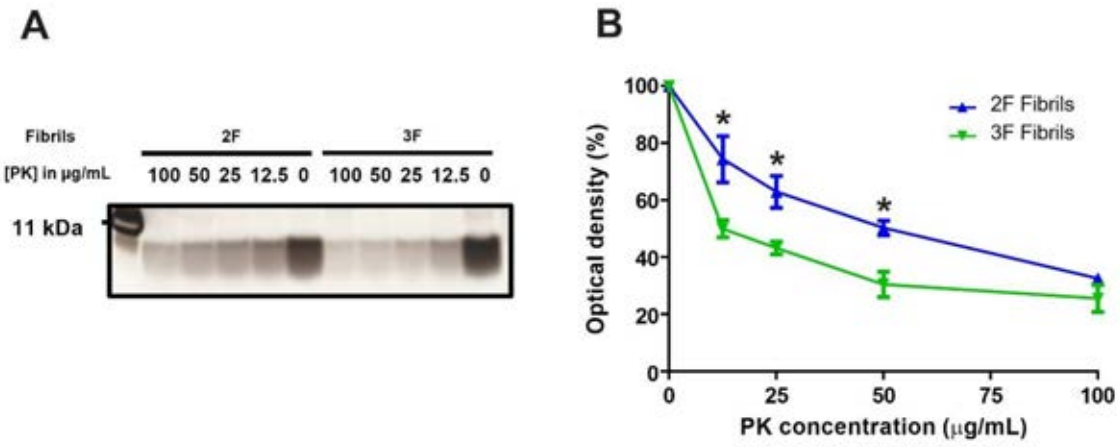

Figure 3.2. Proteolytic resistance of 2F and 3F fibrils. (A) PK resistance profile of 2F (blue in B) and 3F (green in B) fibrils. 11 KDa in the left lane represents a molecular weight marker. **(B)** Quantification of Aβ-PK resistant values depicted in **(A).** Values are expressed as the mean densitometric value (percentage in optical density) in each time point (triplicates) ± standard error. Statistical analyses were performed using student's t-test for each data point. * $p<0.05$.

Previous studies have shown that *in vitro* aggregation assays monitored by the fluorescence signal of thioflavin T (ThT) are capable of distinguishing amyloid fibrils with diverse molecular structures. Amyloid fibrils with different conformational structure not only show distinct rate ("speed") of aggregation but also show differences in maximum ThT fluorescence signal (Shahnawaz et al., 2020). Therefore, we tested the *in vitro* seeding activity of 2F and 3F aggregates using the Protein Misfolding Cyclic Amplification (PMCA) technique modified for Aβ. The PMCA technology was originally developed to replicate infectious prions in an accelerated manner and in cell-free conditions (Morales et al., 2012b). Further modifications on this technology allowed its use for misfolded Aβ (Salvadores et al., 2014), α-synuclein (Shahnawaz et al., 2017b) and tau aggregates (data not published). Importantly, in this thesis, the PMCA technique has been further implemented to faithfully offer a consistent assay using recombinant, lab purified, $A\beta_{40}$ protein (**Figure 3.3**) and allowed us to distinguish between conformational variants of $A\beta_{40}$. Purified, aggregate-free $A\beta_{40}$ was tested at 2 different concentrations, 1

µM (**Figure 3.3A and B**) and 2 µM (**Figure 3.3C and D**) This allowed as to reach a critical concentration that would aggregate with an extended lag phase long enough to differentiate between the seeded and the non-seeded aggregations. Specifically, monomeric Aβ40 was incubated in 100 mM Tris-HCl buffer, pH 7.4 and 5 µM ThT, at 20°C with cycles of 1-minute agitation every 30 minutes. Wells containing aggregate-free Aβ40 were seeded with decreasing concentrations of Aβ40 fibrils (Seed) to test which of the 2 concentrations would allow us for a better separation between the different concentrations of seeds, in order to have an assay that is concentration-dependent. Protein aggregation was measured by ThT fluorescence and graphs fitted using Boltzmann equation. We found that Aβ40 aggregation at 1 µM (**Figure 3.3A and B**) had both a longer lag phase (~120 hours vs ~40 hours) than the 2 µM assay (**Figure 3.3C and D**). It displayed a concentration-dependent aggregation, with higher concentration of seeds (Blue line) inducing a faster aggregation than lower concentration seeds (Red line) or non-seeded aggregations (Black line). Importantly, reactions containing only seeds and without monomeric Aβ40 added to the assay (Orange line in **Figure 3.3A and C**) show no ThT fluorescence increase, further showing that the rise in ThT signal is due to the formation of new Aβ40 fibrils that are nucleated by the seeds and not from the seeds itself.

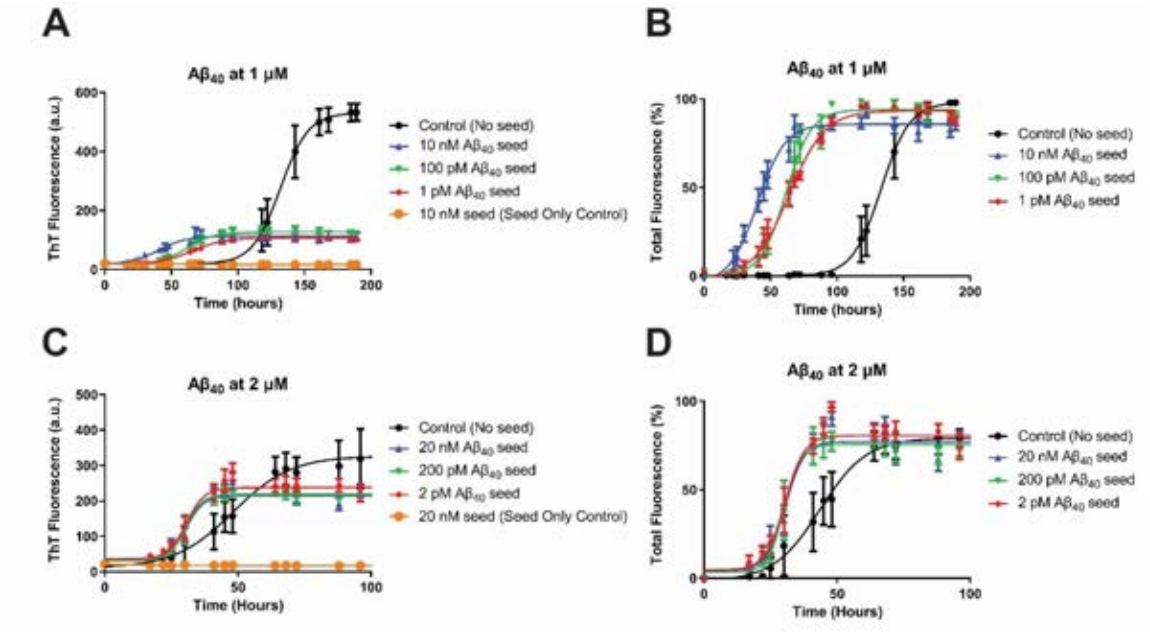

Figure 3.3. Aβ PMCA optimization. *In vitro* Aβ PMCA using aggregate-free Aβ40 at 1 µM **(A and B)** and 2 µM **(C and D)** and different concentrations of Aβ40 fibrils as seeds. Left graphs display graphs with raw data of the mean fluorescence **(A and C)** while right graphs show normalized values as percentage of total aggregation **(B and D)**. Graphs were fitted using Boltzmann equation.

After standardizing the PMCA for Aβ aggregation quantification, we tested 2F and 3F fibrils seeding capability *in vitro*. Similarly, to previously shown, 2F and 3F fibrils were used to act as seeds in the ThT fluorescence assay. Specifically, 3F fibrils displayed a considerably faster seeding activity compared to the 2F fibrils, as evaluated by the time they take to seed 20% (61.77±5.05h vs 77.50±4.00h for 3F and 2F fibrils, respectively); 50% (80.68±3.11h vs 92.19±2.45h for 3F and 2F fibrils, respectively); and 90% (110.6±6.90h vs 115.5±6.04h for 3F and 2F fibrils, respectively) of maximum aggregation (**Figure 3.4A and C**). Importantly, Aβ aggregates generated by 2F and 3F seeding displayed different maximum ThT fluorescence signal at aggregation plateau (323.9±15.67 a.u. vs 129.9±12.66 a.u. at 125 h for 2F and 3F fibrils respectively, **Figure 3.4A and B**). This result further confirms the differential seeding properties of 2F and 3F and demonstrates the differential accessibility and reactivity of ThT to the Aβ aggregates generated by seeding (**Figure 3.4A and B**). Therefore, our assay, using 2F and 3F fibrils as seeds, provided us with relevant information that supported the idea that these two $A\beta_{40}$ *in vitro*-made fibrils have differential pathological activity of misfolded Aβ strains.

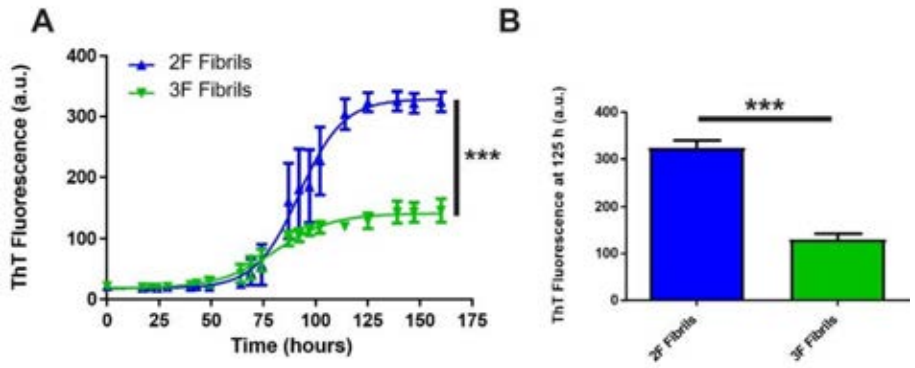

C

	2F Fibrils	3F Fibrils
T20	77.50 ± 4.00	61.77 ± 5.05
T50	92.19 ± 2.45	80.68 ± 3.11
T90	115.5 ± 6.04	110.6 ± 6.90

Figure 3.4. *In vitro* seeding activity of 2F and 3F fibrils. (A) Seeding assays using 100 pM of 2F (blue) and 3F (green) fibrils as seeds. Curves were generated by measuring ThT emission values at different time points. Reaction kinetics were statistically different as assessed by multiple comparisons method to compare pairs of curves. *** $p<0.001$. **(B)** Mean fluorescence (n=5) of the seeding reaction in (A) at 125 h. Statistical differences were assessed by student's t-test. *** $p<0.001$. **(C)** Table of the average time ± standard error at which fluorescence is 20% (T20), 50% (T50) or 90% (T90) of the maximum fluorescence for assays using 2F and 3F fibrils.

3.1.3. Amyloid-conformation-specific dyes confirms that 2F and 3F fibrils are different conformational strains of Aβ$_{40}$.

To further confirm the structural differences between the 2F and 3F fibrils, we tested these two synthetic Aβ aggregates with a battery of luminescent conjugated oligothiophenes (LCOs) provided by Dr. Peter Nilsson (Linköping University, Sweden). LCOs have great conformation-specific affinity for amyloid fibrils and have been previously shown to discriminate between α-synuclein strains (Shahnawaz et al., 2020) and different conformations of misfolded Aβ and tau deposits (Klingstedt et al., 2011, 2013; Nilsson et al., 2007). Here, we tested 9 different LCOs **(See Table 2.1 and Figure 3.5)**. Four of these molecules (HS-68, HS-194, HS-208 and HS-212) were able to discriminate between 2F and 3F fibrils. Specifically, 2F fibrils incubated with HS-68 showed a higher emission when excited at 440 nm, indicating that this conformation of Aβ induces a highly emissive state for HS-68 **(Figure 3.5A)**. Interestingly, 3F fibrils show a higher affinity for HS-194, HS-208 and HS-212 LCOs **(Figure 3.5B-D)**, further supporting the idea that 2F and 3F fibrils are different conformational strains of Aβ$_{40}$. It is worth mentioning that other LCOs, specifically p-FTAA **(Figure 3.6A)**, h-FTAA **(Figure 3.6B)**, HS-169 **(Figure 3.6D)** and HS-199 **(Figure 3.6E)**, revealed similar spectra for both fibrils whereas HS-167 slightly discriminated between the two conformational strains **(Figure 3.6C)**.

Altogether, these results indicate that 2F and 3F fibrils are structurally different at the biochemical and molecular levels. In addition, the findings also show evidence of differential seeding activity between these two conformational strains of Aβ$_{40}$. These data perfectly complement previous structural characterizations performed by the group of Dr. Tycko (Petkova et al., 2005).

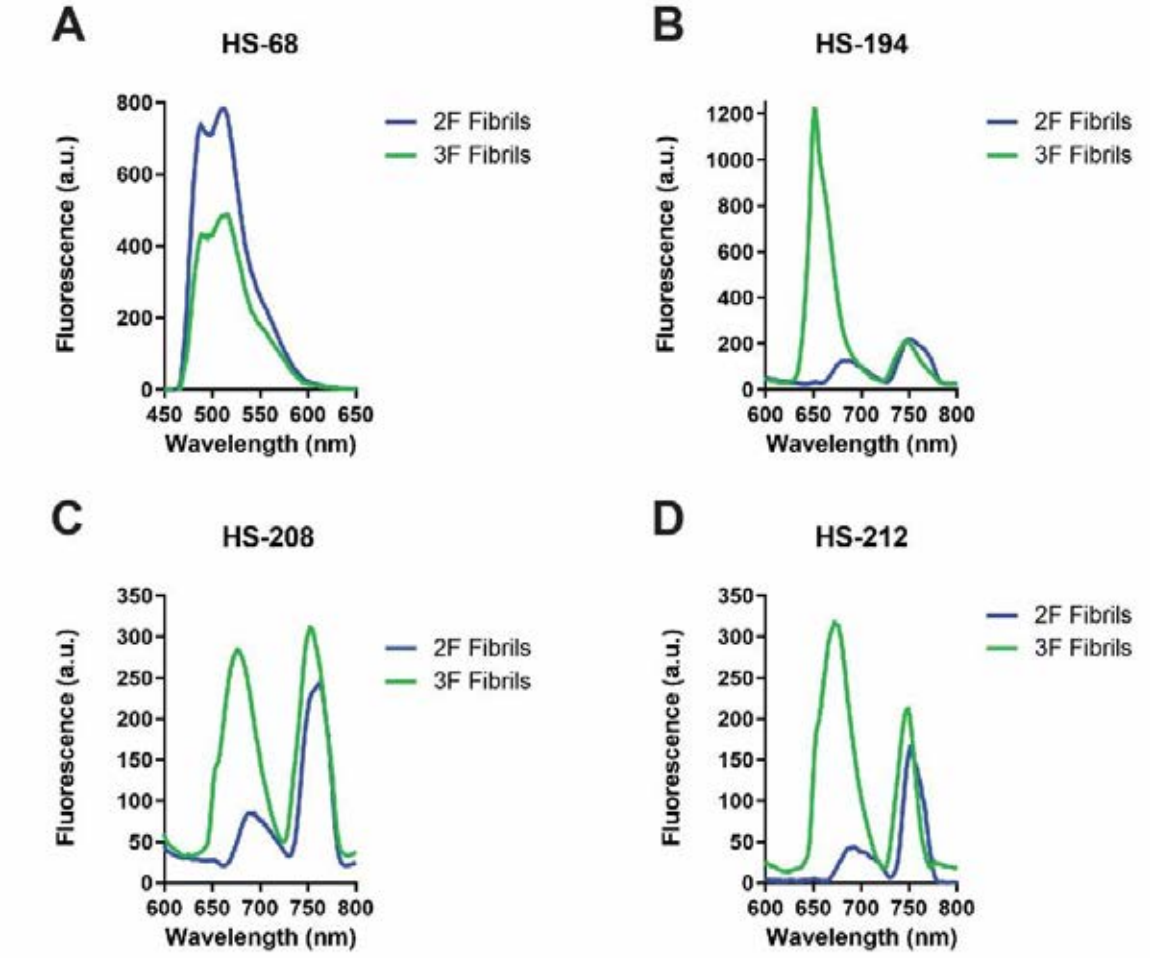

Figure 3.5. 2F and 3F fibrils structural difference by Luminescent Conjugated Thiophenes (LCOs). (A-D) 2F and 3F fibrils were tested for their reactivity against a variety of luminescent conjugated thiophenes (LCOs) able to discriminate among conformational variants of misfolded proteins. **(A)** 2F fibrils show higher excitation with HS-68 than 3F fibrils. **(B-D)** 3F fibrils show higher affinity to HS-194, HS-208 and HS-212 LCOs. All wells contained 10 μM of either 2F or 3F fibrils and LCOs at a final concentration of 0.3 μM. The samples were incubated at 37°C and the emission spectrum of each probe was collected after 30 minutes by exciting the samples at 440 nm (HS-68) or 535 nm (HS-194, HS-208 and HS-212).

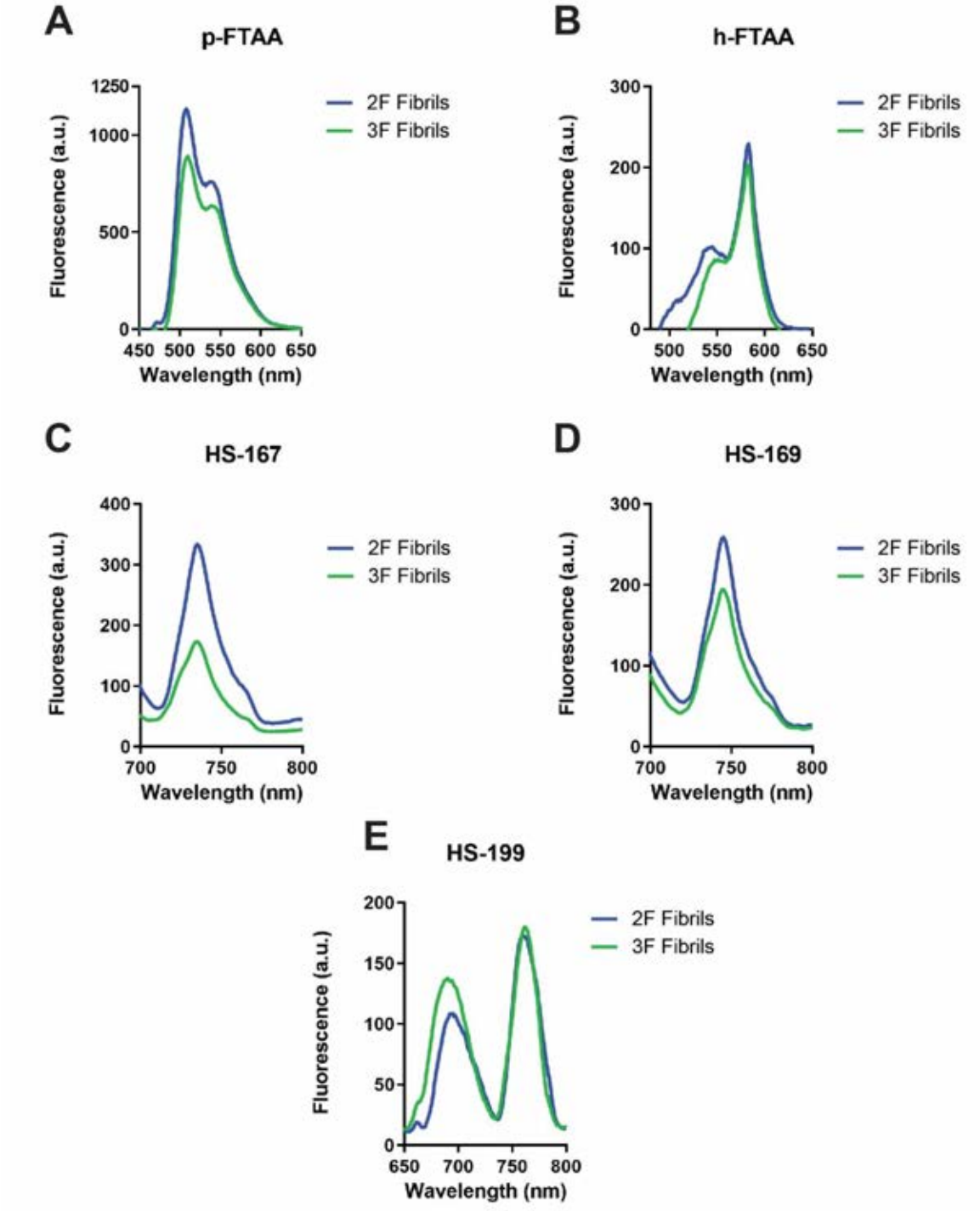

Figure 3.6. Luminescent Conjugated Thiophenes (LCOs) with 2F and 3F fibrils. (A-E) 2F and 3F fibrils were tested for their reactivity against a variety of luminescent conjugated thiophenes (LCOs). p-FTAA **(A)**, h-FTAA **(B)**, HS-169 **(D)** and HS-199 **(E)** shows none or slightly differences between the two synthetic fibrils. HS-167 **(C)** discriminate among conformational variants of misfolded proteins.

3.2. THE 2F AND 3F Aβ$_{40}$ CONFORMATIONAL STRAINS INDUCE DISTINCT PATTERNS OF BRAIN AMYLOIDOSIS AND GLIOSIS IN TG2576 TRANSGENIC MICE

3.2.1. Synthetic Aβ$_{40}$ conformational strains induce amyloid pathology in the brain of seeding-susceptible transgenic mice.

Currently, there is no clear evidence on whether Aβ conformational variants have any pathological or biological relevance in the context of Alzheimer's disease. To evaluate the significance of Aβ strains in Alzheimer´s pathology, we stereotaxically injected well-characterized 2F or 3F fibrils in both brain hippocampi of 50 days old Tg2576 mice (**Figure 2.2**; n=7/strain). Controls for these experiments included animals injected with either monomeric synthetic Aβ$_{40}$ peptides from Biomatik, USA (negative controls; n=4) and 10% w/v brain extracts from old (15 months old) Tg2576 mice (positive controls; n=5) with proven seeding activities (Morales et al., 2015). Animals were euthanized by CO_2 inhalation and brains collected at 300 days of age. At this timepoint, non-treated transgenic mice displayed small amount of Aβ deposits (Hsiao et al., 1996). A short-time group (n=5/strain), in which animals were euthanized at 150 days of age, was used as a control for seeding. In this control group, we expected to see none or just scarce Aβ deposits, since seeding-nucleation polymerization *in vivo* usually takes more than 100 days of incubation in the Tg2576 mice model (Morales et al., 2015). Collected brains from the euthanized mice were separated in both hemispheres, keeping one frozen for biochemical analyses while the other was preserved for histopathological studies (**Figure 2.2A**). Frozen brain hemispheres were homogenized and prepared to isolate PBS-soluble cytokines and PBS-insoluble Aβ peptides as described in methods. Levels of Aβ$_{40}$ and Aβ$_{42}$ were measured from the PBS-insoluble S2 fractions by using commercially available protein-based multiplex immunoassay. Results from this analysis showed that Aβ$_{40}$ levels were not significantly different among the experimental groups (**Figure 3.7A**). As expected, animals injected with brain extract from aged Tg2576 (labeled as "Old Tg BH") showed significant higher level ($F(3,19) = 38.93$, $p < 0.0001$) of PBS-insoluble Aβ$_{42}$ compared to all the other groups (**Figure 3.7B**). Although reduced compared to mice injected with the old Tg2576 brain, animals treated with 2F fibrils displayed significantly higher accumulation of Aβ$_{42}$ (**Figure 3.7B**) compared to the ones challenged with either monomeric Aβ$_{40}$ ($F(3,19) = 38.93$, $p = 0.0385$) or 3F fibrils ($F(3,19) = 38.93$, $p = 0.0074$). When Aβ$_{40}$ and Aβ$_{42}$ levels were combined, a significant

raise of these two Aβ species together in mice treated with the aged Tg2576 brain extract and 2F fibrils was found compared to 3F injected mice and the monomeric $A\beta_{40}$ control (**Figure 3.7C**; $F(3,19) = 12.00$, $p = 0.0009$ (Old Tg BH vs Monomeric $A\beta_{40}$), $p = 0.0004$ (Old Tg BH vs 3F Fibrils), $p = 0.03$ (2F Fibrils vs Monomeric $A\beta_{40}$) and $p = 0.0286$ (2F Fibrils vs 3F Fibrils)). Importantly, the $A\beta_{42}/A\beta_{40}$ ratio did not change in mice injected with either the conformational Aβ strains or monomeric $A\beta_{40}$ and was significantly increased in the positive control group (**Figure 3.7D**) when compared to animals injected with monomeric $A\beta_{40}$ ($F(3,19) = 12.49$, $p = 0.0061$), 2F fibrils ($F(3,19) = 12.49$, $p = 0.0004$) or 3F fibrils ($F(3,19) = 12.49$, $p < 0.0001$). These results further confirmed that presence of $A\beta_{42}$ was more abundant in mice injected with aged Tg2576 brain extracts (**Figure 3.7B**), as expected since the inoculum contains more $A\beta_{42}$ than $A\beta_{40}$ while the two synthetic fibrils are made with $A\beta_{40}$ and will induce more aggregation of $A\beta_{40}$ (homologous seeding). Nevertheless, one of the limitations of this particular analysis was that the results were representative only of the PBS-insoluble S2 fractions. Further studies using the PBS-soluble fraction would be informative on the induction of soluble Aβ species by the different inocula.

3.2.2. Each $A\beta_{40}$ conformational strain induces a unique type of amyloid pathology with brain region-specific tropism in the Tg2576 transgenic mice.

Since results in **section 3.2.1** were representative of whole brain hemispheres, potentially diluting increased seeding events that could be restricted to a particular brain region, the Aβ levels and specific location (tropism) of the induced amyloid deposits were analyzed in the other hemisphere by Aβ immunolabeling (using the monoclonal 4G8 antibody) and Thioflavin-S staining, a dye known to bind dense-core amyloid plaques but not diffuse Aβ deposits. We observed striking differences, specifically in the injected site (hippocampus). Mice treated with monomeric $A\beta_{40}$ peptides displayed slight amount of Aβ deposits by using both 4G8 immunostaining (**Figure 3.8A**) and ThS staining (**Figure 3.8E**). This was corroborated by quantitative image analysis (burden) of amyloid deposits labeled with 4G8 antibody (**Figure 3.8I and K**) and ThS (**Figure 3.8J and L**) in both the hippocampus (Includes alveus and is labeled as "Hippocampus", **Figure 3.8I and J**) and the hippocampal formation, which includes dentate gyrus, hippocampus proper and subiculum but not alveus (**Figure 3.8K and L**), similar to what has been described for untreated mice at the same age (Hsiao et al., 1996).

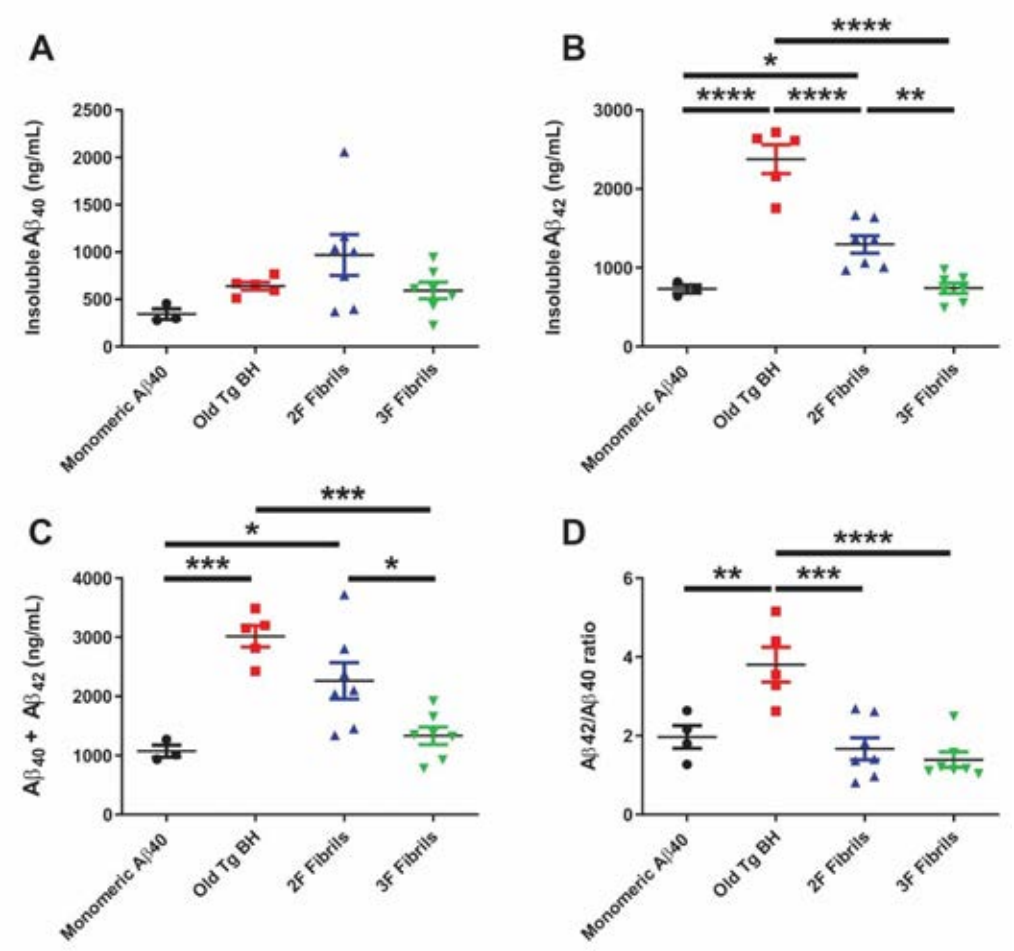

Figure 3.7. Analysis of Aβ$_{40}$ and Aβ$_{42}$ levels in PBS-insoluble fractions by protein-based multiplex immunoassay in Tg2576 animals 250 days post-injection. Levels of insoluble Aβ$_{40}$ (A) and Aβ$_{42}$ **(B)** were measured with a commercially available multiplex immunoassay. **(C)** Levels of both proteins were also added to quantify the total amount of both proteins. **(D)** Ratio of Aβ$_{42}$/Aβ$_{40}$ shows clear increase in the positive controls (animals injected with old Tg2576 brain homogenate). Statistical analyses were performed using One-way ANOVA (*p<0.05, **p<0.01, ***p<0.001, ****p<0.0001).

Furthermore, the group of mice injected with the brain homogenate from old Tg2576 animal showed abundant diffuse (4G8-positive and ThS-negative) amyloid deposition across all hippocampal layers (**Figure 3.8B and F**). After quantification, a significant increase was found in 4G8-positive plaques in the hippocampus (**Figure 3.8I**) when compared to animals injected with monomeric Aβ$_{40}$ ($F(3,19) = 6.114$, $p = 0.0053$) or 3F fibrils ($F(3,19) = 6.114$, $p < 0.0103$), as well as in the hippocampal formation (**Figure 3.8K**) when compared to animals injected with monomeric Aβ$_{40}$ ($F(3,19) = 11.10$, $p = 0.00071$) 2F fibrils ($F(3,19) = 11.10$, $p = 0.0006$) or 3F fibrils ($F(3,19) = 11.10$,

p = 0.0008). These results were in agreement with previous reports using the same model (Morales et al., 2015). These aggregates were poorly reactive against ThS (**Figure 3.8F**), which resulted in no significant changes in the hippocampus (**Figure 3.8J**) and hippocampal formation (**Figure 3.8L**) of animals injected with the aged Tg2576 brain homogenate. Interestingly, brains injected with the synthetic $A\beta_{40}$ 2F or 3F aggregates displayed a unique pattern of amyloid deposition compared to those injected with the aged Tg2576 homogenate. 2F fibrils induced abundant amyloid deposition in the hippocampus of the Tg2576 mice by 300 days of age, displaying a significant increase in ThS-positive plaques (**Figure 3.8J**) when compared to animals injected with monomeric $A\beta_{40}$ ($F(3,19) = 5.139$, $p = 0.0043$). Intriguingly, Aβ deposits induced by 2F fibrils showed a marked tropism towards the alveus region (**Figure 3.9A**) and the dentate gyrus (**Figure 3.8C**), with little or scarce amyloid deposits in the hippocampus proper (CA1, CA2 and CA3 regions) or subiculum regions (**Figure 3.8C and G**). This marked tropism of Aβ deposits towards the alveus region in animals injected with 2F fibrils was confirmed by quantitative studies of both 4G8-positive (**Figure 3.9A and E**) and ThS-positive (**Figure 3.9B and F**) amyloid plaques that showed a significant increase in 4G8-positive Aβ plaques when compared to animals injected with monomeric $A\beta_{40}$ ($F(3,19) = 8.514$, $p = 0.0034$) or 3F fibrils ($F(3,19) = 8.514$, $p = 0.0019$) and a significant increase in ThS-positive Aβ plaques when compared to animals injected with monomeric $A\beta_{40}$ ($F(3,19) = 8.097$, $p = 0.0058$), 3F fibrils ($F(3,19) = 8.097$, $p = 0.0077$) or aged Tg2576 brain extract ($F(3,19) = 8.097$, $p = 0.0035$). In regard to extracellular Aβ deposits induced by the 3F fibrils, most of the deposits were restricted to the dentate gyrus (**Figure 3.8D and H**). The main difference in the amyloid plaques induced by the two synthetic Aβ fibrils, compared to the fibrils induced by the brain homogenate from aged Tg2576 mice, was their reactivity to the ThS dye. Specifically, synthetic fibrils-induced deposits were strongly reactive to ThS (**Figures 3.8 and 3.9**). These results further confirmed that deposits induced by synthetic fibrils have different molecular structure and tropism than those induced by brain homogenates of aged Tg2576 animals. These aggregates are also distinguishable to the ones that this model spontaneously develops at 15-16 months of age, which are mostly found in the cortex and subiculum and are both dense-core and diffuse deposits (Morales et al., 2015).

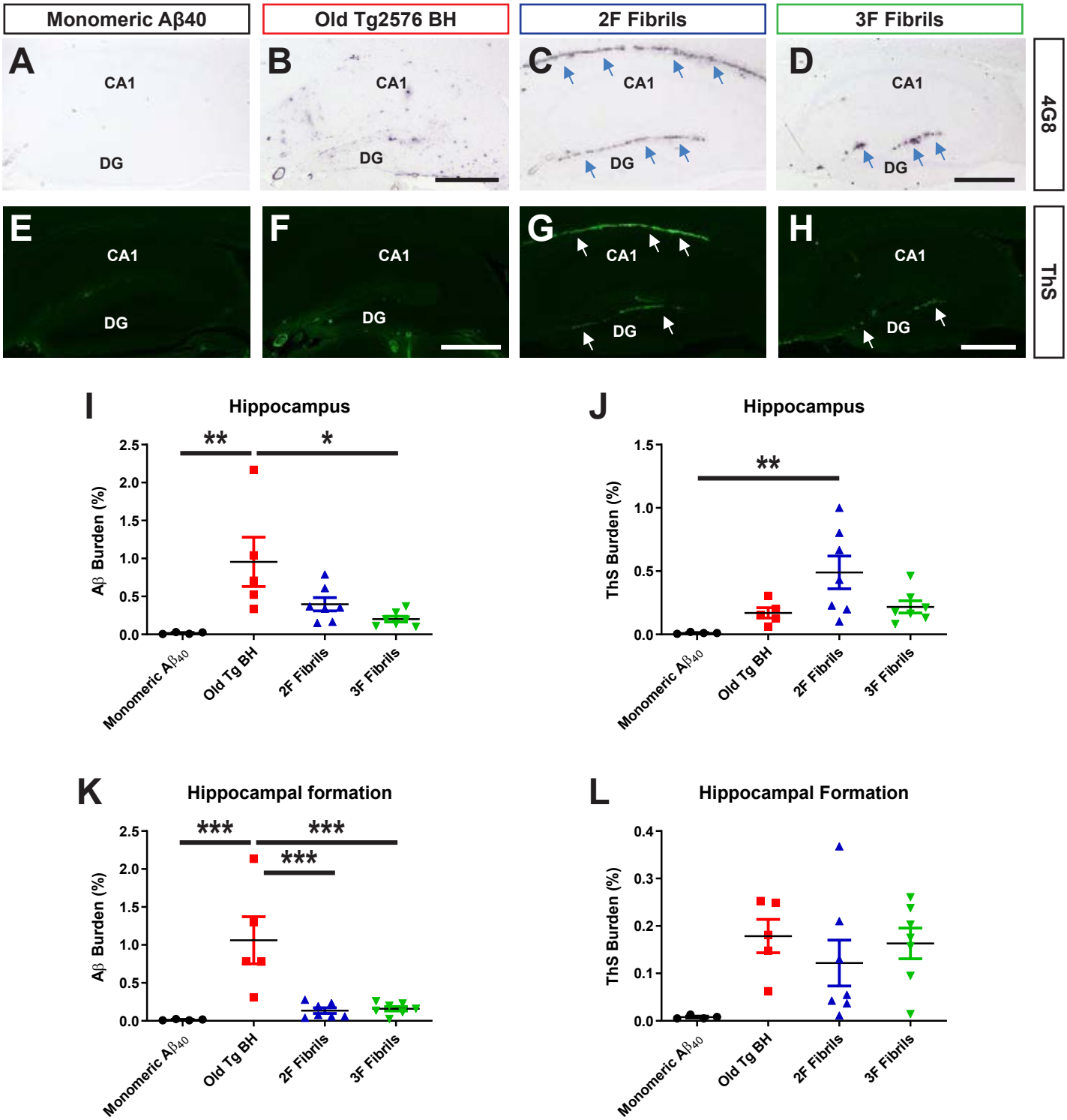

Figure 3.8. Amyloid pathology seeded by 2F and 3F fibrils, and brains extracts from old Tg2576 mice. Representative images of hippocampi from mice treated with 2F-, 3F- and Tg2576-derived seeds after visualization for Aβ deposits using the 4G8 antibody **(A-D)** or Thioflavin-S staining **(E-H)**. Aβ **(I)** and ThS **(J)** burden quantification in hippocampus. Aβ **(K)** and ThS **(L)** burden quantification in the hippocampal formation. *CA1: Cornu Ammonis area 1, DG: dentate gyrus*. Scale bar in **(D)** and **(H)** represents 500 µM and applies to all panels. Statistical analyses performed by One-way ANOVA * $p<0.05$, ** $p<0.01$ and *** $p<0.001$.

3.2.3. $A\beta_{40}$ conformational strains induce accumulation of Aβ in the lateral ventricles and in meningeal blood vessels in the Tg2576 transgenic mice.

An exhaustive quantitative analysis of the amyloid pathology induced in the Tg2576 mice showed differences in the lateral ventricle of animals injected with 2F seeds. These mice displayed a significant increase in both 4G8-positive ($F(3,19) = 28.74$, $p < 0.0001$) and ThS-positive ($F(3,19) = 42.73$, $p < 0.0001$) deposits in the subventricular zone (SVZ), as well as meningeal layers that surround the lateral ventricles when compared to controls and animals injected with the 3F conformational strain (**Figure 3.9C-D and G-H**). 3F fibrils-injected mice also showed increased deposition of 4G8-positive Aβ plaques ($F(3,19) = 28.74$, $p = 0.0316$) in the SVZ and surrounding meningeal layers of the lateral ventricles when compared to animals injected with monomeric $A\beta_{40}$ peptides (**Figure 3.9C-D and G**).

Since Aβ deposits around the lateral ventricles seemed to be mostly associated to the meningeal layers that surround these brain structures, we further explored whether 2F and 3F fibrils induced amyloid deposition in the meningeal blood vessels that surround the whole brain. Interestingly, we found that animals injected with the brain homogenate from aged Tg2576 mice displayed significant increase ($F(3,19) = 5.104$) in 4G8-positive blood vessels compared to 3F-injected mice ($p = 0.0178$) and the negative control group ($p = 0.0122$)(**Figure 3.10**). Naturally, non-treated Tg2576 animals display negligible levels of vascular amyloidosis, however, when challenged with either monomeric $A\beta_{40}$ or the two synthetic $A\beta_{40}$ fibrils, Tg2576 mice displayed increased vascular amyloidosis.

The unique tropism towards the lateral ventricles for Aβ deposits in animals injected with the 2F fibrils, together with the finding that animals injected with the brain homogenate from aged Tg2576 significantly increased their vascular Aβ deposition, further support the idea that Aβ fibrils found in aged Tg2576 brain homogenates, 2F-fibrils and 3F-fibrils represent three different conformational strains of Aβ.

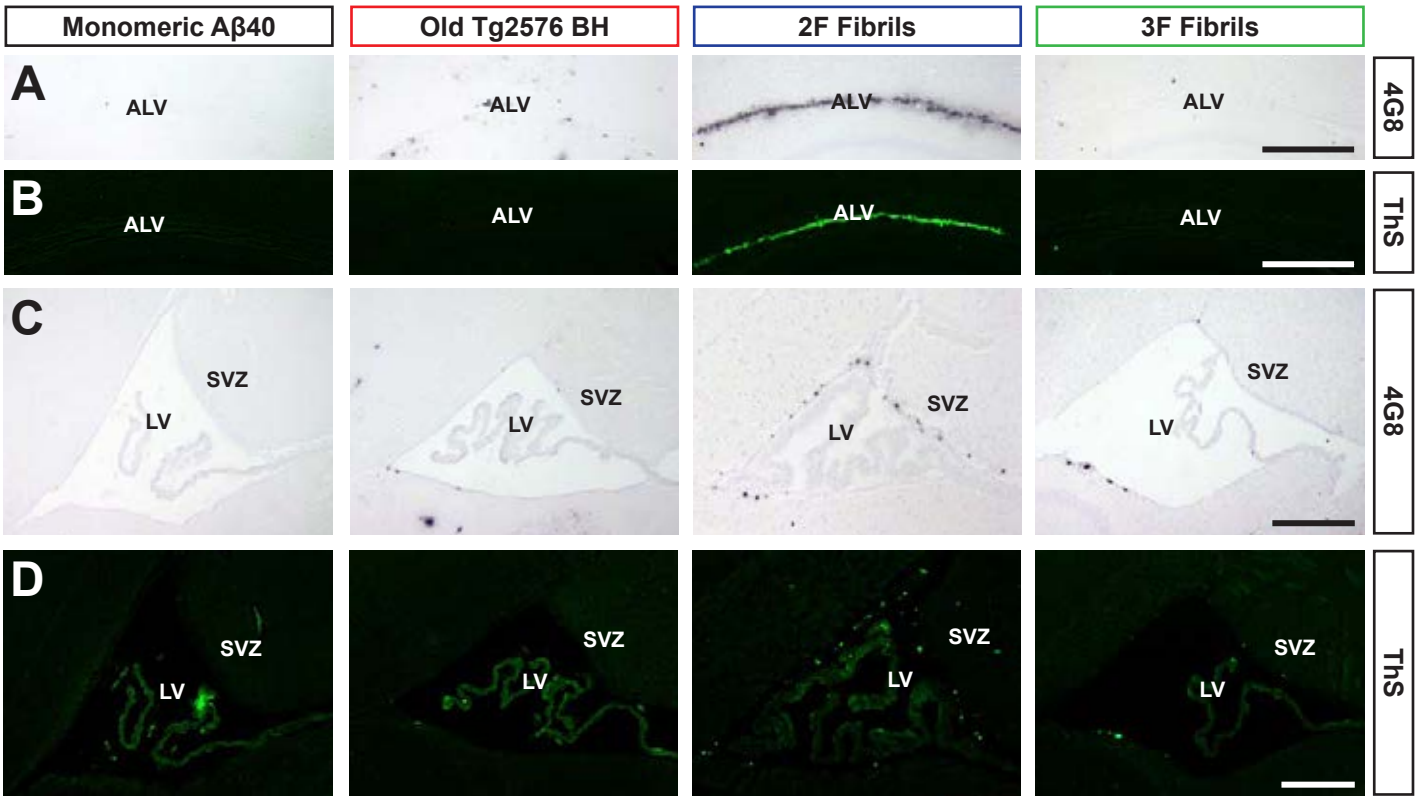

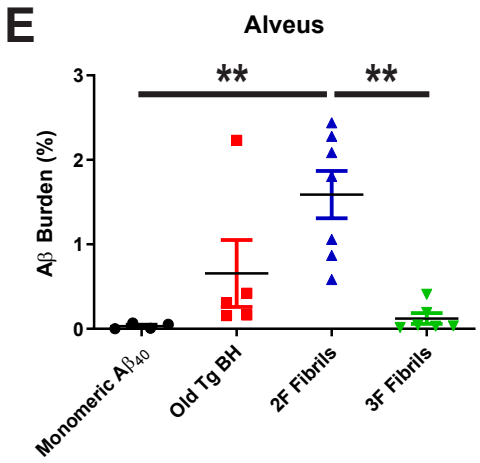

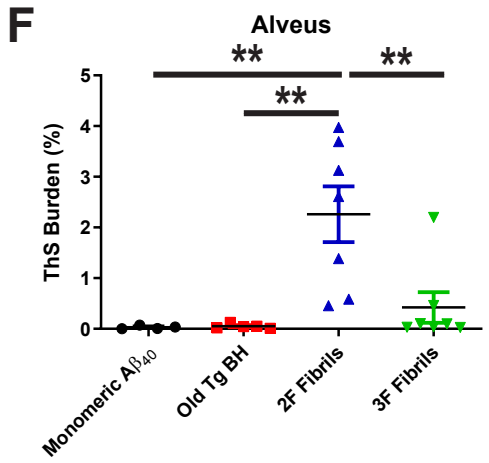

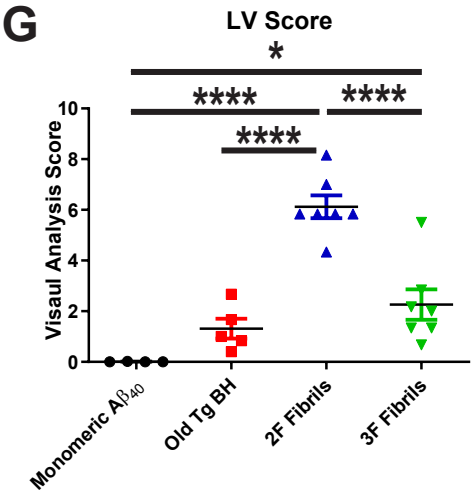

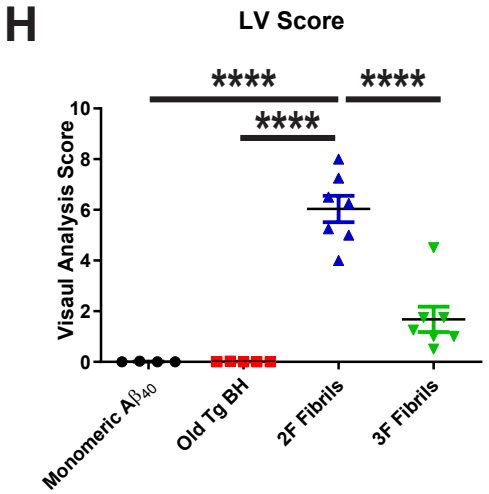

Figure 3.9. Region-specific, alveus and lateral ventricles, analyses of amyloid pathology in animals seeded by 2F and 3F fibrils, and brains extracts from old Tg2576 mice. Representative images of alveus from mice treated with 2F-, 3F- and Tg2576- derived seeds after visualization for Aβ deposits using the 4G8 antibody **(A)** or ThS staining **(B)**. Representative pictures of lateral ventricles from mice treated with 2F-, 3F- and Tg2576- derived seeds after visualization for Aβ deposits using the 4G8 antibody **(C)** or ThS staining **(D)**. Aβ **(E)** and ThS **(F)** burden quantification in alveus. Aβ **(G)** and ThS **(H)** quantification in the lateral ventricles. *ALV: Alveus, LV: Lateral ventricle, SVZ: Subventricular zone*. Scale bars at the right panels represent 500 µM and are applicable to all panels. Statistical analyses performed by One-way ANOVA (* $p<0.05$, ** $p<0.01$ and **** $p<0.0001$).

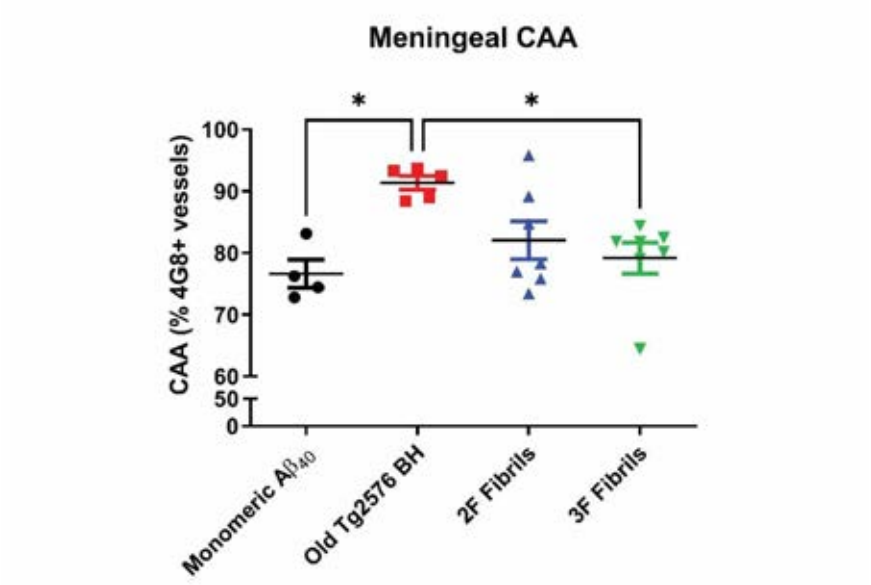

Figure 3.10. Quantification of meningeal Cerebral Amyloid Angiopathy (CAA) in animals injected with 2F and 3F fibrils, monomeric $A\beta_{40}$ and brains extracts from aged Tg2576 mice. Quantification of the percentage of total meningeal vessels that are 4G8-positive in the different animal groups. Statistical analyses performed by One-way ANOVA (* $p<0.05$).

3.2.4. Amyloid deposits found in synthetic fibrils-injected mice result from *de novo* generation of Aβ from the seeded mice and not from inoculum traces.

To confirm that the Aβ deposition in the injected mice, at 300 days of age, corresponded to accumulation of *de novo* generated endogenous Aβ aggregates seeded by administration of the synthetic fibrils and not from the seeds themselves, we injected Tg2576 mice with the same concentration of synthetic fibrils (10 µL of 1 mg/mL fibrils per brain hemisphere) and sacrificed the animals 100 days after exposure. Levels of $A\beta_{40}$ and $A\beta_{42}$ were again measured from the S2 fractions by using commercially available protein-based multiplex immunoassay. Results from this analysis show that both $A\beta_{40}$ and $A\beta_{42}$ levels were not significantly different between the two groups (**Figure 3.11**). Importantly, when we compared the levels of both $A\beta_{40}$ and $A\beta_{42}$ in animals euthanized 100 days post injection (**Figure 3.11**) with the levels of these peptides in animals euthanized 250 days post injection (**Figure 3.7**), we found that animals with longer incubation period displayed around 10 times higher concentration of these peptides (~500-1000 vs ~50 ng/mL for $A\beta_{40}$ and ~1500-2000 vs ~100-200 ng/mL for $A\beta_{42}$).

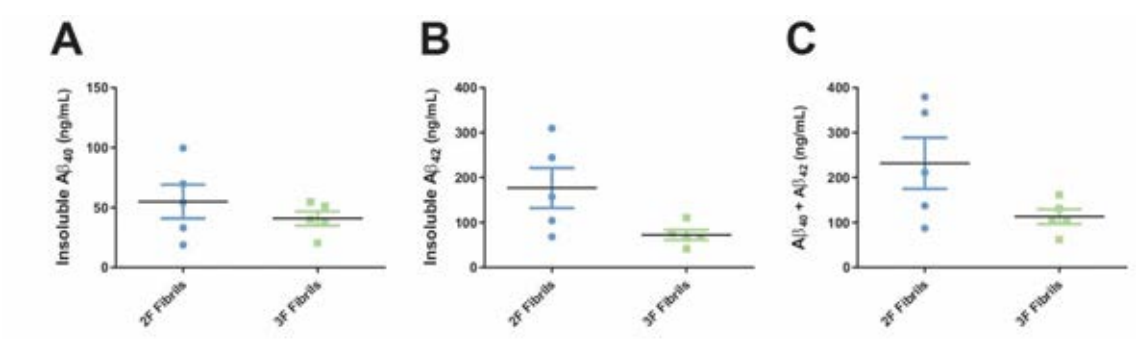

Figure 3.11. Analysis of PBS-insoluble fractions by protein-based multiplex immunoassay for $A\beta_{40}$ and $A\beta_{42}$ in Tg2576 animals 100 days post injection with 2F- and 3F-derived aggregates. Levels of insoluble $A\beta_{40}$ **(A)** and $A\beta_{42}$ **(B)** were measured with a commercially available protein-based multiplex immunoassay in the short time (100 days) of incubation group. **(C)** Levels of both proteins were also added to quantify the total amount of both proteins. Statistical analyses performed by Student's t-test.

In line with the data from brain homogenates (**Figure 3.11**), histological analysis of Aβ deposition in animals sacrificed at the shorter time point demonstrated low amount of Aβ aggregates, even when several brain slices were analyzed (**Figure 3.12A and B**). However, a few animals injected with the 2F aggregates seems to display higher quantities of 4G8-positive deposits compared to mice treated with the 3F fibrils (**Figure 3.12**). Specifically, Aβ deposition was observed in the hippocampal formation and dentate gyrus of 2F treated mice, suggesting that accumulation in these areas might occur before the 300 days old experimental endpoint (**Figure 3.12A, D and E vs Figure 3.8**). Interestingly, a few mice injected with 2F fibrils also displayed an increase in lateral ventricle Aβ deposits as early as 100 days after injection (**Figure 3.12G**). Taken together the data from protein-based multiplex immunoassays and from in-depth histological analysis of animals euthanized 100 days post injection support the hypothesis that Aβ deposits found in injected animals at 300 days of age (**Figure 3.7, 3.8 and 3.9**) results from *de novo* generation of endogenous Aβ and not from the inocula.

3.2.5. Amyloid plaques induced by 2F and 3F aggregates recruits different Aβ peptides and result in differential binding to amyloid-conformation-specific dyes.

As detailed above, we found that the three different types of seeds (brain homogenate from aged Tg2576, 2F- and 3F-fibrils) are able to induce the formation of Aβ deposits with brain region-specific tropism and unique characteristics (dense-core vs diffuse deposits) in the brain of Tg2576 mice. Thus, we performed an in-depth fluorescence microscopy analysis of double $A\beta_{40}$/$A\beta_{42}$ immunofluorescence labeled sections to investigate whether the Aβ aggregates induced by the three inocula display differential recruitment of $A\beta_{40}$ and $A\beta_{42}$ peptides and to explore conformational differences in these induced Aβ plaques. We first focused on the dentate gyrus (**Figure 3.13**), an area of the hippocampus where the three seeds induced amyloidosis. Here, the seeds from aged Tg2576 mice recruited both $A\beta_{40}$ and $A\beta_{42}$ peptides. Both Aβ peptides seemed to co-exist within the induced deposits as shown by their colocalization (**Figure 3.13 a1-a4**). 2F and 3F fibrils also induced the aggregation of both Aβ peptides with predominance of the $A\beta_{40}$ peptide (**Figure 3.13 a9-12 for 2F fibrils, and a13-16 for 3F fibrils**). Interestingly, while some amyloid deposits displayed colocalization for $A\beta_{40}$ and $A\beta_{42}$ immunolabeling, the halo of these plaques appeared to be mostly composed of $A\beta_{40}$. In the 3F-injected animals, plaques were mostly composed by $A\beta_{40}$ and displayed a big halo-like type around small $A\beta_{42}$ aggregates (**Figure 3.13 a13-16**).

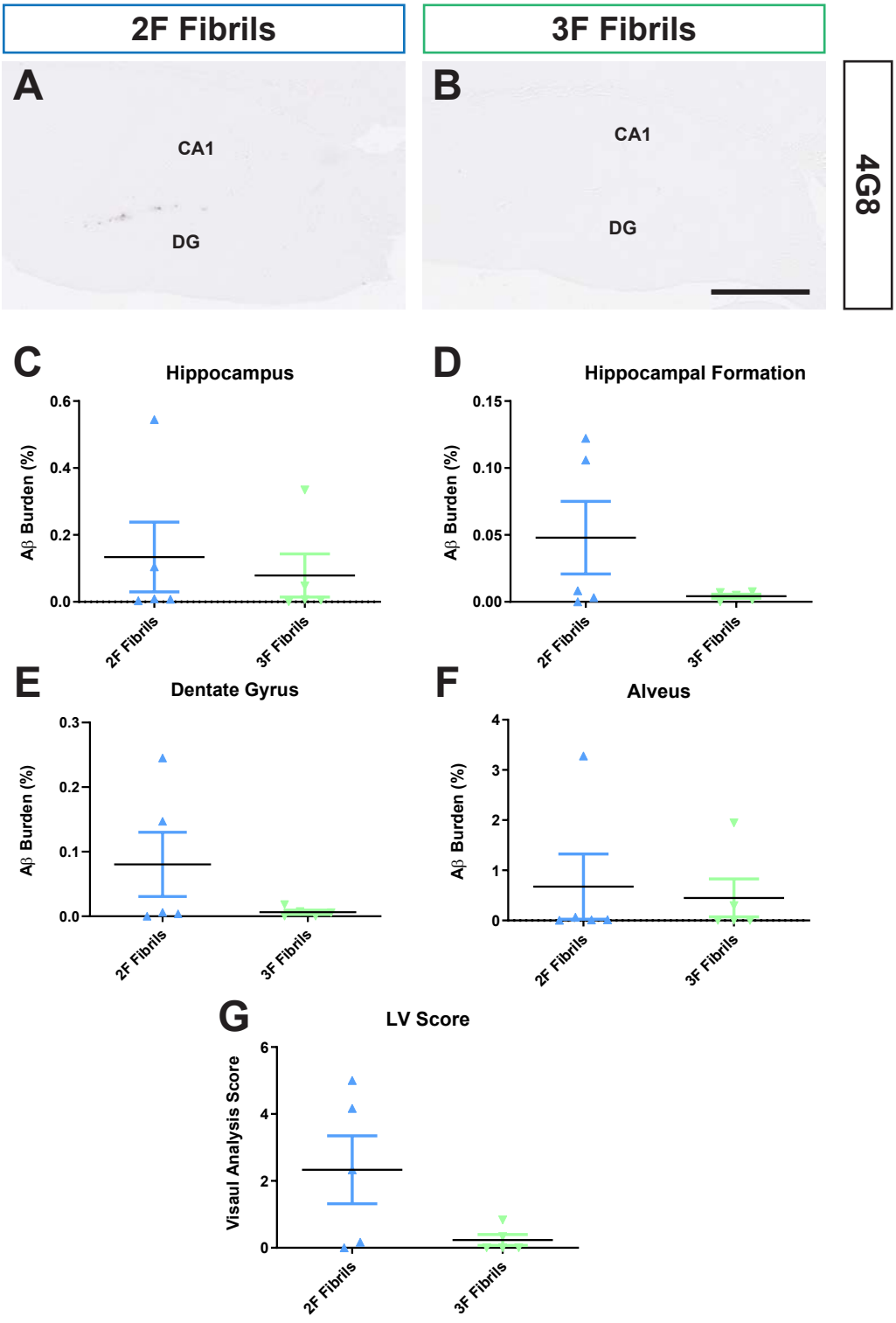

Figure 3.12. Amyloid pathology in Tg2576 animals 100 days after seeding with 2F- and 3F-derived aggregates. Representative pictures of hippocampi from mice treated with 2F- and 3F-derived seeds after visualization for Aβ deposits using the 4G8 antibody **(A-B)**. Scale bar in **(B)** represents 500 µM and applies to both panels. Region-specific Aβ burden quantification in the hippocampus **(C)**, hippocampal formation **(D)**, dentate gyrus **(E)** and alveus **(F)** of 2F- and 3F-fibrils treated mice. **(G)** Aβ visual score analysis in the lateral ventricles. Statistical analyses performed by Student's t-test.

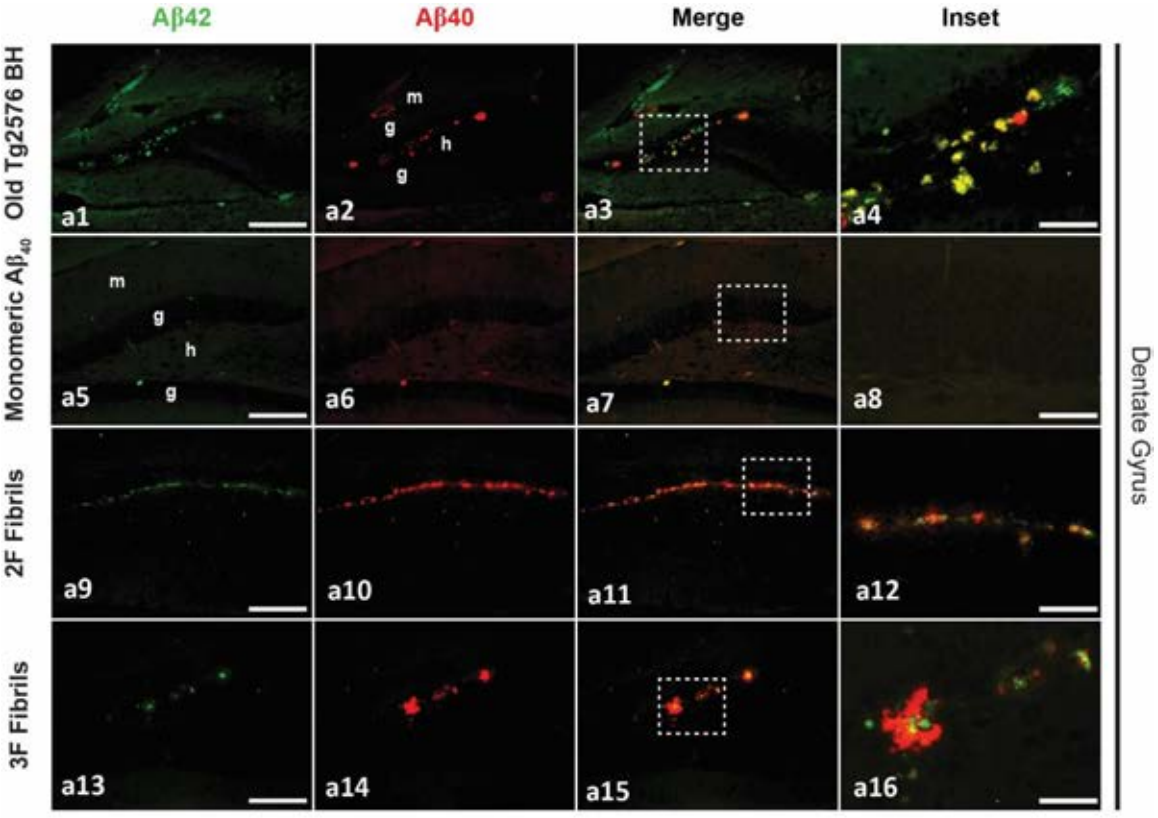

Figure 3.13. $A\beta_{40}$- and $A\beta_{42}$-specific amyloid pathology in the dentate gyrus of the four different experimental groups. Representative pictures of the dentate gyrus from mice treated with Tg2576-derived, monomeric $A\beta_{40}$, 2F- and 3F-seeds after visualization by immunofluorescence of Aβ deposits using the $A\beta_{42}$- (green) and $A\beta_{40}$- (red) specific antibodies. The third column of panels from left to right **(a3, a7, a11 and a15)** depict merged images. Right panels **(a4, a8, a12 and a16)** are insets obtained from the merged images (white punctuated squares). *g: granule cell layer, h: hilus*, *m: molecular layer*. Scale bars at the left panels represent 200 µm and are applicable to the pictures labeled as "$A\beta_{42}$", "$A\beta_{40}$" and "Merge". Scale bars on the right images (inset) represent 50 µm.

Interestingly, additional differences were observed in the alveus layer (**Figure 3.14 a1-16**). Specifically, the extensive amyloidosis exerted by 2F seeds in this region was mostly composed by $A\beta_{40}$, with few deposits showing $A\beta_{42}$-positive immunostaining (**Figure 3.14 a9-12**). Moreover, the scarce deposits induced by the old Tg2576 brain homogenates seeds in this area were mostly formed by $A\beta_{42}$ (**Figure 3.14 a1-4**). Mice treated with monomeric $A\beta_{40}$ (**Figure 3.14 a5-8**) and 3F seeds (**Figure 3.14 a13-16**) generated imperceptible quantities of amyloidosis in this brain region, as discussed above.

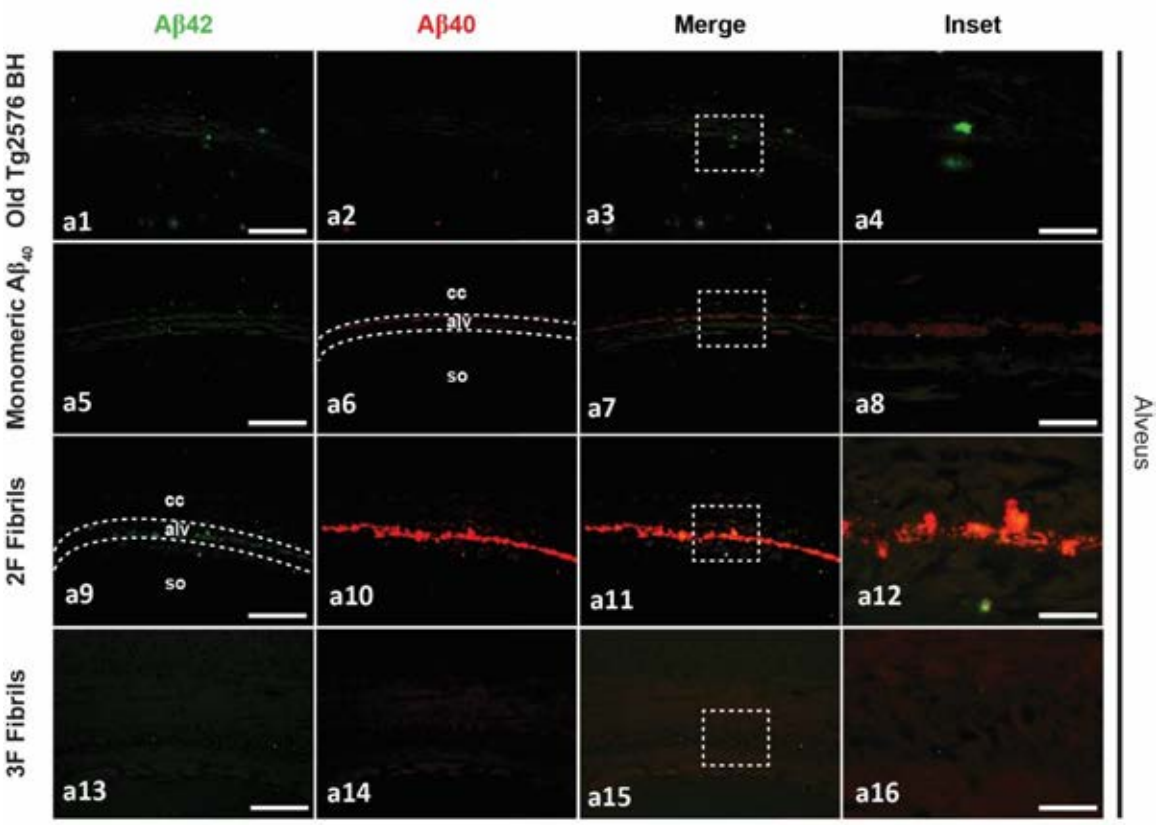

Figure 3.14. $A\beta_{40}$- and $A\beta_{42}$-specific amyloid pathology in the alveus of the four different experimental groups. Representative images of the dentate gyrus from mice treated with Tg2576-derived, monomeric $A\beta_{40}$, 2F- and 3F-seeds after visualization by immunofluorescence of Aβ deposits using the $A\beta_{42}$- (green) and $A\beta_{40}$- (red) specific antibodies. The third column of panels from left to right **(a3, a7, a11 and a15)** depict merged images. Right panels **(a4, a8, a12 and a16)** are insets obtained from the merged images (white punctuated squares). *alv: alveus, cc: corpus callosum, so: stratum oriens*. Scale bars at the left panels represent 200 µm and are applicable to the pictures labeled as "$A\beta_{42}$", "$A\beta_{40}$" and "Merge". Scale bars on the right images (Inset) represent 50 µm.

To further confirm the conformational differences between the deposits induced by the three inocula, we evaluated the Aβ plaques by using the LCOs we used for our *in vitro* analysis of 2F and 3F fibrils (**See Table 2.1 and Figure 3.5**). Based on our *in vitro* data (**Figure 3.5**), we decided to use the HS-68 LCO, which had more affinity for 2F fibrils, and the HS-194 LCO, which had more affinity for 3F fibrils, to potentially differentiate between *in vivo* seeded Aβ strains in the brain of animals injected with the three inocula (**Figure 3.15A and B**).

In the dentate gyrus (**Figure 3.15A**), deposits induced by the old Tg2576 seeds were, in their vast majority, positive to both dyes (**Figure 3.15A a1-4**). Interestingly, 2F-

induced deposits were reactive to both dyes with slightly more reactivity towards the HS-68 LCO (**Figure 3.15A a9-12**). In contrast, 3F-induced deposits in the dentate gyrus were strongly reactive to the HS-194 LCO and poorly reactive against HS-68 (**Figure 3.15A a13-16**). Moreover, 2F-induced amyloidosis in the alveus was reactive almost exclusively to HS-68 (**Figure 3.15B b1-b4**), while no deposits from the other injected animals were found in the alveus region (**Figure 3.15B b5-8**).

These results are strikingly similar to our data from the *in vitro* characterization of the 2F and 3F fibrils with the LCOs, with 2F-induced deposits having better affinity towards the HS-68 LCO and 3F-induced plaques being strongly reactive to the HS-194 LCO. These data are relevant as they confirm the existence of conformational-specific Aβ deposits in the brain of animals injected with different seeds and indicate that these deposits might maintain and propagate some of the characteristics of the initial inocula.

3.2.6. Glial activation induced by 2F- and 3F-fibrils is Aβ strain dependent

We have demonstrated that 2F- and 3F-fibrils induce conformation-specific Aβ aggregates *in vivo*, which strongly support our hypothesis. It is important to bear in mind that the biological significance of misfolding Aβ strains variation in AD pathology is currently unknown. Thus, we performed an in-depth study, both quantitative and qualitative, to test whether *in vivo* seeded aggregates induced by synthetic Aβ seeds resulted in distinct glial responses. In order to achieve this goal, astroglial and microglial reactions were carefully assessed by immunohistochemistry and image analysis quantification in control and experimental groups.

First, astroglial reactivity was measured by immunohistochemistry using an antibody against the astrocyte-specific glial fibrillary acidic protein (GFAP, **Figure 3.16 A-D**) since the upregulation of this protein is a feature of reactive astrocytes (Escartin et al., 2021). Staining with this antibody allows the analysis of astrocytes with reactive phenotype, which are those responding to an insult in the brain parenchyma such as Aβ deposits, showing increased expression of this marker. Thus, increased area of GFAP-positive astrocytes was found in regions with increased Aβ pathology. When GFAP-positive area (astroglial burden) was measured in the whole hippocampus, there was no significant differences between experimental and control groups (**Figure 3.16E**). A similar non-significant outcome was found in the dentate gyrus (**Figure 3.16F**), despite

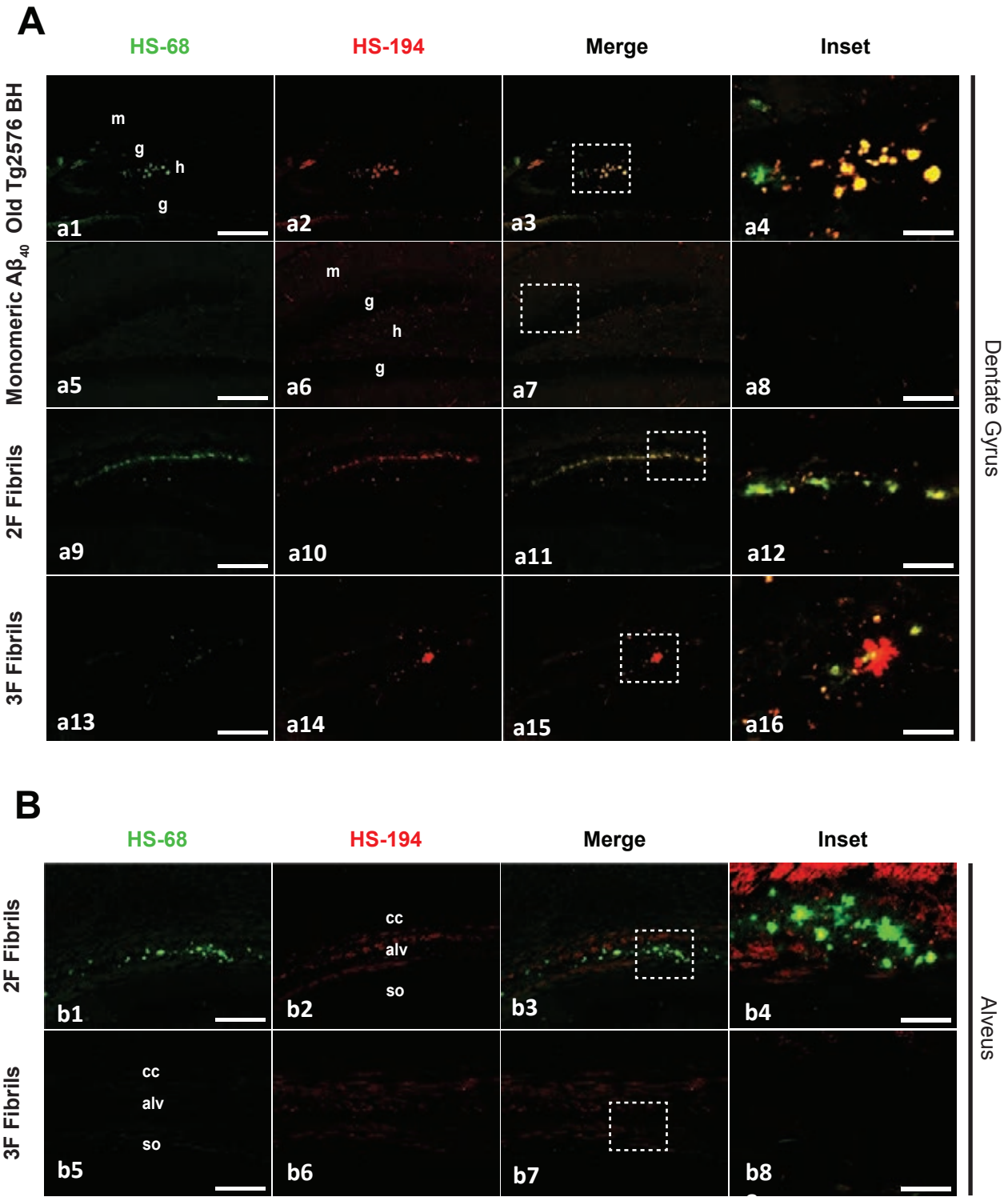

Figure 3.15. Luminescent Conjugated Thiophenes (LCOs) staining in the dentate gyrus and alveus of the four different experimental groups. Representative pictures of the dentate gyrus **(A)** and alveus **(B)** from mice treated with Tg2576-derived, monomeric Aβ40, 2F- and 3F-seeds after visualization by fluorescence of Aβ deposits using the HS-68 (Green, **a1, a5, a9, a13, b1 and b5**) and HS-194 (Red, **a2, a6, a10, a14, b2 and b6**) LCOs. The third column of panels (**a3, a7, a11, a15, b3 and b7**) depict merged images. Right panels **(a4, a8, a12, a16, b4 and b8)** are insets obtained from the merged images (white punctuated squares). *alv: alveus, cc: corpus callosum, g: granule cell layer, h: hilus, m: molecular layer, so: stratum oriens*. Scale bars at the left panels represent 200 µm and are applicable to the pictures labeled as "HS-68", "HS-194" and "Merge". Scale bars on the right images (Inset) represent 50 µm.

the fact that 3F-induced aggregates were predominantly found in that area (**Figure 3.8D and H**). However, the alveus of animals injected with the 2F fibrils displayed a significant increase ($F(3,19) = 6.64$, $p = 0.0238$ vs monomeric $A\beta_{40}$, $p = 0.0297$ vs Old Tg BH, $p = 0.0045$ vs 3F fibrils) of GFAP burden compared to all other groups (**Figure 3.16G**). Since the alveus is the area where most of the induced amyloid plaques were found in 2F seeded mice, we expected that astroglial activation would be exacerbated in this region. This was further assessed by correlation analysis between Aβ burden and astroglial burden ($r = 0.69$; $p = 0.088$; **Figure 3.18A**).

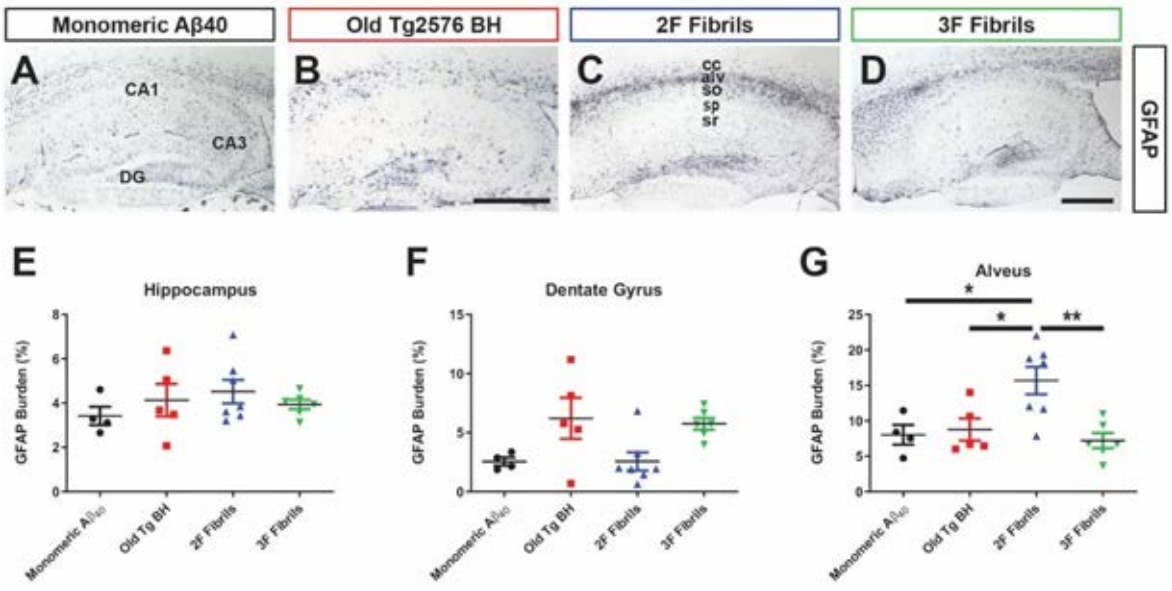

Figure 3.16. Astroglial activation in the brain of mice treated with Tg2576-derived, monomeric $A\beta_{40}$, 2F- and 3F-derived Aβ seeds. Representative images of hippocampi from mice treated with different injectate after visualization for astroglial associated signals using the anti-GFAP antibody **(A-D)**. Scale bar in **(B)** and **(D)** represents 500 µM and applies to all panels. Anti-GFAP burden in hippocampus **(E)**, dentate gyrus **(F)** and alveus **(G)** for all animal groups was quantified for image analysis. *alv: alveus, CA1: Cornu Ammonis area 1, CA3: Cornu Ammonis area 3, cc: corpus callosum, DG: Dentate Gyrus, so: stratum oriens. sp: stratum pyramidale, sr: stratum radiatum.* Statistical analyses performed by One-way ANOVA * $p<0.05$, ** $p<0.01$.

Then, in order to analyze changes in microglial recruitment towards the regions with increased Aβ deposition, we assessed by immunohistochemistry the expression of the microglial-specific ionized calcium binding adaptor molecule 1 (Iba-1) marker (**Figure 3.17A-D**). This marker allows us to measure the areas where microglia is found and, similar to reactive astrocytes, activated microglia will show increased expression of Iba-1, thus allowing us to measure increased inflammatory response towards Aβ deposits by microglial cells. Specifically, we measured by image analysis the area covered by Iba1-positive microglia (**Figure 3.17E-G**) in the hippocampal regions. In agreement with the data obtained with the GFAP marker, no significant differences were found when considering the area covered by Iba-1-positive microglial cells across the whole hippocampus (**Figure 3.17E**). Nonetheless, selective microglial recruitment towards specific areas of the hippocampus was found. In concordance with the amyloid deposition data, 3F injected mice displayed significantly higher levels ($F(3,19) = 6.78$, $p = 0.0063$ vs monomeric $A\beta_{40}$, $p = 0.0060$ vs 2F fibrils) of Iba-1 immunostaining in the dentate gyrus compared to other groups, with the exception of the mice treated with the old Tg2576 brain extract (**Figure 3.17F**). This linear Aβ/glial activation responses correlation was better appreciated when correlation graphs between these parameters were generated ($r = 0.78$; $p < 0.05$; **Figure 3.19F**). In the same line, aggregates in animals seeded with the 2F fibrils, showed significantly higher ($F(3,19) = 10.45$, $p = 0.0078$ vs monomeric $A\beta_{40}$, $p = 0.001$ vs Old Tg BH, $p = 0.0013$ vs 3F fibrils) Iba-1 reactivity in the alveus when compared to all the other groups (**Figure 3.17G**). This linear correlation was further confirmed by correlation analysis ($r = 0.8$; $p < 0.05$; **Figure 3.18A**).

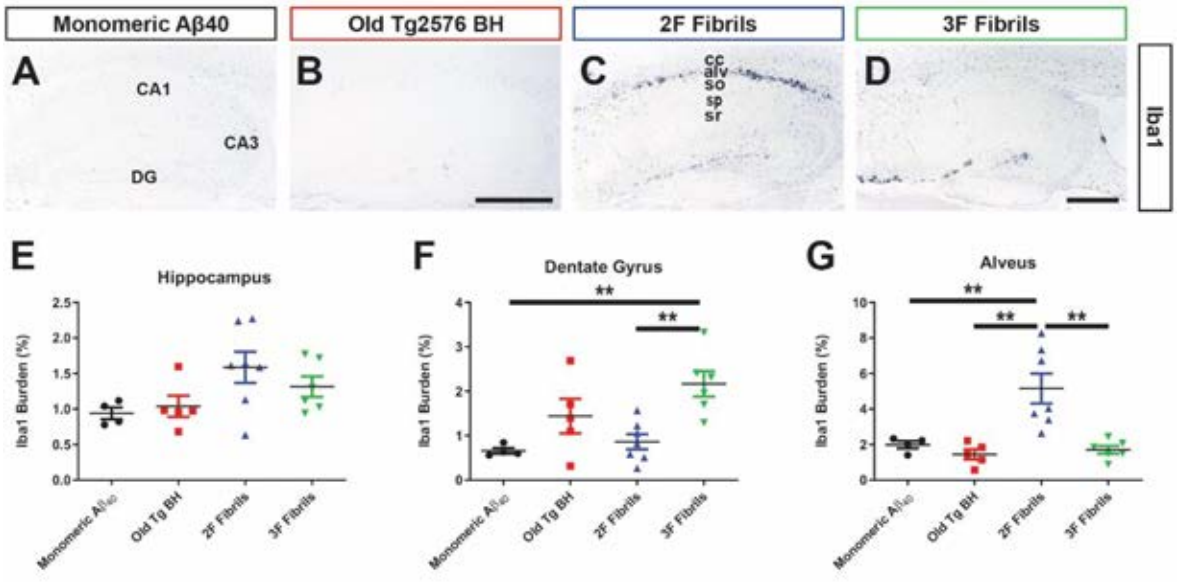

Figure 3.17. Microglial activation in the brain of mice treated with Tg2576-derived, monomeric Aβ$_{40}$, 2F- and 3F-derived Aβ seeds. Representative images of hippocampi from mice treated with different injectate after visualization for microglial associated signals using the anti-Iba1 antibody **(A-D)**. Scale bar in **(B)** and **(D)** represents 500 µM and applies to all panels. Anti-Iba1 burden in hippocampus **(E)**, dentate gyrus **(F)** and alveus **(G)** for all animal groups was quantified for image analysis. *alv: alveus, CA1: Cornu Ammonis area 1, CA3: Cornu Ammonis area 3, cc: corpus callosum, DG: Dentate Gyrus, so: stratum oriens*. *sp: stratum pyramidale*, *sr: stratum radiatum*. Statistical analyses performed by One-way ANOVA ** p<0.01.

Interestingly, correlation analysis in the different hippocampal regions (hippocampal formation, dentate gyrus, alveus, and whole hippocampus) in animals injected with 2F and 3F fibrils, revealed that overall, Aβ deposits from animals injected with the 2F synthetic fibrils tend to induce more astroglial reactivity in comparison to animals injected with 3F synthetic fibrils (**Figure 3.18A-D**; **Figure 3.19E-F and I-J**). However, amyloid deposits from animals injected with 3F synthetic fibrils correlate better with increased microglial activation in these brain regions (**Figure 3.18B and D; Figure 3.19F and J**). These results confirmed that synthetic Aβ strains induce amyloid conformation-specific glial response in Tg2576 mice. It is worth mentioning that Aβ deposits from mice injected with brain homogenate from old Tg2576, mostly correlated with microglial cells recruitment towards those brain regions (**Figure 3.19C, G and K**),

with the exception of the alveus region (**Figure 3.19A**). This is similar to 3F-induced aggregates, despite the fact that aggregates from these two animal groups are conformationally different.

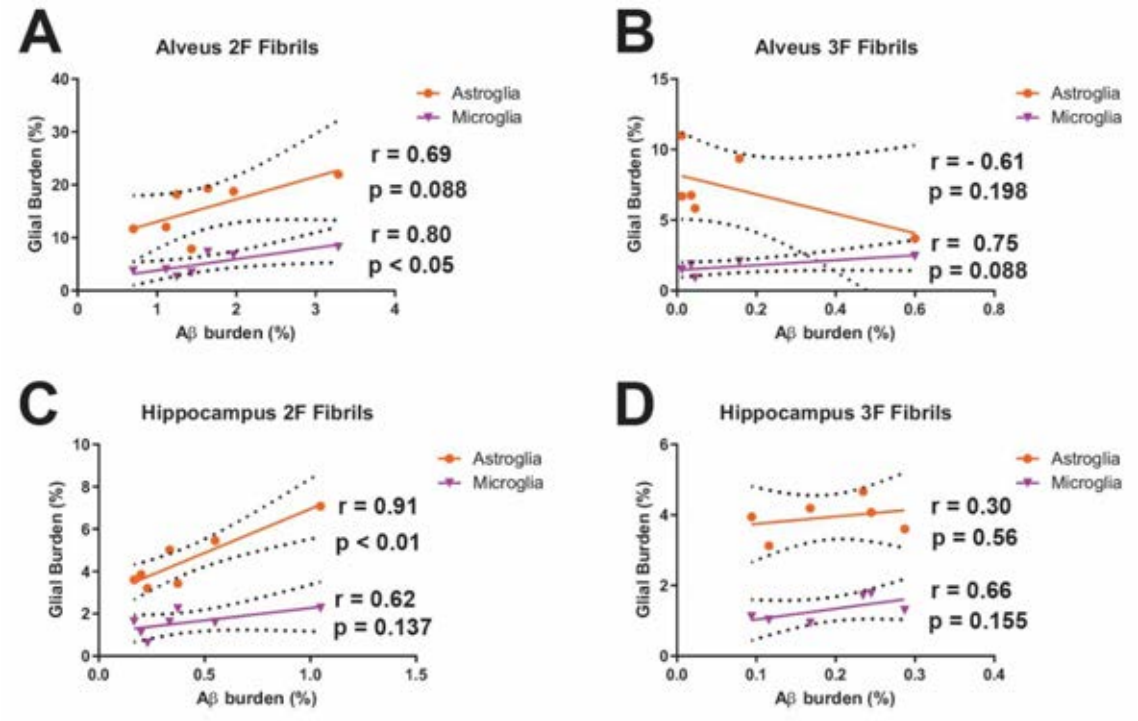

Figure 3.18. Glial burden and Aβ burden correlation in alveus and hippocampus of mice treated with 2F- or 3F-derived Aβ seeds. Correlations between Aβ burden and glial burden were calculated in the alveus for mice injected with 2F **(A)** and 3F **(B)** fibrils. In the same way, the relationship between glial activation and Aβ burden in the hippocampus was calculated for mice treated with 2F **(C)** and 3F **(D)** aggregates. Statistical analyses performed by Pearson correlation coefficients test in which $p<0.05$ was considered significant.

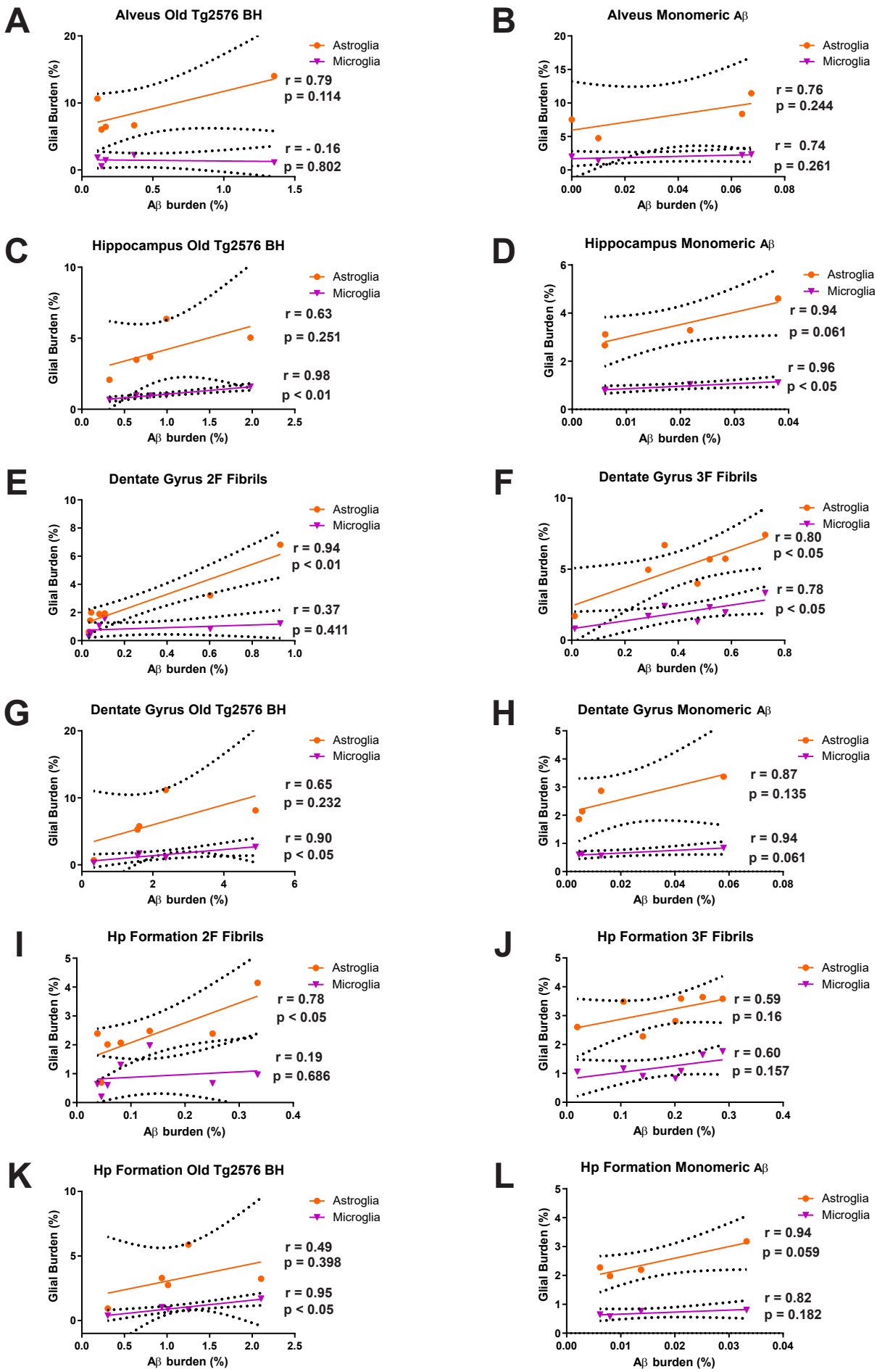

Figure 3.19. Glial burden and Aβ burden correlation in alveus, hippocampus, dentate gyrus, and hippocampus proper in the brain of mice treated with Tg2576-derived, monomeric $A\beta_{40}$, 2F- and 3F-derived Aβ seeds. Correlations between Aβ burden and glial burden in the alveus **(A-B)**, hippocampus **(C-D)**, dentate gyrus **(G-H)** and hippocampus proper **(K-L)** were calculated for mice injected with Tg2576-derived brain homogenate **(A, C, G and K)** or monomeric $A\beta_{40}$ **(B, D, H and L)**. In the same way, the relationship between glial activation and Aβ burden in the dentate gyrus **(E-F)** and hippocampus proper **(I-J)** was calculated for mice injected with 2F **(E and I)** or 3F **(F and J)** fibrils. Statistical analyses performed by Pearson correlation coefficients test in which $p<0.05$ was considered significant.

In order to confirm the results that Aβ strains induce amyloid conformation-specific glial response, we performed a more detailed microscopic analysis on the effect that seeded aggregates exerted over astroglial and microglial cells by double 4G8/GFAP and 4G8/Iba1 immunofluorescence analysis. Specifically, in the dentate gyrus (**Figure 3.20**) astroglial reaction was fairly similar between the groups and regardless of the plaque morphology or nature. Astroglial cells acquired a reactive hypertrophic phenotype around the amyloid plaques in the experimental groups that showed hippocampal amyloid deposition: old Tg2576 BH (**Figure 3.20 a1-4**), 2F (**Figure 3.20 a9-12**) and 3F (**Figure 3.20 a13-16**) injected mice. These results are similar to those obtained in the quantitative studies of the dentate gyrus (**Figure 3.16F**).

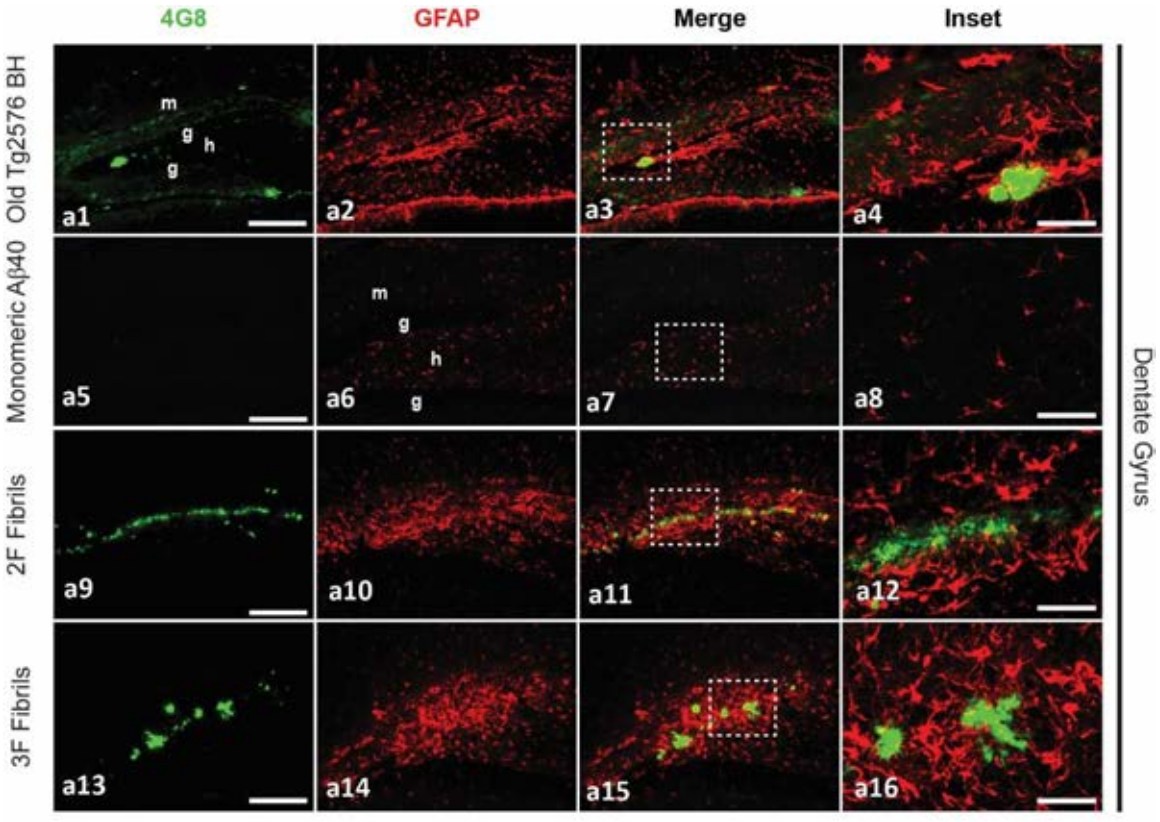

Figure 3.20. Astroglial reactivity to Aβ deposits in the dentate gyrus of animals seeded by Tg2576-derived, monomeric $A\beta_{40}$, 2F- and 3F-derived aggregates. Panels showing representative images of the dentate gyrus of mice treated with experimental and control materials and stained with both 4G8 (green) and anti-GFAP (red) antibodies. The third column of panels from left to right **(a3, a7, a11 and a15)** shows merged images. Right panels **(a4, a8, a12 and a16)** are insets obtained from the merged images (white punctuated squares). *m: molecular layer, g: granule cell layer, h: hilus*. Scale bars at the left panels represent 200 µm and are applicable to the pictures labeled as "4G8", "GFAP" and "Merge". Scale bars on the right images (Inset) represent 50 µm.

GFAP signal in the alveus (**Figure 3.21 a1-16**) was not very prominent, as only 2F aggregates were strongly deposited in this region. The aggregates induced by the 2F fibrils were surrounded by abundant astroglial cells with a reactive phenotype (**Figure 3.21 a9-12**). This finding strongly correlates with the quantitative data for the area covered by GFAP-positive astrocytes (**Figure 3.16G**) and with the correlation studies that showed that 2F synthetic fibrils tend to activate or recruit more astroglial cells (**Figure 3.18A and C and Figure 3.19E**). Importantly, the few diffuse Aβ deposits induced by the Tg2576 brain homogenates in the alveus region did not result in strong astrocyte reactivity around them (**Figure 3.21 a1-4**).

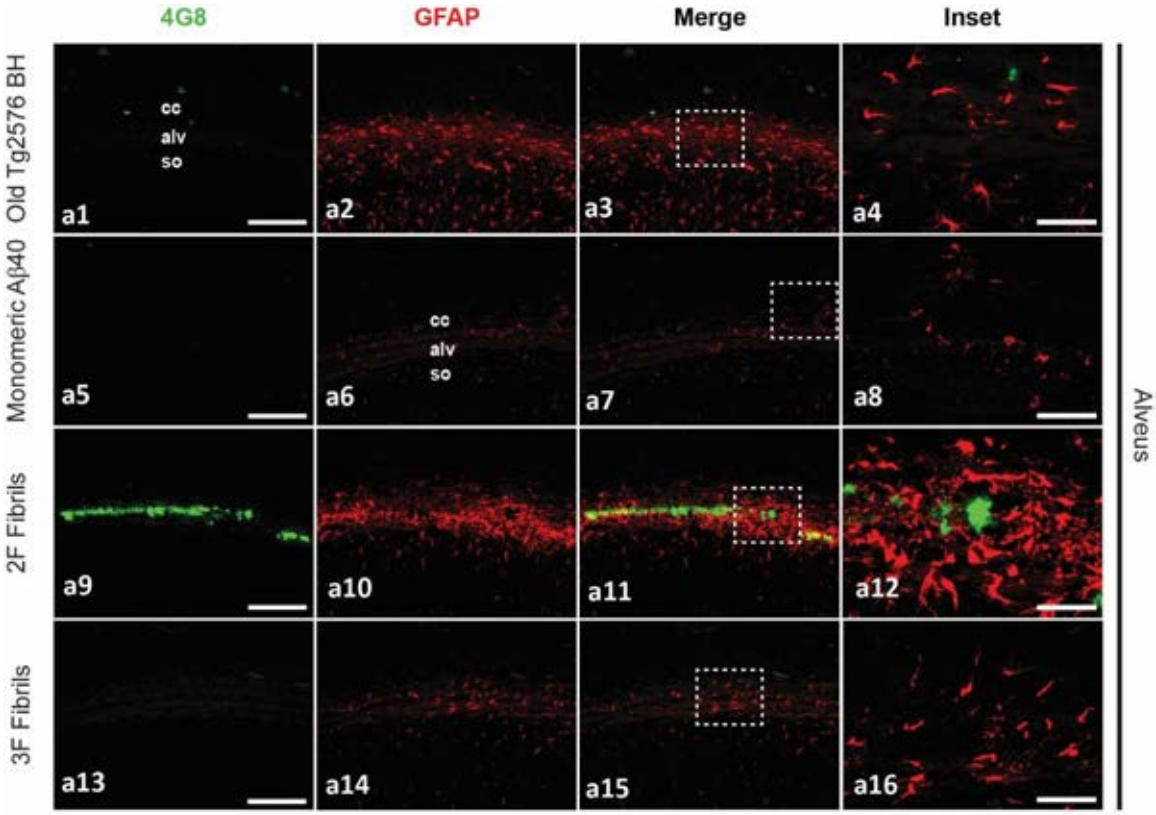

Figure 3.21. Astroglial reactivity to Aβ deposits in the alveus of animals seeded by Tg2576-derived, monomeric $A\beta_{40}$, 2F- and 3F-derived aggregates. Panels showing representative images of the alveus of mice treated with experimental and control materials and stained with both 4G8 (green) and anti-GFAP (red) antibodies. The third column of panels from left to right **(a3, a7, a11 and a15)** shows merged images. Right panels **(a4, a8, a12 and a16)** are insets obtained from the merged images (white punctuated squares). *alv: alveus, cc: corpus callosum, so: stratum oriens*. Scale bars at the left panels represent 200 µm and are applicable to the pictures labeled as "4G8", "GFAP" and "Merge". Scale bars on the right images (Inset) represent 50 µm.

On the other hand, the evaluation of the microglial response (**Figures 3.22 and 3.23**) revealed that microglial cells displayed strong activation towards the amyloid plaques induced only by 3F seeds in the dentate gyrus (**Figure 3.22 a13-16**). In this same region, the response of microglia towards seeded aggregates induced by 2F and the aged Tg2576 seeds was not as strong (**Figure 3.22 a1-4 and a9-12**, respectively). Importantly, microglial cells, as well as astroglial cells, showed a non-reactive or homeostatic phenotype (ramified morphology, **Figure 3.22 a8**) in the dentate gyrus of animals injected with the monomeric Aβ$_{40}$ (**Figure 3.22 a5-8**).

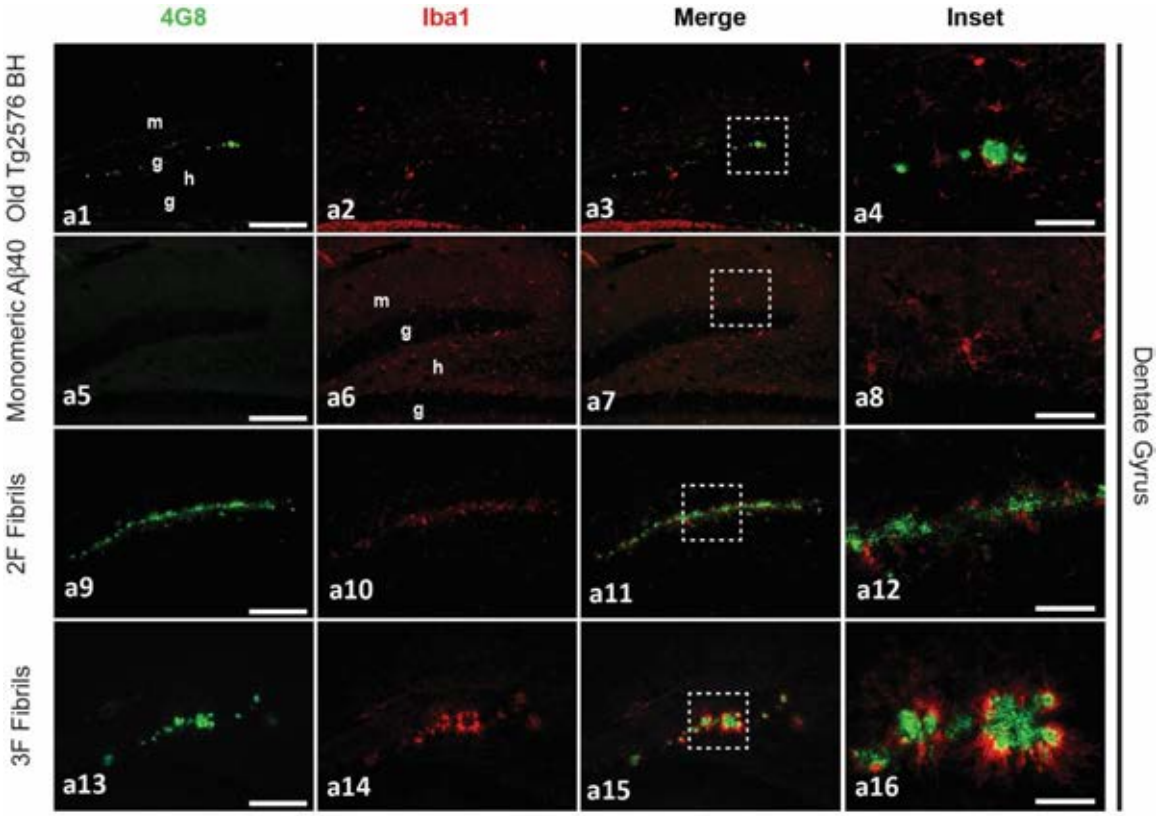

Figure 3.22. Microglial reactivity to Aβ deposits in the dentate gyrus of animals seeded by Tg2576-derived, monomeric Aβ$_{40}$, 2F- and 3F-derived aggregates. Panels showing representative images of the dentate gyrus of mice treated with experimental and control materials and stained with both 4G8 (green) and anti-Iba1 (red) antibodies. The third column of panels from left to right **(a3, a7, a11 and a15)** shows merged images. Right panels **(a4, a8, a12 and a16)** are insets obtained from the merged images (white punctuated squares). *m: molecular layer, g: granule cell layer, h: hilus*. Scale bars at the left panels represent 200 µm and are applicable to the pictures labeled as "4G8", "Iba1" and "Merge". Scale bars on the right images (Inset) represent 50 µm.

In the alveus region (**Figure 3.23**), microglial response towards the 2F seeded aggregates (**Figure 3.23 a9-12**) appeared to be stronger compared to what was found for the same animals in the dentate gyrus. However, this response seemed to be weaker than the response displayed by microglial cells towards the 3F-induced deposits in the dentate gyrus (**Figure 3.22 a13-16**). Specifically, activated microglial cells did not clustered around all the amyloid deposits induced by the 2F fibrils in the alveus (**Figure 3.23 a12**) while those induced by the 3F fibrils in the dentate gyrus seemed to be completely surrounded with activated microglial cells. This finding strongly correlates with our quantitative data for the area of the dentate gyrus covered by microglia (see **Figure 3.17F**) and with the correlation studies that showed that 3F synthetic fibrils tend to recruit more microglial cells (**Figure 3.18B and D, and Figure 19F**). As expected, the few diffuse deposits induced by aged Tg2576 seeds did not induce a strong microglial reactivity in the alveus region (**Figure 3.23 a1-4**). Similar to the dentate gyrus, microglial cells showed a non-reactive/homeostatic phenotype (**Figure 3.23 a8**) in the alveus of animals injected with the monomeric $A\beta_{40}$ (**Figure 3.23 a5-8**). This homeostatic phenotype of microglial cells was also found in the alveus region of animals injected with 3F fibrils (**Figure 3.23 a16**). These results further confirmed that different Aβ arrangements induce differential glial responses in Tg2576 mice.

3.2.7. Distinct cytokine and chemokine profiles induced by 2F- and 3F-fibrils: a multiplex analysis

There is a direct connection between microglial and astroglial activation and cytokine production. Then, we next aimed to investigate whether each of the Aβ strains induced a differential pattern of cytokine expression and, therefore, neuroinflammatory response. Specifically, we used a multiplex immunoassay to quantify 23 cytokines (**Figure 3.24**) in the same brain soluble fractions (S1) in order to gain broad information from the most relevant signaling molecules in the brain and the inflammatory microenvironment. In summary we found that the cytokines levels were significantly different between groups.

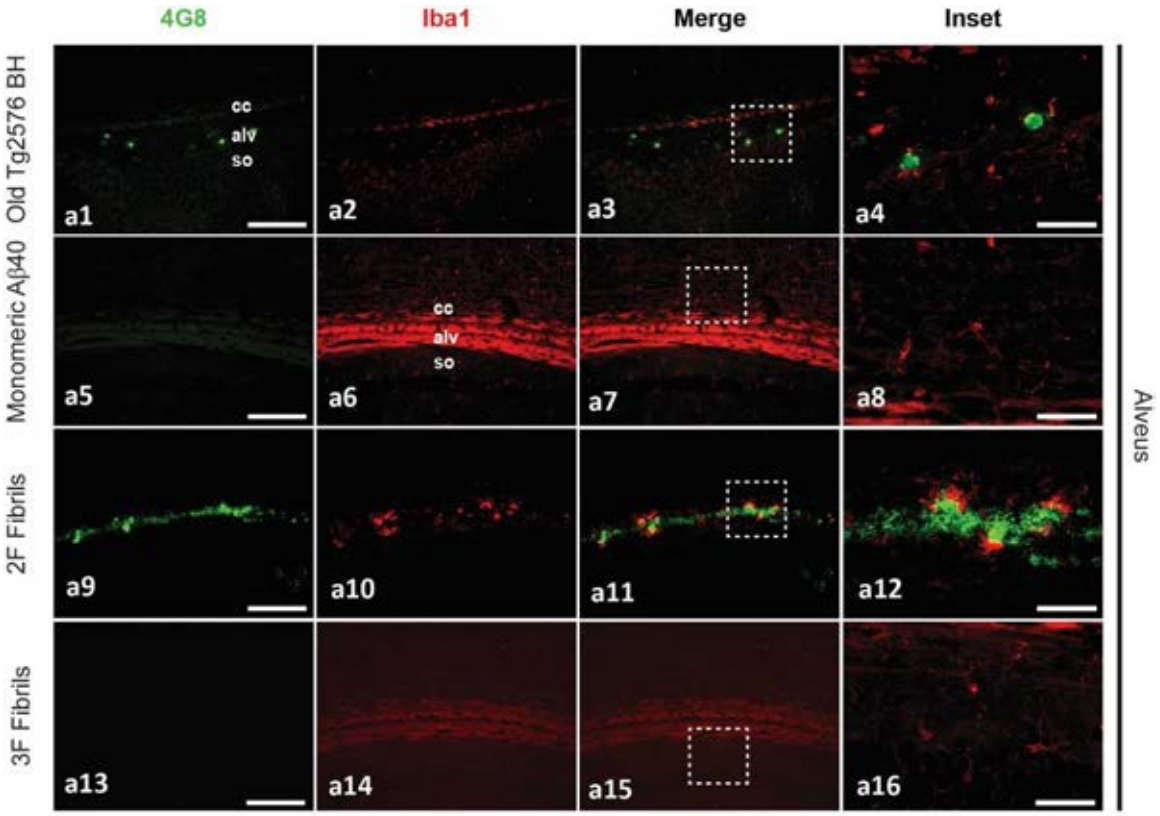

Figure 3.23. Microglial reactivity to Aβ deposits in the alveus of animals seeded by Tg2576-derived, monomeric $A\beta_{40}$, 2F- and 3F-derived aggregates. Panels showing representative images of the alveus of mice treated with experimental and control materials and stained with both 4G8 (green) and anti-Iba1 (red) antibodies. The third column of panels from left to right **(a3, a7, a11 and a15)** shows merged images. Right panels **(a4, a8, a12 and a16)** are insets obtained from the merged images (white punctuated squares). *alv: alveus, cc: corpus callosum, so: stratum oriens*. Scale bars at the left panels represent 200 µm and are applicable to the pictures labeled as "4G8", "Iba1" and "Merge". Scale bars on the right images (Inset) represent 50 µm.

Mice inoculated with the Tg2576-derived seeds displayed greater cytokine alterations, with IL-1α (**Figure 3.24A,** $F(3,19) = 6.902$, $p = 0.0024$), IL-5 (**Figure 3.24F,** $F(3,19) = 6.82$, $p = 0.0168$), IL-6 (**Figure 3.24G,** $F(3,19) = 8.701$, $p = 0.0015$), IL-9 (**Figure 3.24H,** $F(3,19) = 18.94$, $p < 0.0001$), IL-13 (**Figure 3.24L,** $F(3,19) = 24.94$, $p < 0.0001$), CCL3 (**Figure 3.24S,** $F(3,19) = 4.982$, $p = 0.0468$), CCL4 (**Figure 3.24T,** $F(3,19) = 6.427$, $p = 0.002$), INF-γ (**Figure 3.24U,** $F(3,19) = 41.37$, $p < 0.0001$) CCL5 (**Figure 3.24V,** $F(3,19) = 7.319$, $p = 0.0074$) and TNF-α (**Figure 3.24W,** $F(3,19) = 4.272$, $p = 0.0466$) levels significantly increased when compared to control animals challenged with monomeric $A\beta_{40}$. On the contrary, IL-2 (**Figure 3.24C,** $F(3,19) = 31.27$, $p < 0.0001$), IL-3 (**Figure 3.24D,** $F(3,19) = 11.72$, $p = 0.0007$) and IL-17 (**Figure 3.24P,** $F(3,19) = 14.51$, $p = 0.0008$) showed lower levels in mice treated with Tg2576 seeds when compared to control animals challenged with monomeric $A\beta_{40}$. Moreover, Tg2576 seeds induced higher levels of IL-1β (**Figure 3.24B,** $F(3,19) = 3.792$, $p = 0.0347$ vs 2F and $p = 0.0337$ vs 3F), IL-5 (**Figure 3.24F,** $F(3,19) = 6.82$, $p = 0.0127$ vs 2F and $p = 0.0024$ vs 3F), IL-6 (**Figure 3.24G,** $F(3,19) = 8.701$, $p = 0.0052$ vs 2F and $p = 0.0021$ vs 3F), IL-9 (**Figure 3.24H,** $F(3,19) = 18.94$, $p = 0.0002$ vs 2F and $p = 0.0002$ vs 3F), IL-13 (**Figure 3.24L,** $F(3,19) = 24.94$, $p < 0.0001$ vs 2F and $p < 0.0001$ vs 3F) and INF-γ (**Figure 3.24U,** $F(3,19) = 41.37$, $p < 0.0001$ vs 2F and $p < 0.0001$ vs 3F) than 2F and 3F aggregates. Despite these differences these three different Aβ strains also exhibited a common cytokine signature with significant elevations of CCL3 (**Figure 3.24S,** $F(3,19) = 4.982$, $p = 0.0083$ for 2F and $p = 0.0214$ for 3F)and INF-γ (**Figure 3.24U,** $F(3,19) = 41.37$, $p < 0.0001$ for 2F and $p < 0.0001$ for 3F), and reduced IL-2 (**Figure 3.24C,** $F(3,19) = 31.27$, $p < 0.0001$ for 2F and $p < 0.0001$ for 3F), IL-3 (**Figure 3.24D,** $F(3,19) = 11.72$, $p = 0.0001$ for 2F and $p = 0.0011$ for 3F) and IL-17 (**Figure 3.24P,** $F(3,19) = 14.51$, $p < 0.0001$ for 2F and $p < 0.0001$ for 3F) when comparing with the monomeric $A\beta_{40}$ injected group. Levels of the anti-inflammatory cytokines IL-4 and IL-10 were unchanged regardless of the injectate used. In summary, 2F fibrils induced a proinflammatory profile (IL-1α, CCL3, CCL5 and INF-γ) that slightly differed from 3F fibrils (CCL3 and INF-γ).

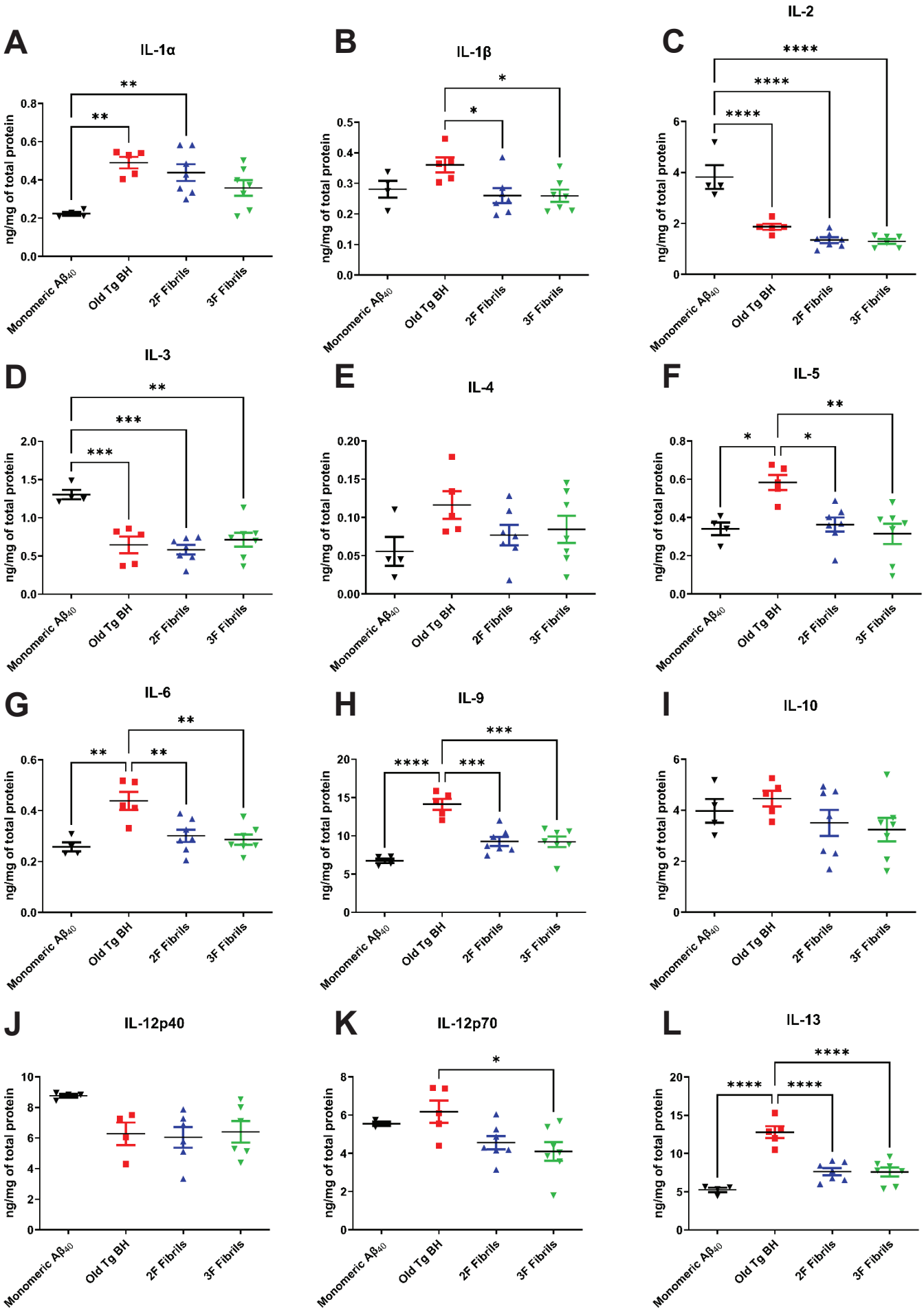

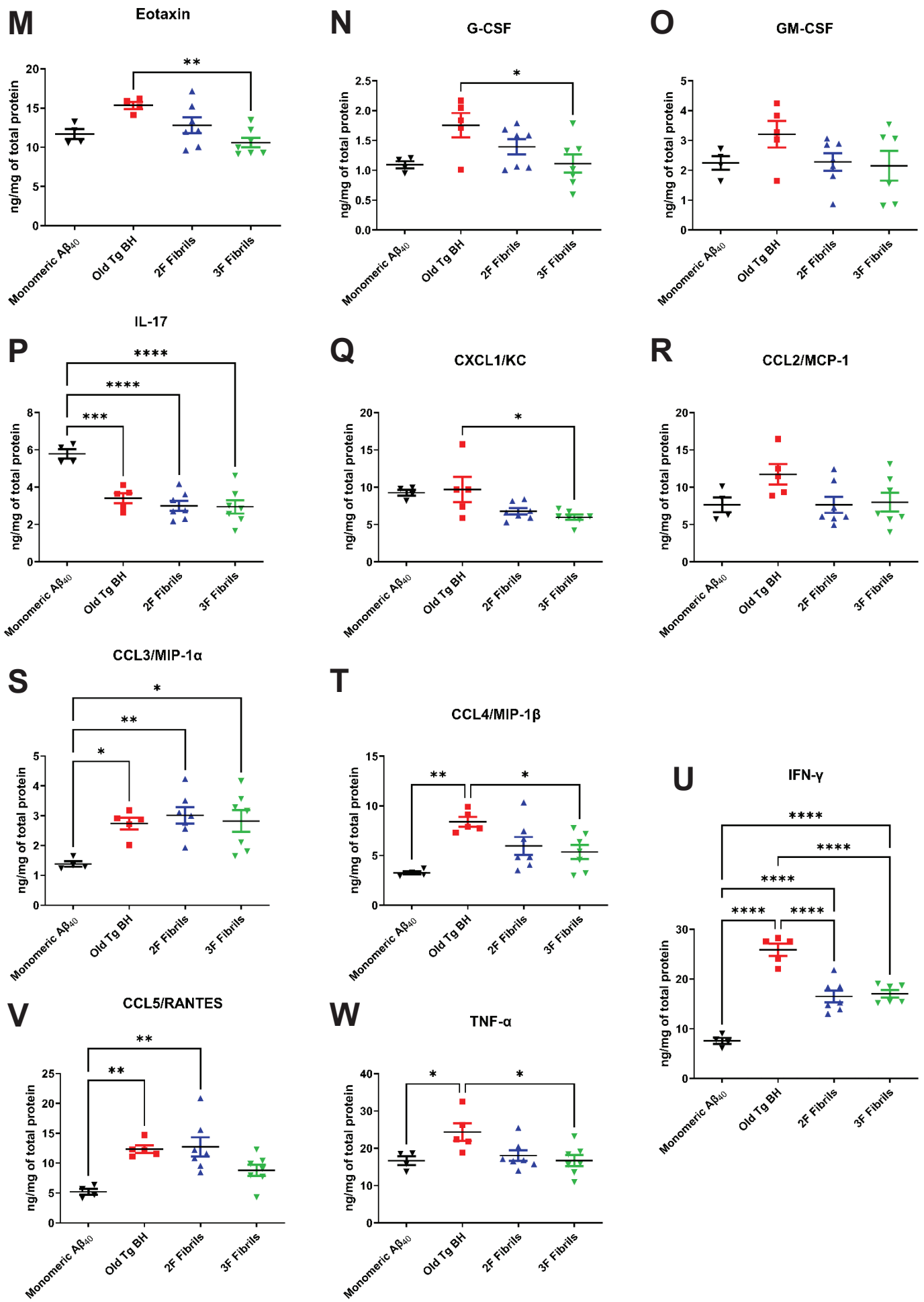

Figure 3.24. 23-plex mouse cytokine/chemokine analyses in the brain of experimental and control mice. A panel of 23 cytokines/chemokines were measured in PBS-soluble (S1) brain fractions samples from mice treated with Tg2576-derived, monomeric $A\beta_{40}$, 2F- and 3F-seeds using the Bio-Plex Pro Mouse Cytokine 23-plex Assay. Concentrations of cytokines/chemokines, normalized to the total amount of protein in the S1 fraction (ng/mL), were significantly different among the groups for IL-1α **(A)**, IL-1β **(B)**, IL-2 **(C)**, IL-3 **(D)**, IL-5 **(F)**, IL-6 **(G)**, IL-9 **(H)**, IL-12p70 **(K)**, IL-13 **(L)**, Eotaxin **(M)**, G-CSF **(N)**, IL-17 **(P)**,CXCL1/KC **(Q)**, CCL3/MIP-1α **(S)**, CCL4/MIP-1β **(T)**, IFN-γ **(U)**, CCL5/RANTES **(V)** and TNF-α **(W)**. Statistical analyses were performed using One-way ANOVA (*p<0.05, **p<0.01, ***p<0.001, ****p<0.0001).

3.2.8. $A\beta_{40}$ conformational strains and brain homogenates from aged Tg2576 induce three unique *in vivo* strains of Aβ: Definitive confirmation by ssNMR.

Previous works have shown that structural variations in Aβ fibrils may correlate with the clinical and pathological variation observed in different subtypes of Alzheimer's disease (Ghosh et al., 2021; Qiang et al., 2017). During this work, we found that Aβ plaques induced by 2F and 3F fibrils, as well as those induced by the brain homogenate of aged Tg2576 mice, were structurally different when measured by different conformation-specific dyes (**Figure 3.15**). The amyloid aggregates also recruited $A\beta_{40}$ and $A\beta_{42}$ differentially (**Figure 3.13 and Figure 3.14**). Furthermore, in collaboration with Dr. Tycko, we decided to unveil the definitive structure of the Aβ fibrils induced by the three different types of seeds by using the most resolutive technique available, the solid-state nuclear magnetic resonance (ssNMR). This is the same key tool that has been previously used for the structural characterization of Aβ fibrils from the amyloid deposits of different AD subtypes (Ghosh et al., 2021; Qiang et al., 2017).

Since ssNMR requires milligram-scale quantities of fibrils and isotopic labeling, fibrils in mouse brain homogenates were amplified by seeded growth *in vitro* (see **section 2.2.15.** in Materials and methods and **Figure 3.26A**), as previously demonstrated in studies of $A\beta_{40}$ fibrils from human brain tissue (Lu et al., 2013; Qiang et al., 2017). $A\beta_{40}$ fibrils for ssNMR were ^{15}N,^{13}C-labeled at all nitrogen and carbon sites in eight residues, namely F19, V24, G25, S26, A30, I31, L34, and M35. NMR frequencies (i.e., chemical shifts) of these residues are sensitive to structural variations among $A\beta_{40}$ polymorphs,

allowing the one-dimensional (1D) and two-dimensional (2D) ssNMR spectra to be used as structural fingerprints (Lu et al., 2013; Qiang et al., 2017).

The 1D ^{13}C ssNMR spectra of $A\beta_{40}$ fibrils grown from amyloid-containing extracts of brain homogenates from mice that had been treated with 2F-, 3F-, or Tg2576-derived seeds is shown (**Figure 3.25A**). These spectra show clear differences, especially in the aliphatic signal region (^{13}C chemical shifts in the 0-70 ppm range). Clear differences in crosspeak positions and crosspeak shapes are also observed in 2D ^{15}N-^{13}C ssNMR spectra, in which signals can be assigned to specific amino acids (**Figure 3.25B**). All labeled residues show differences in ^{13}C and ^{15}N chemical shifts. Two sets of crosspeaks are resolved for F19, G25, and A30 in all three samples, and for I31, S26, and L34 in the sample derived from Tg2576-treated mice. Thus, each brain-derived fibril sample contains at least two distinct polymorphs.

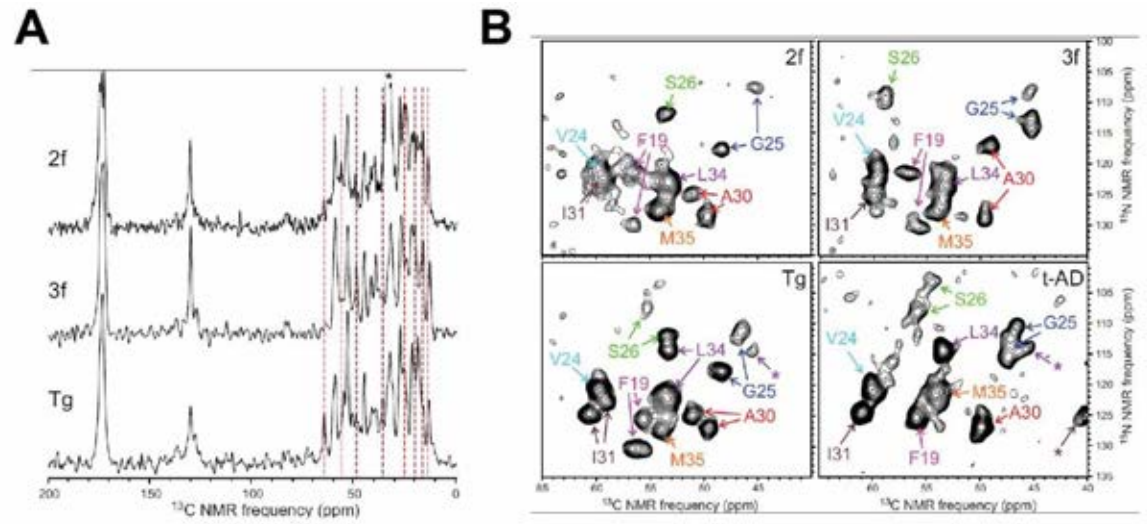

Figure 3.25. Characterization of brain-seeded $A\beta_{40}$ fibrils by ssNMR. (A) 1D ^{13}C ssNMR spectra of fibrils that were prepared *in vitro* by seeded growth from amyloid-containing extracts of mouse brain homogenates from mice injected with 2F-, 3F-, or Tg2576-derived seeds. $A\beta_{40}$ was ^{15}N-,^{13}C-labeled at F19, V24, G25, S26, A30, I31, L34, and M35. Vertical dashed lines indicate some of the ssNMR peaks that vary among the three samples. Asterisk indicates a peak from residual SDS in the 2F sample. **(B)** 2D ^{15}N-^{13}C ssNMR spectra of the same samples, showing intraresidue crosspeaks between chemical shifts of backbone nitrogen and α-carbon sites. Asterisk indicates a crosspeak to the L34 β-carbon. Differences in peak positions in panel **(A)** and differences in crosspeak positions and shapes in panel **(B)** indicate differences in molecular structures of the brain-seeded fibrils.

Superpositions of the 2D ^{15}N-^{13}C ssNMR spectra from the three samples are shown in **Figure 3.26B**. Based on the presence or absence of common crosspeaks in these superpositions, we believe that $A\beta_{40}$ fibrils from 2F- and Tg2576-treated mice may have one polymorph in common but differ in the identity of their second prevalent polymorph.

The most prevalent polymorphs derived from 3F-treated mice are distinct from those derived from 2F- and Tg2576-treated mice. Moreover, one of the prevalent polymorphs in the Tg2576-derived sample may closely resemble the predominant $A\beta_{40}$ polymorph derived from cortical tissue of typical Alzheimer's disease patients (Ghosh et al., 2021; Qiang et al., 2017) based on overlap of ^{15}N-^{13}C crosspeaks (bottom right image in **Figure 3.25B** and green X's in **Figure 3.26B**).

$A\beta_{40}$ fibrils derived from 2F- and 3F-treated mice do not have the same molecular structures as the original 2F and 3F fibrils that were used as seeds to induce amyloid deposition in the mouse brains. Crosspeak positions in 2D ^{15}N-^{13}C ssNMR spectra of the brain-derived samples do not agree with crosspeak positions in similar spectra of 2F and 3F fibrils with the same isotopic labeling pattern (orange and cyan X's in **Figure 3.26C**). Nonetheless, even though molecular structures of synthetic $A\beta_{40}$ seeds do not propagate faithfully *in vivo*, data in **Figure 3.25** and **Figure 3.26** show different molecular structures within amyloid deposits that are induced by structurally distinct $A\beta_{40}$ fibrils.

In summary, ssNMR results definitively confirmed that the aggregates from animals injected with the 2F and 3F fibrils, as well as those injected with the homogenates from aged Tg2576 mice, are structurally different and thus form unique brain-derived fibril polymorphs/strains of Aβ.

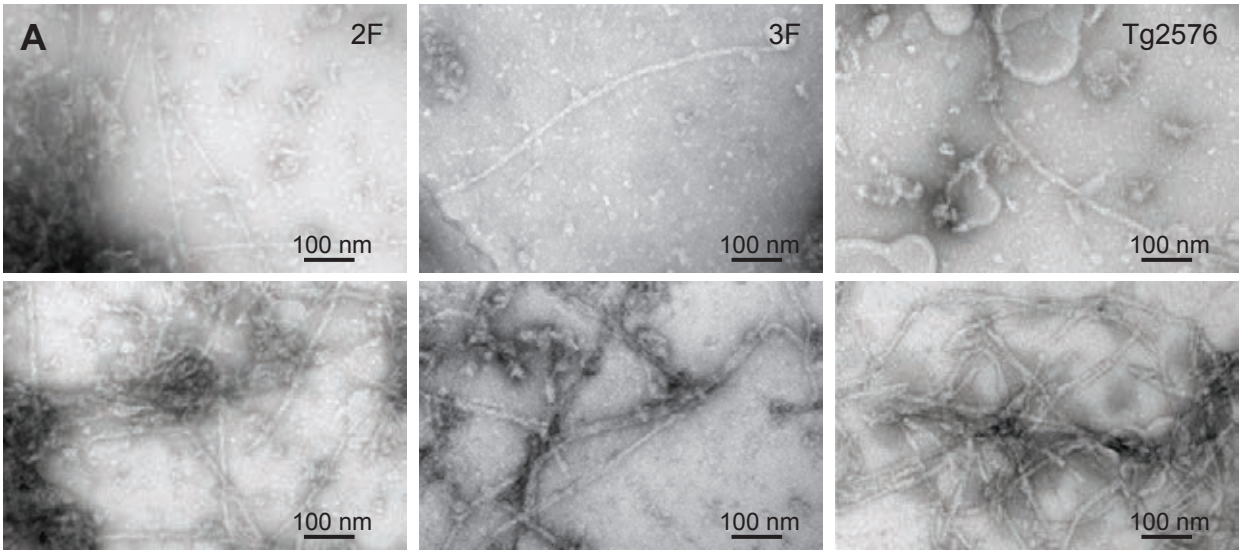

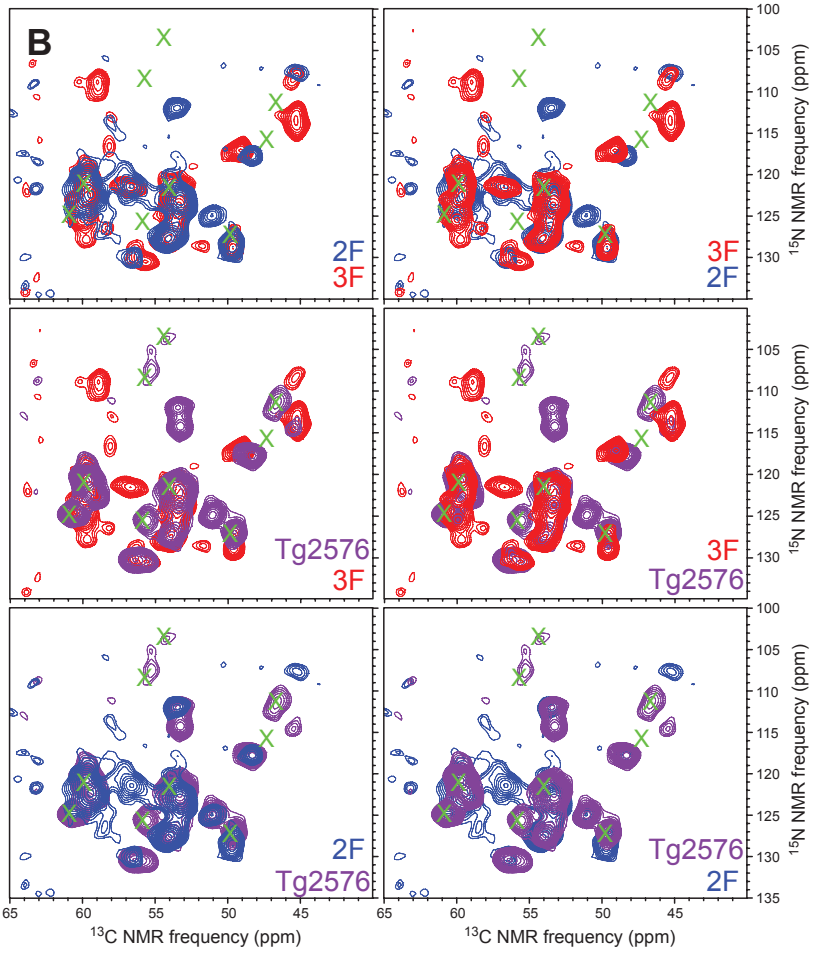

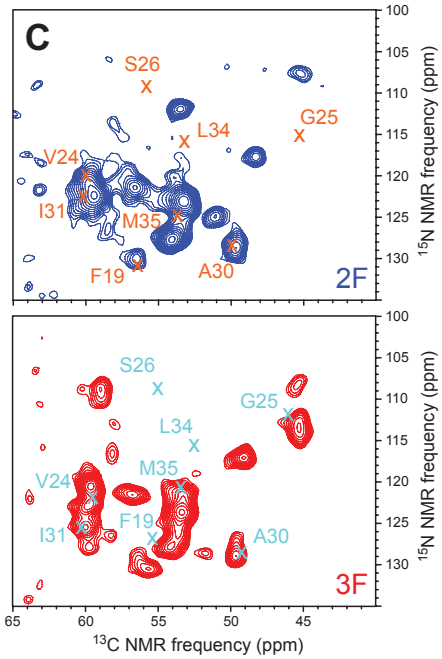

Figure 3.26. Additional characterization of brain-seeded, isotopically labeled Aβ$_{40}$ fibrils and ssNMR data. (A) Negative stained TEM images of fibrils that were prepared *in vitro* by seeded growth from amyloid-containing extracts of mouse brain homogenates from mice injected with 2F-, 3F-, or Tg2576-derived seeds. Images of the 3 samples were acquired after 4 h incubation (top row) and after 4-5 days incubation (bottom row). **(B)** Superpositions of the 2D ^{15}N-^{13}C ssNMR spectra of samples that were derived from mice that had been treated with 2F-(blue contours), 3F-(red contours), or Tg2576- (purple contours). Two superpositions are shown for each pair of spectra, with each of the spectra in the foreground. As an additional comparison, green X's indicate the positions of crosspeaks in spectra of Aβ$_{40}$ fibrils with the same isotopic labeling pattern that were prepared from cortical tissue extracts of typical Alzheimer's disease patients, as reported by Qiang et al. (Nature, vol. 541, pp. 217-221, 2017). **(C)** Comparison of 2D ^{15}N-^{13}C ssNMR spectra of Aβ$_{40}$ fibrils that were derived from 2F- and 3F-treated mice with crosspeak positions in spectra of original 2F (orange X's) and 3F fibrils with the same isotopic labeling pattern (cyan X's).

3.3. THREE DIFFERENT BACTERIAL FUNCTIONAL AMYLOIDS CROSS-SEED THE *IN VITRO* AGGREGATION OF Aβ$_{40}$

3.3.1. CsgA subunit from curli, a bacterial functional amyloid from *Escherichia coli*, accelerates the *in vitro* aggregation of Aβ$_{40}$.

Traditionally associated with debilitating and chronic human diseases, the amyloid structure of proteins has been shown to also assist on important physiological functions, raising the term of functional amyloids. In the case of bacteria, some functions of these amyloids includes the formation of biofilms, adhesion to surfaces, epigenetic control and cytotoxicity (Romero and Kolter, 2014; Shewmaker et al., 2011). The best studied bacterial amyloid protein, made by *Escherichia coli* and *Salmonella spp*, is curli (Barnhart and Chapman, 2006; Chapman et al., 2002). The key element of curli, termed subunit CsgA, has been found to contain amyloidogenic motifs shared by yeast, human prions and α-syn (Cherny et al., 2005; Evans et al., 2015). Interestingly, purified CsgA assembles into curli-like amyloid fibrils upon prolonged incubation *in vitro* (Dueholm et al., 2011; Van Gerven et al., 2015; Wang et al., 2006). Since amyloid proteins found in Alzheimer's and Parkinson's disease are able to self-propagate their morphology and molecular structure in a prion-like manner (Soto, 2012), and fibrils of one misfolded protein have been reported to promote the polymerization of a different amyloid protein in a process known as heterologous seeding or **cross-seeding** (Morales et al., 2013), we **aimed** to investigate whether amyloid fibrils from CsgA subunits were able to cross-seed the polymerization of Aβ$_{40}$. Examples of this mechanism are the crosstalk at the molecular level of prion and AD pathogenic proteins (Morales et al., 2010), and the potentiation of AD pathology by aggregates of IAPP, an amyloid protein that accumulate in pancreatic islets in type-2 diabetes (Moreno-Gonzalez et al., 2017).

In this study, we took advantage of our improved *in vitro* Aβ$_{40}$ aggregation assays (PMCA) to test whether amyloid fibrils from CsgA subunits (curli) were able to nucleate or cross-seed the aggregation of Aβ$_{40}$ monomers. In this aim, we tried two different concentrations of CsgA fibrils, 10 nM and 100 pM. These fibrils were added at the beginning of our aggregation *in vitro* assay, and we found that at both concentrations CsgA fibrils accelerated the aggregation of Aβ$_{40}$ monomers to Aβ$_{40}$ fibrils when compared to samples where no seed was added (**Figure 3.27A-D**). Specifically, CsgA fibrils at 10 nM displayed a considerably faster seeding activity compared to samples without seed, as evaluated by the time they take to seed 20% (81.83±15.5h vs 141.40±16.9h for CsgA

fibrils and No Seed samples respectively for Raw data; ** $p < 0.01$), 50% (138.9±8.1h vs 202.1±23.2h for CsgA fibrils and No Seed samples respectively for Raw data; * $p < 0.05$) and 90% (229.2±22.3h vs 298.3±57h for CsgA fibrils and No Seed samples respectively for Raw data; $p > 0.05$) of maximum aggregation (**Figure 3.27A, C and E**). Furthermore, when we normalized the data for total aggregation (total fluorescence %, **Figure 3.27B and D**), we found similar results on the acceleration of $A\beta_{40}$ aggregation (**Figure 3.27F**). Importantly, CsgA fibrils displayed this phenomenon of cross-seeding even at considerably lower concentration. In this sense, CsgA fibrils at 100 pM concentration displayed also a faster seeding activity compared to samples without seed, as evaluated by the time they take to seed 20% (133.3±9.5h vs 141.40±16.9h for CsgA fibrils and No Seed samples respectively for Raw data; $p > 0.05$), 50% (154.9±6.9h vs 202.1±23.2h for CsgA fibrils and No Seed samples respectively for Raw data; $p = 0.05$) and 90% (189.2±16.5h vs 298.3±57h for CsgA fibrils and No Seed samples respectively for Raw data; $p > 0.05$) of maximum aggregation (**Figure 3.72A, C and E**). Again, when we normalized the data for total aggregation (**Figure 3.27B and D**), we found similar results on the acceleration of $A\beta_{40}$ aggregation (**Figure 3.27F**). It is worth mentioning that our positive controls, in which we seeded with $A\beta_{40}$ fibrils (10 nM and 100 pM as well) to induce homologous seeding, aggregated considerably faster than the samples that were spiked with the CsgA fibrils.

This result confirms that *in vitro* cross-seeding occurs between CsgA fibrils and $A\beta_{40}$. However, this nucleation-polymerization reaction is not as thermodynamically favorable as the reaction between homologous seeds. Interestingly, Aβ aggregates generated by CsgA seeding also displayed different maximum ThT fluorescence signal at plateau (**Figure 3.27A and C**). This result is similar to what we found for 2F and 3F fibrils in the first part of this thesis and suggest that $A\beta_{40}$ amyloid fibrils nucleation by CsgA fibrils results in the formation of $A\beta_{40}$ fibrils polymorphs or strains that could have different toxicity or biological relevance than $A\beta_{40}$ fibrils seeded by homologous seeding.

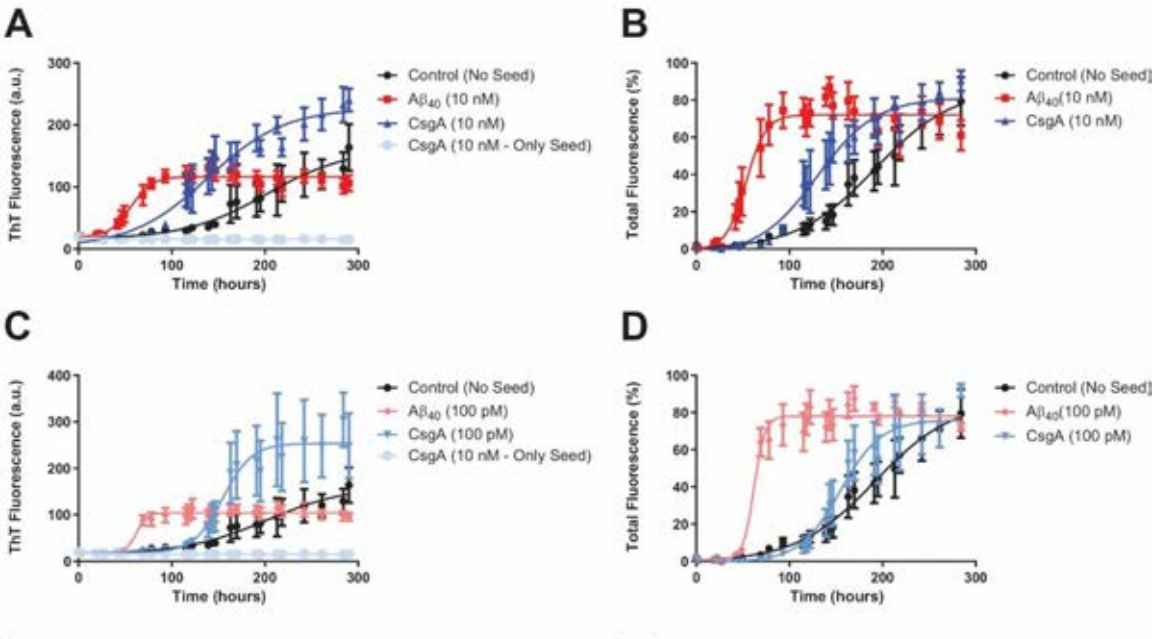

E

Raw Data	T20	T50	T90
No Seed	141.4 ± 16.9	202.1 ± 23.2	298.3 ± 57
$A\beta_{40}$ (10 nM)	40 ± 6.6	56.8 ± 4.2	83.4 ± 8.3
$A\beta_{40}$ (100 pM)	54.29 ± 6.0	62.3 ± 3.96	74.9 ± 5.0
CsgA (10 nM)	81.83 ± 15.5	138.9 ± 8.1	229.2 ± 22.3
CsgA (100 pM)	133.3 ± 9.5	154.9 ± 6.9	189.2 ± 16.5

F

Normalized Data	T20	T50	T90
No Seed	133.5 ± 10.5	191.8 ± 13.9	284.4 ± 34
$A\beta_{40}$ (10 nM)	38.3 ± 5.7	53.8 ± 3.6	78.4 ± 7.7
$A\beta_{40}$ (100 pM)	53.9 ± 3.5	62 ± 2.3	74.9 ± 3.0
CsgA (10 nM)	85.9 ± 12.1	129.8 ± 6.5	199.3 ± 16.8
CsgA (100 pM)	123.9 ± 7.7	154.6 ± 5.8	203.1 ± 14.4

Figure 3.27. Cross-seeding aggregation assay of $A\beta_{40}$ and curli amyloid subunit CsgA. (A-D) Seeding assays using 1 μM of $A\beta_{40}$ monomers and either 10 nM or 100 pM of curli subunit CsgA fibrils or $A\beta_{40}$ fibrils as seeds. Not seeded reaction, containing monomeric $A\beta_{40}$ only, were used as control of spontaneous aggregation. Graphs **(A)** and **(C)** were normalized for total aggregation (Total Fluorescence %) and shown in **(B)** and **(D)**, respectively. Curves were generated by measuring ThT emission values at different time points to show the reaction kinetics. **(E-F)** Table of the average time ± standard error at which fluorescence is 20% (T20), 50% (T50) or 90% (T90) of the maximum fluorescence from raw data **(E)** and normalized data **(F)** of the assays shown in **A-D**.

3.3.2. Microcin E492, a bacterial functional amyloid from *Klebsiella pneumoniae*, accelerates the *in vitro* aggregation of Aβ$_{40}$.

In order to proof that the cross-seeding phenomenon is not specific for CsgA but a common mechanism found in amyloid proteins, we aimed to test other bacterial functional amyloids. In this sense, another amyloidogenic protein found in bacteria is the bacteriocin microcin E492, produced by *Klebsiella pneumoniae*. This bacterial functional amyloid, in its oligomeric state, is able to form pores in the cell surface of competing bacteria and inhibit their growth in order to help *Klebsiella pneumoniae* to colonize this environment, thus providing an adaptive self-benefit (Arranz et al., 2012; Shahnawaz and Soto, 2012; Shahnawaz et al., 2017a).

In this aim, to test whether amyloid fibrils from microcin E492 (Mcc) were able to nucleate or cross-seed the aggregation of Aβ$_{40}$ monomers, we again took advantage of the *in vitro* Aβ$_{40}$ aggregation assays (PMCA). As we did for CsgA, we tried two different concentrations of microcin E492, 10 nM and 100 pM. These fibrils were added at the beginning of our aggregation *in vitro* assay, and we found that at both concentrations microcin fibrils accelerated the *in vitro* formation of Aβ$_{40}$ fibrils when compared to samples where no seed was added (**Figure 3.28A-D**). Specifically, microcin fibrils at 10 nM displayed a considerably faster seeding activity compared to samples without seed, as evaluated by the time they take to seed 20% (46.7±5.5h vs 51.1±16.9h for Mcc fibrils and No Seed samples respectively for Raw data; $p > 0.05$), 50% (57.1±4.3h vs 80.1±9.7h for Mcc fibrils and No Seed samples respectively for Raw data; * $p < 0.05$) and 90% (73.5±8.6h vs 126±26.7h for Mcc fibrils and No Seed samples respectively for Raw data; $p > 0.05$) of maximum aggregation (**Figure 3.28A, C and E**). Furthermore, when we normalized the data for total aggregation (Total Fluorescence %, **Figure 3.28B and D**), we found similar results on the acceleration of Aβ$_{40}$ aggregation (**Figure 3.28F**). Importantly, microcin fibrils also displayed cross-seeding at considerably lower concentration. In this sense, microcin fibrils at 100 pM concentrations induced the aggregation Aβ$_{40}$ at similar speed than the higher concentration, 10 nM, of microcin. Therefore, it also displayed a faster seeding activity compared to samples without seed, as evaluated by the time they take to seed 20% (45.8±4.7h vs 51.1±16.9h for Mcc fibrils and No Seed samples respectively for Raw data; $p > 0.05$), 50% (56.1±3.7h vs 80.1±9.7h for Mcc fibrils and No Seed samples respectively for Raw data; * $p < 0.05$) and 90% (72.5±7.7h vs 126±26.7h for Mcc fibrils and No Seed samples respectively for Raw data;

p = 0.05) of maximum aggregation (**Figure 3.28A, C and E**). Again, when we normalized the data for total aggregation (**Figure 3.28B and D**), we found similar results on the acceleration of Aβ40 aggregation (**Figure 3.28F**). It is worth mentioning that our positive controls, in which we induced homologous seeding with Aβ40 fibrils (10 nM and 100 pM), aggregated considerably faster than the samples that were seeded with the microcin fibrils.

This result further supports the idea that bacterial functional amyloids, in this case microcin, are able to cross-seed Aβ40 *in vitro*. However, this nucleation-polymerization reaction is not as quick as the reaction between homologous seeds. Interestingly, as it happened with the CsgA fibrils, microcin-induced Aβ aggregates displayed different maximum ThT fluorescence signal at plateau (**Figure 3.28A and C**). Thus, this result suggests that Aβ40 amyloid fibrils nucleation by microcin fibrils results in the formation of Aβ40 fibrils polymorphs or strains that could have different toxicity or biological relevance than Aβ40 fibrils seeded by homologous seeding.

3.3.3. The bacterial functional amyloid TasA from *Bacillus subtilis* accelerates the aggregation of Aβ40 *in vitro*.

Besides the CsgA and Mcc amyloids produced by Gram negative bacteria, Gram positive bacteria, such as *Bacillus subtilis* and *Bacillus cereus*, also form amyloid proteins (TasA and CalY) that are critical for biofilms formation derived from this bacteria (Branda et al., 2006; Caro-Astorga et al., 2015; Romero et al., 2010). Therefore, we aimed to proof that the cross-seeding phenomenon seen for CsgA and Mcc was a common mechanism found in amyloid proteins from many bacteria strains. In this sense, we tested the cross-seeding potential of the *Bacillus subtilis* amyloid protein TasA. This amyloid was kindly provided by the lab of professor Dr. Diego Romero.

In this aim, to test whether amyloid fibrils from TasA were able to cross-seed the aggregation of Aβ40 monomers, we again used the *in vitro* Aβ40 aggregation assay (PMCA). As we did for CsgA and Mcc, we tried the same two concentrations of TasA, 10 nM and 100 pM. These fibrils were added again at the beginning of our aggregation *in vitro* assay, and we found that only at low concentration, TasA amyloid fibrils was able to accelerate the *in vitro* formation of Aβ40 fibrils when compared to not seeded samples (**Figure 3.29A-D**). This fascinating result demonstrates that some of these amyloids, at

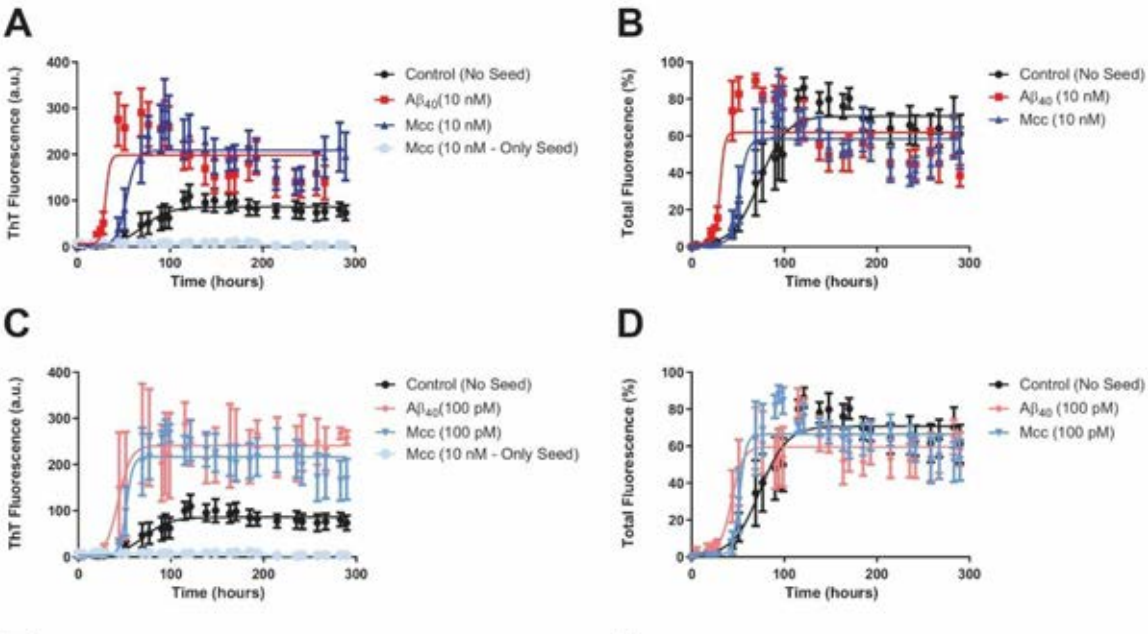

E

Raw Data	T20	T50	T90
No Seed	51.1 ± 16.9	80.1 ± 9.7	126 ± 26.7
$A\beta_{40}$ (10 nM)	31.5 ± 2.9	~ 34	36.5 ± 16.6
$A\beta_{40}$ (100 pM)	33.2 ± 13.4	42.6 ± 7.0	57.6 ± 12.6
Mcc (10 nM)	46.7 ± 5.5	57.1 ± 4.3	73.5 ± 8.6
Mcc (100 pM)	45.8 ± 4.7	56.1 ± 3.7	72.5 ± 7.7

F

Normalized Data	T20	T50	T90
No Seed	53.3 ± 11.2	81.8 ± 6.7	127 ± 18.5
$A\beta_{40}$ (10 nM)	27.7 ± 2.3	~ 33.45	39.2 ± 9.3
$A\beta_{40}$ (100 pM)	33.7 ± 9.4	44.3 ± 4.7	61.2 ± 9.9
Mcc (10 nM)	44.6 ± 4.6	54.1 ± 3.6	69.3 ± 8.8
Mcc (100 pM)	45.7 ± 3.8	55.5 ± 3.0	71 ± 6.7

Figure 3.28. Cross-seeding aggregation assay of $A\beta_{40}$ and microcin (Mcc). (A-D) Seeding assays using 1 μM of $A\beta_{40}$ monomers and either 10 nM or 100 pM of curli microcin-derived fibrils or $A\beta_{40}$ fibrils as seeds. Not seeded reaction, containing monomeric $A\beta_{40}$ only, were used as control of spontaneous aggregation. Graphs **(A)** and **(C)** were normalized for total aggregation (Total Fluorescence %) and shown in **(B)** and **(D)**, respectively. Curves were generated by measuring ThT emission values at different time points to show the reaction kinetics. **(E-F)** Table of the average time ± standard error at which fluorescence is 20% (T20), 50% (T50) or 90% (T90) of the maximum fluorescence from raw data **(E)** and normalized data **(F)** of the assays shown in **A-D**.

high concentration, might induce the opposite activity and thus inhibit the aggregation of other amyloids. Specifically, TasA fibrils at 10 nM displayed a similar seeding activity compared to samples without seed, as evaluated by the time they take to seed 20% (168.6±9.8h vs 141.40±16.9h for TasA fibrils and No Seed samples respectively for Raw data; $p > 0.05$), 50% (173.4±25.1h vs 202.1±23.2h for TasA fibrils and No Seed samples respectively for Raw data ; $p > 0.05$) and 90% (180.9±66.4h vs 298.3±57h for TasA fibrils and No Seed samples respectively for Raw data; $p > 0.05$) of maximum aggregation (**Figure 3.29A, C and E**). The fluorescence level of these aggregations induced by TasA at 10 nM concentrations were really low and thus this higher concentration of TasA fibrils seem to be either inhibiting the nucleation of the $A\beta_{40}$ fibrils or inhibiting the access of ThT to these fibrils. In this case, when we normalized the data for total aggregation (Total Fluorescence %), graphs did not follow a nucleation-polymerization pattern and thus were not added to the figures (**Figure 3.29B, D and F**). Importantly, at considerably lower concentration (100 pM), TasA fibrils significantly induced the aggregation $A\beta_{40}$. The $A\beta_{40}$ monomers seeded with 100 pM of TasA fibrils displayed a faster seeding activity compared to samples without seed, as evaluated by the time they take to seed seed 20% (90.6±10.1h vs 141.40±16.9h for TasA fibrils and No Seed samples respectively for Raw data; * $p < 0.05$), 50% (113.7±5.6h vs 202.1±23.2h for TasA fibrils and No Seed samples respectively for Raw data; *** $p < 0.001$) and 90% (150.4±11.3h vs 298.3±57h for TasA fibrils and No Seed samples respectively for Raw data; * $p < 0.05$) of maximum aggregation (**Figure 3.29A, C and E**). In this sense when we normalized the data for total aggregation (Total Fluorescence %; **Figure 3.29B and D**), we found similar results on the acceleration of $A\beta_{40}$ aggregation (**Figure 3.29F**). It is worth mentioning that our positive controls, in which we induced homologous seeding with $A\beta_{40}$ fibrils (10 nM and 100 pM), aggregated considerably faster than the samples that were seeded with the TasA fibrils.

This result strongly supports the idea that bacterial functional amyloids are able to cross-seed $A\beta_{40}$ *in vitro*. However, the nucleation-polymerization reaction observed with the three functional amyloids (CsgA, Mcc and TasA) was never as quick as the reaction between homologous seeds ($A\beta_{40}$ fibrils). Interestingly, with all three bacterial amyloid fibrils, BFA-induced Aβ aggregates displayed different maximum ThT fluorescence signal at plateau (**Figure 3.27A and C, Figure 3.28A and C; and Figure 3.29A and C**). This result strongly suggests that $A\beta_{40}$ amyloid fibrils nucleation by BFA fibrils results in

the formation of Aβ40 fibrils polymorphs or strains that could have different toxicity or biological relevance than Aβ40 fibrils seeded by homologous seeding.

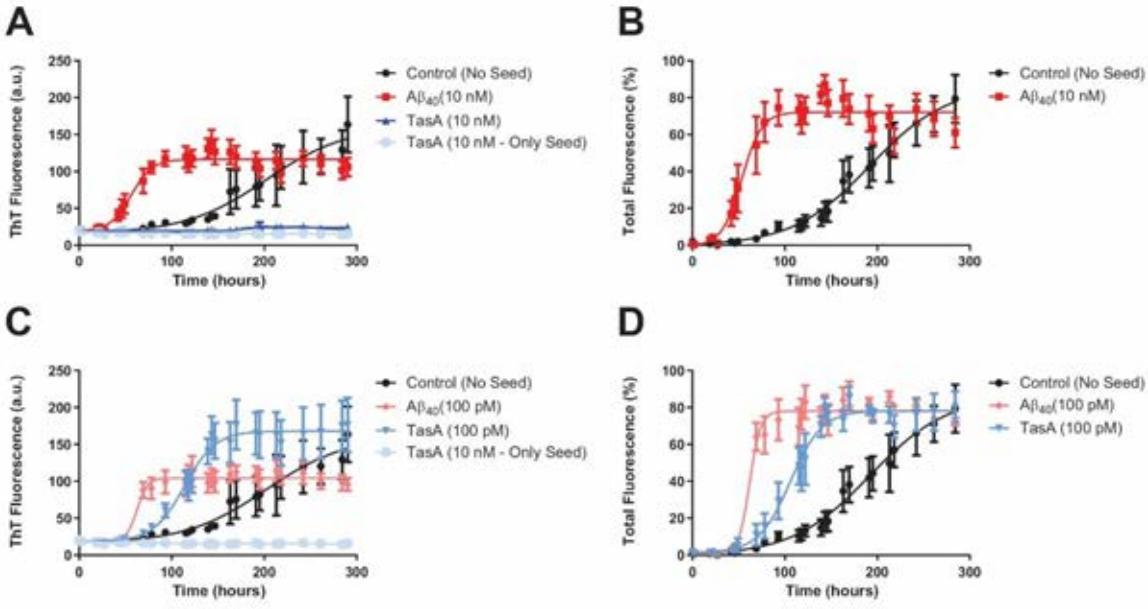

E

Raw Data	T20	T50	T90
No Seed	141.4 ± 16.9	202.1 ± 23.2	298.3 ± 57
$A\beta_{40}$ (10 nM)	40 ± 6.6	56.8 ± 4.2	83.4 ± 8.3
$A\beta_{40}$ (100 pM)	54.29 ± 6.0	62.3 ± 3.96	74.9 ± 5
TasA (10 nM)	168.6 ± 9.8	173.4 ± 25.1	180.9 ± 66.4
TasA (100 pM)	90.6 ± 10.1	113.7 ± 5.6	150.4 ± 11.3

F

Normalized Data	T20	T50	T90
No Seed	133.5 ± 10.5	191.8 ± 13.9	284.4 ± 34
$A\beta_{40}$ (10 nM)	38.3 ± 5.7	53.8 ± 3.6	78.4 ± 7.7
$A\beta_{40}$ (100 pM)	53.9 ± 3.5	62 ± 2.3	74.9 ± 3
TasA (10 nM)	~	~	~
TasA (100 pM)	81.9 ± 6.2	107.7 ± 3.8	~ 147.0

Figure 3.29. Cross-seeding aggregation assay of Aβ40 and TasA from *Bacillus subtilis*. (A-D) Seeding assays using 1 μM of Aβ40 monomers and either 10 nM or 100 pM of TasA fibrils or Aβ40 fibrils as seeds. Not seeded reaction, containing monomeric Aβ40 only, were used as control of spontaneous aggregation. Graphs **(A)** and **(C)** were normalized for total aggregation (Total Fluorescence %) and shown in **(B)** and **(D)**, respectively. Curves were generated by measuring ThT emission values at different time points to show the reaction kinetics. **(E-F)** Table of the average time ± standard error at which fluorescence is 20% (T20), 50% (T50) or 90% (T90) of the maximum fluorescence from raw data **(E)** and normalized data **(F)** of the assays shown in **A-D**.

3.4. BACTERIAL FUNCTIONAL AMYLOIDS INDUCE BRAIN AMYLOIDOSIS IN THE BRAINS OF TG2576 MICE WITH AN INCOMPLETE ATTACK RATE

3.4.1. Bacterial functional amyloids induce amyloid pathology with an incomplete attack rate in the whole-brain of seeding-susceptible amyloidogenic transgenic mice.

To this date, there is no evidence of AD pathology development caused by cross-seeding from bacterial functional amyloids due to a bacterial infection. Therefore, we aimed to investigate whether three different functional amyloids (CsgA, Mcc and TasA) that are found in common pathogens (*Escherichia coli*, *Klebsiella pneumoniae* and *Bacillus subtilis*, respectively) have any pathological and biological relevance in the context of AD. In order to test this idea, we injected 10 µg of well-characterized BFA fibrils (CsgA, Mcc and TasA) in the hippocampus of each brain hemisphere of 50 days old Tg2576 mice (**Figure 2.2**). The negative control animals for these experiments were uninjected Tg2576 mice at 300 days of age. It is worth mentioning that controls injected with monomeric bacterial proteins were not possible due their high rate of aggregation. It was not possible to maintain these amyloids in their monomeric state in PBS buffer, which was the buffer used to inject all the amyloid fibrils in this study.

Animals injected at 50 days of age were euthanized at 300 days of age and their brains were collected. At this timepoint, non-treated Tg2576 mice display small amount of Aβ deposits (Hsiao et al., 1996). Collected brains from the euthanized mice were separated in both hemispheres, keeping one hemisphere frozen for biochemical analyses while the other hemisphere was preserved for histopathological studies (**Figure 2.2A)**. Frozen brain hemispheres were homogenized and prepared to isolate PBS-soluble cytokines and PBS-insoluble Aβ peptides as described in methods. Levels of $A\beta_{40}$ and $A\beta_{42}$ were measured from the PBS-insoluble S2 fractions by using commercially available protein-based multiplex immunoassay.

Results from this analysis showed that $A\beta_{40}$ and $A\beta_{42}$ levels were not significantly different among the groups of animals injected with BFAs when compared to uninjected animals (**Figure 3.30A and B**). Although non-significant, increased levels of these peptides were observed in some individual mice injected with CsgA or TasA fibrils (**Figure 3.30A and B**). Similar results were observed when we added the levels of $A\beta_{40}$ and $A\beta_{42}$ (**Figure 3.30C**). Interestingly, animals injected with microcin fibrils displayed significantly increased ($F(3,31) = 3.119$, $p = 0.0467$) $A\beta_{42}/A\beta_{40}$ ratio (**Figure 3.30D**). This result suggests that microcin fibrils might not induce a significant increase of any of

the individual peptides (Aβ40 and Aβ42) but overall cause a small switch from Aβ40 deposition to Aβ42 deposition, a peptide that is more prone to aggregation. Nevertheless, one of the limitations of this particular analysis was that the results were representative of whole brain hemispheres, potentially diluting increased seeding events that could be restricted to a particular brain region.

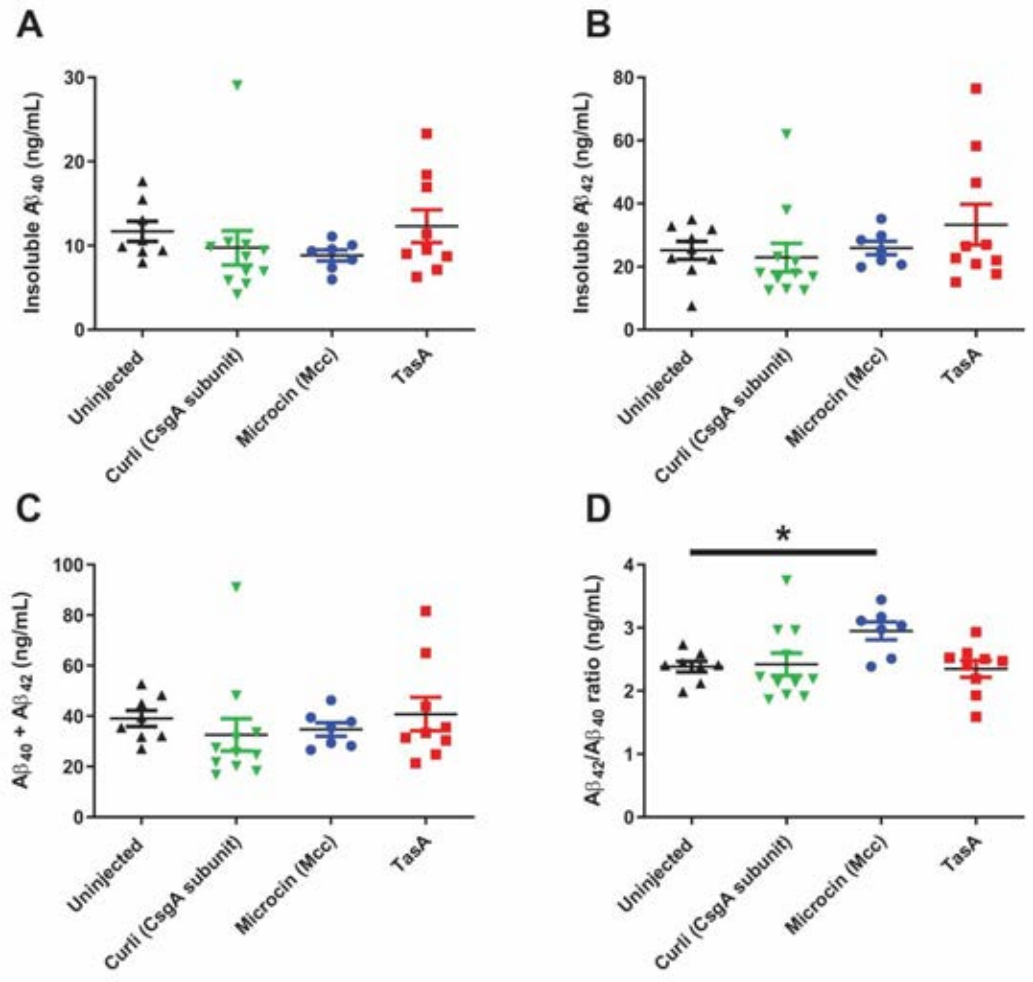

Figure 3.30. Analysis of PBS-insoluble fractions by protein-based multiplex immunoassay for both Aβ40 and Aβ42 in Tg2576 animals 250 days post injection with Bacterial Functional Amyloids (BFAs). Levels of insoluble Aβ40 **(A)** and Aβ42 **(B)** were measured with a commercially available multiplex immunoassay. **(C)** Levels of both proteins were also added to quantify the total amount of both proteins. **(D)** Ratio of Aβ42/Aβ40 shows significant increase in animals injected with microcin (Mcc) fibrils. Statistical analyses were performed using One-way ANOVA (*p<0.05).

3.4.2. CsgA fibrils induce amyloid pathology in the hippocampus of Tg2576 mice while Mcc and TasA fail to induce a robust amyloid pathology.

In order to address the potential issue of diluting brain region-specific seeding events due to studying the whole-hemisphere, we analyzed the Aβ levels and specific location (tropism) of the induced amyloid deposits in the opposite brain hemisphere from the same mice by immunohistochemical methods. By performing this region-specific analysis, we observed significant differences, specifically in the injected site (hippocampus). Mice injected with CsgA fibrils (second column in **Figure 3.31A and B**) displayed a significant increase ($F(3,31) = 3.119$, $p = 0.028$ vs Uninjected, $p = 0.0104$ vs Mcc and $p = 0.0204$ vs TasA) in the hippocampal amyloid burden compared to other groups (**Figure 3.31D**) On the other hand, the groups of mice injected with either microcin or TasA fibrils (third and fourth column, respectively, in **Figure 3.31A and B**). did not show significant increase in Aβ deposition in the hippocampus (**Figure 3.31D**). Interestingly, some animals from these groups displayed small amyloid plaques in the hippocampus (see insets from A in **Figure 3.31B**). In-depth analysis of other regions such as subiculum and cortex resulted in non-significance differences among the groups (**Figure 3.31C, E and F**). Again, few animals for each of the injected group developed small amyloid deposition but overall, the difference between the groups were not significant.

In order to analyze other types of Aβ deposition, we next aimed to study the vascular deposition of Aβ in these animals. Specifically, we focused on the meningeal vessels and calculated the percentage of vessels that were positive for the Aβ-specific antibody 4G8. One more time, we did not find significant changes among the groups (**Figure 3.31G**) but few animals for each of the groups developed meningeal deposition of Aβ.

These results, suggest that functional amyloids from bacteria might not completely induce the development of a robust amyloid pathology in the Tg2576 mice. However, the finding that some of the animals develops amyloid pathology when injected with these bacteria-derived fibrils raise the possibility that CsgA, microcin and TasA amyloids might be inducing amyloid deposition but with an incomplete attack rate. Attack rates have been previously described for both prions- and Aβ-related pathologies and represent the proportion of the total animals per group in which the pathology of the experimental animals is significantly higher than in their controls. Specifically, this term of attack rate has been well-established in previous finding that only a few experimental animals

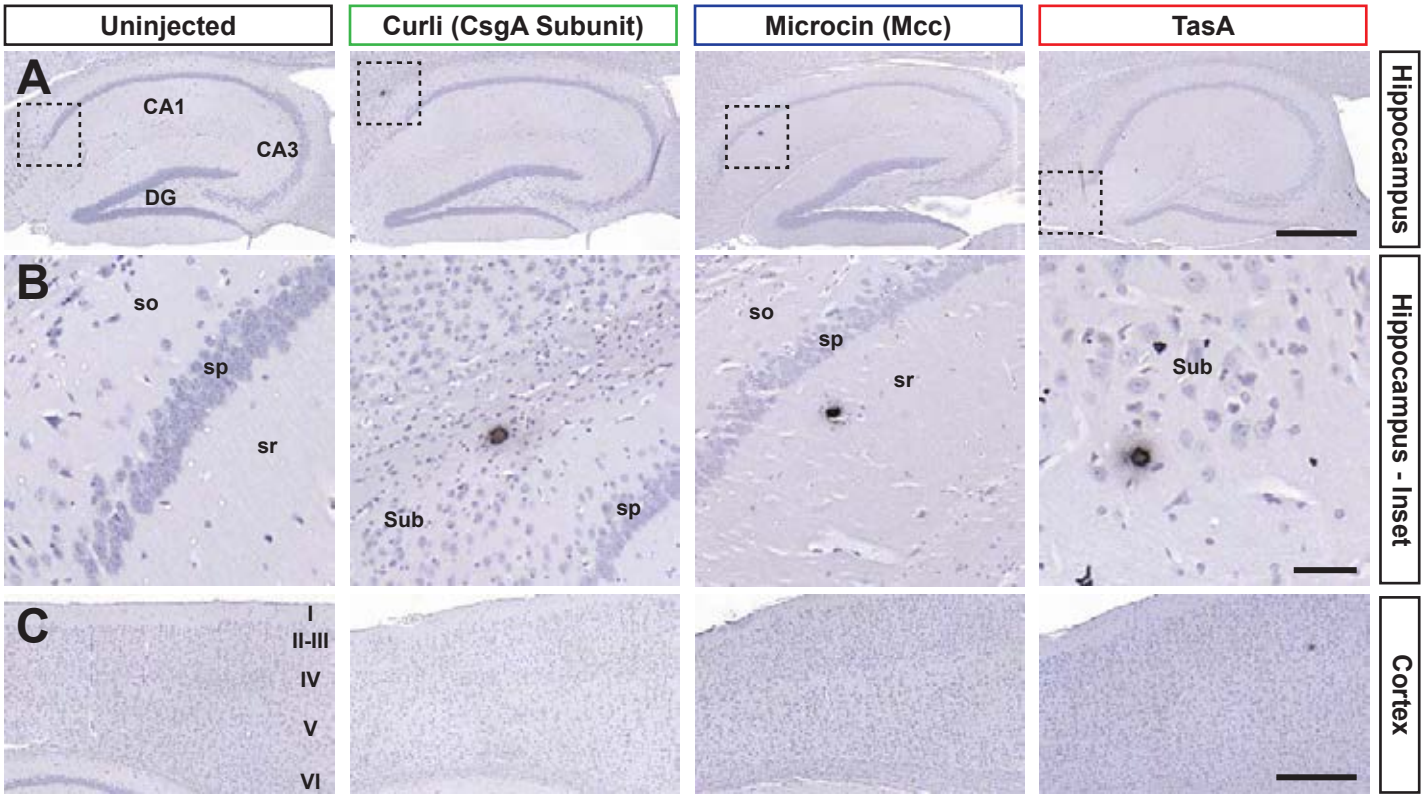

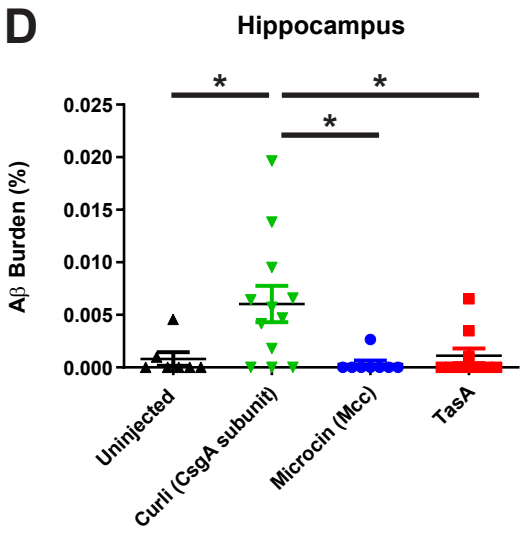

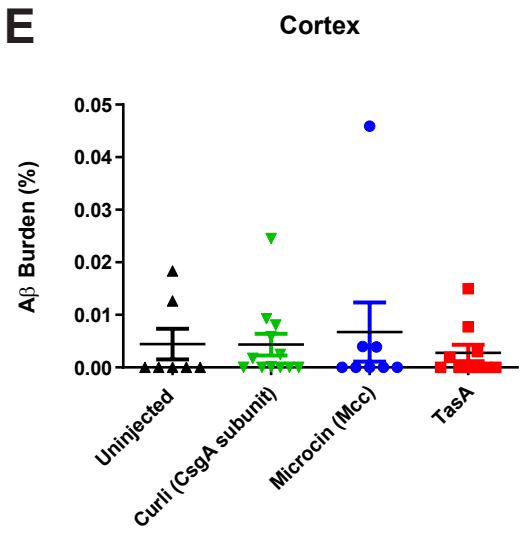

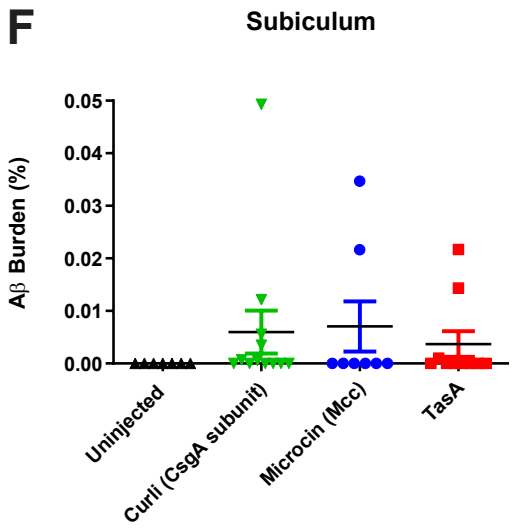

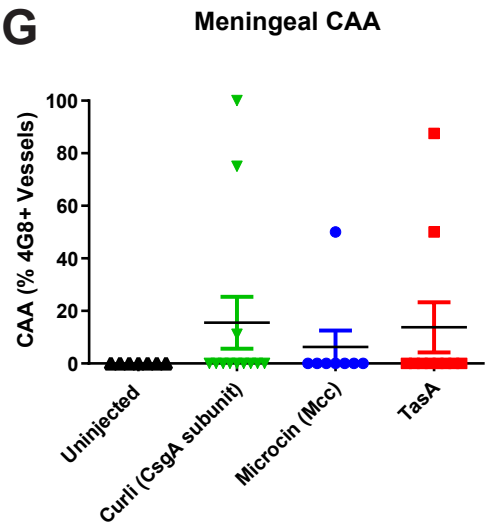

Figure 3.31. Amyloid pathology in Tg2576 mice seeded by CsgA, Microcin and TasA fibrils. Representative pictures of hippocampus **(A)** and cerebral cortex **(C)** from mice uninjected or treated with CsgA-, Mcc- and TasA- derived seeds after visualization for Aβ deposits using the 4G8 antibody. Panels in **(B)** are insets obtained from hippocampi images (white punctuated squares). Scale bars in panels in **(A)** and **(C)** represent 500 µm and are applicable to the pictures labeled as "Uninjected", "Curli (CsgA Subunit)", "Microcin (Mcc)" and "TasA". Scale bars on the right Inset images **(B)** represent 50 µm. *CA1: Cornu Ammonis area 1, CA3: Cornu Ammonis area 3, DG: Dentate Gyrus, so: stratum oriens. sp: stratum pyramidale. sr: stratum radiatum*, *Sub: subiculum*. Cortical layers I through VI are shown in **C**. Aβ burden quantification in hippocampus **(D)**, cortex **(E)** and subiculum **(F)**. Quantification of the percentage of total meningeal vessels that are 4G8-positive in the four different animal groups **(G)**. Statistical analyses performed by One-way ANOVA * $p<0.05$.

develop pathology when receiving intravenous administration of blood that contains prions or Aβ (Brown et al., 2001; Gregori et al., 2004; Morales et al., 2020). This finding in our animals injected with BFA fibrils also raise the question on whether a longer incubation period would result in the development of full amyloid pathology in these animals.

3.5. BACTERIAL FUNCTIONAL AMYLOIDS HAVE LITTLE IMPACT IN THE BRAIN CYTOKINE AND CHEMOKINE PROFILES OF INJECTED MICE

Given the connection between microglial and astroglial activation and cytokine production, and our results with the Aβ strains, we aimed to investigate whether each bacterial functional amyloid induced differential patterns of cytokine and chemokine expression and, therefore, neuroinflammatory response in a similar fashion as the different Aβ strains did. Specifically, we used again a multiplex immunoassay to quantify 22 cytokines (**Figure 3.32**) in the brain soluble fractions (S1) in order to gain broad information from the most relevant signaling molecules in the brain and the inflammatory microenvironment. In summary, we found little difference in cytokines' levels between groups for most of the cytokines/chemokines (16 out 22). However, mice inoculated with the CsgA seeds displayed greater cytokine alterations, with IL-9 (**Figure 3.32H,** $F(3,35) = 3.461$, $p = 0.0232$) and TNF-α (**Figure 3.32U,** $F(3,35) = 3.376$, $p = 0.0377$) levels

significantly increased when compared to control uninjected animals. On the other hand, animals injected with CsgA seeds showed significantly decreased levels of IL-17 (**Figure 3.32O,** $F(3,35) = 15.08$, $p = 0.0071$) when compared to control. Moreover, animals injected with TasA seeds also displayed significantly lower levels of IL-17 when compared to all the other animal groups (**Figure 3.32O,** $F(3,35) = 15.08$, $p < 0.0001$ vs uninjected, $p = 0.0237$ vs CsgA and $p < 0.0001$ vs Mcc). Additionally, animals injected with TasA seeds also showed decreased levels of IL-1α (**Figure 3.32A,** $F(3,35) = 3.034$, $p = 0.0424$) and CXCL1 (**Figure 3.32P,** $F(3,35) = 2.743$, $p = 0.0413$) when compared to animals injected with microcin E492. Interestingly, animals injected with TasA also displayed significantly increased levels of CCL3 when compared to all the other animal groups (**Figure 3.32R,** $F(3,35) = 13.92$, $p = 0.0016$ vs uninjected, $p < 0.0001$ vs CsgA and $p < 0.0001$ vs Mcc). In summary, none of the bacterial functional amyloids induced a robust inflammatory response. Since, the cytokine/chemokine levels were measured 250 days after injection and little Aβ deposition was observed at this time point, this might result in these little changes in inflammatory response. Interestingly, it seems that CsgA fibrils induced a mixed profile with both anti-inflammatory (high IL-9 and low IL-17) and proinflammatory (high TNF-α) signatures. Similar mixed profile was also found in animals injected with TasA fibrils with both anti-inflammatory (low IL-1-α, low CXCL1 and low IL-17) and proinflammatory (High CCL3 and tendency to an increase in TNF-α and IFN-γ). Overall, animals injected with Mcc fibrils displayed similar levels for all of the cytokines/chemokines than uninjected animals (**Figure 3.32**).

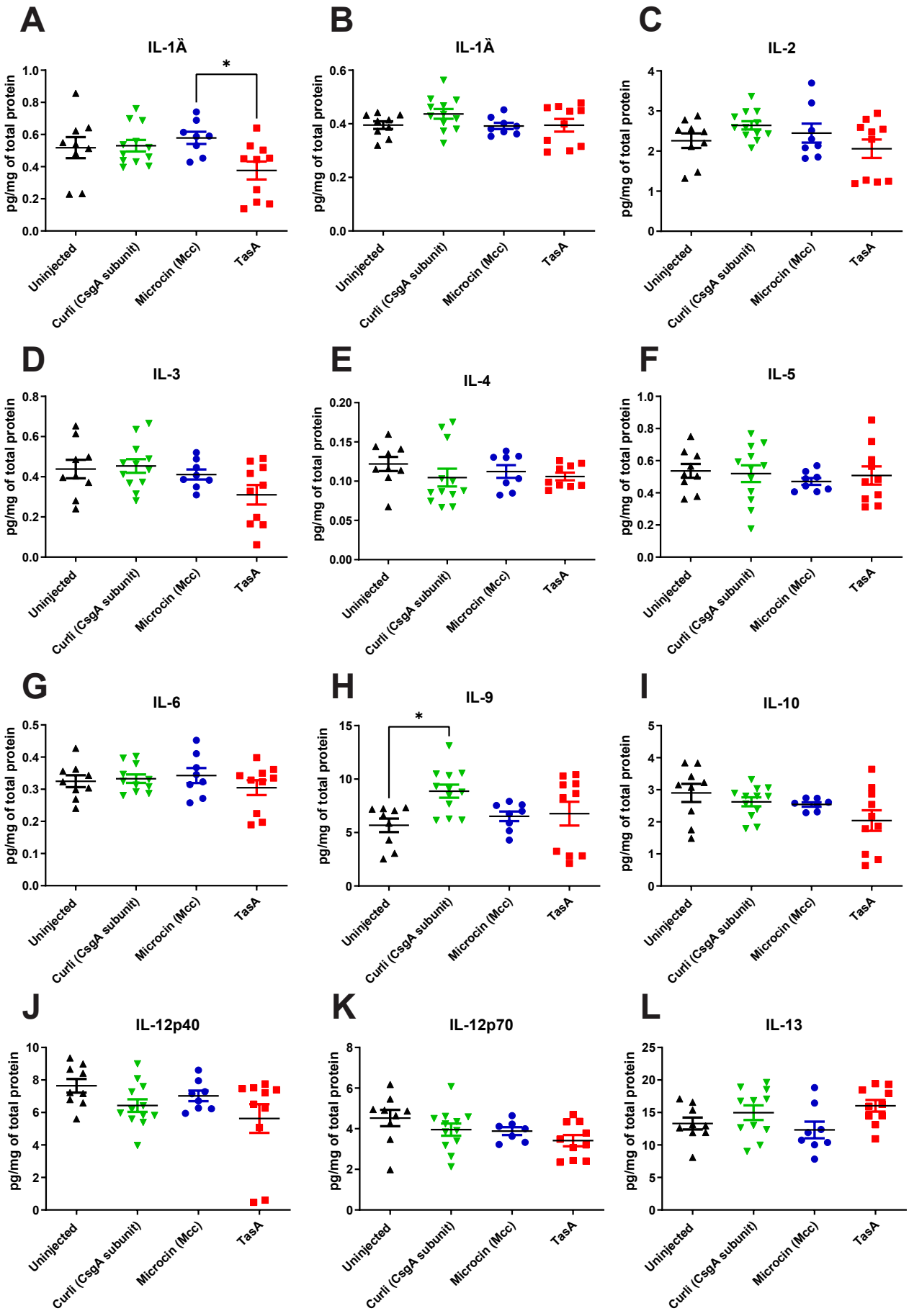

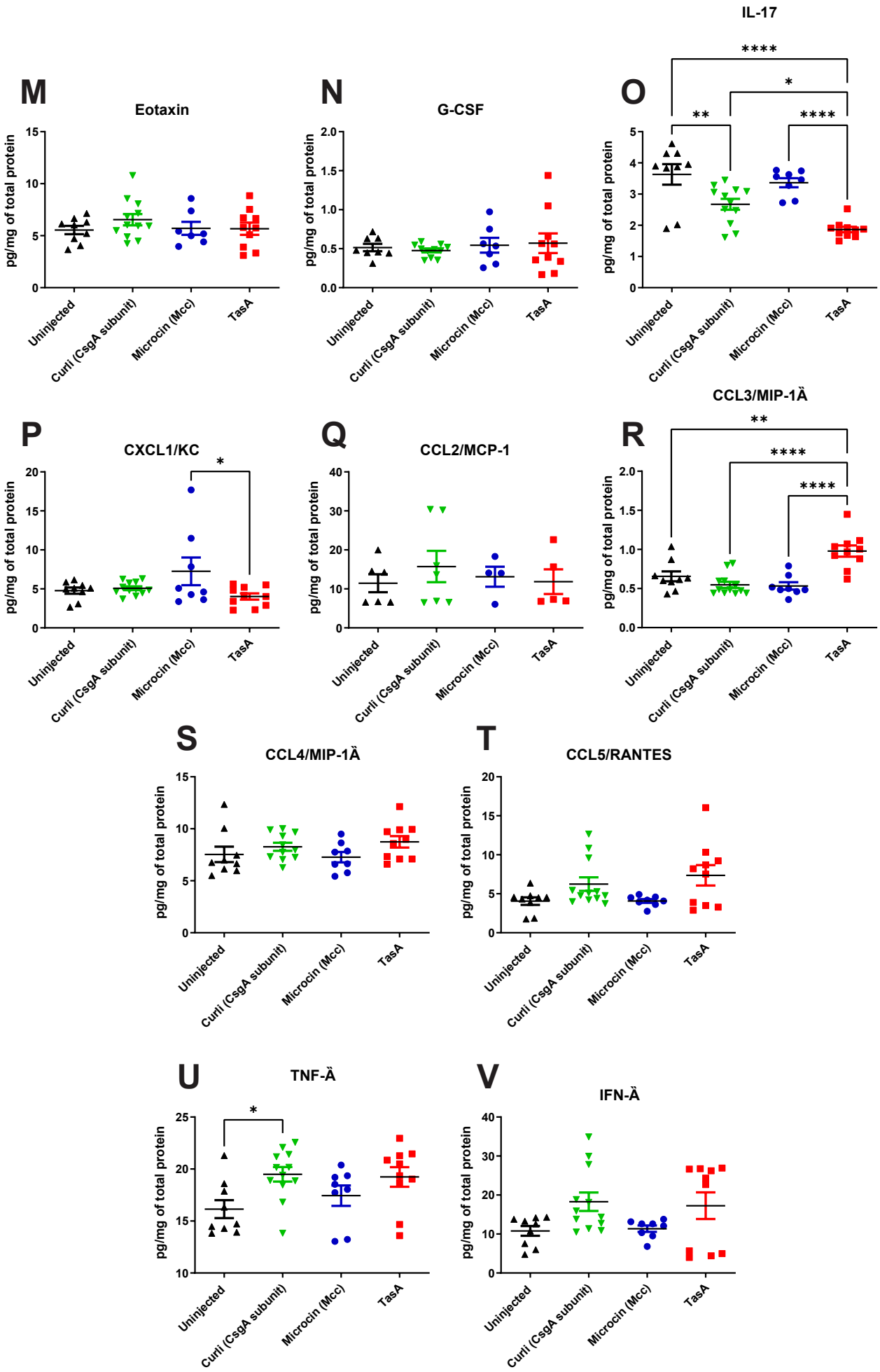

Figure 3.32. 23-plex mouse cytokine/chemokine analyses in the brain of experimental and control mice. A panel of 23 cytokines/chemokines were measured in PBS-soluble (S1) brain fractions samples from mice injected with CsgA fibrils, microcin E492 fibrils and TasA fibrils, and from uninjected mice, using the Bio-Plex Pro Mouse Cytokine 23-plex Assay. Concentrations of cytokines/chemokines, normalized to the total amount of protein in the S1 fraction (mg/mL), were significantly different among the groups for IL-1α **(A)**, IL-9 **(H)**, IL-17 **(O)**, CXCL1/KC **(P)**, CCL3/MIP-1α **(R)** and TNF-α **(U)**. Statistical analyses were performed using One-way ANOVA (*p<0.05, **p<0.01, ****p<0.0001).

4. Discussion

Aimed to gain insight into the biological significance of specific Aβ strains in AD pathology, we inoculated well-characterized synthetic Aβ conformers (2F and 3F fibrils) in the hippocampus of a mouse model of brain amyloidosis (Tg2576 transgenic line). AD pathological features in both, 2F- and 3F-inoculated mice, such as Aβ burden, tropism, and structural features of the amyloid deposits were analyzed. Moreover, microglial and astroglial responses were also evaluated. The main findings from this thesis work are summarized below:

1. Further *in vitro* characterization of the two synthetic Aβ strains shows clear distinct biochemical and structural features. Moreover, these unique conformational arrangements maintain the ability to self-propagate these unique structures, further supporting that these two Aβ conformers are actually two different strains.
2. The inoculation of Tg2576 transgenic mice with these two Aβ strains (2F and 3F) results in higher Aβ deposition in animals injected with the 2F fibrils. These animals also show clear tropism towards the alveus region of the hippocampus, while 3F injected mice display Aβ deposition tropism towards the dentate gyrus. In depth structural analysis of the deposits induced by the 2F and 3F fibrils show clear distinction of these deposits by the staining with conformation specific dyes (LCOs), as well as by their unique ssNMR spectra.
3. *In vivo* seeding experiments result in unique inflammatory responses to the three different inocula (brain homogenate from aged Tg2576 mice, 2F and 3F fibrils). Similar to Aβ deposition, 2F injected animals display an increase in reactive microglial and astroglial cells in the alveus region, while 3F injected animals show a local inflammatory response in dentate gyrus. Specifically, microglial cells show stronger response to 3F induced aggregates than to 2F induced Aβ deposits in the dentate gyrus.

In the second part of this PhD thesis, we aimed to investigate the direct interaction of three bacterial functional amyloids (curli CsgA subunit, microcin E492 and TasA) with the AD-associated peptide Aβ in order to find potential pathological associations between our symbiotic and pathogenic bacteria and AD. In this sense, *in vitro* experiments were performed to analyze the potential cross-seeding mechanism between the three bacterial functional amyloids and Aβ. Moreover, Tg2576 transgenic mice were inoculated with the

three bacterial functional amyloids. The main hallmark of AD, Aβ deposition in the brain parenchyma, was analyzed in these mice. Moreover, the inflammatory response to these functional amyloids was also evaluated. The main findings are summarized below:

1. *In vitro* aggregation assays show clear cross-seeding and thus induction of Aβ aggregation by seeding with CsgA, microcin E492 and TasA fibrils. This supports the ability of bacterial functional amyloids to cross-seed the AD associated pathological peptide, Aβ.
2. The inoculation of Tg2576 transgenic mice with these three bacterial functional amyloids (CsgA, microcin E492 and TasA) demonstrate that microcin E492 and TasA does not induce Aβ deposition in the brain of injected animals. However, CsgA fibrils induce the aggregation of Aβ in the hippocampus of inoculated mice. This result demonstrates the specific *in vivo* cross-seeding between CsgA and Aβ. Results with microcin E492 and TasA point to differences between *in vitro* and *in vivo* experiments and thus highlight the need to re-assess with *in vivo* experiments all the experiments done *in vitro*.

In general, this PhD thesis work has provided new knowledge and deeper understanding on the biological significance of different Aβ conformers in Alzheimer's disease. Moreover, this work has also demonstrated a novel mechanism by which symbiotic and pathogenic bacteria might induce AD neuropathological hallmarks such as Aβ deposition. In the following chapters, the most relevant results obtained in this PhD thesis are discussed.

4.1.1. THE 2F AND 3F AGGREGATES DISPLAY UNIQUE STRUCTURAL AND BIOCHEMICAL FEATURES

It has been thoroughly demonstrated the existence of Aβ strains with unique structural and biochemical features, such as their unique conformational arrangements and ability to self-propagate their unique conformation (Lau et al., 2021). Specifically, the two morphologically distinct synthetic $A\beta_{40}$ fibrils that were used in this PhD work were previously extensively characterized showing clearly different structural features by TEM and ssNMR (Petkova et al., 2005). Briefly, these fibrils showed specific twist, width and mass-per-length and thus displayed 2-fold (2F fibrils) and 3-fold (3F fibrils)

rotational symmetry about the fibril growth axis. Even though this study demonstrated differential mechanical properties, self-propagating features, and distinct toxicity in primary hippocampal neuronal cultures from rats, the *in vivo* propagation and biological significance of these unique structures needed to be further evaluated. This was the main aim of this PhD work and thus, in order to inject these fibrils in mice brain, new 2F and 3F fibrils were synthesized and were consequentially resuspended in PBS, a buffer solution mimicking physiological environments that would not affect the mice upon injection. Therefore, upon new synthesis and resuspension in PBS, it was important for our work that the unique structural and biochemical properties shown by the 2F and 3F fibrils in comparison to the original fibrils was not modified.

In this sense, we first visualized these aggregates by TEM demonstrating clear distinction between the two synthetic fibrils, with 2F fibrils showing a smaller width than 3F fibrils, and 3F fibrils showing a pronounced twist. Therefore, by TEM we demonstrated that newly synthesized 2F and 3F fibrils showed similar characteristic than the original reported 2F and 3F fibrils. Later, these two synthetic fibrils were tested for their specific resistance to proteolytic degradation using increasing concentrations of proteinase K (PK). This conformational stability assay has been reported to distinguish strains formed by disease-associated amyloids such as Aβ (Cohen et al., 2015; Di Fede et al., 2018), prion protein (Pastrana et al., 2006) and α-synuclein (Shahnawaz et al., 2020). Therefore, we believe that our results showing that both 2F and 3F fibrils were clearly distinguishable by this assay, with 2F fibrils displaying a significant higher resistance to proteolytic digestion, support that 2F and 3F fibrils are unique strains of synthetic $A\beta_{40}$.

Furthermore, in order to demonstrate that these two distinct $A\beta_{40}$ conformers retain their ability to self-propagate their structure, we used this fibrils in a PMCA assay modified for $A\beta_{40}$ (Salvadores et al., 2014). Importantly, 2F and 3F fibrils showed both distinct rate of aggregation and unique maximum ThT fluorescence signals. This outcome is strikingly similar to other reports that showed the ability of ThT-based assays to detect structural variations in fibrils comprised of the same polypeptide. Specifically for Aβ, it has been reported that ThT-based aggregation assays were able to detect structural variations in Iowa Mutant Aβ fibrils polymorphs (Qiang et al., 2011). Furthermore, our results were also similar to the one that have been reported for α-synuclein products seeded with Multiple System Atrophy (MSA) and Parkinson's Disease (PD) samples (Shahnawaz et al., 2020). Therefore, this result further confirms the differential self-propagating properties of 2F and 3F and demonstrates the differential accessibility and

reactivity of ThT to the Aβ aggregates generated by seeding. Moreover, given that for α-synuclein different conformations of aggregates are found in two distinct α-synucleinopathies, and these are clearly detected with this *in vitro* technique, our similar results using an equivalent system demonstrate the potential of 2F and 3F fibrils to induce two different and unique Aβ-related pathology. The differential pathological activity of misfolded Aβ strains was later evaluated in this thesis work.

Definitive structural differences between 2F and 3F fibrils were found by using conformation-specific dyes. Specifically, differential binding suggesting unique structural motifs on these two fibrils was demonstrated by four different LCOs (HS-68, HS-194, HS-208 and HS-212). These dyes have been previously shown to discriminate between different conformation of misfolded Aβ and tau deposits (Klingstedt et al., 2011, 2013; Nilsson et al., 2007) and between MSA and PD α-synuclein strains (Shahnawaz et al., 2020). Therefore, our results support, once again, the idea that 2F and 3F are structurally different.

Altogether, our data from TEM, the differential biochemical features displayed by 2F and 3F fibrils such as their differential resistance to proteolytic digestion with PK, their unique *in vitro* seeding activities, and their strain-specific affinities to dyes such as ThT and the four different LCOs, clearly demonstrate distinct structural motifs from 2F and 3F fibrils. These results perfectly complement previous data on these two Aβ strains from the group of Dr. R. Tycko (Petkova et al., 2005). Therefore, these fibrils serve as a perfect inocula to be used in our *in vivo* seeding experiment.

The clinical relevance of the existence of different Aβ strains is discussed in **section 4.1.7.**

4.1.2. UNIQUE PATTERNS OF BRAIN AMYLOIDOSIS ARE SHOWN AFTER *IN VIVO* SEEDING WITH 2F AND 3F $A\beta_{40}$ CONFORMATIONAL STRAINS

It is known that there are three key properties that amyloid aggregates have to fulfill in order to be considered strains. **First**, two different strains should display unique conformational arrangements. **Second**, strains should have the ability to self-propagate their unique structural arrangements. **Finally**, strains should induce distinct disease phenotypes, both pathologically and clinically, which would depend on their conformational variant (Morales, 2017). In the case of Aβ aggregates, it has been demonstrated the existence of different unique conformational arrangements and their

ability to self-propagate their unique conformations (Lau et al., 2021). In the first part of this PhD work, these two key properties were demonstrated by *in vitro* experiments. However, it was necessary to demonstrate these properties *in vivo* and also to demonstrate the third key property of amyloid strains: the ability of these conformational variants to cause distinct disease phenotypes.

Specifically, to fulfill the **criteria for self-propagating Aβ strains**, 2F and 3F fibrils should display spreading of their unique structure into another brain regions and should demonstrate distinct disease phenotypes such as strain-specific tropisms towards specific brain regions, differential seeding activities, unique structural morphology of the aggregates (dense-core *vs* diffuse plaques and with specific binding to conformational specific dyes) and different types of aggregates (parenchymal *vs* vascular). In addition, strain-specific misfolded polymers should induce differential biological responses in the host (Morales, 2017). In order to demonstrate these features in our Aβ strains, 2F and 3F fibrils, we performed stereotaxic injections with these two synthetic $A\beta_{40}$ strains in the hippocampus of 50 days old Tg2576 transgenic mice. In our first analysis, in which we measured the levels of $A\beta_{40}$ and $A\beta_{42}$ from the PBS-insoluble S2 fractions of 300 days old, injected mice, we observed a significant increase of insoluble $A\beta_{42}$ levels in animals injected with aged Tg2576 brain extract and in animals injected with the 2F fibrils, when compared to control (injected with monomeric $A\beta_{40}$) and 3F-injected mice. Importantly, mice injected with aged Tg2576 brain extract displayed significantly higher accumulation of $A\beta_{42}$ than those injected with 2F fibrils. The differences we found between mice treated with aged Tg2576 brain extract and 2F fibrils, are in line with previous reports from the group of Dr. Stanley B. Prusiner (Stöhr et al., 2012). Similar to our results, this group reported that aggregates from synthetic Aβ are sufficient to induce Aβ deposition *in vivo*. Moreover, as in our work, they demonstrated that the aggregates from synthetic Aβ exhibit lower specific biological activity and induce less Aβ deposition compared to animals injected with brain derived aggregates of Aβ.

A concern we had with our results was the high concentration (10 µg/ hippocampi) of synthetic $A\beta_{40}$ peptide in our 2F and 3F fibrils inocula. This raise the possibility that the aggregates observed in the brain of our injected mice could be the result of residual Aβ from the inoculum that has not been cleared from the brain. To tackle this issue, we also euthanized animals 100 days post-injection, instead of the 250 days post-injection we did for the main experimental groups. We found that at this age animals did not display

clear Aβ deposition. Specifically, analysis of the PBS-insoluble S2 fractions of these animals demonstrated a 10-fold decrease of both insoluble $A\beta_{40}$ and $A\beta_{42}$ as measured with protein-based multiplex immunoassay kits. Moreover, immunohistochemical analysis of the brain parenchyma of these animals clearly showed no Aβ deposition 100 days post-injection clearly demonstrating that the original inoculum had been rapidly cleared from the brain and that Aβ deposition found in 300 days old mice was induced *de novo*. This clearance phenomenon after intracerebral inoculation has been previously reported for prion protein (Safar et al., 2005) and Aβ (Morales et al., 2012a; Stöhr et al., 2012).

Going back to the analysis of the PBS-insoluble S2 fractions, one clear limitation of that technique is that is not very resolutive as results were representative of whole brain hemispheres, potentially diluting seeding events restricted to particular brain regions. To address this potential issue, we analyzed Aβ pathology in the opposite brain hemisphere from the same mice by immunohistochemical methods. In order to find **self-propagating Aβ strains properties from 2F and 3F fibrils** we focused on analyzing the specific brain tropism of Aβ pathology induced by these fibrils, the differential seeding activities, unique structural morphology of the aggregates (ThS-positivity and LCO-specific binding) and different type of aggregates (vascular, parenchymal and reactivity to $A\beta_{40}$ and $A\beta_{42}$ antibodies).

In regard to **brain tropism**, we first demonstrated that 2F fibrils induced deposition towards the alveus region of the hippocampus while 3F fibrils induced Aβ pathology mostly in the dentate gyrus. 2F fibrils also induced pathology in the dentate gyrus but included aggregates of different morphology compared to the ones generated by 3F. In the case of animals injected with aged Tg2576 brain extract, Aβ pathology was observed all over the hippocampal formation with no clear tropism towards any specific hippocampus layer. Therefore, each of the three different inocula clearly displayed unique brain tropism. Specifically, the tropism of 2F fibrils towards the alveus region agrees with previous reports that demonstrated a clear tropism towards the alveus of fibrils induced by synthetic Aβ aggregates (Stöhr et al., 2012, 2014). Similar to our results, one of this reports also demonstrated the clear difference in brain tropism between using fibrils from synthetic Aβ and brain-derived aggregates (Stöhr et al., 2012). 2F fibrils tropism towards the alveus region might have enormous pathological consequences. The alveus is mostly comprised of axons from pyramidal cells that are projecting from the CA1 region to the

subiculum or to the entorhinal cortex. Specifically, the interaction between entorhinal cortex neurons and CA1 neurons is thought to be involved in providing strength to previously established memories. Moreover, there is clear atrophy found in the CA1 region in patients with mild AD (Llorens-Martín et al., 2014). Thus, the deposition of Aβ aggregates in the alveus region might have critical pathological consequences. These deposits and the release of Aβ oligomers from them could cause toxicity in the CA1 pyramidal cells, thus inducing memory impairment in these animals. Therefore, this should be further explored by cognitive tests and by histological analysis that measure pyramidal cells loss.

Other specific **tropism** shown by Aβ aggregates induced by 2F fibrils was towards the lateral ventricles. This novel tropism found for the 2F fibrils might have critical physiological consequences. Previous reports have shown that the presence of Aβ oligomers cause disruption of the blood-CSF barrier and is associated with long-term cognitive impairment (Brkic et al., 2015; Schmid et al., 2017), therefore 2F fibrils tropism towards the lateral ventricles might result in long-term cognitive impairment. However, and as mentioned above, this should be tested by behavioral tests such as the modified hole board test or Morris water maze.

4.1.3. DIFFERENTIAL SEEDING ACTIVITIES ARE OBSERVED AFTER *IN VIVO* SEEDING WITH 2F AND 3F $A\beta_{40}$ CONFORMATIONAL STRAINS

Regarding the **seeding activities** found in animals injected with the two synthetic Aβ strains and with brain extract from aged Tg2576 mice, we found similar results to those we observed when we used the PBS-insoluble S2 fractions. There was a significant increase in Aβ aggregates in animals injected with aged Tg2576 brain homogenates and a tendency towards an increase in animals injected with 2F and 3F fibrils. Since all these animals were euthanized at the same time (300 days of age), a clear temporal line in Aβ deposition that would be informative for differentiating incubation periods was not present in this work. However, the analysis in animals that were euthanized only 100 days post-injection showed a tendency to an increase in Aβ parenchymal deposits in the animals injected with 2F fibrils. This tendency, together with our data from the animals at 300 days of age (250 days post-inoculation), points towards an increased seeding activity in animals injected with the 2F fibrils when compared to the 3F fibril-injected mice. Moreover, the animals injected with the aged Tg2576 brain extract potentially had

an even higher seeding activity than animals injected with the 2F fibrils, since they showed greater Aβ deposition at 300 days of age. As mentioned above, the higher specific biological activity (greater seeding potency) of the aggregates derived from brain extract compared to the fibrils from synthetic Aβ have been also supported by data from the group of Dr. Prusiner (Stöhr et al., 2012).

The reason for this differential biological activity observed for synthetic Aβ fibrils and aged Tg2576 brain extracts might be the result that only a subset of the aggregates found in synthetic Aβ fibrils might have the ability to induce a seeding-nucleation mechanism. An alternative explanation would be that Aβ fibrils found in the brain extract from aged Tg2576 might in fact constitute another strain of Aβ than 2F and 3F synthetic fibrils. Hence, this would mean that we are working with three different strains of Aβ: Aβ fibrils from aged Tg2576, 2F Aβ fibrils and 3F Aβ fibrils. This possibility is supported by data from Dr. Robert Tycko demonstrating that the molecular structure of fibrils formed by seeding with AD patient brain extracts are different than the structures of the purely synthetic, 2F and 3F, $A\beta_{40}$ fibrils (Paravastu et al., 2009). In fact, further analysis using conformation-specific dyes and ssNMR studies demonstrated that in this thesis we worked with three different strains of Aβ. These data are discussed further below.

4.1.4. AGGREGATES INDUCED BY THE DIFFERENT INOCULA DISPLAY UNIQUE STRUCTURAL AND BIOCHEMICAL FEATURES

As mentioned before, another specific property of *in vivo* self-propagating Aβ strains would be a unique **structural morphology** of the aggregates. In this sense, we analyzed the structural morphology of the aggregates induced by the two synthetic Aβ strains and the brain extract from aged Tg2576 mice by staining these aggregates with Thioflavin-S (ThS) and different LCOs. Specifically, ThS is an amyloid-specific dye that binds to dense-core plaques (Bussière et al., 2004). These plaques display a spherical core with tightly packed Aβ and have been associated to dystrophic neurites pathology and higher glial cells reactivity (Thal et al., 2015). Interestingly, we found that the deposits induced by both the 2F and 3F synthetic fibrils stained positive with ThS. This is in line with previous research that reported that deposits induced by fibrils from synthetic Aβ strains bind to ThS (Stöhr et al., 2012). Both the Aβ plaques induced by 2F fibrils, and the ones induced by 3F fibrils stained intensely with ThS, demonstrating that in the case of the synthetic Aβ strains ThS binding specificity to was independent of the Aβ isoform

used for inoculation. This result is similar to the ones reported by the group of Dr. Prusiner showing no differences in ThS binding when using two different Aβ strains formed by synthetic peptides (Stohr 2014). Moreover, the deposits induced by the brain extract from aged Tg2576 did not show binding to ThS. Thus, the deposits induced by these brain homogenates were mostly diffuse plaques. Similar type of diffuse deposits have been reported in the past using the same animal model and same inoculum (Morales et al., 2015).

Further **conformational differences** of the aggregates induced by the three different strains of Aβ were reported in this PhD work by using two different LCOs (HS-68 and HS-194). Interestingly, we found that aggregates induced by the brain extract from aged Tg2576 mice were reactive to both LCOs. However, aggregates induced by the synthetic Aβ strains displayed high specificity towards each of the LCOs with fibrils from 2F-induced mice binding mostly to the HS-68 LCO, while aggregates from 3F-seeded mice bound mostly to the HS-194 LCO. These results correlated perfectly with our *in vitro* data in which we found that 2F synthetic Aβ fibrils show specific binding towards the HS-68 LCO and 3F synthetic Aβ fibrils towards the HS-194 LCO. These data is in agreement with previous research reports that found that LCOs have conformation-specific affinities that are able to discriminate between different molecular structures of Aβ (Åslund et al., 2009; Klingstedt et al., 2011, 2013; Nilsson et al., 2007; Psonka-Antonczyk et al., 2016). Moreover, recent data have also shown that these conformation-specific dyes are also able to differentiate between structurally different Aβ deposits in mice (Burwinkel et al., 2018; Michno et al., 2019; Nyström et al., 2013). Even more relevant, these dyes have been reported to distinguish conformational variants of Aβ among patients with certain subtypes of AD (Rasmussen et al., 2017) and have also shown to discriminate between α-synuclein strains distinguishing the Parkinson's disease-associated strain from the strains associated to Multiple System Atrophy (Shahnawaz et al., 2020). Thus, our data, together with previous findings from other groups, supports that the 2F and 3F strains might be inducing the deposition of Aβ aggregates with distinctives arrangements and somehow with similar molecular structure than those from the original inoculum. These results also provide proof that the deposits induced by aged Tg2576 brain extracts, 2F and 3F fibrils are in fact three distinct groups of aggregates of Aβ with distinct molecular structures that affect their specific binding to ThS and

conformation-specific dyes (HS-68 and HS-194), further supporting the idea that these three inocula are actually three different strains of Aβ.

Definitive proof of the unique molecular structures found in the deposits induced by each of the three inocula was shown in this PhD work with the results we obtained by ssNMR, which is a high-resolution technique. Since ssNMR requires milligram-scale quantities of Aβ fibrils and isotopic labeling, the fibrils from brain homogenates of our inoculated mice were amplified by seeded growth *in vitro*. This technique has been previously demonstrated by our collaborators in studies of Aβ fibrils from human AD brain (Lu et al., 2013; Qiang et al., 2017). Therefore, our measurement was an indirect product from what we found in the brain of our mice. Perhaps, one of the most **relevant results** reported in this thesis manuscript is the structural differences observed at the molecular level by ssNMR in the Aβ aggregates from the three different seeded-brain. Specifically, it was found that $A\beta_{40}$ fibrils derived from 2F- and Tg2576-treated mice had one Aβ polymorph in common but also showed a second prevalent polymorph that was unique for each of the animal groups, thus demonstrating that the Aβ aggregates induced by the aged Tg2576 brain extract were structurally different than those induced by the fibrils from the 2F Aβ strain. Moreover, the most prevalent polymorphs derived from 3F-treated mice were distinct to those found in animals injected with either aged Tg2576 brain extract or 2F fibrils. Interestingly, one of the most prevalent polymorphs found in the brain of animals injected with aged Tg2576 brain homogenate closely resembled the predominant $A\beta_{40}$ polymorph derived from cortical tissue from patients with typical AD (Ghosh et al., 2021; Qiang et al., 2017). This is of high relevance, since these studies found different molecular structures of Aβ aggregates when they compared two atypical Alzheimer's disease clinical subtypes (rapidly progressive form (r-AD) and the posterior cortical atrophy variant (PCA-AD) with a typical prolonged-duration form (t-AD), with common structures in t-AD and PCA-AD that differ from those found in r-AD. Thus, the differences we find in molecular structure by ssNMR in the aggregates induced by our three different inocula might have different pathological and clinical consequences. As expected, $A\beta_{40}$ fibrils derived from mice injected with the 2F and 3F strains did not have the same molecular structures as the original 2F and 3F fibrils that were used as seeds. This observation was expected because the pathology induced by *in vivo* seeding of mice are likely to be a result of both, the seeds administered and the endogenous aggregates that are normally displayed by the Tg2576 mice as they age as it has been previously

reported (Meyer-Luehmann et al., 2006). Specifically, we believe that his result may indicate that Aβ fibril molecular structures evolve as they propagate in brain tissue, presumably due to the pronounced differences in chemical, physical, and biological environments between a mouse brain and the simple phosphate buffer used to grow the original 2F and 3F fibrils *in vitro*. The fact that Aβ fibril structures can evolve during multiple rounds of self-propagation in a new environment has been actually demonstrated by both *in vitro* (Qiang et al., 2011) and *in vivo* experiments (Hérard et al., 2020).

Taking together our data using ThS, the LCOs HS-68 and HS-194, and the molecular structures resolved by the ssNMR spectra, we believe that our three different seeds (aged Tg2576 brain extracts, 2F and 3F fibrils) induced the deposition of Aβ aggregates with unique structural morphology, hence supporting once again the idea that 2F and 3F fibrils are distinguishable Aβ strains with varying biological activities.

4.1.5. *IN VIVO* SEEDING WITH THE THREE DIFFERENT INOCULA RESULTS IN DISTINCT TYPE OF AGGREGATES

The last specific property of *in vivo* self-propagating Aβ strains that we analyzed was the **type of aggregates**. Specifically, we focused on the presence of vascular Aβ deposits in the meningeal layers of the brain of the injected mice. Interestingly, we found that animals injected with aged Tg2576 mice brain extract displayed increased Aβ deposition in blood vessels, at cortical meningeal layers, compared to 3F-injected mice and the negative control group. 2F-injected mice showed a tendency to an increase in this type of deposits, but this was not significant. These results further support that the three different types of inocula induce distinguishable type of aggregates. It is worth noting that severe vascular deposition of Aβ can lead to microscopic infarcts and microhemorrhages, worsening cognitive deficits in AD patients (Thal et al., 2003), thus this unique type of Aβ deposition shown by animals injected with aged Tg2576 brain homogenate could lead to cognitive deficits in these mice. However, this have not been analyzed in this work and should be explore in further research. It is important to mention that both of our synthetic Aβ strains and monomeric $A\beta_{40}$ induced deposition in the vessels. The finding that both synthetic fibrils induced Aβ deposition in the vessels with no clear difference between the groups is supported by data from other groups showing that Aβ deposition in the blood vessels was not influenced by Aβ strain-specific information (Hamaguchi et al., 2021). However, our finding that these types of deposits are increased in animals injected with

aged Tg2576 brain extract, might point towards that specific inoculum having a differential biological activity in regard to vascular Aβ pathology. Moreover, the presence of these type of deposits even in control animals (injected with monomeric $A\beta_{40}$) results were expected since it was reported in previous publications from our group (Morales et al., 2015) and might be associated to clearance mechanisms of the seeds injected into the animals, or might be the result of the inocula containing negligible amount of oligomers formed in the short time (minutes) between resuspending the monomeric $A\beta_{40}$ peptide and injecting. It would be of great interest to the field to find the mechanism behind monomeric $A\beta_{40}$ induction of Aβ deposition in meningeal vessels, however this was out of the scope of this work and was not investigated further. Interestingly, Aβ deposition in vessels (CAA) have been found in most of the iatrogenic cases of AD pathology (Gomez-Gutierrez and Morales, 2020; Yamada et al., 2019). Our data, in which we found vascular deposition of Aβ in all animals, further support that iatrogenic cases of AD might be induced by contamination with seeds from cadaveric dura mater grafts, cadaveric human growth hormone or surgical tools containing little amounts of Aβ.

Furthermore, an in-depth analysis of the differential recruitment of $A\beta_{40}$ and $A\beta_{42}$ peptides by the different type of aggregates was also performed. As expected, we found that both synthetic Aβ strains predominantly induced $A\beta_{40}$ deposition. Since both 2F and 3F fibrils are made our of synthetic $A\beta_{40}$, this result was consistent with the homologous *in vivo* seeding observed in previous work (Ruiz-Riquelme et al., 2021; Stöhr et al., 2014). Moreover, animals injected with aged Tg2576 brain extracts predominantly showed higher deposition of $A\beta_{42}$ when compared with animals injected with the synthetic Aβ fibrils. This again is supported by previous work that reported that the brain homogenates of aged Tg2576 mice, which was the inoculum in this thesis work, contain higher amounts of insoluble $A\beta_{42}$ than $A\beta_{40}$ (Morales et al., 2015). Since these animals contains fibrils from both $A\beta_{40}$ and $A\beta_{42}$, it is normal that we observed deposition of both peptides in animals injected with this inoculum. Interestingly, we found that aggregates induced by the 2F-fibrils in the alveus were almost entirely formed by $A\beta_{40}$, while deposits in the dentate gyrus of the same animals also contained $A\beta_{42}$ deposits, in a similar manner to 3F-fibrils injected mice. This further support that 2F and 3F fibrils induce different type of aggregates and also open the possibility that 2F fibrils might be forming additional fibril structures in the brain of injected mice. The latter has been previously reported in brain samples from patients. Specifically, the group of Dr. R. Tycko found that there is a

predominant fibril structure of Aβ40 in the brain of patients with t-AD and PCA-AD clinical subtypes of AD, while brain from patients with r-AD shows greater heterogeneity in fibril structures related to additional fibril structures found in these brains (Qiang et al., 2017). This data is also supported by our own data on ssNMR, in which we found that 2F-injected mice and animals injected with aged Tg2576 brain homogenate have one Aβ40 polymorph in common, but they also have a second prevalent polymorph that is completely different. The common polymorph might be the one found in the dentate gyrus Aβ plaques which somehow show similar binding properties to Aβ40 and Aβ42 antibodies and to conformational specific dyes (HS-68 and HS-194), while the deposits found in the alveus of 2F-injected mice might contain mostly the second prevalent polymorph, since these deposits are mostly specific to Aβ40 antibodies and to the HS-68 LCO. On the other hand, slightly higher affinity to Aβ40 antibodies of the deposits is found in the dentate gyrus of 3F-injected mice. These deposits also display higher specificity to the HS-194 LCO, and the results obtained by ssNMR show that the most prevalent Aβ40 polymorph found in these animals is unique compared to those derived from 2F-injected mice and animals injected with aged Tg2576 brain homogenate. Therefore, our data supports that Aβ deposits induced by the 3F fibrils are distinct that those induced by the other inocula.

In summary and **discussed in sections 4.1.2. through 4.1.5.**, our two synthetic Aβ40 strains showed clear *in vivo* seeding properties with induction of Aβ aggregates with unique brain tropism and with distinguishable seeding activities and structural morphologies. Therefore, our results show clear properties of self-propagating Aβ strains from 2F and 3F fibrils.

4.1.6. DIFFERENTIAL NEUROINFLAMMATORY RESPONSE IS INDUCED BY THE THREE DIFFERENT INOCULA

An important contribution of this work is to describe the pathological significance of strain-specific replication of Aβ misfolding *in vivo*. We show that the induction of amyloid pathology in different patterns resulted in different glial responses. Specifically, by correlation analysis, we found that animals injected with the 2F synthetic fibrils tend to induce more astroglial reactivity, while amyloid deposits from animals injected with 3F synthetic fibrils correlate better with increased microglial activation. These results confirmed that the two synthetic Aβ strains induce amyloid conformation-specific glial response in Tg2576 mice. Moreover, Aβ deposits from mice injected with aged Tg2576

brain extract mostly correlated with activated microglial cells recruitment. This is similar to 3F-induced aggregates, despite the fact that the inoculated aggregates in these two animal groups were conformationally different. Interestingly, in the case of 2F-injected mice we observed that microglial response was stronger towards the aggregates found in the alveus compared to the response towards the aggregates formed in the dentate gyrus of this same animals. This further support our aforementioned idea that 2F fibrils might induce two distinct $A\beta_{40}$ polymorph in the brain of the injected mice, with one predominantly found in the alveus and the other found mostly in the dentate gyrus. As expected, and previously reported by others, diffuse deposits found in animals injected with aged Tg2576 brain homogenate did not induce a strong microglial response compare to the dense-core plaques found in animals injected with the two distinct $A\beta_{40}$ strains (Wang et al., 2016). This phenotype is of critical importance since it has been demonstrated that activated microglial cells are an important physical barrier to prevent toxicity from the plaques, with high microglial coverage being associated to compacting the plaques and inducing dense-core plaques and uncovered areas showing diffuse, and more toxic, deposits (Condello et al., 2015). In fact, the disruption of this microglia barrier around plaques is associated with the increase of dystrophic neurites (Wang et al., 2016; Yuan et al., 2016). This phenomenon have been further supported by new research from other groups (Casali et al., 2020; Zhao et al., 2017). Furthermore, a recent work by Huang et al. (2021) conclude that dense-core plaques are built by activated microglia as a mechanisms to limit the brain damage from soluble Aβ. Therefore, microglia seem to mitigate AD pathology by regulating/constructing compact plaques and delimiting diffuse-like plaque expansion, providing a neuroprotective mechanism. TREM2 variants, one of several genes for which expression is restricted to microglial in the brain and that enables microglia to acquire a fully mature activated disease-associated microglia (DAM) profile defined by a set of upregulated/downregulated genes, have been linked to increased risk of sporadic AD supporting a key role of microglia in the pathogenesis of this neurodegenerative disease (reviewed in Ulland and Colonna, 2018). Therefore, TREM2 deficiency leads to incomplete activation of the microglial DAM phenotype decreasing its ability to surround and compact plaques with increased neuritic pathology (Ulrich et al., 2014; Yuan et al., 2016). In our study we have not evaluated the toxicity of the plaques (measured by the amount of dystrophic neurites surrounding plaques) induced by the different inocula and this deserve further investigation. In addition, it will be important to identify the inocula-induced microglial molecular phenotype since microglia

might present distinct activated signatures and function under the different seeding conditions. Transcriptomic studies by single-cell RNAseq has revealed a diversity of microglial phenotypes in aging and AD (reviewed in Boche and Gordon, 2021). In transgenic mouse models with amyloid pathology activated microglia populations named DAM, MGnD (neurodegenerative disease microglia) or ARM (activated response microglia) have been reported (Keren-Shaul et al., 2017; Krasemann et al., 2017; Sala Frigerio et al., 2019). However, human AD microglial (named HAM) are transcriptionally quite distinct from the reported mice microglia (Srinivasan et al., 2020). Distinct microglial subtypes defined by differential gene expression may coexist in a brain region, though regional differences and changes along disease-stage might contribute to microglial heterogeneity. It's tempting to speculate that the different Aβ strains induce a specific microglial gene profile, and a better understanding of this diversity will be required for the future development of microglial targeted therapies.

Restricting plaques, or building dense plaques, seems to be a protective mechanism, thus plaques induced by aged Tg2576 brain extracts would be more toxic than those induced by the two synthetic $A\beta_{40}$ strains. Since 3F fibrils-induced plaques seem to be recruiting more microglial cells than 2F fibrils-induced ones, we could argue that 3F fibrils induce amyloid deposits that are less toxic than those induced by 2F fibrils. Since microglial cells response seem to be affecting Aβ plaque morphologies (Casali et al., 2020; Huang et al., 2021), we cannot rule out the possibility that glial cells response could be affecting the molecular structure of Aβ protofilaments resulting in the different polymorphs we found by ssNMR.

Recently, it has been proven that activation of the NLRP3 inflammasome induce the formation of ASC specks in microglial cells, that later binds to Aβ inducing its aggregation through a cross-seeding mechanism (Venegas et al., 2017). Therefore, even though our in vitro data support a direct cross-seeding mechanism, we should consider that the induction of amyloid deposition by our inocula might be also caused by a cross-seeding mechanism through the NLRP3 inflammasome. Moreover, the binding of Aβ to ASC specks seem to cause toxicity in microglia causing pyroptotic cell death (Friker et al., 2020). Thus, the differential inflammatory response we have seen in each inoculated group might result in distinct neurotoxicity in the brain of injected mice. Finally, microglial cells have been found to exacerbate tau pathology by either the release of extracellular vesicles containing pTau or through the NLRP3–ASC inflammasome

mechanism (Clayton et al., 2021; Stancu et al., 2019). Given the correlation of tau pathology with the cognitive deficits developed in AD, it would be of critical importance to study whether the different Aβ strains induce tau pathology either by a direct cross-seeding mechanism (protein to protein) or through a microglial mediated mechanism. This is currently undergoing in our lab.

Though a more comprehensive inflammatory characterization of the Aβ seed-specific inflammatory profiles would be necessary, our multiplex analysis show a predominance of the proinflammatory cytokines expression in mice receiving the Tg2576-derived seeds. This indicates that neuroinflammation is exacerbated by this specific Aβ strain compared to those challenged with the other seeds. 2F and 3F fibrils elicited a moderate proinflammatory signature characterized by INF-γ and CCL3 production, with 2F also increasing IL-1α and CCL5 production. These findings indicate the existence of differential glial responses to the pathological seed inocula. Cytokines can be produced by microglia astroglia and neurons, however the exact sources for each cytokine in the different seeded mice need to be further investigated. Moreover, the biological impact of the Aβ strains in the innate immunity response may be underestimated by the complexity of microglial and astroglial responses in the disease context, with the co-existence of multiple functional phenotypes including spatial and temporal variations (Escartin et al., 2021). Interestingly, the three inocula induced similar CCL3 upregulation, a chemokine involved in chemotaxis and shown to contribute to T cell recruitment to the brain (Laurent et al., 2017). Moreover, these seeds also induced IFN-γ elevation, an essential element of the neuroinflammatory network involved in leukocyte trafficking (Kunis et al., 2013). Future research in this line may help to link specific conformational motifs on misfolded Aβ with strain-specific pathological profiles.

4.1.7. 2F AND 3F FIBRILS ARE UNIQUE SYNTHETIC Aβ40 STRAINS WITH VARYING BIOLOGICAL ACTIVITIES. CLINICAL RELEVANCE

In summary, our data (discussed in **section 4.1.6.**) suggest that 2F and 3F fibrils are polymorphic synthetic $A\beta_{40}$ strains with varying biological activities. These activities are also different than those induced by the aggregates from aged Tg2576 brain extracts. As mentioned above, there are three key properties that amyloid aggregates have to fulfill in order to be considered strains. **First**, strains should display unique conformational arrangements. **Second**, strains should have the ability to self-propagate unique structural

arrangements and **finally**, strains should induce distinct disease phenotypes, both pathologically and clinically, that depends on their conformational variant (Morales, 2017). Taking together all the **data discussed in sections 4.1.1. through section 4.1.6.,** we can certainly conclude that 2F and 3F fibrils are unique synthetic $A\beta_{40}$ strains. To our knowledge this is the first study demonstrating the existence of two distinguishable Aβ strains formed by the same peptide ($A\beta_{40}$). Previous reports demonstrated the formation of different strains with different biological activity both from synthetic Aβ peptides or brain homogenates from AD patients, but these preparations were always a mixture of Aβ peptides ($A\beta_{40}$, $A\beta_{42}$, etc…) and not preparations from a single pure peptide (Condello et al., 2018; Duran-Aniotz et al., 2021; Ghosh et al., 2021; Michno et al., 2019; Qiang et al., 2017; Rasmussen et al., 2017; Stöhr et al., 2012, 2014; Watts et al., 2014).

Alzheimer's disease is a highly heterogenous disorder with various defined neuropathological subtypes. Four major subtypes have been defined based on the distribution of tau pathology and brain atrophy: typical AD (55% of cases), limbic-predominant AD (21% of cases), hippocampal-sparing AD (17% of cases), and minimal atrophy AD (15% of cases). These subtypes are not only neuropathological subtypes but also different clinical subtypes, with distinct ages of onset and different rates of progression (Ferreira et al., 2020; Jellinger, 2021; Murray et al., 2011). Other clinical variants with distinct regional patterns of tau deposition have also been identified. Examples of this are the posterior cortical atrophy, primary progressive aphasia, nonamnestic, corticobasal syndromal, and mild dementia variants (Jellinger, 2021). Recently, a new clinical subtype of AD with rapid progressive cognitive decline has been characterized and named as rapidly progressive AD (Abu-Rumeileh et al., 2018; Schmidt et al., 2011, 2012). Moreover, advances in tau PET imaging and machine learning algorithms have permitted the identification of new subtypes of AD (Mitelpunkt et al., 2020; Vogel et al., 2021). Therefore, AD is a highly heterogenous, both pathologically and clinically, disorder, that have shown differences in age at onset, sex distribution, global cognitive status, disease duration, CSF biomarker levels and APOE ε4 genotype (Ferreira et al., 2020). Most of these studies have associated these clinical subtypes to distinct distribution of tau pathology and brain atrophy, thus supporting the idea that different structural arrangements or strains of tau protein, with different rate of toxicity, could be the cause of these different patterns in tau pathology distribution and brain atrophy. This was somehow observed for tau fibrils from Pick's disease, which showed a

different conformation than tau filaments from AD patients (Falcon et al., 2018). However, recent data from studies that resolved the structure of tau filaments in different AD subtypes by Cryo-EM, showed no structural differences between the fibrils from each of the subtypes (Fitzpatrick et al., 2017; Shi et al., 2021).

Since similar structure was observed for tau filaments of different AD subtypes, potential explanation for the heterogeneity found within AD patients could be brain region-dependent susceptibility to tau aggregates, even though the structure of these aggregates has identical molecular conformation. Since Aβ pathology is known to precede tau pathology and neurodegeneration (Hampel et al., 2021b; Zetterberg and Bendlin, 2021) another potential mechanism that could be driving the heterogeneity found in AD was the existence of different strains of Aβ, which then could be induced differential tau pathology, unique brain tropism and distinct neurodegeneration. Unlike tau filaments, existence of distinct strains of Aβ in different clinical subtypes have been reported by different groups using both low- and high-resolution techniques (Condello et al., 2018; Duran-Aniotz et al., 2021; Di Fede et al., 2018; Ghosh et al., 2021; Lau et al., 2021; Michno et al., 2019; Qiang et al., 2017; Rasmussen et al., 2017; Watts et al., 2014; Wildburger et al., 2017), thus supporting the idea that Aβ strains might be the driver of the heterogeneity found in AD patients. Moreover, recent transcriptomic data obtained from different brain regions in AD patients have further supported Aβ, and specifically Aβ-mediated neuroinflammation, as one of the main molecular subtypes of AD that drive heterogeneity in AD patients (Neff et al., 2021).

Even though all the aforementioned studies found different molecular structures of Aβ aggregates when comparing AD clinical subtypes, none of these studies were able to find which are the most deleterious structures of Aβ. The reason for this is that very likely Aβ aggregates in AD brains are composed by a multitude of different structural arrangements, making hard to define a specific biological response to a unique structural arrangement. Therefore, working with homogeneous samples or unique conformers of Aβ is indispensable to be able to associate a specific conformation of Aβ to a specific biological response. This was the **main strength of our work** because we employed pure Aβ strains, with a unique molecular structure. Moreover, we found unique biological activities for each of the strains, thus demonstrating the capabilities of Aβ conformers to induce differential biological responses. However, we acknowledge that in this study we used synthetic Aβ seeds and not pathologically associated Aβ strains. Future studies using

purified Aβ strains isolated from each of the clinical subtypes will definitively confirm or discard the hypothesis that Aβ strains are at the core of the clinical variability observed across AD patients. Moreover, these studies will be essential in the clinic since these results will allow for subtyping of AD patients leading to personalized diagnosis and for implementing precision medicine approaches with the ultimate goal of developing successful preventative and disease-modifying drugs for each of the AD subtypes.

4.2.1. BACTERIAL FUNCTIONAL AMYLOIDS INDUCE *IN VITRO* AGGREGATION OF $A\beta_{40}$ BY A CROSS-SEEDING MECHANISM

As it was explained in depth in section 1.3.1. of the introduction, the amyloid structure of proteins is not only associated with protein misfolding disorders (PMDs), such as Alzheimer's disease or Parkinson's disease, but also to important physiological functions, rising the term of functional amyloids (Loquet et al., 2018; Otzen and Riek, 2019). Functional amyloids have been described in mammals but also in prokaryote organisms such as bacteria. In these organisms, functional amyloids have shown to be involved in the formation of biofilms, hence supporting bacterial adhesion to surfaces and cell-to-cell adhesion and also show both antimicrobials and cytotoxic activities (Levkovich et al., 2021). Given that increasing amounts of scientific research have shown the presence of bacteria in AD brains and that gut microbiome is altered in AD patients (Kamer et al., 2015; Miklossy, 2016; Vogt et al., 2017), it has been proposed that bacteria could be involved in AD pathogenesis by several mechanisms such as direct toxicity to neuronal cells, the induction of an inflammatory environment that could lead to the aggregation of amyloid proteins and tissue damage, oxidative stress and even the direct induction of Aβ aggregation (Bulgart et al., 2020). Since the specific mechanisms by which bacteria may induce the pathological hallmarks of AD, such as amyloid plaques and neurofibrillary tangles, have not been elucidated we decided to explore the potential cross-seeding of three bacterial functional amyloids (curli CsgA subunit, microcin E492 and TasA) with the AD-associated peptide Aβ as the potential pathological mechanism underlying the link between our microbiome and AD pathology. By cross-seeding, bacterial functional amyloids would induce the aggregation of Aβ by directly nucleating the polymerization of Aβ fibrils and increasing the formation of Aβ aggregates in animals exposed to bacterial functional amyloids. This mechanism has already been reported for

several amyloidogenic proteins such as Aβ, PrP, tau and α-synuclein both *in vitro* and *in vivo* (Morales et al., 2013; Moreno-Gonzalez et al., 2017; Vaneyck et al., 2021).

In this sense, this PhD work has demonstrated that the three bacterial functional amyloids (curli CsgA subunit, microcin E492 and TasA) were able to induce the aggregation of $A\beta_{40}$ *in vitro*, thus supporting our hypothesis that bacterial functional amyloids are able to cross-seed the aggregation of the AD-associated amyloid peptide Aβ. Interestingly, we also found that both microcin E492 and TasA showed a better cross-seeding activity at lower concentrations, with TasA even inhibiting the aggregation of $A\beta_{40}$ at 10 nM concentration. This type of mechanism by which one amyloid protein could inhibit the aggregation or change the structure of another amyloid protein thus avoiding the formation of toxic fibrils has been described for other amyloidogenic proteins such as PrP (Diaz-Espinoza et al., 2018). However, it should not be ruled out the possibility that TasA fibrils could be inhibiting the access of the fluorochrome ThT at high concentrations.

Our findings also pointed towards two interesting mechanisms. First, we observed that the aggregation induced by homologous seeds ($A\beta_{40}$ seeds) was always more rapid than the aggregation induced by the heterologous seeds (CsgA, Mcc E492 and TasA), hence demonstrating that the nucleation-polymerization reaction was not as thermodynamically favorable when cross-seeding was observed. Second, we found that for all of the cross-seeding reactions, $A\beta_{40}$ aggregates displayed a different maximum ThT fluorescence signal at plateau than those $A\beta_{40}$ aggregates produced by self-polymerization, with no seeds. The latter is a similar result to what we observed in the first part of the thesis with the 2F and 3F fibrils, and similar to what others have observed for other amyloidogenic proteins that showed structural variations by ThT assays (Qiang et al., 2011; Shahnawaz et al., 2020). Therefore, this observation suggests that $A\beta_{40}$ cross-seeding with the bacterial functional amyloids results in the formation of $A\beta_{40}$ fibrils polymorphs or strains that could have different toxicity or biological activity than $A\beta_{40}$ fibrils seeded by homologous seeding or self-polymerization. However, in order to decipher whether the $A\beta_{40}$ fibrils formed by cross-seeding with bacterial amyloids exacerbate or on the other hand are less detrimental, *in vitro* cell studies exposing neuronal cells to these fibrils or *in vivo* studies injecting the $A\beta_{40}$ cross-seeded fibrils should be further explored.

Taken together, our results show that *E. coli*-derived CsgA fibrils, *K. pneumoniae*-derived Mcc E492 fibrils and *B. subtilis*-derived TasA fibrils are able to cross-seed the

formation of $A\beta_{40}$ fibrils *in vitro*. Moreover, it was demonstrated that these bacterial amyloids might be inducing the formation of $A\beta_{40}$ fibrils with different structural arrangements, thus forming new $A\beta_{40}$ polymorphs or strains. However, definitive proof of this should be shown by high-resolution techniques These results are of high relevance due to the known involvement of bacteria in AD.

It is worth noting that the bacterial functional amyloids used in this study are naturally formed by bacteria known to naturally reside in the human body or known to be common pathogens in human. Specifically, CsgA is formed by *Escherichia coli* species. These species are almost exclusively non-pathogenic and has been found to be in the intestinal microbiome of more than 90% of healthy human adults living in symbiosis with its host, however *E. coli* can become a harmful pathogen when introduced in the host by exposure of the host to uncooked food and drinking water (Martinson and Walk, 2020; Tenaillon et al., 2010). Interestingly, recent studies have shown increased abundance of *Escherichia* bacteria in individuals with increased amyloid deposition, as measured by PET imaging (Cattaneo et al., 2017). Indeed, the presence of *E. coli* have been confirmed in the human brain and *E. coli* molecules such as LPS and K99 pili protein have been found in higher levels in the brain of AD patients when compared to healthy controls, with LPS showing colocalization with amyloid plaques and CAA pathology (Zhan et al., 2016, 2018). Related to our work, other groups have shown the potential of CsgA to induce the aggregation of mammalian amyloid proteins such as α-synuclein, amyloid protein A and HIV-related Semen Enhancer of Viral Infection or SEVI (Chen et al., 2016; Hartman et al., 2013; Lundmark et al., 2005; Sampson et al., 2020). Even though these studies used the term cross-seeding, only one of them showed direct interaction of CsgA with mammalian amyloidogenic proteins (α-synuclein) such as what we showed in our *in vitro* experiments (Sampson et al., 2020). However, the induction of seeding by other mechanisms such as inflammation, as explained below, should not be ruled out.

In the case of microcin E492, this is a functional amyloid formed by the gram-negative bacteria *Klebsiella pneumoniae*. This bacterium is part of the normal human flora but has been also associated to hospital-acquired infections, such as urinary tract infections, septicemia and pneumonia, and is increasingly becoming resistant to antibiotics such as carbapenemase (Conlan et al., 2012). *K. pneumoniae* is usually found in the oral microbiome and have been shown to be resistant to long-term starvation (Baker et al., 2019). Moreover, it has been demonstrated that Klebsiella can induce dysbiosis and

inflammation of the gut by ectopic colonization (Atarashi et al., 2017). Since these bacteria is found frequently in the human body, demonstrating the cross-seeding of mammalian amyloids by microcin E492, the amyloid produced by these bacteria, is of critical importance.

Finally, the other bacterial amyloid demonstrated to cross-seed the formation of $A\beta_{40}$ fibrils *in vitro* was TasA. This amyloid is produced by gram-positive bacteria such as *Bacillus subtilis* and *Bacillus cereus* (Álvarez-Mena et al., 2020; Romero et al., 2010). In our case, we demonstrated the *in vitro* cross-seeding by using TasA fibrils from *Bacillus subtilis*. This bacteria is of high relevance in humans since it is not only a normal gut commensal but it is also commonly used as a probiotic with the ability to attenuate and prevent inflammation in the human gut (Colom et al., 2021; Lee et al., 2019; Rhayat et al., 2019). Moreover, probiotics containing *B. subtilis* have been demonstrated to positively affect neurochemical activities (Cheng et al., 2019; Lyte, 2011).

In summary, the normal presence of the amyloid-producing bacteria used in this PhD work in the human microbiome and our results showing the ability of the bacterial-derived functional amyloids to cross-seed the formation of $A\beta_{40}$ fibrils *in vitro* is of **critical relevance**, since this would demonstrate that the Aβ protein misfolding associated with Alzheimer's disease might be induced by functional bacterial amyloids from normal gut commensal bacteria through a cross-seeding mechanism, providing a **novel pathogenic mechanism associated with AD pathology**. However, this has to be demonstrated *in vivo* and with that goal in mind we injected these bacterial functional amyloids in AD transgenic mice.

4.2.2. BACTERIAL FUNCTIONAL AMYLOIDS INDUCE BRAIN AMYLOIDOSIS WITH AN INCOMPLETE ATTACK RATE

In order to finally prove the *in vivo* cross-seeding mechanism between the three bacterial functional amyloids and Aβ, we injected 10 µg of well-characterized BFA fibrils (CsgA, Mcc and TasA) in each hippocampus of 50 days old Tg2576 mice. By biochemical techniques, we did not find significant differences in $A\beta_{40}$ and $A\beta_{42}$ levels among the groups of animals injected with BFAs when compared to uninjected animals. However, we found that animals injected with microcin fibrils displayed significantly increased $A\beta_{42}/A\beta_{40}$ ratio, which would be associated to increase AD-like pathology in these mice. This result suggests that microcin fibrils might not induce a significant

increase of any of the individual peptides (Aβ40 or Aβ42) but overall cause a small switch from Aβ40 deposition to Aβ42 deposition, a peptide that is more prone to aggregation. Interestingly, in each of the groups we observed increased levels of Aβ40 and Aβ42 in some individual mice injected with bacterial functional amyloids. As in the first part of this thesis, one of the limitations of the biochemical analysis was that the results were representative of whole brain hemispheres, potentially diluting increased seeding events that could be restricted to a particular brain region. To address this potential issue, we again analyzed the Aβ deposition and specific location (tropism) of the induced amyloid deposits in the opposite brain hemisphere from the same mice by immunohistochemical methods. Interestingly, we found that mice injected with CsgA fibrils displayed a significant increase in Aβ deposition in the hippocampus compared to other groups. Mice injected with either microcin E492 or TasA amyloid fibrils did not displayed increased Aβ deposition, however we again observed that few animals for each of the injected group developed small amyloid deposition, even though the difference between the groups were not significant overall. This pattern was found both by biochemical and immunohistochemical methods, therefore it seems to be a real event happening in our injected mice. This phenomenon in which just a percentage of the injected mice develops amyloid pathology after injection with seeds, is a well-known phenomenon in prion diseases known as **incomplete attack rate** (Rossi et al., 2019). In prion diseases, this phenomenon is observed during interspecies transmission, where there is a barrier effect (Bartz et al., 2000; Bessen and Marsh, 1992) and also when the inoculum titer is either lower, coming from a synthetic prion protein or by the existence of different strains (Colby et al., 2009; Makarava et al., 2010; Morales et al., 2016). Therefore, an incomplete attack rate is caused by either low titers or by structural differences in the amyloid arrangement of the seeds respect to the inoculated animal. Attack rates are usually expressed as the percentage of injected animals that develop pathology and, in our experiments, we found about 2-3 animals per group that actually showed increased levels of Aβ40 and Aβ42. Therefore, it is possible that bacterial functional amyloids induced Aβ pathology with an incomplete attack rate. This would be caused by either the different conformational arrangement of these amyloids compared to Aβ, or by low concentration of the injected material, which would be solved by injecting higher concentrations of the BFAs in Tg2576 mice. Another way we could approach this issue is by extending the incubation periods or by performing subsequent passages with the brain homogenates from animals injected with the three BFAs. This approach have been proven successful

in the past in prion diseases (Raymond et al., 2007). Given that previous studies have shown that curli fibrils from *Escherichia coli* enhance α-synuclein aggregation and induce motor impairment in mice (Chen et al., 2016; Sampson et al., 2020), we strongly believe that a cross-seeding mechanism might occur *in vivo*. The main difference between these studies and ours, is that their approach was to colonize these animals' gut with curli-producing *Escherichia coli*. Therefore, these animals were subject to constant release and production of curli fibrils by the bacteria that colonized their gut. This support the idea that a single injection of bacterial functional amyloids might not be sufficient to induce a complete attack rate with all animals showing induced Aβ deposition by these amyloids. Our *in vitro* cross-seeding aggregation assays also supported this idea, since we observed that bacterial functional amyloids are not as efficient inducing seeding of Aβ as their homologous seeds. Since many different groups have reported the presence of bacteria in the brain of AD patients (Balin et al., 2008; Bulgart et al., 2020; Dominy et al., 2019; Gérard et al., 2006; Hammond et al., 2010; Kamer et al., 2015; Miklossy, 2011, 2016; Sparks Stein et al., 2012), it is highly possible that the exposure to bacterial amyloids in the brain is constant and not a single event as what we exposed our animals to. This issue should be addressed in future experiments. We propose that these should be approached by two different ways: colonizing mice gut with curli-producing *Escherichia coli* or by implantation of a pump in the brain of these mice which would allow us for constant delivery of fibrils from bacterial functional amyloids. These two methods would also allow for further separating the pathology induced by peripheral routes compare to direct inoculation of the brain, an important concern since it has been shown that different route of inoculation might result in distinct Aβ deposition in mice (Eisele et al., 2009, 2010; Morales et al., 2021). Finally, we should not rule out that the cross-seeding mechanism *in vitro* is totally different that the *in vivo* cross-seeding mechanism and probably what seems to happen *in vitro* does not happen *in vivo* due to *in vitro* experiments not being performed in a real physiological setting with the exact pH and exposure to other metabolites/proteins (Nguyen and Endres, 2021). Overall, this highlights the need for caution when interpreting *in vitro* cross-seeding data and suggest that such mechanisms should be monitored by bioassays.

Even though the cross-seeding mechanism was the main mechanism studied in this work, we agree that alternative mechanisms by which bacterial amyloids and other bacteria by-products could influence AD should be considered. In this sense, it has been shown that gut bacteria could control the function and maturation of microglial cells (Erny

et al., 2015). Moreover, it has been demonstrated that Aβ could be playing a beneficial role and serve as antimicrobial peptide (AMP) that protects the brain from microbes' infection, thus supporting that the increase in Aβ observed in AD patients is due to prior bacterial or viral infections, linking microbes with AD through a different mechanism that cross-seeding and hence serving as a link between the amyloid cascade hypothesis and the infection hypothesis of AD (Kumar et al., 2016; Moir et al., 2018). Interestingly, bacterial amyloids such as curli are pathogen-associated molecular pattern recognized by the innate immune system inducing an inflammatory response similar to the one triggered by amyloid proteins associated to neurodegenerative diseases such as Aβ and thus could be altering brain homeostasis (Tükel et al., 2005, 2009, 2010; Venegas and Heneka, 2017). In fact, these bacterial amyloids induce the activation of toll-like receptors 1 and 2 and the NLRP3 inflammasome. Neuroinflammatory response to neurodegeneration related amyloids have been demonstrated to be enhanced by the exposure to bacterial amyloids and thus, this mechanism should be considered as a plausible mechanism by which bacteria could cause brain dysfunction in neurodegenerative diseases (Chen et al., 2016; Friedland, 2015; Friedland and Chapman, 2017). Another potential mechanism by which bacteria could induced neurodegeneration in humans is by activation of oxidative toxicity processes (Tükel et al., 2005, 2009). Indeed, the influence gut microbiota on oxidative processes has been recently demonstrated (Jones and Neish, 2017). Furthermore, metabolites produced by bacteria, such as short-chain fatty acids (SCFAs) have also been proven to be involved in microglial activation and seem to be contributing to the aggregation of α-synuclein, another neurodegenerative associated amyloid, resulting in worsened motor deficits in animal models of Parkinson's disease (Sampson et al., 2016). Interestingly, other groups have found a decrease in the concentrations SCFA in fecal samples from PD patients (Unger et al., 2016). These bacterial metabolites have shown ability to pass the blood-brain barrier and to influence systemic immunity, potentially playing a critical role in human neurodegenerative diseases (Arpaia and Rudensky, 2014; Desai et al., 2016). In addition, they could be transmitted through the vagus nerve which connects the enteric nervous system to the brain stem (Rutsch et al., 2020). Other metabolites produced by bacteria such a trimethylamine N-oxide (TMAO) or lipopolysaccharides (LPS) should be also taken into account since those have been demonstrated to regulate vascular functions and neuroinflammation-induced cognitive impairment (Zhan et al., 2018; Zhao et al., 2019; Zhu et al., 2016). Therefore, bacterial influence in neurodegenerative diseases might not only induced by cross-seeding

mechanisms, neuroinflammation activation or oxidative stress but also by the metabolites produced by the human microbiome which could have pathogenic or health sustaining functions (Friedland and Chapman, 2017).

In summary, it is clear that the nervous system communicate in a bidirectional manner with the gut a pathway known as the gut-brain axis, which is done directly through the vagus nerve or by immune system mediators or bacterial metabolites and byproducts (Rutsch et al., 2020). Moreover, microbiota gut dysbiosis has been demonstrated to cause neuroinflammation by increasing pro-inflammatory cytokines levels, systemic inflammation and disruption of gut barrier compromising immune protection. Alterations in the composition of gut bacteria have been associated to neurodegeneration and other disorders (Cryan et al., 2020; Lynch and Pedersen, 2016). In fact, there is increasing evidence that gut dysbiosis is linked to Alzheimer's disease by inducing Aβ aggregation, oxidative stress and neuroinflammation (Liu et al., 2020; Rutsch et al., 2020; Vogt et al., 2017). Interestingly, recent reports have shown that alterations in the gut microbiome are not only associated to neurodegenerative diseases but also to aging and medication use, with two bacterial species used in this PhD thesis, *Escherichia* and *Klebsiella*, increasing their population in older subjects and in subjects with more medication use respectively (Leite et al., 2021). The definitive mechanism by which gut dysbiosis cause neural dysfunction has not been elucidated and further research is needed. Another interesting mechanism is the inflammasome, which is known to be activated by exposure to bacteria and bacterial amyloids (Rutsch et al., 2020). As stated previously, it has been proven that activation of the NLRP3 inflammasome induce the formation of ASC specks in microglial cells, that later binds to Aβ inducing its aggregation through a cross-seeding mechanism (Venegas et al., 2017). Therefore, even though our hypothesis was that bacterial amyloids induce the aggregation of Aβ by a direct cross-seeding mechanism, we should consider that bacterial amyloids might induce Aβ deposition by a cross-seeding mechanism through the NLRP3 inflammasome. The binding of Aβ to ASC specks seem to cause toxicity in microglia causing pyroptotic cell death (Friker et al., 2020), hence it is possible that bacterial functional amyloids could be inducing cell death directly resulting in distinct neurotoxicity in the brain of injected mice. Induction of the NLRP3 inflammasome by the three bacterial functional amyloids used in this thesis and cross-seeding mechanism through ASC specks is currently being investigated in collaboration with the lab of Dr. Michael T. Heneka (Bonn, Germany).

Taken together the increasing among of data demonstrating a causal relationship between the gut microbiome and AD pathology, modulation of the gut microbes through specific interventions such as dietary changes and supplementation with probiotics, fecal transplants, caloric restriction, lifestyle changes, food preparation and hygiene practices improvement and even genetic manipulation of the human gut microbial populations could be an effective strategy to prevent or reduce the risk of developing neurodegenerative disorders (Bonfili et al., 2021; Pistollato et al., 2016). Interestingly, some of these practices are currently under investigation (Arora et al., 2020; Hazan, 2020; Kesika et al., 2021; Park et al., 2021; Sun et al., 2019). It is always important to keep in mind that in the human body there are the same amount of bacterial cells than human cells (Sender et al., 2016), further supporting their critical relevance in human health and disease.

4.2.3. BACTERIAL FUNCTIONAL AMYLOIDS FAIL TO INDUCE A STRONG NEUROINFLAMMATORY RESPONSE

Though a more comprehensive inflammatory characterization of the BFA- induced inflammatory profiles would be necessary, our multiplex analysis show little differences in the expression of pro- and anti-inflammatory cytokines in mice receiving bacterial functional amyloid fibrils. The few changes observed in cytokines/chemokines levels in these mice indicate that CsgA fibrils induced a mixed profile with both anti-inflammatory (high IL-9 and low IL-17) and proinflammatory (high TNF-α) signatures. In a similar fashion, a mixed profile was also found in animals injected with TasA fibrils with both anti-inflammatory (low IL-1α, low CXCL1 and low IL-17) and proinflammatory (High CCL3 and tendency to an increase in TNF-α and IFN-γ). However, animals injected with Mcc fibrils displayed similar levels for all of the cytokines/chemokines than uninjected animals. Even though these responses were weak, these findings indicate the existence of differential glial responses to the bacterial functional amyloids CsgA and TasA. Cytokines can be produced by microglia astroglia and neurons, however the exact sources for each cytokine in the different seeded mice need to be further investigated. Moreover, the biological impact of CsgA and TasA fibrils in the innate immunity response may be underestimated by the complexity of microglial and astroglial responses in the disease context, with the co-existence of multiple functional phenotypes including spatial and temporal variations (Escartin et al., 2021). Interestingly, TasA fibrils induced CCL3

upregulation, a chemokine involved in chemotaxis and shown to contribute to T cell recruitment to the brain (Laurent et al., 2017). Moreover, these seeds also induced IFN-γ elevation, an essential element of the neuroinflammatory network involved in leukocyte trafficking (Kunis et al., 2013). In the case of CsgA fibrils, an increase in TNF-α levels was observed. This pro-inflammatory cytokine has been associated to detrimental effects in AD such as neuronal cell death, increased synthesis and lower clearance of Aβ, as well as increased tau hyperphosphorylation (Wang et al., 2015). Therefore, the little inflammatory response observed in these animals might have some detrimental biological effects. On the other hand, increased levels of anti-inflammatory cytokine IL-9 and decreased levels of proinflammatory cytokines such as IL-1α, CXCL1 and IL-17, might be inducing the opposite effects in biological functions. Future research in this line may help to link bacterial functional amyloids with specific pathological responses.

5. Conclusions

1. The 2F and 3F Aβ strains, as well as Aβ-containing brain extracts from aged Tg2576 mice, self-propagate *in vivo* and induce amyloid pathology with unique structural arrangements, specific brain tropism, and induce different type of amyloid deposits. Moreover, the three different types of Aβ aggregates, induced distinctive biological responses in the brains of injected mice as seen by their differential glial responses and associated patterns of cytokine/chemokine levels.

2. The Aβ deposits induced by the three different inocula have unique molecular structures as evaluated by high-resolution techniques (ssNMR). Interestingly, one of the most prevalent $A\beta_{40}$ polymorphs found in the brain of animals injected with brain extracts from aged Tg2576 mice closely resembled the predominant polymorph found in patients with typical AD. Given the heterogeneity in Aβ fibrils found in AD, our findings support the idea that misfolded Aβ conformational diversity explain the existence of different AD subtypes. Therefore, deciphering the most pathologically relevant Aβ conformations in AD patients will allow for personalized diagnosis and precision medicine approaches against each of the clinical AD subtypes.

3. The three different bacterial functional amyloids, CsgA subunit of curli from *E. coli*, microcin E492 from *K. pneumoniae* and TasA from *B. subtilis*, have the ability to cross-seed the aggregation of Aβ *in vitro*. These bacterial functional amyloids might induce the formation of $A\beta_{40}$ fibrils polymorphs or strains that could exhibit different toxicity or biological relevance than $A\beta_{40}$ fibrils seeded by homologous seeding.

4. CsgA fibrils induced the aggregation of Aβ *in vivo* through a cross-seeding mechanism. However, the other bacterial amyloids failed to induce significant increases in Aβ pathology. Similar to what is observed in prion diseases during interspecies transmissions, bacterial functional amyloids seem to induce Aβ pathology with an incomplete attack rate. These results support Aβ pathology being induced by normal gut commensal or pathogenic bacteria as a novel pathogenic mechanism associated with AD. Therefore, individualized gut microbiome interventions represent potential therapeutic targets for Alzheimer's disease.

6. Resumen

TESIS DOCTORAL – 2021

CEPAS CONFORMACIONALES DE Aβ Y MECANISMO DE *CROSS-SEEDING* EN LA PATOGÉNESIS DE LA ENFERMEDAD DE ALZHEIMER: ESTUDIOS *IN VIVO* EN MODELOS ANIMALES TRANSGENICOS

6.1. INTRODUCCION

La enfermedad de Alzheimer (EA) es la causa más común de demencia en las personas mayores de 65 años. Esta enfermedad es una proteinopatía neurodegenerativa que se caracteriza por un deterioro cognitivo progresivo e imparable, resultando finalmente en un estado de demencia y de dependencia total de los pacientes. Según la Organización Mundial de la Salud (www.who.int/es), la EA es responsable del 60-70% de los casos diagnosticados con demencia, actualmente unos 50 millones de personas a nivel mundial. Se prevé que para el año 2050 se triplique los afectados con demencia, alcanzando los 150 millones (Scheltens et al., 2021). La EA ocurre en un proceso continuo que comienza con una fase preclínica o asintomática de larga duración, que puede durar de 15 a 20 años y que se caracteriza por cambios fisiopatológicos en el cerebro que comienzan décadas antes de la aparición de síntomas. Esta fase preclínica es seguida por una fase clínica sintomática que comienza con un estadio prodrómico conocido como deterioro cognitivo leve (o MCI, *mild cognitive impairment*), el cual progresa hacia una fase con demencia leve, posteriormente moderada, finalizando con una fase de demencia severa (Alzheimer Association Report 2020). Esta fase clínica de demencia tiene normalmente una duración de 8-10 años y se caracteriza por la pérdida substancial de la memoria y otros deterioros funcionales que afectan a la capacidad de razonamiento, al lenguaje (afasia), funciones ejecutivas (apraxia), atención (agnosia) así como al procesamiento espacio visual y capacidad de socializar. Estas alteraciones son consecuencia del daño selectivo de regiones cerebrales implicadas en estos procesos como son el hipocampo, la corteza entorrinal, la amígdala, los ganglios basales y zonas neocorticales. A nivel neuropatológico, estas regiones sufren perdida sináptica y muerte neuronal, junto con la agregación y acumulación extracelular del péptido beta-amiloide (Aβ) formando las placas seniles, la acumulación intraneuronal de agregados de proteína tau hiperfosforilada formando los ovillos neurofibrilares, así como por la activación de

células gliales (microglía y astroglía) asociada a una respuesta neuroinflamatoria (Scheltens et al., 2021).

Aunque últimamente se hayan hecho grandes avances en investigación biomédica, actualmente no existe ninguna terapia farmacológica capaz de curar, prevenir o retrasar la progresión de la EA. Las terapias que se encontraban hasta ahora disponibles tan solo reducían los síntomas y ninguna era completamente efectiva (Cummings et al., 2021; Scheltens et al., 2021). Sin embargo, en este año la agencia de Estados Unidos del medicamento (FDA, del inglés *Food and Drug Administration*) ha aprobado por primera vez una terapia para modificar el curso de la enfermedad de Alzheimer, que se basa en un anticuerpo monoclonal (Aducanumab) que tiene al péptido Aβ como diana y que ha sido desarrollado por la compañía Biogen (Fillit and Green, 2021; Hooker, 2021; Tampi et al., 2021). Aunque la aprobación de esta inmunoterapia haya sido objeto de bastante controversia en la comunidad científica, al no haber demostrado los ensayos clínicos un beneficio clínico significativo a nivel cognitivo, su apuesta como potencial terapia apoya la importancia de seguir estudiando la patología de Aβ como diana de futuras intervenciones clínicas dirigidas a modular la enfermedad de Alzheimer.

A nivel microscópico, la patología de Aβ se presenta en dos formas principales en el cerebro de los pacientes de EA. Por un lado, se observan acumulaciones extracelulares de este péptido en el parénquima cerebral, más en concreto en las regiones del hipocampo y la corteza cerebral, conocidas como placas amiloides y por otro lado se observan agregados de Aβ en el espacio perivascular de los vasos sanguíneos, formando lo que se conoce como angiopatía amiloide cerebral (o CAA) y que puede provocar daños en las paredes de los vasos, resultando en microhemorragias (Knopman et al., 2021; Long and Holtzman, 2019; Selkoe and Hardy, 2016). La morfología de las placas amiloides es variada, siendo clasificadas principalmente en dos grupos: las **placas amiloides compactas o neuríticas**, que se caracterizan por tener un núcleo compacto de Aβ y que son reactivas a colorantes específicos para amiloides fibrilares como son el rojo Congo y la Tioflavina S. Estas placas están rodeadas de neuritas distróficas (axones y elementos presinápticos dilatados por acumulación de material vesicular autofágico) y células gliales reactivas (Thal et al., 2015). Por otro lado, se encuentran las **placas difusas**, que se caracterizan por ser depósitos laxos de Aβ no fibrilar y que no son reactivas a tinciones con rojo Congo o Tioflavina S. Estas placas no presentan neuritas distróficas y non inducen la activación de de células gliales a su alrededor (Calderon-Garcidueñas and

Duyckaerts, 2018). Además de estos dos tipos principales de depósitos de Aβ, se han descrito otros tipos de depósitos como las placas ‘’*cotton-wool’’* y las placas asociadas a ovillos neurofibrilares, así como dos tipos de angiopatía amiloide cerebral dependiendo del tipo de vasos sanguíneos al que se asocia. Por otro lado, también se ha descrito la agregación y acumulación de Aβ intracelular en las neuronas (Hampel et al., 2021b). Por lo tanto, y dado que la patología Aβ comienza en el cerebro décadas antes de la aparición de síntomas, la acumulación de este péptido ha sido considerado el agente causativo de la enfermedad de Alzheimer (hipótesis de la cascada amiloide, revisada en Selkoe and Hardy, 2016). A nivel molecular existe una gran diversidad de formas, conformaciones y estados de agregación de Aβ pudiendo ser responsable de la gran heterogeneidad neuropatológica y clínica en la EA (Cohen et al., 2016; Ghosh et al., 2021; Qiang et al., 2017).

La patología de Aβ, además de observarse de diversas formas, comparte mecanismos patológicos con las enfermedades priónicas y otras enfermedades neurodegenerativas ya que el Aβ, al igual que los priones y otras proteínas como la α-sinucleina y el TDP-43, tiene la capacidad de malplegarse, agregarse y propagar su conformación amiloide. Igualmente comparten características estructurales, biológicas y bioquímicas como es su insolubilidad, toxicidad, resistencia a degradación proteolítica y la reactividad con tinciones específicas para proteínas amiloides como son el rojo Congo y la tioflavina S (Jucker and Walker, 2018; Lau et al., 2021). En concreto, la capacidad de propagar su conformación, también conocido como un mecanismo de propagación tipo-priónico (o *prion-like propagation*), ha sido demostrado tanto *in vitro* como *in vivo* y ha evidenciado la posibilidad de que la patología de Aβ pueda ser transmitible entre individuos (Gomez-Gutierrez and Morales, 2020). El péptido Aβ, además de demostrar una capacidad auto propagativa, también tiene en común con los priones la existencia de cepas. En concreto, se consideran cepas todas aquellas variantes conformacionales y estructurales del Aβ que son estables y tienen capacidad de propagar esta estructura especifica tanto *in vitro* como *in vivo* (Cohen et al., 2016; Lau et al., 2021). Estas cepas de Aβ se puede demostrar que presentan distintas estructuras mediante técnicas bioquímicas como la degradación proteolítica con proteinasa K (PK) o con agentes caotrópicos como el GdnHCl (Di Fede et al., 2018; Lau et al., 2018), así como con tinciones especificas como el rojo Congo y la Tioflavina S (Condello et al., 2018). Además, el desarrollo de compuestos luminiscentes como los LCOs, así como los

anticuerpos conformacionales, han evidenciado la existencia de cepas de Aβ (Cohen et al., 2015; Nilsson et al., 2007; Rasmussen et al., 2017). Finalmente, estudios de alta resolución como la criomicroscopía electrónica (del inglés *Cryo-EM*) y la resonancia magnética nuclear en estado sólido (ssNMR) demostraron la existencia de distintas cepas de Aβ tanto formadas a partir de Aβ sintético como a partir de cerebros de pacientes con EA (Cendrowska et al., 2020; Ghosh et al., 2021; Qiang et al., 2017), evidenciando de esta manera que en el cerebro de humanos también se aprecia la existencia de distintas cepas de Aβ en los distintos subtipos clínicos de Alzheimer.

Respecto a las cepas formadas a partir de Aβ sintético, dos cepas distintas fueron desarrolladas por el laboratorio del Profesor Robert Tycko (Petkova et al., 2005). Estas cepas fueron caracterizadas tanto por microscopia electrónica como por ssNMR y demostraron tener características morfológicas específicas como son el giro y la anchura de las fibras, así como la longitud por masa (MPL). Debido a estos datos, se reconoció que las fibras formadas por agitación del péptido Aβ tenían aproximadamente una simetría rotacional doble, con dos capas moleculares por protofilamento, mientras que las fibras amiloides formadas por quiescencia del péptido Aβ tenían aproximadamente una simetría triple, con tres capas moleculares por protofilamento, recibiendo de esta manera el nombre de fibras o cepas 2F y 3F respectivamente (Petkova et al., 2005; Tycko, 2014, 2015). Estas cepas de Aβ sintético demostraron tener la capacidad de propagar su conformación *in vitro*, distinta susceptibilidad a la fragmentación y diferente toxicidad en cultivos neuronales primarios de hipocampo de rata (Petkova et al., 2005). Sin embargo, la capacidad de propagar su conformación *in vivo*, así como la posibilidad de inducir efectos biológicos específicos relacionados a sus estructuras, no han sido estudiados. Con ese objetivo en mente, las cepas 2F y 3F procedentes del laboratorio del Profesor Robert Tycko fueron utilizadas en esta tesis doctoral.

Como ha sido mencionado anteriormente, enfermedades neurodegenerativas como la EA o la enfermedad de Parkinson, han sido históricamente asociadas a la agregación y deposición de proteínas organizadas en conformaciones amiloides. Entre las proteínas mayormente involucradas en estos procesos y consideradas amiloides se incluyen el péptido Aβ, tau y α-sinucleína (Soto and Pritzkow, 2018). Hoy en día se conoce que las proteínas amiloides no solo están relacionadas con enfermedades neurodegenerativas, sino que también ejercen funciones fisiológicas importantes, adoptándose el termino de **amiloides funcionales** (Loquet et al., 2018; Otzen and Riek, 2019). Los amiloides

funcionales no están únicamente presentes en mamíferos, sino también en otros seres vivos, como bacterias, hongos, insectos y peces. En todos ellos, los amiloides pueden ejercer una gran diversidad de funciones, incluyendo roles adaptativos y de soporte (Kosolapova et al., 2020; Sergeeva and Galkin, 2020; Shewmaker et al., 2011). Trabajos anteriores, han demostrado que la agregación de proteínas amiloides puede ser inducida por otras proteínas amiloides mediante un mecanismo de siembra cruzada (del inglés *cross-seeding)*, en el que una "semilla" (del inglés *seed*) o pequeño agregado de una proteína induce la agregación especifica de otra (Morales et al., 2013). Este mecanismo ha sido ampliamente estudiado en el contexto de las enfermedades neurodegenerativas. Específicamente, para el Aβ se ha demostrado la capacidad de hacer *cross-seeding* con otras proteínas como son los priones (Morales et al., 2010), tau (Guo et al., 2006), amilina (Moreno-Gonzalez et al., 2017) o α-sinucleína (Clinton et al., 2010; Masliah et al., 2001), evidenciando de esta manera la posibilidad de que enfermedades como la diabetes, el Parkinson y las enfermedades priónicas puedan estar potenciando la aparición de la enfermedad de Alzheimer. Sin embargo, todavía se desconoce si el mecanismo de *cross-seeding* pudiera estar ocurriendo entre amiloides funcionales bacterianos (producidos por la flora intestinal humana) y amiloides de mamíferos como el Aβ. De esta manera, se podría demostrar que la enfermedad de Alzheimer puede estar provocada por proteínas amiloides que son producidas por las bacterias presentes en nuestra flora intestinal. Ejemplos de proteínas amiloides producidas por bacterias que se podrían encontrar en abundancia en humanos son la proteína **curli**, producida principalmente por enterobacterias como *Escherichia coli* y *Salmonella spp* (Chapman et al., 2002), la bacteriocina **microcina E492**, producida por la bacteria gram-negativa *Klebsiella pneumoniae* (Shahnawaz et al., 2017a), y la proteína **TasA**, producida por bacterias gram-positivas como *Bacillus subtilis* y *Bacillus cereus* y que tienen gran similitud a la proteína curli (Romero et al., 2010). Aunque existan otros mecanismos por el cual las bacterias de nuestra flora intestinal podrían inducir la patología de la EA (Dominy et al., 2019; Moir et al., 2018), en esta Tesis Doctoral nuestro estudio se centró en demostrar mediante ensayos *in vitro* e *in vivo* la posibilidad de que esto ocurriera por un mecanismo de *cross-seeding*, intentando identificar así un nuevo mecanismo relacionado con la progresión de enfermedades asociadas al mal plegamiento de proteínas.

6.2. HIPOTESIS Y OBJETIVOS

Teniendo en cuenta todo lo expuesto anteriormente acerca de las cepas de Aβ y la posibilidad de que los amiloides bacterianos puedan inducir la EA, se ha propuesto como **hipótesis principal** de esta Tesis Doctoral que diferentes cepas de Aβ son las responsables de la progresión patológica de la enfermedad de Alzheimer, incluyendo la toxicidad, el tropismo celular y tisular, la propagación de tipo priónico y la neuroinflamación, resultando de esta manera en las diversas variantes clínicas de la EA. Además, hemos propuesto que el mal plegamiento de Aβ asociado a la enfermedad de Alzheimer podría ser inducido por amiloides funcionales bacterianos a través de un mecanismo de *cross-seeding*. De este modo, de ser demostrada que ambas hipótesis son correctas, esta Tesis Doctoral revelaría nuevos mecanismos patológicos asociados a enfermedades neurodegenerativas y esto permitiría el futuro desarrollo de terapias para prevenir y tratar esta devastadora enfermedad.

Por lo tanto, el **objetivo principal** de este trabajo *es asociar las distintas conformaciones de Aβ con diferentes respuestas biológicas utilizando las cepas de Aβ producidas in vitro que han sido ampliamente caracterizadas con anterioridad*. De este modo, también tenemos como **objetivo** *demostrar y caracterizar, mediante experimentos in vitro e in vivo, la interacción entre amiloides funcionales bacterianos y amiloides relacionados con la enfermedad de Alzheimer como el Aβ*. Para ello, se proponen los siguientes objetivos específicos:

Objetivo 1. Relevancia fisiológica de las cepas de Aβ en la enfermedad de Alzheimer

1.1. Análisis de la interacción *in vitro* entre las cepas de Aβ sintéticas (2F y 3F) que han sido previamente caracterizadas y el Aβ sintético monomérico. Mediante el uso de ensayos de agregación *in vitro*, tenemos como objetivo evaluar la capacidad de iniciar la agregación de Aβ monomérico de estas dos cepas de Aβ. Estas dos cepas también se caracterizarán mediante el uso de tinciones específicas de conformación (LCOs) y ensayos de resistencia a PK.

1.2. Determinar la capacidad de iniciar la agregación de Aβ de estas dos cepas en modelos animales transgénicos de la enfermedad de Alzheimer. En resumen, se evaluará la aceleración de la patología de la EA (patología de Aβ y respuesta glial) por medios convencionales (inmunohistoquímica y ensayos de citoquinas por Multiplex) en el cerebro de animales transgénicos de la EA que han sido

inyectados intracerebralmente con estas cepas sintéticas de Aβ, con agregados derivados de cerebro de ratón o con Aβ monomérico/soluble. La conformación de los agregados inducidos en animales inyectados se analizará con tinciones específicas de conformación (LCOs) y ssNMR en colaboración con Dr. Robert Tycko (NIH, USA).

Objetivo 2. Interacción entre proteínas amiloides de mamíferos y de bacterias

2.1. Análisis de la interacción *in vitro* entre amiloides de mamíferos (Aβ) y amiloides bacterianos (subunidad CsgA de curli, microcina E492 y TasA). Mediante el uso de ensayos de agregación *in vitro*, tenemos como objetivo evaluar la capacidad que tienen los amiloides bacterianos de hacer *cross-seeding* con las formas solubles de Aβ.

2.2. Determinar la capacidad de iniciar la agregación de Aβ de estos amiloides bacterianos en modelos animales transgénicos de la Enfermedad de Alzheimer. En este trabajo, se evaluará la aceleración de la patología de Aβ por medios convencionales (inmunohistoquímica y ensayos de citoquinas por Multiplex) en el cerebro de animales transgénicos de la EA que han sido inyectados intracerebralmente con agregados formados a partir de los amiloides bacterianos (subunidad CsgA de curli, microcina E492 y TasA). Diversos marcadores de inflamación también serán evaluados mediante ensayos Multiplex.

Todos los experimentos desarrollados durante esta tesis doctoral han constado de la correspondiente aprobación del comité ético para la experimentación con animales.

6.3. MATERIAL Y METODOS

En el transcurso de la presente tesis doctoral se realizó una gran diversidad de métodos experimentales y se encuentran completamente explicados en la **sección 2** de esta tesis doctoral. A continuación, se exponen los principales métodos empleados en ella en forma de resumen:

6.3.1. Animales de experimentación

En el presente trabajo de Tesis Doctoral se utilizó el modelo murino transgénico Tg2576, el cual es un modelo para la patología de Aβ que sobreexpresa la isoforma 695 de la proteína precursora amiloide (APP) con una mutación (KM670/671NL) bajo el control del promotor de la proteína priónica. Estos animales se mantuvieron en un fondo genético B6;SJL. Este modelo animal comienza a desarrollar depósitos extracelulares de Aβ a partir de los 8 meses de edad y presenta numerosas placas de Aβ en el parénquima cerebral a los 15 meses de edad (Hsiao et al., 1996; Irizarry et al., 1997).

6.3.2. Preparación de los inóculos

Para nuestro estudio, se prepararon una gran diversidad de inóculos. En primer lugar, como control positivo y para estudiar la patología inducida por el Aβ propio de los animales Tg2576, se homogeneizó un cerebro de un animal adulto (15 meses) de este modelo con un homogeneizador de vidrio a una concentración del 10% peso volumen en tampón fosfato salino (PBS, HyClone™ Dulbecco's PBS, GE Healthcare Life Sciences, USA). Como control negativo, $A\beta_{40}$ (Biomatik, USA) sintético monomérico se disolvió en PBS a una concentración de 1 mg/mL segundos antes de ser inyectado para así evitar la agregación del péptido. Para los grupos experimentales inoculados con fibras 2F y 3F, así como con los amiloides bacterianos (CsgA, microcina E492 y TasA), las fibras amiloides de estos péptidos fueron ultracentrifugadas a 100.000 x g usando una ultracentrífuga Optima L-100K (Beckman-Coulter, USA) por 1 hora y posteriormente resuspendidos en PBS a una concentración de 1 mg/Ml. Todos los inóculos preparados fueron mantenidos a -80°C hasta ser utilizadas. Antes de ser inyectados en los animales, los inóculos fueron sonicados por 30 segundos en un baño de agua con hielo.

6.3.3. Procedimientos animales

Para estudiar nuestras hipótesis, animales Tg2576 fueron inyectado con los inóculos (fibras 2F, n=7; fibras 3F, n=7; extracto de cerebros de animales adultos (15 meses)

Tg2576, n=5; Aβ40 sintético monomérico, n=4; fibras de CsgA, n=12; microcina, n=8 y fibras de TasA, n=10) a los 50 días de edad y fueron sacrificados a los 150 días de edad o 300 días de edad dependiendo del grupo experimental.

Los animales fueron anestesiados e inyectados estereotaxicamente con los inóculos en ambos hipocampos usando las siguientes coordenadas desde bregma: anteroposterior: -1.8 mm; medio-lateral: ±1.8 mm; dorsoventral: -1.8 mm. En concreto se inyectaron 10 µL de inoculo usando una jeringa Hamilton 1700 Series (Hamilton company, USA). Puesto que todos los procedimientos animales descritos en esta tesis doctoral se realizaron durante la estancia doctoral en UTHealth, los procedimientos contaron con la aprobación del comité ético del comité de la universidad (AWC) y siguieron la regulación del centro de medicina y cuidado animal (CLAMC).

6.3.4. Ensayos de agregación *in vitro* (PMCA)

Para los ensayos de agregación *in vitro* de Aβ40 se utilizó péptido recombinante purificado a partir de células *E. coli* (BL21 (DE3) que contenían el plásmido pET28 GroES-Ub-Aβ40 siguiendo el protocolo descrito en la **sección 2.2.6.1**. El péptido monomérico de Aβ40 liofilizado se disolvió a una concentración de 1 mg/ml en hidróxido de amonio (NH_4OH) al 0,1%. A continuación, se filtró a través de un filtro de 30 kDa (Amicon Ultra Centrifugal Filter Units, Millipore, Ref. UFC503096) a 14.000 x g durante 12 minutos para eliminar los agregados de gran tamaño. La concentración de proteína filtrada se midió posteriormente empleando el kit Micro BCA™ (Pierce, Ref.23235) y se mantuvieron a -80°C hasta su uso.

Posteriormente se realizaron los ensayos de agregación *in vitro* de Aβ40 siguiendo el protocolo descrito por Salvadores et al., 2014 y explicado en profundidad en el **apartado 2.2.6.3** de esta tesis. En resumen, el Aβ40 fue incubado a una concentración de 1 µM en tampón Tris-HCl 100 mM (pH 7.4) y con 5 µM de Tioflavina-T (ThT), a 20°C en una placa opaca de 96 pocillos, empleando ciclos de 1 minuto de agitación a 500 rpm cada 30 minutos. Las fibras amiloides de los mismos inóculos empleados en las inyecciones de animales transgénicos se añadieron a los pocillos que contenían Aβ40, a diversas diluciones. La agregación fue monitorizada midiendo la fluorescencia de la Tioflavina-T a 485 nm tras la excitación a 435 nm, usando un espectrofluorómetro de placas (SpectraMax® iD3, Molecular Devices, USA), y las gráficas se ajustaron empleando la ecuación de Boltzmann. Las curvas fueron posteriormente comparadas

empleando la prueba de Tukey de comparaciones múltiples. Todos los cálculos se realizaron mediante el software GraphPad Prism 9.

6.3.5. Microscopía óptica

Durante el presente trabajo de Tesis Doctoral se realizaron estudios tanto de microscopía óptica a campo claro como de microscopia óptica de fluorescencia. Para estos estudios se emplearon tanto técnicas de inmunohistoquímica como tinciones con Tioflavina-S o los LCOs. Para las técnicas inmunohistoquímicas se emplearon anticuerpos primarios dirigidos hacia las dianas de estudio (ver **tabla 2.3**) que fueron posteriormente detectados por anticuerpos secundarios acoplados a biotina y al complejo molecular extravidina-peroxidasa (ver **tabla 2.4**, campo claro) o por anticuerpos secundarios acoplados a fluorocromos (ver **tabla 2.5**, inmunofluorescencia). Para una información más detallada acerca de la realización de estos experimentos, se recomienda revisar los **apartados 2.2.9 al 2.2.14** donde se explican detalladamente los protocolos seguidos para cada uno de los marcadores empleados en esta tesis doctoral.

Posteriormente, las secciones teñidas tanto por técnicas inmunohistoquímicas como por tinciones con Tioflavina-S o los LCOs, se visualizaron usando un microscopio (DMI6000B, Leica Microsystems, Germany) conectado a un ordenador con el software Leica Application Suite (LAS; Leica Microsystems, Germany). Las muestras se fotografiaron empleando una cámara digital (DFC310 FX Leica, Germany). Las imágenes fueron tomadas con un tamaño de 2560x1920 píxeles y en formato .tiff.

Las imágenes digitales obtenidas fueron posteriormente procesadas en el software Adobe PhotoShop versión 22.4.1 (2021) en el que, cuando se estimó necesario, se ajustaron el tamaño, brillo y contraste en todas las imágenes por igual. Finalmente, las imágenes fueron montadas en láminas con la aplicación Adobe Illustrator, versión 25.2.3 (2021).

6.3.6. Análisis estadístico

Los análisis estadísticos de este trabajo se realizaron empleando el programa GraphPad Prism 9 (GraphPad Software Inc, USA). En concreto, para los experimentos de agregación *in vitro* se realizaron los ensayos al menos dos veces y las reacciones se realizaron por quintuplicado (5 réplicas técnicas por condición) y los datos fueron expresados como a media del grupo ± error standard de la media (SEM). Las gráficas de estos ensayos se ajustaron empleando la ecuación de Boltzmann. Para los análisis de los

datos obtenidos en los experimentos bioquímicos e histológicos, la comparación entre los grupos se realizó aplicando el análisis de la varianza (ADEVA o ANOVA) de una vía, y para las pruebas *post-hoc* se aplicó Tukey. Para todos los análisis, se empleó un intervalo de confianza del 95% y por lo tanto se consideraron estadísticamente significativos todos aquellos análisis con un valor de $p < 0,05$, señalado con una estrella (*) a los valores con $p < 0,05$, con dos estrellas (**) a los valores con $p < 0,01$, con tres estrellas (***) a los valores con $p < 0,001$ y con cuatro estrellas (****) a los valores con $p < 0,0001$.

6.4. RESULTADOS Y DISCUSIÓN

A continuación, se exponen en forma de resumen los resultados más relevantes, así como una discusión de ellos, que han sido obtenidos durante el transcurso de la presente tesis doctoral:

6.4.1. Los agregados 2F y 3F demuestran características estructurales y bioquímicas únicas

Pese a que los agregados 2F y 3F empleados en este trabajo han sido previamente caracterizados por ssNMR (Petkova et al., 2005), en esta Tesis Doctoral se realizó una extensa caracterización de estos agregados *in vitro*. Estas fibras demostraron tener distintas características por microscopia electrónica y diferente resistencia a la proteólisis con proteinasa K, siendo las fibras 2F más resistentes a la digestión proteolítica que las fibras 3F. Este tipo de ensayos ha demostrado previamente la capacidad de diferenciar distintas cepas de amiloides asociados enfermedades neurodegenerativas como son el Aβ (Cohen et al., 2015; Di Fede et al., 2018), la proteína priónica (Pastrana et al., 2006) y la α-sinucleina (Shahnawaz et al., 2020). Posteriormente, las fibras 2F y las fibras 3F también demostraron, en los ensayos de agregación *in vitro* con $A\beta_{40}$ (PMCA) una velocidad de agregación distinta, así como un máximo de fluorescencia de Tioflavina-T único, para cada una de las fibras. Este tipo de ensayos de agregación *in vitro* han demostrado también con anterioridad que son capaces de distinguir distintas cepas de Aβ (Qiang et al., 2011) y de α-sinucleina (Shahnawaz et al., 2020). Por último, haciendo uso de tinciones específicas de conformación, con las moléculas conocidas como LCOs, se demostró que las fibras 2F mostraron una unión especifica a la molécula HS-68 mientras que las fibras 3F demostraron mayor afinidad con las moléculas HS-194, HS-208 y HS-212. De nuevo, este tipo de ensayos ha demostrado con anterioridad ser capaz de

distinguir distintas cepas de proteínas amiloides como el Aβ y tau (Klingstedt et al., 2011, 2013; Nilsson et al., 2007) así como cepas de α-sinucleína (Shahnawaz et al., 2020).

Por lo tanto, tomando en conjunto los resultados obtenidos por: microscopía electrónica, ensayos de resistencia a la digestión proteolítica por PK, ensayos de agregación *in vitro* con $A\beta_{40}$ (PMCA) y ensayos de afinidad a los LCOs, hemos demostrado en este trabajo que las fibras 2F y 3F son claramente cepas conformacionales distintas formadas ambas por $A\beta_{40}$ sintético. Estos datos complementan perfectamente a los resultados obtenidos previamente por el grupo del Dr. Robert Tycko (Petkova et al., 2005) y por lo tanto apoyan el uso de estas fibras como inóculo en nuestro trabajo, para así poder descifrar la actividad biológica de estos agregados *in vivo*, lo cual podría ser de gran relevancia clínica.

6.4.2. Los agregados de Aβ muestran un tropismo único en el cerebro de animales Tg2576 inyectados con las cepas 2F y 3F

A continuación, nos dispusimos a analizar el efecto que tienen *in vivo* las cepas 2F y 3F en animales inyectados intracerebralmente (hipocampo) con ellas y con otros inóculos como son el extracto de cerebro de animales adultos Tg2576 (modelo amiloidogénico), así como con proteína $A\beta_{40}$ sintética monomérica, para así poder evaluar la capacidad de propagación de su estructura única de estas fibras, así como la posibilidad de inducir efectos biológicos únicos dependientes de su estructura única. En primer lugar, analizamos los niveles de $A\beta_{40}$ y $A\beta_{42}$ en las fracciones S2 insolubles en PBS en animales de 300 días de edad (250 días después de la inyección con los inóculos). En estos análisis observamos que los animales inyectados con fibras 2F, así como los animales inyectados con extracto de cerebro de animales transgénicos adultos, demostraron un aumento significativo de los niveles de $A\beta_{42}$ insoluble en comparación con los animales inyectados con las fibras 3F o el péptido monomérico. Además, los animales inyectados con los extractos de cerebro demostraron tener niveles más altos de $A\beta_{42}$ insoluble que los animales inyectados con las fibras 2F. Este resultado, en el cual los agregados formados por Aβ sintético son capaces de inducir la agregación de Aβ *in vivo* y además lo hacen con una actividad biológica menos especifica que los agregados derivados de cerebros, ha sido igualmente reportado con anterioridad por el grupo del Dr. Stanley B. Prusiner (Stöhr et al., 2012)

Posteriormente, para evaluar la capacidad de estas cepas de propagar sus propiedades *in vivo*, analizamos por métodos inmunohistoquímicos la patología de Aβ en

estos ratones para así comprobar si en estos animales mostraban características propias de cepas como son la inducción de la patología con un tropismo diferencial hacia regiones específicas del cerebro. Este tipo de efectos ha sido demostrado anteriormente como una característica diferencial de las cepas tanto en priones (Morales, 2017) como en cepas de Aβ (Stöhr et al., 2012, 2014). En nuestro estudio, observamos que los animales inyectados con las fibras 2F acumularon Aβ extracelular principalmente en la región del alveus del hipocampo mientras que las fibras 3F indujeron mayormente esta patología en la región del giro dentado. Por otro lado, los animales inyectados con extracto de cerebro de animales transgénicos adultos no mostraron un claro tropismo hacia una región especifica ya que contenían placas de Aβ distribuidas por todas las subregiones del hipocampo. Por lo tanto, en este trabajo demostramos que cada uno de los inóculos indujo un tropismo único de la patología Aβ, apoyando así la idea de que cada uno de nuestros inóculos constituye una cepa única de Aβ.

Específicamente, el tropismo observado en animales inyectados con las fibras 2F podría tener consecuencias patológicas enormes, ya que la región del alveus, donde hemos observado la mayoría de depósitos de Aβ en estos animales, es una región que contiene axones de las células piramidales del hipocampo y por lo tanto cumplen una función critica en el establecimiento de la memoria (Llorens-Martín et al., 2014). Por ello, la acumulación de estos agregados de Aβ en esta región y su toxicidad podrían tener consecuencias patológicas importantes, aunque esta hipótesis debería ser explorada en futuros experimentos. Además, los depósitos de Aβ en animales inyectados con las fibras 2F también mostraron un claro tropismo hacia los ventrículos laterales. Puesto que experimentos anteriores han demostrado que la presencia de oligómeros de Aβ en estas regiones pueden alterar la barrera hematoencefálica provocando de esa manera déficits cognitivos (Brkic et al., 2015; Schmid et al., 2017), existe la posibilidad que la cepa 2F induzca deterioro cognitivo a largo plazo en estos animales. De nuevo, esta hipótesis debería de ser explorada en futuros experimentos utilizando estudios de comportamiento en estos animales.

6.4.3. Los agregados de Aβ inducidos por los distintos inóculos muestran características estructurales y bioquímicas únicas

Como se ha mencionado con anterioridad, una de las principales propiedades de las cepas de Aβ es la capacidad de producir agregados *in vivo* con una morfología estructural única. En este sentido, analizamos si los agregados inducidos *in vivo* por las cepas 2F y

3F, así como por los agregados de extracto de cerebro de animales adultos Tg2576. Por un lado, empleando la tinción con Tioflavina-S (TioS) observamos que los agregados inducidos por las fibras 2F y 3F fueron positivos para TioS, mientras que las placas inducidas por el extracto de cerebro adulto fueron negativas. Esto demuestra que las placas amiloides inducidas por las fibras sintéticas son placas compactas o neuríticas, mientras que las placas inducidas por el extracto de cerebro son de naturaleza difusa. Este resultado va en línea con trabajos previos que demostraron que las fibras formadas por Aβ sintético producen depósitos positivos para TioS (Stöhr et al., 2012) y trabajos que demostraron que distintas cepas formadas por péptido sintético no son distinguibles por tinción con TioS (Stöhr et al., 2014). además, las placas difusas inducidas por los extractos de cerebros también han sido demostradas con anterioridad (Morales et al., 2015).

A continuación, realizamos análisis en detalle de la conformación de los agregados inducidos por estos tres inóculos empleando las tinciones de tejido de cerebro con los dos LCOs (HS-68 y HS-194) que mejor resultado dieron en nuestros ensayos *in vitro*. Al igual que en nuestros resultados *in vitro*, los depósitos inducidos por las fibras 2F demostraron tener gran especificidad con la molécula HS-68, mientras que las placas inducidas por las fibras 3F mostraron mayor especificidad con la molécula HS-194. Por otro lado, los agregados inducidos por el extracto de cerebro de animales adultos demostraron reactividad hacia ambas moléculas. Estas moléculas han demostrado con anterioridad la capacidad de discriminar entre distintas estructuras moleculares del Aβ *in vitro* (Åslund et al., 2009; Klingstedt et al., 2011, 2013; Nilsson et al., 2007; Psonka-Antonczyk et al., 2016), así como depósitos estructuralmente distintos en ratones (Burwinkel et al., 2018; Michno et al., 2019; Nyström et al., 2013) y en pacientes de ciertos subtipos de la enfermedad de Alzheimer (Rasmussen et al., 2017), e incluso entre distintas cepas de α-sinucleína, siendo capaces de distinguir entre dos tipos de sinucleinopatías como son la enfermedad de Parkinson y la atrofia multisistémica (Shahnawaz et al., 2020). Por lo tanto, nuestros datos junto con el apoyo de los datos de otros grupos demuestran que la deposición de Aβ inducida por cada uno de los tres inóculos contienen estructuras moleculares únicas y por lo tanto constituyen tres tipos distintos de cepas de Aβ.

Por último, la estructura molecular definitiva de estos depósitos fue demostrada por ensayos de alta resolución como son el ssNMR. Esta técnica ha demostrado con anterioridad la capacidad de distinguir distintas conformaciones o cepas de Aβ a partir de

tejido de pacientes de EA, distinguiendo incluso distintas estructuras moleculares en las fibras de Aβ producidas por cada uno de los subtipos de EA (Ghosh et al., 2021; Lu et al., 2013; Qiang et al., 2017). Utilizando el cerebro de los ratones tratados con los distintos inóculos y en colaboración con el grupo del Dr. R. Tycko, se demostró en este trabajo que las fibras de $A\beta_{40}$ derivadas de animales inyectados con 2F y animales inyectados con extracto de cerebro de Tg2576, tienen un polimorfismo de fibras de Aβ en común, mientras que la segunda conformación mas prevalente en sus fibras fue estructuralmente distinta. Por su parte, los animales inyectados con las fibras 3F demostraron tener un polimorfismo de fibras de Aβ totalmente distinto a los animales inyectados con los otros dos inóculos. Es interesante destacar que una de las conformaciones estructurales encontradas en los animales inyectados con el extracto de cerebro adulto mostró tener gran semejanza con el polimorfismo de $A\beta_{40}$ predominantemente observado en el tejido cortical de pacientes con EA típico (Ghosh et al., 2021; Qiang et al., 2017). Por lo tanto, en este trabajo demostramos por ssNMR que los depósitos de Aβ inducidos por los tres tipos de inóculos fueron estructuralmente distintos a nivel molecular.

En resumen, nuestros datos utilizando tinciones con TioS y con los LCOs HS-68 y HS-194, así como las estructuras moleculares resueltas por ssNMR, apoyan la idea de que los tres inóculos (fibras 2F y 3F, así como los extractos de cerebros de Tg2576 adultos) son tres tipos de cepas de Aβ únicas con actividades biológicas únicas.

6.4.4. Los agregados de Aβ inducidos por los distintos inóculos estimulan respuestas neuroinflamatorias únicas

Una contribución importante de esta Tesis Doctoral fue analizar la significancia patológica de las distintas cepas de Aβ *in vivo*. En concreto, demostramos que la patología de Aβ inducida por los distintos tipos de inóculos resultó en respuestas gliales diferenciales en las que los depósitos inducidos por las fibras 2F mostraron una mayor inducción de respuesta astroglial, mientras que las placas amiloides inducidas por las fibras 3F, al igual que los depósitos inducidos por extractos de cerebro, mostraron mayor activación de la respuesta microglial. Sin embargo, es importante destacar que los depósitos difusos inducidos por los extractos cerebrales presentaron una respuesta microglial menor que las fibras sintéticas, en concordancia con trabajos previos por otros grupos (Wang et al., 2016)

Aunque se debería hacer un estudio más detallado de la respuesta inflamatoria en estos animales, como por ejemplo mediante el uso de técnicas de secuenciación de ARN de células individuales, el análisis multiplex realizado en este trabajo demostró que los animales inyectados con extracto de cerebro mostraron una expresión mayoritariamente de citoquinas proinflamatorias y se observó que esta respuesta neuroinflamatoria se encontraba exacerbada en comparación con los animales inyectados con los otros inóculos. Igualmente, los animales inyectados con las fibras 2F y 3F mostraron un aumento moderado de citoquinas proinflamatorias como el INF-γ y CCL3, con los animales inyectados con fibras 2F aumentando también la producción de IL-1α y CCL5. Por lo tanto, en esta tesis doctoral se demostró que distintas conformaciones o cepas de Aβ son capaces de inducir respuestas gliales diferenciales. Esto es de gran importancia, ya que se conoce que la patología de la enfermedad de Alzheimer está fuertemente influenciada por la respuesta glial observada en el cerebro de estos pacientes (Boche and Gordon, 2021; Escartin et al., 2021; Ulland and Colonna, 2018). Trabajos futuros que sigan esta línea, pero empleando cepas de Aβ encontradas en el cerebro de pacientes de EA, ayudaran a elucidar las cepas de Aβ que tienen mayores efectos en la respuesta inflamatoria en el cerebro de pacientes.

6.4.5. Las fibras 2F y 3F son cepas únicas de Aβ sintético. Relevancia clínica.

En resumen, todos los datos discutidos anteriormente apoyan que las fibras 2F y 3F son cepas de Aβ sintético con estructuras moleculares y actividades biológicas únicas. Estas también fueron distintas que los agregados de extractos de cerebro de Tg2576 adulto. Puesto que la enfermedad de Alzheimer es una enfermedad muy heterogénea, con cuatros subtipos claramente definidos neuropatológicamente y clínicamente (Ferreira et al., 2020; Jellinger, 2021; Vogel et al., 2021), y se ha demostrado por diversas técnicas que el cerebro de los pacientes con distintos subtipos contiene distintas cepas de Aβ (Condello et al., 2018; Duran-Aniotz et al., 2021; Di Fede et al., 2018; Ghosh et al., 2021; Lau et al., 2021; Michno et al., 2019; Qiang et al., 2017), se ha postulado que las distintas cepas de Aβ podrían ser la causa de la gran heterogeneidad observada en pacientes de EA. Resultados recientes de transcriptómica han apoyado nuevamente esta idea (Neff et al., 2021). Por lo tanto, una contribución importante de esta Tesis Doctoral ha sido demostrar la significancia patológica de las distintas cepas de Aβ *in vivo*. Sin embargo, pensamos que experimentos futuros empleando cepas de Aβ encontradas en el cerebro de pacientes de EA de cada uno de los subtipos, serán definitivos para confirmar o descartar

esta hipótesis de que las cepas de Aβ son la causa de la gran heterogeneidad observada en pacientes de EA. Estos estudios, serian de gran relevancia ya que ayudarían a definir los distintos subtipos de EA, así como a desarrollar herramientas de diagnóstico y terapias personalizadas, pudiendo finalmente resultar en el desarrollo de fármacos con capacidad de prevenir o modificar el curso de la EA para cada uno de los subtipos.

6.4.6. Los amiloides funcionales bacterianos inducen la agregación *in vitro* de $A\beta_{40}$ por mecanismo de *cross-seeding*.

Como ha sido explicado con anterioridad, las estructuras amiloides de las proteínas no están únicamente asociadas a patologías sino que también cumplen importante funciones biológicas, recibiendo así el nombre de amiloides funcionales (Loquet et al., 2018; Otzen and Riek, 2019). Debido a que gran cantidad de trabajos científicos han demostrado la presencia de bacterias en el cerebro de pacientes de EA y se ha observado una alteración de las bacterias flora intestinal en estos pacientes (Itzhaki et al., 2016; Kamer et al., 2015; Miklossy, 2016; Vogt et al., 2017), se ha propuesto que las bacterias podrían estar involucradas en la patología de la EA a través de diversos mecanismos como son la toxicidad directa, la inducción de una respuesta inflamatoria o incluso induciendo directamente la agregación de Aβ, siendo el Aβ un péptido anti-microbiano que se agregaría en respuesta a una infección para evitar la propagación de la infección bacteriana (Bulgart et al., 2020; Moir et al., 2018). Puesto que bacterias de gran relevancia en humanos como son *Escherichia coli, Klebsiella pneumoniae* y *Bacillus subtilis* producen amiloides bacterianos como son curli, microcina E492 y TasA respectivamente (Chapman et al., 2002; Romero et al., 2010; Shahnawaz et al., 2017a), y es conocido que distintos tipos de amiloides pueden inducir la agregación de otros amiloides heterólogos por un mecanismo de *cross-seeding*, en este trabajo decidimos analizar la capacidad de estos amiloides bacterianos de hacer *cross-seeding* e inducir la agregación *in vitro* de $A\beta_{40}$. Concretamente, en este trabajo demostramos que los tres amiloides funcionales bacterianos utilizados (subunidad CsgA, microcina E492 y TasA) fueron capaces de inducir la agregación *in vitro* de $A\beta_{40}$, aunque con una velocidad menor que la agregación inducida por semillas homologas (fibras amiloides de $A\beta_{40}$) y con una fluorescencia máxima de Tioflavina-T distinta, apoyando la idea de que los agregados producidos por estos amiloides bacterianos posiblemente representan distintas cepas o polimorfismos estructural de $A\beta_{40}$ y quizás tengan diferente toxicidad o actividad biológica. Futuros estudios de toxicidad y análisis con técnicas de alta resolución como

el ssNMR serán esenciales para corroborar esta existencia de cepas inducidas por amiloides bacterianos y la posible toxicidad de cada una de ellas.

En resumen, la presencia normal de bacterias que producen estos amiloides funcionales en la flora intestinal humana junto con nuestros resultados demostrando la capacidad de estos de inducir la agregación de $A\beta_{40}$ *in vitro* por un mecanismo de *cross-seeding*, es de gran relevancia ya que demuestra un nuevo posible mecanismo patogénico asociado a la EA. Sin embargo, esto debería de ser demostrado *in vivo* y por ello inyectamos estos amiloides bacterianos en el hipocampo de animales transgénicos de EA.

6.4.7. Los amiloides funcionales bacterianos inducen amiloidosis cerebral de una manera incompleta y produce una respuesta inflamatoria leve

Tras inyectar 10 µg de cada uno de los amiloides bacterianos (CsgA, Mcc and TasA) en cada hipocampo de animales Tg2576 de 50 días de edad y analizar los niveles de Aβ tanto por ensayos bioquímicos como por ensayos inmunohistoquímicos observamos que los animales inyectados con microcina mostraron un aumento en el ratio de $A\beta_{42}/A\beta_{40}$ por análisis bioquímicos mientras que los animales inyectados con CsgA desarrollaron una mayor acumulación de Aβ en el hipocampo cuando fueron analizados por técnicas de inmunohistoquímica. Sin embargo, no se encontraron diferencias significativas en los otros grupos analizados. Curiosamente, en todos los grupos inyectados con amiloides bacterianos se observo que algunos animales sí que desarrollan deposición de Aβ extracelular, fenómeno que no se observó en los animales no inyectados. Este fenómeno por el cual solo cierto porcentaje de los animales desarrollan patología amiloide tras ser inyectados, es un fenómeno conocido en el campo de priones como un ataque o inducción incompleta (Rossi et al., 2019). Este fenómeno normalmente se observa en la transmisión de priones entre distintas especies en las que existe un efecto de barrera (Bartz et al., 2000; Bessen and Marsh, 1992) y en experimentos con inóculos en baja concentración, con priones sintéticos o con distintas cepas (Colby et al., 2009; Makarava et al., 2010; Morales et al., 2016). Por lo tanto, es posible que aumentando la concentración del material inyectado o haciendo una inyección continua de agregados mediante el uso de bombas de inyección intracerebrales sea posible inducir de manera robusta la agregación de Aβ *in vivo* por los amiloides bacterianos. También, se podría explorar la posibilidad de inducir la exposición continua a estos amiloides bacterianos mediante la introducción de bacterias que expresan estos amiloides en el sistema digestivo de animales transgénicos de EA. Este último enfoque se ha realizado con existo usando *Escherichia*

coli que expresa fibras de curli y fueron capaces de inducir agregación de α-sinucleína y déficits motores en ratones (Chen et al., 2016; Sampson et al., 2020). Otros mecanismos como son el control de la función y maduración de las células gliales por bacterias (Erny et al., 2015), el posible rol del Aβ como péptido antimicrobiano (Moir et al., 2018), así como la posible inducción del inflamasoma NLRP3 que a su vez podría provocar el *cross-seeding* del Aβ (Venegas and Heneka, 2017), deberían de ser explorados como mecanismos alternativos al mecanismos de *cross-seeding* directo entre los amiloides bacterianos y el Aβ. Por otro lado, también se analizó la **respuesta inflamatoria** en el cerebro de los animales inyectados con los amiloides bacterianos mediante el uso de un análisis Multiplex de diversas citoquinas. En concreto, se observaron pequeños cambios en los niveles de citoquinas pro-inflamatorias y anti-inflamatorias, observándose un perfil mixto con respuestas tanto proinflamatorias (niveles altos de TNF-α) como anti-inflamatorias (niveles altos de IL-9 y niveles bajos de IL-17) en los animales inyectados con CsgA. Una respuesta similar se observó en animales inyectados con fibras de TasA con respuestas tanto proinflamatorias (niveles altos de CCL3 and con tendencia al aumento de TNF-α e IFN-γ) como antiinflamatorias (niveles bajos de IL-1α, CXCL1 y IL-17). Por su parte, los animales inyectados con las fibras de microcina no mostraron cambios en los niveles de citoquinas analizados. Aunque algunas de estas respuestas inflamatorias podrían tener efectos biológicamente negativos, otras respuestas observadas en estos análisis parecen ser protectores. Por lo tanto, se debería de realizar un análisis más exhaustivo de esta respuesta en animales en los que se observe una deposición robusta de Aβ inducidos por los amiloides bacterianos. Esto ayudara a conectar estos amiloides funcionales bacterianos con respuestas patológicas específicas.

Puesto que una gran cantidad de datos de otros grupos demuestran la más que posible relación causal entre la flora intestinal y la patología de la EA (Friedland and Chapman, 2017; Rutsch et al., 2020), se piensa que la modulación de los organismos de nuestra flora intestinal mediante intervenciones como el cambio de dieta y la suplementación con probióticos, trasplantes fecales, restricción calórica o prácticas de higiene, así como manipulaciones genéticas de nuestra flora intestinal, podrían ser estrategias efectivas para prevenir o reducir el riesgo de desarrollar enfermedades neurodegenerativas (Bonfili et al., 2021; Pistollato et al., 2016). De hecho, estas prácticas están bajo investigación en la actualidad (Arora et al., 2020; Hazan, 2020; Kesika et al., 2021; Park et al., 2021; Sun et al., 2019)

6.5. CONCLUSIONES

1. Tantos las cepas sintéticas 2F y 3F, como los agregados de Aβ provenientes de extracto de cerebro de ratones Tg2576 adultos, demostraron la capacidad de propagarse *in vivo* induciendo patología Aβ con características morfológicas específicas, un tropismo único e induciendo distintos tipos de agregados. Además, estos tres tipos de agregados de Aβ indujeron una respuesta biológica distintiva en el cerebro de los animales inyectados como demuestra la existencia de respuestas gliales diferenciales.

2. Los depósitos de Aβ inducidos por los tres inóculos mostraron tener estructuras moleculares únicas cuando se analizaron por técnicas de alta resolución (ssNMR). El polimorfismo estructural de $A\beta_{40}$ más prevalente en el cerebro de animales inyectados con extractos de cerebro de ratones Tg2576 adulto mostró características estructurales similares a las fibras que se encuentran en los pacientes de EA típica. Dada la gran heterogeneidad de fibras de Aβ observada en la EA, estos resultados apoyan la idea de que la diversidad de morfologías de los agregades de Aβ podría explicar la existencia de distintos subtipos de EA. Por lo tanto, descifrar las conformaciones de Aβ que son patológicamente más relevantes permitirá el desarrollo de herramientas de diagnóstico y terapias personalizadas, para cada uno de los subtipos de la EA.

3. Los tres amiloides funcionales bacterianos, subunidad CsgA de curli de *E. coli*, microcina E492 de *K. pneumoniae* y TasA de *B. subtilis*, tienen la habilidad de inducir la agregación de Aβ *in vitro* mediante un mecanismo de *cross-seeding*. Los amiloides funcionales bacterianos indujeron la formación de cepa de $A\beta_{40}$ que podrían resultar en actividades biológicas y toxicidad diferente a las fibras formadas por nucleación homologa.

4. Las fibras de CsgA indujeron la agregación de Aβ *in vitro* mediante un mecanismo de *cross-seeding*, sin embargo, los otros amiloides bacterianos no demostraron esa misma actividad. De manera similar a lo observado en algunas enfermedades priónicas, los amiloides bacterianos indujeron patología de Aβ con una inducción incompleta. Estos resultados apoyan un nuevo mecanismo patogénico de la EA por el que la patología de Aβ podría ser inducida por bacterias comensales de la flora intestinal. Por lo tanto, la modulación del microbioma podría ser una estrategia efectiva para la EA.

7. References

Abramov, E., Dolev, I., Fogel, H., Ciccotosto, G.D., Ruff, E., and Slutsky, I. (2009). Amyloid-β as a positive endogenous regulator of release probability at hippocampal synapses. Nat. Neurosci. 12, 1567–1576.

Abu-Rumeileh, S., Capellari, S., and Parchi, P. (2018). Rapidly Progressive Alzheimer's Disease: Contributions to Clinical-Pathological Definition and Diagnosis. J. Alzheimer's Dis. 63, 887–897.

Allen, N., Robinson, a. C., Snowden, J., Davidson, Y.S., and Mann, D.M. a (2014). Patterns of cerebral amyloid angiopathy define histopathological phenotypes in Alzheimer's disease. Neuropathol. Appl. Neurobiol. 40, 136–148.

Alonso, R., Pisa, D., Rábano, A., Rodal, I., and Carrasco, L. (2015). Cerebrospinal fluid from Alzheimer's disease patients contains fungal proteins and DNA. J. Alzheimer's Dis. 47, 873–876.

Álvarez-Mena, A., Cámara-Almirón, J., de Vicente, A., and Romero, D. (2020). Multifunctional amyloids in the biology of gram-positive bacteria. Microorganisms 8, 1–20.

Ando, K., De Decker, R., Vergara, C., Yilmaz, Z., Mansour, S., Suain, V., Sleegers, K., de Fisenne, M.-A., Houben, S., Potier, M.-C., et al. (2020). Picalm reduction exacerbates tau pathology in a murine tauopathy model. Acta Neuropathol. 2020 1394 139, 773–789.

Andrews, S.J., Fulton-Howard, B., and Goate, A. (2020). Interpretation of risk loci from genome-wide association studies of Alzheimer's disease. Lancet Neurol. 19, 326–335.

Arora, K., Green, M., and Prakash, S. (2020). The Microbiome and Alzheimer's Disease: Potential and Limitations of Prebiotic, Synbiotic, and Probiotic Formulations. Front. Bioeng. Biotechnol. 8.

Arpaia, N., and Rudensky, A.Y. (2014). Microbial metabolites control gut inflammatory responses. Proc. Natl. Acad. Sci. U. S. A. 111, 2058–2059.

Arranz, R., Mercado, G., Martín-Benito, J., Giraldo, R., Monasterio, O., Lagos, R., and Valpuesta, J.M. (2012). Structural characterization of microcin E492 amyloid formation: Identification of the precursors. J. Struct. Biol. 178, 54–60.

Aschenbrenner, A.J., Gordon, B.A., Benzinger, T.L.S., Morris, J.C., and Hassenstab, J.J. (2018). Influence of tau PET, amyloid PET, and hippocampal volume on cognition in Alzheimer disease. Neurology 91, e859–e866.

Ashton, N.J., Leuzy, A., Karikari, T.K., Dodich, A., Boccardi, M., Barthel, H., Bischof, G.N., Carrillo, M.C., Chiotis, K., Corre, J., et al. (2020). Alzheimer's disease biomarker roadmap 2020: Fluid biomarkers. Alzheimer's Dement. 16, e039557.

Ashton, N.J., Pascoal, T.A., Karikari, T.K., Benedet, A.L., Lantero-Rodriguez, J., Brinkmalm, G., Snellman, A., Schöll, M., Troakes, C., Hye, A., et al. (2021). Plasma p-tau231: a new biomarker for incipient Alzheimer's disease pathology. Acta Neuropathol. 141, 709–724.

Åslund, A., Sigurdson, C.J., Klingstedt, T., Grathwohl, S., Bolmont, T., Dickstein, D.L., Glimsdal, E., Prokop, S., Lindgren, M., Konradsson, P., et al. (2009). Novel Pentameric Thiophene Derivatives for in Vitro and in Vivo Optical Imaging of a Plethora of Protein Aggregates in Cerebral Amyloidoses. ACS Chem. Biol. 4, 673–684.

Atarashi, K., Suda, W., Luo, C., Kawaguchi, T., Motoo, I., Narushima, S., Kiguchi, Y., Yasuma, K., Watanabe, E., Tanoue, T., et al. (2017). Ectopic colonization of oral bacteria in the intestine drives TH1 cell induction and inflammation. Science (80-.). 358, 359–365.

References

Atkins, J.L., Masoli, J.A.H., Delgado, J., Pilling, L.C., Kuo, C.L., Kuchel, G.A., and Melzer, D. (2020). Preexisting Comorbidities Predicting COVID-19 and Mortality in the UK Biobank Community Cohort. Journals Gerontol. - Ser. A Biol. Sci. Med. Sci. 75, 2224–2230.

Ayodele, T., Rogaeva, E., Kurup, J.T., Beecham, G., and Reitz, C. (2021). Early-Onset Alzheimer's Disease: What Is Missing in Research? Curr. Neurol. Neurosci. Rep. 21, 1–10.

Baik, S.H., Kang, S., Lee, W., Choi, H., Chung, S., Kim, J. Il, and Mook-Jung, I. (2019). A Breakdown in Metabolic Reprogramming Causes Microglia Dysfunction in Alzheimer's Disease. Cell Metab. 30, 493-507.e6.

Baker, H.F., Ridley, R.M., Duchen, L.W., Crow, T.J., and Bruton, C.J. (1993). Evidence for the experimental transmission of cerebral beta-amyloidosis to primates. Int. J. Exp. Pathol. 74, 441–454.

Baker, J.L., Hendrickson, E.L., Tang, X., Lux, R., He, X., Edlund, A., McLean, J.S., and Shi, W. (2019). Klebsiella and Providencia emerge as lone survivors following long-term starvation of oral microbiota. Proc. Natl. Acad. Sci. U. S. A. 116, 8499–8504.

Balin, B.J., Gérard, H.C., Arking, E.J., Appelt, D.M., Branigan, P.J., Abrams, J.T., Whittum-Hudson, J.A., and Hudson, A.P. (1998). Identification and localization of Chlamydia pneumoniae in the Alzheimer's brain. Med. Microbiol. Immunol. 187, 23–42.

Balin, B.J., Little, C.S., Hammond, C.J., Appelt, D.M., Whittum-Hudson, J.A., Gérard, H.C., and Hudson, A.P. (2008). Chlamydophila pneumoniae and the etiology of late-onset Alzheimer's disease. J. Alzheimers. Dis. 13, 371–380.

Ballard, C., Gauthier, S., Corbett, A., Brayne, C., Aarsland, D., and Jones, E. (2011). Alzheimer's disease. Lancet 377, 1019–1031.

Banerjee, G., Adams, M.E., Jaunmuktane, Z., Alistair Lammie, G., Turner, B., Wani, M., Sawhney, I.M.S., Houlden, H., Mead, S., Brandner, S., et al. (2019). Early onset cerebral amyloid angiopathy following childhood exposure to cadaveric dura. Ann. Neurol. 85, 284–290.

Barnhart, M.M., and Chapman, M.R. (2006). Curli Biogenesis and Function. Annu. Rev. Microbiol. 60, 131–147.

Barthélemy, N.R., Horie, K., Sato, C., and Bateman, R.J. (2020). Blood plasma phosphorylated-tau isoforms track CNS change in Alzheimer's disease. J. Exp. Med. 217, 1–12.

Bartz, J.C., Bessen, R.A., McKenzie, D., Marsh, R.F., and Aiken, J.M. (2000). Adaptation and Selection of Prion Protein Strain Conformations following Interspecies Transmission of Transmissible Mink Encephalopathy. J. Virol. 74, 5542–5547.

Bateman, R.J., Aisen, P.S., De Strooper, B., Fox, N.C., Lemere, C.A., Ringman, J.M., Salloway, S., Sperling, R.A., Windisch, M., and Xiong, C. (2011). Autosomal-dominant Alzheimer's disease: a review and proposal for the prevention of Alzheimer's disease. Alzheimers. Res. Ther. 3, 1.

Bennett, A.E., Rienstra, C.M., Auger, M., Lakshmi, K. V., and Griffin, R.G. (1995). Heteronuclear decoupling in rotating solids. J. Chem. Phys. 103, 6951–6958.

Bertini, I., Gonnelli, L., Luchinat, C., Mao, J., and Nesi, A. (2011). A new structural model of Aβ 40 fibrils. J. Am. Chem. Soc. 133, 16013–16022.

Bessen, R.A., and Marsh, R.F. (1992). Identification of two biologically distinct strains of transmissible mink encephalopathy in hamsters. J. Gen. Virol. 73, 329–334.

Bhattacharyya, R., Black, S.E., Lotlikar, M.S., Fenn, R.H., Jorfi, M., Kovacs, D.M., and Tanzi, R.E. (2021). Axonal generation of amyloid-β from palmitoylated APP in mitochondria-associated endoplasmic reticulum membranes. Cell Rep. 35, 109134.

Bieler, S., Estrada, L., Lagos, R., Baeza, M., Castilla, J., and Soto, C. (2005). Amyloid formation modulates the biological activity of a bacterial protein. J. Biol. Chem. 280, 26880–26885.

Biessels, G.J., and Kappelle, L.J. (2005). Increased risk of Alzheimer's disease in Type II diabetes: insulin resistance of the brain or insulin-induced amyloid pathology? Biochem. Soc. Trans. 33, 1041–1044.

Billings, L.M., Oddo, S., Green, K.N., McGaugh, J.L., and LaFerla, F.M. (2005). Intraneuronal Aβ causes the onset of early Alzheimer's disease-related cognitive deficits in transgenic mice. Neuron 45, 675–688.

Boccardi, M., Bocchetta, M., Apostolova, L.G., Barnes, J., Bartzokis, G., Corbetta, G., Decarli, C., Detoledo-Morrell, L., Firbank, M., Ganzola, R., et al. (2015). Delphi definition of the EADC-ADNI harmonized protocol for hippocampal segmentation on magnetic resonance. Alzheimer's Dement. 11, 126–138.

Boche, D., and Gordon, M.N. (2021). Diversity of transcriptomic microglial phenotypes in aging and Alzheimer's disease. Alzheimer's Dement.

Bode, D.C., Baker, M.D., and Viles, J.H. (2017). Ion channel formation by amyloid-β42 oligomers but not amyloid-β40 in cellular membranes. J. Biol. Chem. 292, 144–1413.

Bonfili, L., Cecarini, V., Gogoi, O., Gong, C., Cuccioloni, M., Angeletti, M., Rossi, G., and Eleuteri, A.M. (2021). Microbiota modulation as preventative and therapeutic approach in Alzheimer's disease. FEBS J. 288, 2836–2855.

Boukhvalova, M.S., Mortensen, E., Mbaye, A., Lopez, D., Kastrukoff, L., and Blanco, J.C.G. (2019). Herpes Simplex Virus 1 Induces Brain Inflammation and Multifocal Demyelination in the Cotton Rat Sigmodon hispidus. J. Virol. 94.

Bourgade, K., Garneau, H., Giroux, G., Le Page, A.Y., Bocti, C., Dupuis, G., Frost, E.H., and Fülöp, T. (2015). β-Amyloid peptides display protective activity against the human Alzheimer's disease-associated herpes simplex virus-1. Biogerontology 16, 85–98.

Bourgade, K., Le Page, A., Bocti, C., Witkowski, J.M., Dupuis, G., Frost, E.H., and Fülöp, T. (2016). Protective Effect of Amyloid-β Peptides Against Herpes Simplex Virus-1 Infection in a Neuronal Cell Culture Model. J. Alzheimer's Dis. 50, 1227–1241.

Braak, H., and Braak, E. (1991). Neuropathological stageing of Alzheimer-related changes. Acta Neuropathol. 82, 239–259.

Braak, H., Zetterberg, H., Del Tredici, K., and Blennow, K. (2013). Intraneuronal tau aggregation precedes diffuse plaque deposition, but amyloid-β changes occur before increases of tau in cerebrospinal fluid. Acta Neuropathol. 126, 631–641.

Branda, S.S., Chu, F., Kearns, D.B., Losick, R., and Kolter, R. (2006). A major protein component of the Bacillus subtilis biofilm matrix. Mol. Microbiol. 59, 1229–1238.

References

Breydo, L., and Uversky, V.N. (2015). Structural, morphological, and functional diversity of amyloid oligomers. FEBS Lett. 589, 2640–2648.

Brkic, M., Balusu, S., Van Wonterghem, E., Gorlé, N., Benilova, I., Kremer, A., Van Hove, I., Moons, L., De Strooper, B., Kanazir, S., et al. (2015). Amyloid β oligomers disrupt blood–CSF barrier integrity by activating matrix metalloproteinases. J. Neurosci. 35, 12766–12778.

Brown, A., and Török, M. (2021). Functional amyloids in the human body. Bioorganic Med. Chem. Lett. 40, 127914.

Brown, P., Cervenáková, L., and Diringer, H. (2001). Blood infectivity and the prospects for a diagnostic screening test in Creutzfeldt-Jakob disease. J. Lab. Clin. Med. 137, 5–13.

Bulgart, H.R., Neczypor, E.W., Wold, L.E., and Mackos, A.R. (2020). Microbial involvement in Alzheimer disease development and progression. Mol. Neurodegener. 2020 151 15, 1–12.

Burwinkel, M., Lutzenberger, M., Heppner, F.L., Schulz-Schaeffer, W., and Baier, M. (2018). Intravenous injection of beta-amyloid seeds promotes cerebral amyloid angiopathy (CAA). Acta Neuropathol. Commun. 6, 23.

Bussière, T., Bard, F., Barbour, R., Grajeda, H., Guido, T., Khan, K., Schenk, D., Games, D., Seubert, P., and Buttini, M. (2004). Morphological characterization of Thioflavin-S-positive amyloid plaques in transgenic Alzheimer mice and effect of passive Aβ immunotherapy on their clearance. Am. J. Pathol. 165, 987–995.

Butovsky, O., and Weiner, H.L. (2018). Microglial signatures and their role in health and disease. Nat. Rev. Neurosci. 19, 622–635.

Butterfield, D.A., and Halliwell, B. (2019). Oxidative stress, dysfunctional glucose metabolism and Alzheimer disease. Nat. Rev. Neurosci. 20, 148–160.

Calderon-Garcidueñas, A.L., and Duyckaerts, C. (2018). Alzheimer disease. In Handbook of Clinical Neurology, (Elsevier), pp. 325–337.

Cali, I., Castellani, R., Yuan, J., Al-Shekhlee, A., Cohen, M.L., Xiao, X., Moleres, F.J., Parchi, P., Zou, W.Q., and Gambetti, P. (2006). Classification of sporadic Creutzfeldt-Jakob disease revisited. Brain 129, 2266–2277.

Cali, I., Cohen, M.L., Haik, S., Parchi, P., Giaccone, G., Collins, S.J., Kofskey, D., Wang, H., McLean, C.A., Brandel, J.P., et al. (2018). Iatrogenic Creutzfeldt-Jakob disease with Amyloid-β pathology: an international study. Acta Neuropathol. Commun. 6, 5.

Cámara-Almirón, J., Navarro, Y., Díaz-Martínez, L., Magno-Pérez-Bryan, M.C., Molina-Santiago, C., Pearson, J.R., de Vicente, A., Pérez-García, A., and Romero, D. (2020). Dual functionality of the amyloid protein TasA in Bacillus physiology and fitness on the phylloplane. Nat. Commun. 11, 1–21.

Caro-Astorga, J., Perez-Garcia, A., de Vicente, A., and Romero, D. (2015). A genomic region involved in the formation of adhesin fibers in Bacillus cereus biofilms. Front. Microbiol. 5, 745.

Carter, C.J. (2017). Genetic, Transcriptome, Proteomic, and Epidemiological Evidence for Blood-Brain Barrier Disruption and Polymicrobial Brain Invasion as Determinant Factors in Alzheimer's Disease. J. Alzheimer's Dis. Reports 1, 125–157.

Casali, B.T., MacPherson, K.P., Reed-Geaghan, E.G., and Landreth, G.E. (2020). Microglia depletion rapidly and reversibly alters amyloid pathology by modification of plaque compaction and morphologies. Neurobiol. Dis. 142, 104956.

Cassel, J.C., Duconseille, E., Jeltsch, H., and Will, B. (1997). The fimbria-fornix/cingular bundle pathways: A review of neurochemical and behavioural approaches using lesions and transplantation techniques. Prog. Neurobiol. 51, 663–716.

Castellani, R.J., Rolston, R.K., and Smith, M. a (2010). Alzheimer Disease. Dis. a Mon. 56, 1–60.

Cattaneo, A., Cattane, N., Galluzzi, S., Provasi, S., Lopizzo, N., Festari, C., Ferrari, C., Guerra, U.P., Paghera, B., Muscio, C., et al. (2017). Association of brain amyloidosis with pro-inflammatory gut bacterial taxa and peripheral inflammation markers in cognitively impaired elderly. Neurobiol. Aging 49, 60–68.

Cendrowska, U., Silva, P.J., Ait-Bouziad, N., Müller, M., Guven, Z.P., Vieweg, S., Chiki, A., Radamaker, L., Kumar, S.T., Fändrich, M., et al. (2020). Unraveling the complexity of amyloid polymorphism using gold nanoparticles and cryo-EM. Proc. Natl. Acad. Sci. U. S. A. 117, 6866–6874.

Chapman, M.R., Robinson, L.S., Pinkner, J.S., Roth, R., Heuser, J., Hammar, M., Normark, S., and Hultgren, S.J. (2002). Role of Escherichia coli Curli Operons in Directing Amyloid Fiber Formation. Science (80-.). 295, 851–855.

Chatila, Z.K., and Bradshaw, E.M. (2021). Alzheimer's Disease Genetics: A Dampened Microglial Response? Neuroscientist.

Chen, F., Swartzlander, D.B., Ghosh, A., Fryer, J.D., Wang, B., and Zheng, H. (2021). Clusterin secreted from astrocyte promotes excitatory synaptic transmission and ameliorates Alzheimer's disease neuropathology. Mol. Neurodegener. 2021 161 16, 1–16.

Chen, S.G., Stribinskis, V., Rane, M.J., Demuth, D.R., Gozal, E., Roberts, A.M., Jagadapillai, R., Liu, R., Choe, K., Shivakumar, B., et al. (2016). Exposure to the Functional Bacterial Amyloid Protein Curli Enhances Alpha-Synuclein Aggregation in Aged Fischer 344 Rats and Caenorhabditis elegans. Sci. Rep. 6, 1–10.

Cheng, H.-W., Jiang, S., and Hu, J. (2019). Gut-Brain Axis: Probiotic, Bacillus subtilis, Prevents Aggression via the Modification of the Central Serotonergic System. In Oral Health by Using Probiotic Products, (IntechOpen), p.

Cherny, I., Rockah, L., Levy-Nissenbaum, O., Gophna, U., Ron, E.Z., and Gazit, E. (2005). The Formation of Escherichia coli Curli Amyloid Fibrils is Mediated by Prion-like Peptide Repeats. J. Mol. Biol. 352, 245–252.

Chételat, G., Arbizu, J., Barthel, H., Garibotto, V., Law, I., Morbelli, S., van de Giessen, E., Agosta, F., Barkhof, F., Brooks, D.J., et al. (2020). Amyloid-PET and 18F-FDG-PET in the diagnostic investigation of Alzheimer's disease and other dementias. Lancet Neurol. 19, 951–962.

De Chiara, G., Piacentini, R., Fabiani, M., Mastrodonato, A., Marcocci, M.E., Limongi, D., Napoletani, G., Protto, V., Coluccio, P., Celestino, I., et al. (2019). Recurrent herpes simplex virus-1 infection induces hallmarks of neurodegeneration and cognitive deficits in mice. PLoS Pathog. 15.

References

Clayton, K., Delpech, J.C., Herron, S., Iwahara, N., Ericsson, M., Saito, T., Saido, T.C., Ikezu, S., and Ikezu, T. (2021). Plaque associated microglia hyper-secrete extracellular vesicles and accelerate tau propagation in a humanized APP mouse model. Mol. Neurodegener. 16, 1–16.

Clinton, L.K., Blurton-Jones, M., Myczek, K., Trojanowski, J.Q., and LaFerla, F.M. (2010). Synergistic interactions between Aβ, tau, and α-synuclein: Acceleration of neuropathology and cognitive decline. J. Neurosci. 30, 7281–7289.

Cloe, A.L., Orgel, J.P.R.O., Sachleben, J.R., Tycko, R., and Meredith, S.C. (2011). The Japanese Mutant Aβ (ΔE22-Aβ1−39) Forms Fibrils Instantaneously, with Low-Thioflavin T Fluorescence: Seeding of Wild-Type Aβ1−40 into Atypical Fibrils by ΔE22-Aβ1−39. Biochemistry 50, 2026–2039.

Cohen, M., Appleby, B., and Safar, J.G. (2016). Distinct prion-like strains of amyloid beta implicated in phenotypic diversity of Alzheimer's disease. Prion 10, 9–17.

Cohen, M.L., Kim, C., Haldiman, T., ElHag, M., Mehndiratta, P., Pichet, T., Lissemore, F., Shea, M., Cohen, Y., Chen, W., et al. (2015). Rapidly progressive Alzheimer's disease features distinct structures of amyloid-β. Brain 138, 1009–1022.

Colby, D.W., Giles, K., Legname, G., Wille, H., Baskakov, I. V., DeArmond, S.J., and Prusiner, S.B. (2009). Design and construction of diverse mammalian prion strains. Proc. Natl. Acad. Sci. U. S. A. 106, 20417–20422.

Colom, J., Freitas, D., Simon, A., Brodkorb, A., Buckley, M., Deaton, J., and Winger, A.M. (2021). Presence and Germination of the Probiotic Bacillus subtilis DE111® in the Human Small Intestinal Tract: A Randomized, Crossover, Double-Blind, and Placebo-Controlled Study. Front. Microbiol. 12, 2189.

Colvin, M.T., Silvers, R., Ni, Q.Z., Can, T. V., Sergeyev, I., Rosay, M., Donovan, K.J., Michael, B., Wall, J., Linse, S., et al. (2016). Atomic Resolution Structure of Monomorphic Aβ42 Amyloid Fibrils. J. Am. Chem. Soc. 138, 9663–9674.

Condello, C., and Stöehr, J. (2018). Aβ propagation and strains: Implications for the phenotypic diversity in Alzheimer's disease. Neurobiol. Dis. 109, 191–200.

Condello, C., Yuan, P., Schain, A., and Grutzendler, J. (2015). Microglia constitute a barrier that prevents neurotoxic protofibrillar Aβ42 hotspots around plaques. Nat. Commun. 6, 6176.

Condello, C., Lemmin, T., Stöhr, J., Nick, M., Wu, Y., Maxwell, A.M., Watts, J.C., Caro, C.D., Oehler, A., Keene, C.D., et al. (2018). Structural heterogeneity and intersubject variability of Aβ in familial and sporadic Alzheimer's disease. Proc. Natl. Acad. Sci. 115, E782–E791.

Conlan, S., Kong, H.H., and Segre, J.A. (2012). Species-Level Analysis of DNA Sequence Data from the NIH Human Microbiome Project. PLoS One 7, e47075.

Crews, L., and Masliah, E. (2010). Molecular mechanisms of neurodegeneration in Alzheimer's disease. Hum. Mol. Genet. 19, R12–R20.

Cryan, J.F., and Dinan, T.G. (2012). Mind-altering microorganisms: The impact of the gut microbiota on brain and behaviour. Nat. Rev. Neurosci. 13, 701–712.

Cryan, J.F., O'Riordan, K.J., Sandhu, K., Peterson, V., and Dinan, T.G. (2020). The gut microbiome in neurological disorders. Lancet Neurol. 19, 179–194.

Cummings, J., Lee, G., Zhong, K., Fonseca, J., and Taghva, K. (2021). Alzheimer's disease drug development pipeline: 2021. Alzheimer's Dement. Transl. Res. Clin. Interv. 7, e12179.

Daskalov, A., Martinez, D., Coustou, V., Mammeri, N. El, Mélanie Berbon, Andreas, L.B., Bardiaux, B., Stanek, J., Noubhani, A., Kauffmann, B., et al. (2020). Structural and molecular basis of cross-seeding barriers in amyloids. Proc. Natl. Acad. Sci. U. S. A. 118.

Debatin, L., Streffer, J., Geissen, M., Matschke, J., Aguzzi, A., and Glatzel, M. (2008). Association between deposition of beta-amyloid and pathological prion protein in sporadic Creutzfeldt-Jakob disease. Neurodegener. Dis. 5, 347–354.

Deczkowska, A., Keren-Shaul, H., Weiner, A., Colonna, M., Schwartz, M., and Amit, I. (2018). Disease-Associated Microglia: A Universal Immune Sensor of Neurodegeneration. Cell 173, 1073–1081.

Delaglio, F., Grzesiek, S., Vuister, G.W., Zhu, G., Pfeifer, J., and Bax, A. (1995). NMRPipe: A multidimensional spectral processing system based on UNIX pipes. J. Biomol. NMR 6, 277–293.

Desai, M.S., Seekatz, A.M., Koropatkin, N.M., Kamada, N., Hickey, C.A., Wolter, M., Pudlo, N.A., Kitamoto, S., Terrapon, N., Muller, A., et al. (2016). A Dietary Fiber-Deprived Gut Microbiota Degrades the Colonic Mucus Barrier and Enhances Pathogen Susceptibility. Cell 167, 1339-1353.e21.

Destoumieux-Garzón, D., Thomas, X., Santamaria, M., Goulard, C., Barthélémy, M., Boscher, B., Bessin, Y., Molle, G., Pons, A.M., Letellier, L., et al. (2003). Microcin E492 antibacterial activity: Evidence for a TonB-dependent inner membrane permeabilization on Escherichia coli. Mol. Microbiol. 49, 1031–1041.

Deture, M.A., and Dickson, D.W. (2019). The neuropathological diagnosis of Alzheimer's disease. Mol. Neurodegener. 14, 1–18.

Diaz-Espinoza, R., Morales, R., Concha-Marambio, L., Moreno-Gonzalez, I., Moda, F., and Soto, C. (2018). Treatment with a non-toxic, self-replicating anti-prion delays or prevents prion disease in vivo. Mol. Psychiatry 23, 777–788.

Diehl, A., Roske, Y., Ball, L., Chowdhury, A., Hiller, M., Molière, N., Kramer, R., Stöppler, D., Worth, C.L., Schlegel, B., et al. (2018). Structural changes of TasA in biofilm formation of Bacillus subtilis. Proc. Natl. Acad. Sci. U. S. A. 115, 3237–3242.

Dominy, S.S., Lynch, C., Ermini, F., Benedyk, M., Marczyk, A., Konradi, A., Nguyen, M., Haditsch, U., Raha, D., Griffin, C., et al. (2019). Porphyromonas gingivalis in Alzheimer's disease brains: Evidence for disease causation and treatment with small-molecule inhibitors. Sci. Adv. 5.

Dueholm, M.S., Nielsen, S.B., Hein, K.L., Nissen, P., Chapman, M., Christiansen, G., Nielsen, P.H., and Otzen, D.E. (2011). Fibrillation of the major curli subunit CsgA under a wide range of conditions implies a robust design of aggregation. Biochemistry 50, 8281–8290.

Duran-Aniotz, C., Morales, R., Moreno-Gonzalez, I., Hu, P.P., Fedynyshyn, J., and Soto, C. (2014). Aggregate-depleted brain fails to induce Aβ deposition in a mouse model of Alzheimer's disease. PLoS One 9.

Duran-Aniotz, C., Moreno-Gonzalez, I., Gamez, N., Perez-Urrutia, N., Vegas-Gomez, L., Soto, C., and Morales, R. (2021). Amyloid pathology arrangements in Alzheimer's disease brains modulate in vivo seeding capability. Acta Neuropathol. Commun. 9, 1–13.

Duyckaerts, C., Delatour, B., and Potier, M.C. (2009). Classification and basic pathology of Alzheimer disease. Acta Neuropathol. 118, 5–36.

Dyrks, T., Weidemann, A., Multhaup, G., Salbaum, J.M., Lemaire, H.G., Kang, J., Müller-Hill, B., Masters, C.L., and Beyreuther, K. (1988). Identification, transmembrane orientation and biogenesis of the amyloid A4 precursor of Alzheimer's disease. EMBO J. 7, 949–957.

Edwards III, G.A., Gamez, N., Escobedo Jr., G., Calderon, O., and Moreno-Gonzalez, I. (2019). Modifiable Risk Factors for Alzheimer's Disease. Front. Aging Neurosci. 0, 146.

Efthymiou, A.G., and Goate, A.M. (2017). Late onset Alzheimer's disease genetics implicates microglial pathways in disease risk. Mol. Neurodegener. 12, 1–12.

Eisele, Y.S., Bolmont, T., Heikenwalder, M., Langer, F., Jacobson, L.H., Yan, Z.X., Roth, K., Aguzzi, A., Staufenbiel, M., Walker, L.C., et al. (2009). Induction of cerebral β-amyloidosis: Intracerebral versus systemic Aβ inoculation. Proc. Natl. Acad. Sci. U. S. A. 106, 12926–12931.

Eisele, Y.S., Obermuller, U., Heilbronner, G., Baumann, F., Kaeser, S.A., Wolburg, H., Walker, L.C., Staufenbiel, M., Heikenwalder, M., and Jucker, M. (2010). Peripherally Applied Aβ-Containing Inoculates Induce Cerebral β-Amyloidosis. Science (80-.). 330, 980–982.

Erny, D., De Angelis, A.L.H., Jaitin, D., Wieghofer, P., Staszewski, O., David, E., Keren-Shaul, H., Mahlakoiv, T., Jakobshagen, K., Buch, T., et al. (2015). Host microbiota constantly control maturation and function of microglia in the CNS. Nat. Neurosci. 18, 965–977.

Escartin, C., Galea, E., Lakatos, A., O'Callaghan, J.P., Petzold, G.C., Serrano-Pozo, A., Steinhäuser, C., Volterra, A., Carmignoto, G., Agarwal, A., et al. (2021). Reactive astrocyte nomenclature, definitions, and future directions. Nat. Neurosci. 24, 312–325.

Esparza, T.J., Wildburger, N.C., Jiang, H., Gangolli, M., Cairns, N.J., Bateman, R.J., and Brody, D.L. (2016). Soluble amyloid-beta aggregates from human Alzheimer's disease brains. Sci. Rep. 6, 1–16.

Evans, M.L., Chorell, E., Taylor, J.D., Åden, J., Götheson, A., Li, F., Koch, M., Sefer, L., Matthews, S.J., Wittung-Stafshede, P., et al. (2015). The Bacterial Curli System Possesses a Potent and Selective Inhibitor of Amyloid Formation. Mol. Cell 57, 445–455.

Evin, G., and Weidemann, A. (2002). Biogenesis and metabolism of Alzheimer's disease Abeta amyloid peptides. Peptides 23, 1285–1297.

Fakhoury, M. (2018). Microglia and astrocytes in Alzheimer's disease: implications for therapy. Curr. Neuropharmacol. 16.

Falcon, B., Zhang, W., Murzin, A.G., Murshudov, G., Garringer, H.J., Vidal, R., Crowther, R.A., Ghetti, B., Scheres, S.H.W., and Goedert, M. (2018). Structures of filaments from Pick's disease reveal a novel tau protein fold. Nature 561, 137–140.

Di Fede, G., Catania, M., Maderna, E., Ghidoni, R., Benussi, L., Tonoli, E., Giaccone, G., Moda, F., Paterlini, A., Campagnani, I., et al. (2018). Molecular subtypes of Alzheimer's disease. Sci. Rep. 8.

Ferreira, D., Verhagen, C., Hernández-Cabrera, J.A., Cavallin, L., Guo, C.J., Ekman, U., Muehlboeck, J.S., Simmons, A., Barroso, J., Wahlund, L.O., et al. (2017). Distinct subtypes of

Alzheimer's disease based on patterns of brain atrophy: Longitudinal trajectories and clinical applications. Sci. Rep. 7, 1–13.

Ferreira, D., Nordberg, A., and Westman, E. (2020). Biological subtypes of Alzheimer disease: A systematic review and meta-analysis. Neurology 94, 436–448.

Ferrer, I., Blanco, R., Carmona, M., Puig, B., Ribera, R., Rey, M.J., and Ribalta, T. (2001). Prion protein expression in senile plaques in Alzheimer's disease. Acta Neuropathol. 101, 49–56.

Fillit, H., and Green, A. (2021). Aducanumab and the FDA — where are we now? Nat. Rev. Neurol. 17, 129–130.

Fitzpatrick, A.W.P., Falcon, B., He, S., Murzin, A.G., Murshudov, G., Garringer, H.J., Crowther, R.A., Ghetti, B., Goedert, M., and Scheres, S.H.W. (2017). Cryo-EM structures of tau filaments from Alzheimer's disease. Nature 547, 185–190.

Fleeman, R.M., and Proctor, E.A. (2021). Astrocytic Propagation of Tau in the Context of Alzheimer's Disease. Front. Cell. Neurosci. 15, 63.

Fowler, D.M., Koulov, A. V., Alory-Jost, C., Marks, M.S., Balch, W.E., and Kelly, J.W. (2006). Functional amyloid formation within mammalian tissue. PLoS Biol. 4, 0100–0107.

Fraser, H., and Dickinson, A.G. (1968). The sequential development of the brain lesions of scrapie in three strains of mice. J. Comp. Pathol. 78.

Friedland, R.P. (2015). Mechanisms of Molecular Mimicry Involving the Microbiota in Neurodegeneration. J. Alzheimer's Dis. 45, 349–362.

Friedland, R.P., and Chapman, M.R. (2017). The role of microbial amyloid in neurodegeneration. PLoS Pathog. 13, e1006654.

Friker, L.L., Scheiblich, H., Hochheiser, I. V, Brinkschulte, R., Riedel, D., Latz, E., Geyer, M., and Heneka, M.T. (2020). β-Amyloid Clustering around ASC Fibrils Boosts Its Toxicity in Microglia. Cell Rep. 30, 3743-3754.e6.

Frontzek, K., Lutz, M.I., Aguzzi, A., Kovacs, G.G., and Budka, H. (2016). Amyloid-β pathology and cerebral amyloid angiopathy are frequent in iatrogenic Creutzfeldt-Jakob disease after dural grafting. Swiss Med. Wkly. 146, w14287.

Fulop, T., Witkowski, J.M., Bourgade, K., Khalil, A., Zerif, E., Larbi, A., Hirokawa, K., Pawelec, G., Bocti, C., Lacombe, G., et al. (2018). Can an Infection Hypothesis Explain the Beta Amyloid Hypothesis of Alzheimer's Disease? Front. Aging Neurosci. 10, 1–11.

Gérard, H.C., Dreses-Werringloer, U., Wildt, K.S., Deka, S., Oszust, C., Balin, B.J., Frey, W.H., Bordayo, E.Z., Whittum-Hudson, J.A., and Hudson, A.P. (2006). Chlamydophila (Chlamydia) pneumoniae in the Alzheimer's brain. FEMS Immunol. Med. Microbiol. 48, 355–366.

Van Gerven, N., Klein, R.D., Hultgren, S.J., and Remaut, H. (2015). Bacterial amyloid formation: structural insights into curli biogensis. Trends Microbiol. 23, 693–706.

Ghosh, U., Thurber, K.R., Yau, W.-M., and Tycko, R. (2021). Molecular structure of a prevalent amyloid-β fibril polymorph from Alzheimer's disease brain tissue. Proc. Natl. Acad. Sci. 118, e2023089118.

References

Giuffrida, M.L., Tomasello, M.F., Pandini, G., Caraci, F., Battaglia, G., Busceti, C., Di Pietro, P., Pappalardo, G., Attanasio, F., Chiechio, S., et al. (2015). Monomeric ß-amyloid interacts with type-1 insulin-like growth factor receptors to provide energy supply to neurons. Front. Cell. Neurosci. 9, 297.

Golde, T.E. (2016). Alzheimer disease: Host immune defence, amyloid-β peptide and Alzheimer disease. Nat. Rev. Neurol. 12, 433.

Gomez-Gutierrez, R., and Morales, R. (2020). The prion-like phenomenon in Alzheimer's disease: Evidence of pathology transmission in humans. PLoS Pathog. 16, e1009004.

Gotz, J., Chen, F., van Dorpe, J., and Nitsch, R.M. (2001). Formation of Neurofibrillary Tangles in P301L Tau Transgenic Mice Induced by Abeta 42 Fibrils. Science (80-.). 293, 1491–1495.

Gregori, L., McCombie, N., Palmer, D., Birch, P., Sowemimo-Coker, S.O., Giulivi, A., and Rohwer, R.G. (2004). Effectiveness of leucoreduction for removal of infectivity of transmissible spongiform encephalopathies from blood. Lancet 364, 529–531.

Gremer, L., Schölzel, D., Schenk, C., Reinartz, E., Labahn, J., Ravelli, R.B.G., Tusche, M., Lopez-Iglesias, C., Hoyer, W., Heise, H., et al. (2017). Fibril structure of amyloid-β (1–42) by cryo–electron microscopy. Science (80-.). 358, 116–119.

Griciuc, A., and Tanzi, R.E. (2021). The role of innate immune genes in Alzheimer's disease. Curr. Opin. Neurol. 34, 228–236.

Grochowska, K.M., Yuanxiang, P., Bär, J., Raman, R., Brugal, G., Sahu, G., Schweizer, M., Bikbaev, A., Schilling, S., Demuth, H., et al. (2017). Posttranslational modification impact on the mechanism by which amyloid-β induces synaptic dysfunction. EMBO Rep. 18, 962–981.

Guo, J.P., Arai, T., Miklossy, J., and McGeer, P.L. (2006). Aβ and tau form soluble complexes that may promote self aggregation of both into the insoluble forms in Alzheimer's diseases. Proc. Natl. Acad. Sci. U. S. A. 103, 1953–1958.

Gutierrez, A., and Vitorica, J. (2018). Toward a New Concept of Alzheimer's Disease Models: A Perspective from Neuroinflammation. J. Alzheimer's Dis. 64, S329–S338.

Haass, C., Kaether, C., Thinakaran, G., and Sisodia, S. (2012). Trafficking and proteolytic processing of APP. Cold Spring Harb. Perspect. Med. 2, a006270.

Habib, N., McCabe, C., Medina, S., Varshavsky, M., Kitsberg, D., Dvir-Szternfeld, R., Green, G., Dionne, D., Nguyen, L., Marshall, J.L., et al. (2020). Disease-associated astrocytes in Alzheimer's disease and aging. Nat. Neurosci. 23, 701–706.

Hamaguchi, T., Taniguchi, Y., Sakai, K., Kitamoto, T., Takao, M., Murayama, S., Iwasaki, Y., Yoshida, M., Shimizu, H., Kakita, A., et al. (2016). Significant association of cadaveric dura mater grafting with subpial Aβ deposition and meningeal amyloid angiopathy. Acta Neuropathol. 132, 313–315.

Hamaguchi, T., Kim, J.H., Hasegawa, A., Goto, R., Sakai, K., Ono, K., Itoh, Y., and Yamada, M. (2021). Exogenous Aβ seeds induce Aβ depositions in the blood vessels rather than the brain parenchyma, independently of Aβ strain-specific information. Acta Neuropathol. Commun. 9, 1–17.

Hamilton, R.L. (2000). Lewy bodies in Alzheimer's Disease: A neuropathological review of 145 cases using α-synuclein immunohistochemistry. Brain Pathol. 10, 378–384.

Hammer, N.D., Schmidt, J.C., and Chapman, M.R. (2007). The curli nucleator protein, CsgB, contains an amyloidogenic domain that directs CsgA polymerization. Proc. Natl. Acad. Sci. U. S. A. 104, 12494–12499.

Hammond, C.J., Hallock, L.R., Howanski, R.J., Appelt, D.M., Little, C.S., Balin, B.J., Duyckaerts, C., Delatour, B., Potier, M., Savva, G., et al. (2010). Immunohistological detection of Chlamydia pneumoniae in the Alzheimer's disease brain. BMC Neurosci. 11, 121.

Hampel, H., Cummings, J., Blennow, K., Gao, P., Jack, C.R., and Vergallo, A. (2021a). Developing the ATX(N) classification for use across the Alzheimer disease continuum. Nat. Rev. Neurol. 17, 580–589.

Hampel, H., Hardy, J., Blennow, K., Chen, C., Perry, G., Kim, S.H., Villemagne, V.L., Aisen, P., Vendruscolo, M., Iwatsubo, T., et al. (2021b). The Amyloid-β Pathway in Alzheimer's Disease. Mol. Psychiatry.

Hansen, D. V., Hanson, J.E., and Sheng, M. (2018). Microglia in Alzheimer's disease. J. Cell Biol. 217, 459–472.

Hansson, O. (2021). Biomarkers for neurodegenerative diseases. Nat. Med. 27, 954–963.

Hansson, O., Zetterberg, H., Buchhave, P., Londos, E., Blennow, K., and Minthon, L. (2006). Association between CSF biomarkers and incipient Alzheimer's disease in patients with mild cognitive impairment: a follow-up study. Lancet Neurol. 5, 228–234.

Harada, R., Okamura, N., Furumoto, S., Furukawa, K., Ishiki, A., Tomita, N., Tago, T., Hiraoka, K., Watanuki, S., Shidahara, M., et al. (2016). 18F-THK5351: A novel PET radiotracer for imaging neurofibrillary pathology in Alzheimer disease. J. Nucl. Med. 57, 208–214.

Harari, O., Cruchaga, C., Kauwe, J.S.K., Ainscough, B.J., Bales, K., Pickering, E.H., Bertelsen, S., Fagan, A.M., Holtzman, D.M., Morris, J.C., et al. (2014). Phosphorylated tau-Aβ42 ratio as a continuous trait for biomarker discovery for early-stage Alzheimer's disease in multiplex immunoassay panels of cerebrospinal fluid. Biol. Psychiatry 75, 723–731.

Hardy, J.A., and Higgins, G.A. (1992). Alzheimer's disease: the amyloid cascade hypothesis. Science 256, 184–185.

Harold, D., Abraham, R., Hollingworth, P., Sims, R., Gerrish, A., Hamshere, M.L., Pahwa, J.S., Moskvina, V., Dowzell, K., Williams, A., et al. (2009). Genome-wide association study identifies variants at CLU and PICALM associated with Alzheimer's disease. Nat. Genet. 41, 1088–1093.

Hartman, K., Brender, J.R., Monde, K., Ono, A., Evans, M.L., Popovych, N., Chapman, M.R., and Ramamoorthy, A. (2013). Bacterial curli protein promotes the conversion of PAP248-286 into the amyloid SEVI: cross-seeding of dissimilar amyloid sequences. PeerJ 2013, e5.

Hasan Mohajeri, M., La Fata, G., Steinert, R.E., and Weber, P. (2018). Relationship between the gut microbiome and brain function. Nutr. Rev. 76, 481–496.

Hatami, A., Albay, R., Monjazeb, S., Milton, S., and Glabe, C. (2014). Monoclonal antibodies against Aβ42 fibrils distinguish multiple aggregation state polymorphisms in vitro and in Alzheimer disease brain. J. Biol. Chem. 289, 32131–32143.

Hazan, S. (2020). Rapid improvement in Alzheimer's disease symptoms following fecal microbiota transplantation: a case report. J. Int. Med. Res. 48.

References

Heilbronner, G., Eisele, Y.S., Langer, F., Kaeser, S.A., Novotny, R., Nagarathinam, A., Åslund, A., Hammarström, P., Nilsson, K.P.R., and Jucker, M. (2013). Seeded strain-like transmission of β-amyloid morphotypes in APP transgenic mice. EMBO Rep. 14, 1017–1022.

Hemonnot, A.L., Hua, J., Ulmann, L., and Hirbec, H. (2019). Microglia in Alzheimer disease: Well-known targets and new opportunities. Front. Cell. Infect. Microbiol. 9, 233.

Heneka, M.T., Golenbock, D.T., and Latz, E. (2015). Innate immunity in Alzheimer's disease. Nat. Immunol. 16, 229–236.

Heppner, F.L., Ransohoff, R.M., and Becher, B. (2015). Immune attack: The role of inflammation in Alzheimer disease. Nat. Rev. Neurosci. 16, 358–372.

Hérard, A.S., Petit, F., Gary, C., Guillermier, M., Boluda, S., Garin, C.M., Letournel, F., Martin-Négrier, M.L., Faisant, M., Godfraind, C., et al. (2020). Induction of amyloid-β deposits from serially transmitted, histologically silent, Aβ seeds issued from human brains. Acta Neuropathol. Commun. 8, 1–10.

Herrup, K. (2015). The case for rejecting the amyloid cascade hypothesis. Nat. Neurosci. 18, 794–799.

Hervé, D., Porché, M., Cabrejo, L., Guidoux, C., Tournier-Lasserve, E., Nicolas, G., Adle-Biassette, H., Plu, I., Chabriat, H., and Duyckaerts, C. (2018). Fatal Aβ cerebral amyloid angiopathy 4 decades after a dural graft at the age of 2 years. Acta Neuropathol. 135, 801–803.

Hoban, A.E., Stilling, R.M., Ryan, F.J., Shanahan, F., Dinan, T.G., Claesson, M.J., Clarke, G., and Cryan, J.F. (2016). Regulation of prefrontal cortex myelination by the microbiota. Transl. Psychiatry 6.

Hodges, A.K., Piers, T.M., Collier, D., Cousins, O., and Pocock, J.M. (2021). Pathways linking Alzheimer's disease risk genes expressed highly in microglia. Neuroimmunol. Neuroinflammation 2020.

Hong, W., Wang, Z., Liu, W., O'Malley, T.T., Jin, M., Willem, M., Haass, C., Frosch, M.P., and Walsh, D.M. (2018). Diffusible, highly bioactive oligomers represent a critical minority of soluble Aβ in Alzheimer's disease brain. Acta Neuropathol. 136, 19–40.

Hooker, J.M. (2021). FDA Approval of Aducanumab Divided the Community but Also Connected and United It. ACS Chem. Neurosci. acschemneuro.1c00393.

Hsiao, K., Chapman, P., Nilsen, S., Eckman, C., Harigaya, Y., Younkin, S., Yang, F., and Cole, G. (1996). Correlative memory deficits, Abeta elevation, and amyloid plaques in transgenic mice. Science 274, 99–102.

Huang, Y., Happonen, K.E., Burrola, P.G., O'Connor, C., Hah, N., Huang, L., Nimmerjahn, A., and Lemke, G. (2021). Microglia use TAM receptors to detect and engulf amyloid β plaques. Nat. Immunol. 22, 586–594.

Iba, M., Guo, J.L., McBride, J.D., Zhang, B., Trojanowski, J.Q., and Lee, V.M.Y. (2013). Synthetic tau fibrils mediate transmission of neurofibrillary tangles in a transgenic mouse model of alzheimer's-like tauopathy. J. Neurosci. 33, 1024–1037.

Irizarry, M.C., McNamara, M., Fedorchak, K., Hsiao, K., and Hyman, B.T. (1997). APP(Sw) transgenic mice develop age-related Aβ deposits and neuropil abnormalities, but no neuronal loss in CA1. J. Neuropathol. Exp. Neurol. 56, 965–973.

Ironside, J.W., and Head, M.W. (2004). Neuropathology and Molecular Biology of Variant Creutzfeldt-Jakob Disease. Curr. Top. Microbiol. Immunol. 284, 133–159.

Itzhaki, R.F. (2016). Herpes and Alzheimer's Disease: Subversion in the Central Nervous System and How It Might Be Halted. J. Alzheimer's Dis. 54, 1273–1281.

Itzhaki, R.F., Lin, W.R., Shang, D., Wilcock, G.K., Faragher, B., and Jamieson, G.A. (1997). Herpes simplex virus type 1 in brain and risk of Alzheimer's disease. Lancet 349, 241–244.

Itzhaki, R.F., Lathe, R., Balin, B.J., Ball, M.J., Bearer, E.L., Braak, H., Bullido, M.J., Carter, C., Clerici, M., Cosby, S.L., et al. (2016). Microbes and Alzheimer's Disease. J. Alzheimer's Dis. 51, 979–984.

Ivanova, M.I., Lin, Y., Lee, Y.H., Zheng, J., and Ramamoorthy, A. (2021). Biophysical processes underlying cross-seeding in amyloid aggregation and implications in amyloid pathology. Biophys. Chem. 269.

Iwata, N., Tsubuki, S., Takaki, Y., Shirotani, K., Lu, B., Gerard, N.P., Gerard, C., Hama, E., Lee, H.J., and Saido, T.C. (2001). Metabolic regulation of brain Aβ by neprilysin. Science (80-.). 292, 1550–1552.

Jack, C.R., Bennett, D.A., Blennow, K., Carrillo, M.C., Dunn, B., Haeberlein, S.B., Holtzman, D.M., Jagust, W., Jessen, F., Karlawish, J., et al. (2018). NIA-AA Research Framework: Toward a biological definition of Alzheimer's disease. Alzheimer's Dement. 14, 535–562.

Jain, N., and Chapman, M.R. (2019). Bacterial functional amyloids: Order from disorder. Biochim. Biophys. Acta - Proteins Proteomics 1867, 954–960.

Jarrett, J.T., and Lansbury, P.T. (1993). Seeding "one-dimensional crystallization" of amyloid: A pathogenic mechanism in Alzheimer's disease and scrapie? Cell 73, 1055–1058.

Jaunmuktane, Z., Mead, S., Ellis, M., Wadsworth, J.D.F., Nicoll, A.J., Kenny, J., Launchbury, F., Linehan, J., Richard-Loendt, A., Walker, A.S., et al. (2015). Evidence for human transmission of amyloid-β pathology and cerebral amyloid angiopathy. Nature 525, 247–250.

Jaunmuktane, Z., Quaegebeur, A., Taipa, R., Viana-Baptista, M., Barbosa, R., Koriath, C., Sciot, R., Mead, S., and Brandner, S. (2018). Evidence of amyloid-β cerebral amyloid angiopathy transmission through neurosurgery. Acta Neuropathol. 135, 671–679.

Jawhar, S., Wirths, O., and Bayer, T.A. (2011). Pyroglutamate amyloid-β (Aβ): A hatchet man in alzheimer disease. J. Biol. Chem. 286, 38825–38832.

Jefferies, K., and Agrawal, N. (2009). Early-onset dementia. Adv. Psychiatr. Treat. 15, 380–388.

Jellinger, K.A. (2021). Pathobiological Subtypes of Alzheimer Disease. Dement. Geriatr. Cogn. Disord. 49, 321–333.

Jeong, H.J., Lee, H., Lee, S.Y., Seo, S., Park, K.H., Lee, Y.B., Shin, D.J., Kang, J.M., Yeon, B.K., Kang, S.G., et al. (2020). [18F]THK5351 PET imaging in patients with mild cognitive impairment. J. Clin. Neurol. 16, 202–214.

References

Jiang, M., Vanan, S., Tu, H.-T., Zhang, W., Zhang, Z.-W., Chia, S.-Y., Jang, S.E., Zeng, X.-X., Yu, W.-P., Xu, J., et al. (2020). Amyloid precursor protein intracellular domain-dependent regulation of FOXO3a inhibits adult hippocampal neurogenesis. Neurobiol. Aging 95, 250–263.

Jones, R.M., and Neish, A.S. (2017). Redox signaling mediated by the gut microbiota. Free Radic. Biol. Med. 105, 41–47.

Jucker, M., and Walker, L.C. (2018). Propagation and spread of pathogenic protein assemblies in neurodegenerative diseases. Nat. Neurosci. 21, 1341–1349.

Kakuda, N., Yamaguchi, H., Akazawa, K., Hata, S., Suzuki, T., Hatsuta, H., Murayama, S., Funamoto, S., and Ihara, Y. (2020). γ-Secretase Activity Is Associated with Braak Senile Plaque Stages. Am. J. Pathol. 190, 1323–1331.

Kamer, A.R., Pirraglia, E., Tsui, W., Rusinek, H., Vallabhajosula, S., Mosconi, L., Yi, L., McHugh, P., Craig, R.G., Svetcov, S., et al. (2015). Periodontal disease associates with higher brain amyloid load in normal elderly. Neurobiol. Aging 36, 627–633.

Kane, M.D., Lipinski, W.J., Callahan, M.J., Bian, F., Durham, R.A., Schwarz, R.D., Roher, A.E., and Walker, L.C. (2000). Evidence for Seeding of β-Amyloid by Intracerebral Infusion of Alzheimer Brain Extracts in β-Amyloid Precursor Protein-Transgenic Mice. J. Neurosci. 20, 3606–3611.

Kang, J., Lemaire, H.G., Unterbeck, A., Salbaum, J.M., Masters, C.L., Grzeschik, K.H., Multhaup, G., Beyreuther, K., and Müller-Hill, B. (1987). The precursor of Alzheimer's disease amyloid A4 protein resembles a cell-surface receptor. Nature 325, 733–736.

van der Kant, R., Goldstein, L.S.B., and Ossenkoppele, R. (2020). Amyloid-β-independent regulators of tau pathology in Alzheimer disease. Nat. Rev. Neurosci. 21, 21–35.

Karikari, T.K., Pascoal, T.A., Ashton, N.J., Janelidze, S., Benedet, A.L., Rodriguez, J.L., Chamoun, M., Savard, M., Kang, M.S., Therriault, J., et al. (2020). Blood phosphorylated tau 181 as a biomarker for Alzheimer's disease: a diagnostic performance and prediction modelling study using data from four prospective cohorts. Lancet Neurol. 19, 422–433.

Kaur, D., Sharma, V., and Deshmukh, R. (2019). Activation of microglia and astrocytes: a roadway to neuroinflammation and Alzheimer's disease. Inflammopharmacology 27, 663–677.

Keren-Shaul, H., Spinrad, A., Weiner, A., Matcovitch-Natan, O., Dvir-Szternfeld, R., Ulland, T.K., David, E., Baruch, K., Lara-Astaiso, D., Toth, B., et al. (2017). A Unique Microglia Type Associated with Restricting Development of Alzheimer's Disease. Cell 169, 1276-1290.e17.

Kern, S., Syrjanen, J.A., Blennow, K., Zetterberg, H., Skoog, I., Waern, M., Hagen, C.E., Van Harten, A.C., Knopman, D.S., Jack, C.R., et al. (2019). Association of Cerebrospinal Fluid Neurofilament Light Protein with Risk of Mild Cognitive Impairment among Individuals Without Cognitive Impairment. JAMA Neurol. 76, 187–193.

Kesika, P., Suganthy, N., Sivamaruthi, B.S., and Chaiyasut, C. (2021). Role of gut-brain axis, gut microbial composition, and probiotic intervention in Alzheimer's disease. Life Sci. 264, 118627.

Khachaturian, Z.S. (1985). Diagnosis of Alzheimer's disease. Arch. Neurol. 42, 1097–1105.

Kim, D., and Tsai, L.-H. (2009). Bridging physiology and pathology in AD. Cell 137, 997–1000.

Kim, D.H., Yeo, S.H., Park, J.-M., Choi, J.Y., Lee, T.-H., Park, S.Y., Ock, M.S., Eo, J., Kim, H.-S., and Cha, H.-J. (2014). Genetic markers for diagnosis and pathogenesis of Alzheimer's disease. Gene 545, 185–193.

Klingstedt, T., Åslund, A., Simon, R.A., Johansson, L.B.G., Mason, J.J., Nyström, S., Hammarström, P., and Nilsson, K.P.R. (2011). Synthesis of a library of oligothiophenes and their utilization as fluorescent ligands for spectral assignment of protein aggregates. Org. Biomol. Chem. 9, 8356–8370.

Klingstedt, T., Shirani, H., Åslund, K.O.A., Cairns, N.J., Sigurdson, C.J., Goedert, M., and Nilsson, K.P.R. (2013). The structural basis for optimal performance of oligothiophene-based fluorescent amyloid ligands: Conformational flexibility is essential for spectral assignment of a diversity of protein aggregates. Chem. - A Eur. J. 19, 10179–10192.

Klunk, W.E., Engler, H., Nordberg, A., Wang, Y., Blomqvist, G., Holt, D.P., Bergström, M., Savitcheva, I., Huang, G.F., Estrada, S., et al. (2004). Imaging Brain Amyloid in Alzheimer's Disease with Pittsburgh Compound-B. Ann. Neurol. 55, 306–319.

Knopman, D.S., Amieva, H., Petersen, R.C., Chételat, G., Holtzman, D.M., Hyman, B.T., Nixon, R.A., and Jones, D.T. (2021). Alzheimer disease. Nat. Rev. Dis. Prim. 7, 33.

Knowles, T.P.J., Vendruscolo, M., and Dobson, C.M. (2014). The amyloid state and its association with protein misfolding diseases. Nat. Rev. Mol. Cell Biol. 15, 384–396.

Kodali, R., Williams, A.D., Chemuru, S., and Wetzel, R. (2010). Aβ(1–40) Forms Five Distinct Amyloid Structures whose β-Sheet Contents and Fibril Stabilities Are Correlated. J. Mol. Biol. 401, 503–517.

Koffie, R.M., Hyman, B.T., and Spires-Jones, T.L. (2011). Alzheimer's disease: synapses gone cold. Mol. Neurodegener. 6, 63.

Kollmer, M., Close, W., Funk, L., Rasmussen, J., Bsoul, A., Schierhorn, A., Schmidt, M., Sigurdson, C.J., Jucker, M., and Fändrich, M. (2019). Cryo-EM structure and polymorphism of Aβ amyloid fibrils purified from Alzheimer's brain tissue. Nat. Commun. 10, 1–8.

Kosolapova, A.O., Antonets, K.S., Belousov, M. V., and Nizhnikov, A.A. (2020). Biological functions of prokaryotic amyloids in interspecies interactions: Facts and assumptions. Int. J. Mol. Sci. 21, 1–26.

Kovacs, G.G., Lutz, M.I., Ricken, G., Ströbel, T., Höftberger, R., Preusser, M., Regelsberger, G., Hönigschnabl, S., Reiner, A., Fischer, P., et al. (2016). Dura mater is a potential source of Aβ seeds. Acta Neuropathol. 131, 911–923.

Krafft, G. a., and Klein, W.L. (2010). ADDLs and the signaling web that leads to Alzheimer's disease. Neuropharmacology 59, 230–242.

Krasemann, S., Madore, C., Cialic, R., Baufeld, C., Calcagno, N., Fatimy, R. El, Beckers, L., O'Loughlin, E., Xu, Y., Fanek, Z., et al. (2017). The TREM2-APOE Pathway Drives the Transcriptional Phenotype of Dysfunctional Microglia in Neurodegenerative Diseases. Immunity 47, 566-581.e9.

Kraus, A., Hoyt, F., Schwartz, C.L., Hansen, B., Artikis, E., Hughson, A.G., Raymond, G.J., Race, B., Baron, G.S., and Caughey, B. (2021). High-resolution structure and strain comparison of infectious mammalian prions. Mol. Cell 81, 4540-4551.e6.

References

Krebs, M.R.H., Morozova-Roche, L.A., Daniel, K., Robinson, C. V., and Dobson, C.M. (2004). Observation of sequence specificity in the seeding of protein amyloid fibrils. Protein Sci. 13, 1933–1938.

Kulenkampff, K., Wolf Perez, A.M., Sormanni, P., Habchi, J., and Vendruscolo, M. (2021). Quantifying misfolded protein oligomers as drug targets and biomarkers in Alzheimer and Parkinson diseases. Nat. Rev. Chem. 5, 277–294.

Kumar, D., Kumar, V., Choi, S.H., Washicosky, K.J., Eimer, W.A., Tucker, S., Ghofrani, J., Lefkowitz, A., Mccoll, G., Goldstein, L.E., et al. (2016). Amyloid-β peptide protects against microbial infection in mouse and worm models of Alzheimer's disease. Sci. Transl. Med. 8.

Kunis, G., Baruch, K., Rosenzweig, N., Kertser, A., Miller, O., Berkutzki, T., and Schwartz, M. (2013). IFN-γ-dependent activation of the brain's choroid plexus for CNS immune surveillance and repair. Brain 136, 3427–3440.

Kunkle, B.W., Grenier-Boley, B., Sims, R., Bis, J.C., Damotte, V., Naj, A.C., Boland, A., Vronskaya, M., van der Lee, S.J., Amlie-Wolf, A., et al. (2019). Genetic meta-analysis of diagnosed Alzheimer's disease identifies new risk loci and implicates Aβ, tau, immunity and lipid processing. Nat. Genet. 51, 414–430.

Lacor, P.N., Buniel, M.C., Furlow, P.W., Clemente, A.S., Velasco, P.T., Wood, M., Viola, K.L., and Klein, W.L. (2007). Aβ oligomer-induced aberrations in synapse composition, shape, and density provide a molecular basis for loss of connectivity in Alzheimer's disease. J. Neurosci. 27, 796–807.

LaFerla, F.M., Green, K.N., and Oddo, S. (2007). Intracellular amyloid-β in Alzheimer's disease. Nat. Rev. Neurosci. 8, 499–509.

Laforce, R., Tosun, D., Ghosh, P., Lehmann, M., Madison, C.M., Weiner, M.W., Miller, B.L., Jagust, W.J., and Rabinovici, G.D. (2014). Parallel ICA of FDG-PET and PiB-PET in three conditions with underlying Alzheimer's pathology. NeuroImage Clin. 4, 508–516.

Lambert, J.-C., Heath, S., Even, G., Campion, D., Sleegers, K., Hiltunen, M., Combarros, O., Zelenika, D., Bullido, M.J., Tavernier, B., et al. (2009). Genome-wide association study identifies variants at CLU and CR1 associated with Alzheimer's disease. Nat. Genet. 41, 1094–1099.

Lau, H.H.C., Lau, A., and Watts, J.C. (2018). Discriminating strains of self-propagating protein aggregates using a conformational stability assay. In Methods in Molecular Biology, (Methods Mol Biol), pp. 339–354.

Lau, H.H.C., Ingelsson, M., and Watts, J.C. (2021). The existence of Aβ strains and their potential for driving phenotypic heterogeneity in Alzheimer's disease. Acta Neuropathol. 142, 17–39.

Laurent, C., Dorothée, G., Hunot, S., Martin, E., Monnet, Y., Duchamp, M., Dong, Y., Légeron, F.P., Leboucher, A., Burnouf, S., et al. (2017). Hippocampal T cell infiltration promotes neuroinflammation and cognitive decline in a mouse model of tauopathy. Brain 140, 184–200.

Le, T. V, Crook, R., Hardy, J., and Dickson, D.W. (2001). Cotton wool plaques in non-familial late-onset Alzheimer disease. J. Neuropathol. Exp. Neurol. 60, 1051–1061.

Lee, N.K., Kim, W.S., and Paik, H.D. (2019). Bacillus strains as human probiotics: characterization, safety, microbiome, and probiotic carrier. Food Sci. Biotechnol. 28, 1297–1305.

Lee, S.H., Kang, J., Ho, A., Watanabe, H., Bolshakov, V.Y., and Shen, J. (2020). APP Family Regulates Neuronal Excitability and Synaptic Plasticity but Not Neuronal Survival. Neuron 108, 676-690.e8.

Lehmann, M., Douiri, A., Kim, L.G., Modat, M., Chan, D., Ourselin, S., Barnes, J., and Fox, N.C. (2010). Atrophy patterns in Alzheimer's disease and semantic dementia: a comparison of FreeSurfer and manual volumetric measurements. Neuroimage 49, 2264–2274.

Leite, G., Pimentel, M., Barlow, G.M., Chang, C., Hosseini, A., Wang, J., Parodi, G., Sedighi, R., Rezaie, A., and Mathur, R. (2021). Age and the aging process significantly alter the small bowel microbiome. Cell Rep. 36, 109765.

Leng, F., and Edison, P. (2021). Neuroinflammation and microglial activation in Alzheimer disease: where do we go from here? Nat. Rev. Neurol. 2020 173 17, 157–172.

Lesné, S.E. (2014). Toxic oligomer species of amyloid-β in Alzheimer's disease, a timing issue. Swiss Med. Wkly. 144, w14021.

Levkovich, S.A., Gazit, E., and Laor Bar-Yosef, D. (2021). Two Decades of Studying Functional Amyloids in Microorganisms. Trends Microbiol. 29, 251–265.

Lewcock, J.W., Schlepckow, K., Di Paolo, G., Tahirovic, S., Monroe, K.M., and Haass, C. (2020). Emerging Microglia Biology Defines Novel Therapeutic Approaches for Alzheimer's Disease. Neuron 108, 801–821.

Lewis, H., Beher, D., Cookson, N., Oakley, A., Piggott, M., Morris, C.M., Jaros, E., Perry, R., Ince, P., Kenny, R. a, et al. (2006). Quantification of Alzheimer pathology in ageing and dementia: age-related accumulation of amyloid-beta (42) peptide in vascular dementia. Neuropathol. Appl. Neurobiol. 32, 103–118.

Lewis, J., Dickson, D.W., Lin, W.L., Chisholm, L., Corral, A., Jones, G., Yen, S.H., Sahara, N., Skipper, L., Yager, D., et al. (2001). Enhanced Neurofibrillary Degeneration in Transgenic Mice Expressing Mutant Tau and APP. Science (80-.). 293, 1487–1491.

Li, S., and Selkoe, D.J. (2020). A mechanistic hypothesis for the impairment of synaptic plasticity by soluble Aβ oligomers from Alzheimer's brain. J. Neurochem. 154, 583–597.

Li, H., Wolfe, M.S., and Selkoe, D.J. (2009). Toward structural elucidation of the gamma-secretase complex. Structure 17, 326–334.

Li, J., McQuade, T., Siemer, A.B., Napetschnig, J., Moriwaki, K., Hsiao, Y.S., Damko, E., Moquin, D., Walz, T., McDermott, A., et al. (2012). The RIP1/RIP3 necrosome forms a functional amyloid signaling complex required for programmed necrosis. Cell 150, 339–350.

Li, J., Long, X., Huang, H., Tang, J., Zhu, C., Hu, S., Wu, J., Li, J., Lin, Z., and Xiong, N. (2020). Resilience of Alzheimer's Disease to COVID-19. J. Alzheimer's Dis. 77, 67–73.

Lier, J., Streit, W.J., and Bechmann, I. (2021). Beyond Activation: Characterizing Microglial Functional Phenotypes. Cells 10, 2236.

Lilly S.A. (2012). Estado del arte de la enfermedad de Alzheimer en España. Consult. PwC.

Liu, H., Kim, C., Haldiman, T., Sigurdson, C.J., Nyström, S., Nilsson, K.P.R., Cohen, M.L., Wisniewski, T., Hammarström, P., and Safar, J.G. (2021). Distinct conformers of amyloid beta

accumulate in the neocortex of patients with rapidly progressive Alzheimer's disease. J. Biol. Chem. 101267.

Liu, S., Gao, J., Zhu, M., Liu, K., and Zhang, H.L. (2020). Gut Microbiota and Dysbiosis in Alzheimer's Disease: Implications for Pathogenesis and Treatment. Mol. Neurobiol. 57, 5026–5043.

Llorens-Martín, M., Blazquez-Llorca, L., Benavides-Piccione, R., Rabano, A., Hernandez, F., Avila, J., and DeFelipe, J. (2014). Selective alterations of neurons and circuits related to early memory loss in Alzheimer's disease. Front. Neuroanat. 8.

Long, J.M., and Holtzman, D.M. (2019). Alzheimer Disease: An Update on Pathobiology and Treatment Strategies. Cell 179, 312–339.

Loquet, A., Saupe, S.J., and Romero, D. (2018). Functional Amyloids in Health and Disease. J. Mol. Biol. 430, 3629–3630.

Lord, A., Kalimo, H., Eckman, C., Zhang, X.Q., Lannfelt, L., and Nilsson, L.N.G. (2006). The Arctic Alzheimer mutation facilitates early intraneuronal Aβ aggregation and senile plaque formation in transgenic mice. Neurobiol. Aging 27, 67–77.

Lord, A., Englund, H., Söderberg, L., Tucker, S., Clausen, F., Hillered, L., Gordon, M., Morgan, D., Lannfelt, L., Pettersson, F.E., et al. (2009). Amyloid-β protofibril levels correlate with spatial learning in Arctic Alzheimer's disease transgenic mice. FEBS J. 276, 995–1006.

Lövheim, H., Olsson, J., Weidung, B., Johansson, A., Eriksson, S., Hallmans, G., and Elgh, F. (2018). Interaction between Cytomegalovirus and Herpes Simplex Virus Type 1 Associated with the Risk of Alzheimer's Disease Development. J. Alzheimer's Dis. 61, 939–945.

Lu, J.X., Qiang, W., Yau, W.M., Schwieters, C.D., Meredith, S.C., and Tycko, R. (2013). Molecular structure of β-amyloid fibrils in alzheimer's disease brain tissue. Cell 154, 1257.

Lührs, T., Ritter, C., Adrian, M., Riek-Loher, D., Bohrmann, B., Döbeli, H., Schubert, D., and Riek, R. (2005). 3D structure of Alzheimer's amyloid-β (1-42) fibrils. Proc. Natl. Acad. Sci. U. S. A. 102, 17342–17347.

Lundmark, K., Westermark, G.T., Olsén, A., and Westermark, P. (2005). Protein fibrils in nature can enhance amyloid protein A amyloidosis in mice: Cross-seeding as a disease mechanism. Proc. Natl. Acad. Sci. U. S. A. 102, 6098–6102.

Lynch, S. V., and Pedersen, O. (2016). The Human Intestinal Microbiome in Health and Disease. N. Engl. J. Med. 375, 2369–2379.

Lyte, M. (2011). Probiotics function mechanistically as delivery vehicles for neuroactive compounds: Microbial endocrinology in the design and use of probiotics. BioEssays 33, 574–581.

Magusali, N., Graham, A.C., Piers, T.M., Panichnantakul, P., Yaman, U., Shoai, M., Reynolds, R.H., Botia, J.A., Brookes, K.J., Guetta-Baranes, T., et al. (2021). A genetic link between risk for Alzheimer's disease and severe COVID-19 outcomes via the OAS1 gene. Brain.

Maji, S.K., Perrin, M.H., Sawaya, M.R., Jessberger, S., Vadodaria, K., Rissman, R.A., Singru, P.S., Nilsson, K.P.R., Simon, R., Schubert, D., et al. (2009). Functional amyloids as natural storage of peptide hormones in pituitary secretory granules. Science (80-.). 325, 328–332.

Makarava, N., Kovacs, G.G., Bocharova, O., Savtchenko, R., Alexeeva, I., Budka, H., Rohwer, R.G., and Baskakov, I. V. (2010). Recombinant prion protein induces a new transmissible prion disease in wild-type animals. Acta Neuropathol. 119, 177–187.

Makowski, L. (2020). The Structural Basis of Amyloid Strains in Alzheimer's Disease. ACS Biomater. Sci. Eng. 6, 2498–2505.

Mammeri, N. El, Hierrezuelo, J., Tolchard, J., Cámara-Almirón, J., Caro-Astorga, J., Álvarez-Mena, A., Dutour, A., Berbon, M., Shenoy, J., Morvan, E., et al. (2019). Molecular architecture of bacterial amyloids in Bacillus biofilms. FASEB J. 33, 12146–12163.

Mandal, P.K., Pettegrew, J.W., Masliah, E., Hamilton, R.L., and Mandal, R. (2006). Interaction between Aβ peptide and α synuclein: Molecular mechanisms in overlapping pathology of Alzheimer's and Parkinson's in dementia with Lewy body disease. Neurochem. Res. 31, 1153–1162.

Mapstone, M., Cheema, A.K., Fiandaca, M.S., Zhong, X., Mhyre, T.R., MacArthur, L.H., Hall, W.J., Fisher, S.G., Peterson, D.R., Haley, J.M., et al. (2014). Plasma phospholipids identify antecedent memory impairment in older adults. Nat. Med. 20, 415–418.

Marschallinger, J., Iram, T., Zardeneta, M., Lee, S.E., Lehallier, B., Haney, M.S., Pluvinage, J. V., Mathur, V., Hahn, O., Morgens, D.W., et al. (2020). Lipid-droplet-accumulating microglia represent a dysfunctional and proinflammatory state in the aging brain. Nat. Neurosci. 23, 194–208.

Martinson, J.N. V., and Walk, S.T. (2020). Escherichia coli Residency in the Gut of Healthy Human Adults. EcoSal Plus 9.

Masliah, E., Rockenstein, E., Veinbergs, I., Sagara, Y., Mallory, M., Hashimoto, M., and Mucke, L. (2001). β-Amyloid peptides enhance α-synuclein accumulation and neuronal deficits in a transgenic mouse model linking Alzheimer's disease and Parkinson's disease. Proc. Natl. Acad. Sci. U. S. A. 98, 12245–12250.

Masters, C.L., Bateman, R., Blennow, K., Rowe, C.C., Sperling, R.A., and Cummings, J.L. (2015). Alzheimer's disease. Nat. Rev. Dis. Prim. 1, 15056.

Mathis, C.A., Wang, Y., Holt, D.P., Huang, G.F., Debnath, M.L., and Klunk, W.E. (2003). Synthesis and evaluation of C-11-labeled 6-substituted 2-arylbenzothiazoles as amyloid imaging agents. J. Med. Chem. 46, 2740–2754.

Meinhardt, J., Sachse, C., Hortschansky, P., Grigorieff, N., and Fändrich, M. (2009). Aβ(1-40) Fibril Polymorphism Implies Diverse Interaction Patterns in Amyloid Fibrils. J. Mol. Biol. 386, 869–877.

Meyer-Luehmann, M., Coomaraswamy, J., Bolmont, T., Kaeser, S., Schaefer, C., Kilger, E., Neuenschwander, A., Abramowski, D., Frey, P., Jaton, A.L., et al. (2006). Exogenous induction of cerebral β-amyloidogenesis is governed by agent and host. Science (80-.). 313, 1781–1784.

Michaels, T.C.T., Šarić, A., Curk, S., Bernfur, K., Arosio, P., Meisl, G., Dear, A.J., Cohen, S.I.A., Dobson, C.M., Vendruscolo, M., et al. (2020). Dynamics of oligomer populations formed during the aggregation of Alzheimer's Aβ42 peptide. Nat. Chem. 12, 445–451.

Michno, W., Nyström, S., Wehrli, P., Lashley, T., Brinkmalm, G., Guerard, L., Syvänen, S., Sehlin, D., Kaya, I., Brinet, D., et al. (2019). Pyroglutamation of amyloid-βx-42 (Aβx-42) followed by Aβ1-40 deposition underlies plaque polymorphism in progressing Alzheimer's disease pathology. J. Biol. Chem. 294, 6719–6732.

Miklossy, J. (2011). Alzheimer's disease - a neurospirochetosis. Analysis of the evidence following Koch's and Hill's criteria. J. Neuroinflammation 8, 90.

Miklossy, J. (2016). Bacterial Amyloid and DNA are Important Constituents of Senile Plaques: Further Evidence of the Spirochetal and Biofilm Nature of Senile Plaques. J. Alzheimer's Dis. 53, 1459–1473.

Miners, S., Kehoe, P.G., and Love, S. (2020). Cognitive impact of COVID-19: looking beyond the short term. Alzheimer's Res. Ther. 12, 1–16.

Miravalle, L., Calero, M., Takao, M., Roher, A.E., Ghetti, B., and Vidal, R. (2005). Amino-terminally truncated Aβ peptide species are the main component of cotton wool plaques. Biochemistry 44, 10810–10821.

Mirbaha, H., Chen, D., Morazova, O.A., Ruff, K.M., Sharma, A.M., Liu, X., Goodarzi, M., Pappu, R. V., Colby, D.W., Mirzaei, H., et al. (2018). Inert and seed-competent tau monomers suggest structural origins of aggregation. Elife 7.

Mitelpunkt, A., Galili, T., Kozlovski, T., Bregman, N., Shachar, N., Markus-Kalish, M., and Benjamini, Y. (2020). Novel Alzheimer's disease subtypes identified using a data and knowledge driven strategy. Sci. Rep. 10, 1–13.

Miyazono, M., Kitamoto, T., Iwaki, T., and Tateishi, J. (1992). Colocalization of prion protein and β protein in the same amyloid plaques in patients with Gerstmann-Sträussler Syndrome. Acta Neuropathol. 83, 333–339.

Moir, R.D., Lathe, R., and Tanzi, R.E. (2018). The antimicrobial protection hypothesis of Alzheimer's disease. Alzheimer's Dement. 1–13.

Molinuevo, J.L., Ayton, S., Batrla, R., Bednar, M.M., Bittner, T., Cummings, J., Fagan, A.M., Hampel, H., Mielke, M.M., Mikulskis, A., et al. (2018). Current state of Alzheimer's fluid biomarkers. Acta Neuropathol. 136.

Montalbano, M., McAllen, S., Cascio, F. Lo, Sengupta, U., Garcia, S., Bhatt, N., Ellsworth, A., Heidelman, E.A., Johnson, O.D., Doskocil, S., et al. (2020). TDP-43 and Tau Oligomers in Alzheimer's Disease, Amyotrophic Lateral Sclerosis, and Frontotemporal Dementia. Neurobiol. Dis. 146.

Morales, R. (2017). Prion strains in mammals: Different conformations leading to disease. PLoS Pathog. 13, e1006323.

Morales, R., Estrada, L.D., Diaz-Espinoza, R., Morales-Scheihing, D., Jara, M.C., Castilla, J., and Soto, C. (2010). Molecular cross talk between misfolded proteins in animal models of Alzheimer's and prion diseases. J. Neurosci. 30, 4528–4535.

Morales, R., Duran-Aniotz, C., Castilla, J., Estrada, L.D., and Soto, C. (2012a). De novo induction of amyloid-β deposition in vivo. Mol. Psychiatry 17, 1347–1353.

Morales, R., Duran-Aniotz, C., Diaz-Espinoza, R., Camacho, M. V, and Soto, C. (2012b). Protein misfolding cyclic amplification of infectious prions. Nat. Protoc. 7, 1397–1409.

Morales, R., Moreno-Gonzalez, I., and Soto, C. (2013). Cross-Seeding of Misfolded Proteins: Implications for Etiology and Pathogenesis of Protein Misfolding Diseases. PLoS Pathog. 9, e1003537.

Morales, R., Bravo-Alegria, J., Duran-Aniotz, C., and Soto, C. (2015). Titration of biologically active amyloid–β seeds in a transgenic mouse model of Alzheimer's disease. Sci. Rep. 5, 9349.

Morales, R., Hu, P.P., Duran-Aniotz, C., Moda, F., Diaz-Espinoza, R., Chen, B., Bravo-Alegria, J., Makarava, N., Baskakov, I. V, and Soto, C. (2016). Strain-dependent profile of misfolded prion protein aggregates. Sci. Rep. 6, 20526.

Morales, R., Duran-Aniotz, C., Bravo-Alegria, J., Estrada, L.D., Shahnawaz, M., Hu, P.P., Kramm, C., Morales-Scheihing, D., Urayama, A., and Soto, C. (2020). Infusion of blood from mice displaying cerebral amyloidosis accelerates amyloid pathology in animal models of Alzheimer's disease. Acta Neuropathol. Commun. 8, 213.

Morales, R., Bravo-Alegria, J., Moreno-Gonzalez, I., Duran-Aniotz, C., Gamez, N., Edwards, G., and Soto, C. (2021). Transmission of cerebral amyloid pathology by peripheral administration of misfolded Aβ aggregates. Mol. Psychiatry 1–12.

Moreno-Gonzalez, I., Edwards, G., Salvadores, N., Shahnawaz, M., Diaz-Espinoza, R., and Soto, C. (2017). Molecular interaction between type 2 diabetes and Alzheimer's disease through cross-seeding of protein misfolding. Mol. Psychiatry 22, 1327–1334.

Moreno-Jiménez, E.P., Flor-García, M., Terreros-Roncal, J., Rábano, A., Cafini, F., Pallas-Bazarra, N., Ávila, J., and Llorens-Martín, M. (2019). Adult hippocampal neurogenesis is abundant in neurologically healthy subjects and drops sharply in patients with Alzheimer's disease. Nat. Med. 25, 554–560.

Morley, J.E., and Farr, S. a (2014). The role of amyloid-beta in the regulation of memory. Biochem. Pharmacol. 88, 479–485.

Mukherjee, A., Morales-Scheihing, D., Salvadores, N., Moreno-Gonzalez, I., Gonzalez, C., Taylor-Presse, K., Mendez, N., Shahnawaz, M., Gaber, A.O., Sabek, O.M., et al. (2017). Induction of IAPP amyloid deposition and associated diabetic abnormalities by a prion-like mechanism. J. Exp. Med. 214, 2591–2610.

Murray, M.E., Graff-Radford, N.R., Ross, O.A., Petersen, R.C., Duara, R., and Dickson, D.W. (2011). Neuropathologically defined subtypes of Alzheimer's disease with distinct clinical characteristics: A retrospective study. Lancet Neurol. 10, 785–796.

Musiek, E.S., and Holtzman, D.M. (2015). Three dimensions of the amyloid hypothesis: time, space and "wingmen." Nat Neurosci 18, 800–806.

Navarro, V., Sanchez-Mejias, E., Jimenez, S., Muñoz-Castro, C., Sanchez-Varo, R., Davila, J.C., Vizuete, M., Gutierrez, A., and Vitorica, J. (2018). Microglia in Alzheimer's disease: Activated, dysfunctional or degenerative. Front. Aging Neurosci. 10, 140.

Nayeri Chegeni, T., Sarvi, S., Moosazadeh, M., Sharif, M., Aghayan, S.A., Amouei, A., Hosseininejad, Z., and Daryani, A. (2019). Is Toxoplasma gondii a potential risk factor for Alzheimer's disease? A systematic review and meta-analysis. Microb. Pathog. 137, 103751.

Neff, R.A., Wang, M., Vatansever, S., Guo, L., Ming, C., Wang, Q., Wang, E., Horgusluoglu-Moloch, E., Song, W.M., Li, A., et al. (2021). Molecular subtyping of Alzheimer's disease using RNA sequencing data reveals novel mechanisms and targets. Sci. Adv. 7.

References

Nelson, P.T., Dickson, D.W., Trojanowski, J.Q., Jack, C.R., Boyle, P.A., Arfanakis, K., Rademakers, R., Alafuzoff, I., Attems, J., Brayne, C., et al. (2019). Limbic-predominant age-related TDP-43 encephalopathy (LATE): Consensus working group report. Brain 142, 1503–1527.

Neuner, S.M., TCW, J., and Goate, A.M. (2020). Genetic architecture of Alzheimer's disease. Neurobiol. Dis. 143, 104976.

Newcombe, E.A., Camats-Perna, J., Silva, M.L., Valmas, N., Huat, T.J., and Medeiros, R. (2018). Inflammation: The link between comorbidities, genetics, and Alzheimer's disease 11 Medical and Health Sciences 1109 Neurosciences 11 Medical and Health Sciences 1107 Immunology. J. Neuroinflammation 15, 1–26.

Nguyen, V.T.T., and Endres, K. (2021). A crate of Pandora: Do amyloids from bacteria promote Alzheimer's disease? Neural Regen. Res. 16, 988–989.

Nilsson, K.P.R., Åslund, A., Berg, I., Nyström, S., Konradsson, P., Herland, A., Inganäs, O., Stabo-Eeg, F., Lindgren, M., Westermark, G.T., et al. (2007). Imaging distinct conformational states of amyloid-β fibrils in Alzheimer's disease using novel luminescent probes. ACS Chem. Biol. 2, 553–560.

Nixon, R.A. (2017). Amyloid precursor protein & endosomal-lysosomal dysfunction in Alzheimer's disease: Inseparable partners in a multifactorial disease. FASEB J. 31, 2729–2743.

Noble, G.P., Wang, D.W., Walsh, D.J., Supattapone, S., Miller, M.B., Nishina, K.A., Li, S., and Supattapone, S. (2015). A Structural and Functional Comparison Between Infectious and Non-Infectious Autocatalytic Recombinant PrP Conformers. PLoS Pathog. 11, e1005017.

Nussbaum, J.M., Schilling, S., Cynis, H., Silva, A., Swanson, E., Wangsanut, T., Tayler, K., Wiltgen, B., Hatami, A., Rönicke, R., et al. (2012). Prion-like behaviour and tau-dependent cytotoxicity of pyroglutamylated amyloid-β. Nature 485, 651–655.

Nyström, S., Psonka-Antonczyk, K.M., Ellingsen, P.G., Johansson, L.B.G., Reitan, N., Handrick, S., Prokop, S., Heppner, F.L., Wegenast-Braun, B.M., Jucker, M., et al. (2013). Evidence for age-dependent in vivo conformational rearrangement within Aβ amyloid deposits. ACS Chem. Biol. 8, 1128–1133.

O'Nuallain, B., Williams, A.D., Westermark, P., and Wetzel, R. (2004). Seeding Specificity in Amyloid Growth Induced by Heterologous Fibrils. J. Biol. Chem. 279, 17490–17499.

Ogbonnaya, E.S., Clarke, G., Shanahan, F., Dinan, T.G., Cryan, J.F., and O'Leary, O.F. (2015). Adult Hippocampal Neurogenesis Is Regulated by the Microbiome. Biol. Psychiatry 78, e7–e9.

Olah, M., Menon, V., Habib, N., Taga, M.F., Ma, Y., Yung, C.J., Cimpean, M., Khairallah, A., Coronas-Samano, G., Sankowski, R., et al. (2020). Single cell RNA sequencing of human microglia uncovers a subset associated with Alzheimer's disease. Nat. Commun. 11, 1–18.

Olajide, O.J., Suvanto, M.E., and Chapman, C.A. (2021). Molecular mechanisms of neurodegeneration in the entorhinal cortex that underlie its selective vulnerability during the pathogenesis of Alzheimer's disease. Biol. Open 10.

Onuska, K.M. (2020). The dual role of microglia in the progression of Alzheimer's disease. J. Neurosci. 40, 1608–1610.

Orvedahl, A., Alexander, D., Tallóczy, Z., Sun, Q., Wei, Y., Zhang, W., Burns, D., Leib, D.A., and Levine, B. (2007). HSV-1 ICP34.5 Confers Neurovirulence by Targeting the Beclin 1 Autophagy Protein. Cell Host Microbe 1, 23–35.

Otzen, D., and Riek, R. (2019). Functional amyloids. Cold Spring Harb. Perspect. Biol. 11, a033860.

Pacheco-Quinto, J., and Eckman, E.A. (2013). Endothelin-converting enzymes degrade intracellular β-amyloid produced within the endosomal/lysosomal pathway and autophagosomes. J. Biol. Chem. 288, 5606–5615.

Palmqvist, S., Janelidze, S., Quiroz, Y.T., Zetterberg, H., Lopera, F., Stomrud, E., Su, Y., Chen, Y., Serrano, G.E., Leuzy, A., et al. (2020). Discriminative Accuracy of Plasma Phospho-tau217 for Alzheimer Disease vs Other Neurodegenerative Disorders. JAMA - J. Am. Med. Assoc. 324, 772–781.

Paniz-Mondolfi, A., Bryce, C., Grimes, Z., Gordon, R.E., Reidy, J., Lednicky, J., Sordillo, E.M., and Fowkes, M. (2020). Central nervous system involvement by severe acute respiratory syndrome coronavirus-2 (SARS-CoV-2). J. Med. Virol. 92, 699–702.

Paravastu, A.K., Leapman, R.D., Yau, W.M., and Tycko, R. (2008). Molecular structural basis for polymorphism in Alzheimer's β-amyloid fibrils. Proc. Natl. Acad. Sci. U. S. A. 105, 18349–18354.

Paravastu, A.K., Qahwash, I., Leapman, R.D., Meredith, S.C., and Tycko, R. (2009). Seeded growth of β-amyloid fibrils from Alzheimer's brain-derived fibrils produces a distinct fibril structure. Proc. Natl. Acad. Sci. 106, 7443–7448.

Park, S.H., Lee, J.H., Shin, J., Kim, J.S., Cha, B., Lee, S., Kwon, K.S., Shin, Y.W., and Choi, S.H. (2021). Cognitive function improvement after fecal microbiota transplantation in Alzheimer's dementia patient: a case report. Curr. Med. Res. Opin. 37, 1739–1744.

Pascoal, T.A., Benedet, A.L., Ashton, N.J., Kang, M.S., Therriault, J., Chamoun, M., Savard, M., Lussier, F.Z., Tissot, C., Karikari, T.K., et al. (2021). Microglial activation and tau propagate jointly across Braak stages. Nat. Med. 27, 1592–1599.

Pastore, A., Raimondi, F., Rajendran, L., and Temussi, P.A. (2020). Why does the Aβ peptide of Alzheimer share structural similarity with antimicrobial peptides? Commun. Biol. 3, 1–7.

Pastrana, M.A., Sajnani, G., Onisko, B., Castilla, J., Morales, R., Soto, C., and Requena, J.R. (2006). Isolation and characterization of a proteinase K-sensitive PrPSc fraction. Biochemistry 45, 15710–15717.

Paxinos, G., and Franklin, K. (2008). The Mouse Brain in Stereotaxic Coordinates.

Perez-Nievas, B.G., and Serrano-Pozo, A. (2018). Deciphering the astrocyte reaction in Alzheimer's disease. Front. Aging Neurosci. 10, 114.

Petkova, A.T., Leapman, R.D., Guo, Z., Yau, W.-M., Mattson, M.P., and Tycko, R. (2005). Self-Propagating, Molecular-Level Polymorphism in Alzheimer's β-Amyloid Fibrils. Science (80-.). 307, 262–265.

Petkova, A.T., Yau, W.M., and Tycko, R. (2006). Experimental constraints on quaternary structure in Alzheimer's β-amyloid fibrils. Biochemistry 45, 498–512.

Pezzini, A., and Padovani, A. (2020). Lifting the mask on neurological manifestations of COVID-19. Nat. Rev. Neurol. 2020 1611 16, 636–644.

Pisa, D., Alonso, R., Juarranz, A., Rábano, A., and Carrasco, L. (2015a). Direct visualization of fungal infection in brains from patients with Alzheimer's disease. J. Alzheimer's Dis. 43, 613–624.

Pisa, D., Alonso, R., Rábano, A., Rodal, I., and Carrasco, L. (2015b). Different Brain Regions are Infected with Fungi in Alzheimer's Disease. Sci. Rep. 5.

Pisa, D., Alonso, R., Rábano, A., Horst, M.N., and Carrasco, L. (2016a). Fungal Enolase, β-Tubulin, and Chitin Are Detected in Brain Tissue from Alzheimer's Disease Patients. Front. Microbiol. 0, 1772.

Pisa, D., Alonso, R., Rábano, A., and Carrasco, L. (2016b). Corpora amylacea of brain tissue from neurodegenerative diseases are stained with specific antifungal antibodies. Front. Neurosci. 10.

Pisa, D., Alonso, R., Marina, A.I., Rábano, A., and Carrasco, L. (2018). Human and Microbial Proteins From Corpora Amylacea of Alzheimer's Disease. Sci. Reports 2018 81 8, 1–12.

Pistollato, F., Cano, S.S., Elio, I., Vergara, M.M., Giampieri, F., and Battino, M. (2016). Role of gut microbiota and nutrients in amyloid formation and pathogenesis of Alzheimer disease. Nutr. Rev. 74, 624–634.

Plácido, a I., Pereira, C.M.F., Duarte, a I., Candeias, E., Correia, S.C., Santos, R.X., Carvalho, C., Cardoso, S., Oliveira, C.R., and Moreira, P.I. (2014). The role of endoplasmic reticulum in amyloid precursor protein processing and trafficking: Implications for Alzheimer's disease. Biochim. Biophys. Acta 1842, 1444–1453.

Powell-Doherty, R.D., Abbott, A.R.N., Nelson, L.A., and Bertke, A.S. (2020). Amyloid-β and p-Tau Anti-Threat Response to Herpes Simplex Virus 1 Infection in Primary Adult Murine Hippocampal Neurons. J. Virol. 94.

Preische, O., Schultz, S.A., Apel, A., Kuhle, J., Kaeser, S.A., Barro, C., Gräber, S., Kuder-Buletta, E., LaFougere, C., Laske, C., et al. (2019). Serum neurofilament dynamics predicts neurodegeneration and clinical progression in presymptomatic Alzheimer's disease. Nat. Med. 25, 277–283.

Preman, P., Alfonso-Triguero, M., Alberdi, E., Verkhratsky, A., and Arranz, A.M. (2021). Astrocytes in alzheimer's disease: Pathological significance and molecular pathways. Cells 10, 1–19.

Prince, M., Bryce, R., Albanese, E., Wimo, A., Ribeiro, W., and Ferri, C.P. (2013). The global prevalence of dementia: A systematic review and metaanalysis. Alzheimer's Dement. 9, 63-75.e2.

Prusiner, S. (1982). Novel proteinaceous infectious particles cause scrapie. Science (80-.). 216, 136–144.

Psonka-Antonczyk, K.M., Hammarström, P., Johansson, L.B.G., Lindgren, M., Stokke, B.T., Nilsson, K.P.R., and Nyström, S. (2016). Nanoscale structure and spectroscopic probing of aβ1-40 fibril bundle formation. Front. Chem. 4.

Purro, S.A., Farrow, M.A., Linehan, J., Nazari, T., Thomas, D.X., Chen, Z., Mengel, D., Saito, T., Saido, T., Rudge, P., et al. (2018). Transmission of amyloid-β protein pathology from cadaveric pituitary growth hormone. Nature 564, 415–419.

Qiang, W., Yau, W.M., and Tycko, R. (2011). Structural evolution of Iowa mutant β-amyloid fibrils from polymorphic to homogeneous states under repeated seeded growth. J. Am. Chem. Soc. 133, 4018–4029.

Qiang, W., Kelley, K., and Tycko, R. (2013). Polymorph-specific kinetics and thermodynamics of β-amyloid fibril growth. J. Am. Chem. Soc. 135, 6860–6871.

Qiang, W., Yau, W.-M., Lu, J.-X., Collinge, J., and Tycko, R. (2017). Structural variation in amyloid-β fibrils from Alzheimer's disease clinical subtypes. Nature 541, 217–221.

Qiao, O., Ji, H., Zhang, Y., Zhang, X., Zhang, X., Liu, N., Huang, L., Liu, C., and Gao, W. (2021). New insights in drug development for Alzheimer's disease based on microglia function. Biomed. Pharmacother. 140, 111703.

Rajan, K.B., Weuve, J., Barnes, L.L., McAninch, E.A., Wilson, R.S., and Evans, D.A. (2021). Population estimate of people with clinical Alzheimer's disease and mild cognitive impairment in the United States (2020–2060). Alzheimer's Dement. 1–10.

Rasmussen, J., Mahler, J., Beschorner, N., Kaeser, S.A., Häsler, L.M., Baumann, F., Nyström, S., Portelius, E., Blennow, K., Lashley, T., et al. (2017). Amyloid polymorphisms constitute distinct clouds of conformational variants in different etiological subtypes of Alzheimer's disease. Proc. Natl. Acad. Sci. U. S. A. 114, 13018–13023.

Raymond, G.J., Raymond, L.D., Meade-White, K.D., Hughson, A.G., Favara, C., Gardner, D., Williams, E.S., Miller, M.W., Race, R.E., and Caughey, B. (2007). Transmission and Adaptation of Chronic Wasting Disease to Hamsters and Transgenic Mice: Evidence for Strains. J. Virol. 81, 4305–4314.

Reinke, A.A., and Gestwicki, J.E. (2011). Insight into Amyloid Structure Using Chemical Probes. Chem. Biol. Drug Des. 77, 399–411.

Reitz, C., Rogaeva, E., and Beecham, G.W. (2020). Late-onset vs nonmendelian early-onset Alzheimer disease: A distinction without a difference? Neurol. Genet. 6.

Rhayat, L., Maresca, M., Nicoletti, C., Perrier, J., Brinch, K.S., Christian, S., Devillard, E., and Eckhardt, E. (2019). Effect of Bacillus subtilis Strains on Intestinal Barrier Function and Inflammatory Response. Front. Immunol. 10, 564.

Ritchie, D.L., Adlard, P., Peden, A.H., Lowrie, S., Le Grice, M., Burns, K., Jackson, R.J., Yull, H., Keogh, M.J., Wei, W., et al. (2017). Amyloid-β accumulation in the CNS in human growth hormone recipients in the UK. Acta Neuropathol. 134, 221–240.

Romero, D., and Kolter, R. (2014). Functional amyloids in bacteria. Int. Microbiol. 17, 65–73.

Romero, D., Aguilar, C., Losick, R., and Kolter, R. (2010). Amyloid fibers provide structural integrity to Bacillus subtilis biofilms. Proc. Natl. Acad. Sci. U. S. A. 107, 2230–2234.

Romero, D., Vlamakis, H., Losick, R., and Kolter, R. (2011). An accessory protein required for anchoring and assembly of amyloid fibres in B. subtilis biofilms. Mol. Microbiol. 80, 1155–1168.

Rosen, R.F., Fritz, J.J., Dooyema, J., Cintron, A.F., Hamaguchi, T., Lah, J.J., LeVine, H., Jucker, M., and Walker, L.C. (2012). Exogenous seeding of cerebral β-amyloid deposition in βAPP-transgenic rats. J. Neurochem. 120, 660–666.

Rossi, M., Baiardi, S., and Parchi, P. (2019). Understanding prion strains: Evidence from studies of the disease forms affecting humans. Viruses 11.

Ruiz-Riquelme, A., Mao, A., Barghash, M.M., Lau, H.H.C., Stuart, E., Kovacs, G.G., Nilsson, K.P.R., Fraser, P.E., Schmitt-Ulms, G., and Watts, J.C. (2021). Aβ43 aggregates exhibit enhanced prion-like seeding activity in mice. Acta Neuropathol. Commun. 9, 1–19.

Rutsch, A., Kantsjö, J.B., and Ronchi, F. (2020). The Gut-Brain Axis: How Microbiota and Host Inflammasome Influence Brain Physiology and Pathology. Front. Immunol. 0, 3237.

Ryan, N.S., Rossor, M.N., and Fox, N.C. (2015). Alzheimer's disease in the 100 years since Alzheimer's death. Brain 138, 3816–3821.

Ryan, N.S., Nicholas, J.M., Weston, P.S.J., Liang, Y., Lashley, T., Guerreiro, R., Adamson, G., Kenny, J., Beck, J., Chavez-Gutierrez, L., et al. (2016). Clinical phenotype and genetic associations in autosomal dominant familial Alzheimer's disease: a case series. Lancet Neurol. 15, 1326–1335.

Sachse, C., Fändrich, M., and Grigorieff, N. (2008). Paired β-sheet structure of an Aβ(1-40) amyloid fibril revealed by electron microscopy. Proc. Natl. Acad. Sci. U. S. A. 105, 7462–7466.

Safar, J.G., Kellings, K., Serban, A., Groth, D., Cleaver, J.E., Prusiner, S.B., and Riesner, D. (2005). Search for a Prion-Specific Nucleic Acid. J. Virol. 79, 10796–10806.

Safar, J.G., Xiao, X., Kabir, M.E., Chen, S., Kim, C., Haldiman, T., Cohen, Y., Chen, W., Cohen, M.L., and Surewicz, W.K. (2015). Structural Determinants of Phenotypic Diversity and Replication Rate of Human Prions. PLoS Pathog. 11, e1004832.

Sahlin, C., Lord, A., Magnusson, K., Englund, H., Almeida, C.G., Greengard, P., Nyberg, F., Gouras, G.K., Lannfelt, L., and Nilsson, L.N.G. (2007). The Arctic Alzheimer mutation favors intracellular amyloid-β production by making amyloid precursor protein less available to α-secretase. J. Neurochem. 101, 854–862.

Sait, A., Angeli, C., Doig, A.J., and Day, P.J.R. (2021). Viral Involvement in Alzheimer's Disease. ACS Chem. Neurosci. 12, 1049–1060.

Sala Frigerio, C., Wolfs, L., Fattorelli, N., Thrupp, N., Voytyuk, I., Schmidt, I., Mancuso, R., Chen, W.T., Woodbury, M.E., Srivastava, G., et al. (2019). The Major Risk Factors for Alzheimer's Disease: Age, Sex, and Genes Modulate the Microglia Response to Aβ Plaques. Cell Rep. 27, 1293-1306.e6.

Salvadores, N., Shahnawaz, M., Scarpini, E., Tagliavini, F., and Soto, C. (2014). Detection of Misfolded Aβ Oligomers for Sensitive Biochemical Diagnosis of Alzheimer's Disease. Cell Rep. 7, 261–268.

Sampson, T.R., Debelius, J.W., Thron, T., Janssen, S., Shastri, G.G., Ilhan, Z.E., Challis, C., Schretter, C.E., Rocha, S., Gradinaru, V., et al. (2016). Gut Microbiota Regulate Motor Deficits and Neuroinflammation in a Model of Parkinson's Disease. Cell 167, 1469-1480.e12.

Sampson, T.R., Challis, C., Jain, N., Moiseyenko, A., Ladinsky, M.S., Shastri, G.G., Thron, T., Needham, B.D., Horvath, I., Debelius, J.W., et al. (2020). A gut bacterial amyloid promotes a-synuclein aggregation and motor impairment in mice. Elife 9, 1–19.

Sanchez-Mejias, E., Navarro, V., Jimenez, S., Sanchez-Mico, M., Sanchez-Varo, R., Nuñez-Diaz, C., Trujillo-Estrada, L., Davila, J.C., Vizuete, M., Gutierrez, A., et al. (2016). Soluble phospho-tau from Alzheimer's disease hippocampus drives microglial degeneration. Acta Neuropathol. 132, 897–916.

Sanchez-Mejias, E., Nuñez-Diaz, C., Sanchez-Varo, R., Gomez-Arboledas, A., Garcia-Leon, J.A., Fernandez-Valenzuela, J.J., Mejias-Ortega, M., Trujillo-Estrada, L., Baglietto-Vargas, D., Moreno-Gonzalez, I., et al. (2020). Distinct disease-sensitive GABAergic neurons in the perirhinal cortex of Alzheimer's mice and patients. Brain Pathol. 30, 345–363.

Sanchez-Varo, R., Trujillo-Estrada, L., Sanchez-Mejias, E., Torres, M., Baglietto-Vargas, D., Moreno-Gonzalez, I., De Castro, V., Jimenez, S., Ruano, D., Vizuete, M., et al. (2012). Abnormal accumulation of autophagic vesicles correlates with axonal and synaptic pathology in young Alzheimer's mice hippocampus. Acta Neuropathol. 123, 53–70.

Scheltens, P., De Strooper, B., Kivipelto, M., Holstege, H., Chételat, G., Teunissen, C.E., Cummings, J., and van der Flier, W.M. (2021). Alzheimer's disease. Lancet 397, 1577–1590.

Schindler, S.E., Bollinger, J.G., Ovod, V., Mawuenyega, K.G., Li, Y., Gordon, B.A., Holtzman, D.M., Morris, J.C., Benzinger, T.L.S., Xiong, C., et al. (2019). High-precision plasma β-amyloid 42/40 predicts current and future brain amyloidosis. Neurology 93, E1647–E1659.

Schmid, S., Jungwirth, B., Gehlert, V., Blobner, M., Schneider, G., Kratzer, S., Kellermann, K., and Rammes, G. (2017). Intracerebroventricular injection of beta-amyloid in mice is associated with long-term cognitive impairment in the modified hole-board test. Behav. Brain Res. 324, 15–20.

Schmidt, C., Wolff, M., Weitz, M., Bartlau, T., Korth, C., and Zerr, I. (2011). Rapidly progressive alzheimer disease. Arch. Neurol. 68, 1124–1130.

Schmidt, C., Haïk, S., Satoh, K., Rábano, A., Martinez-Martin, P., Roeber, S., Brandel, J.P., Calero-Lara, M., De Pedro-Cuesta, J., Laplanche, J.L., et al. (2012). Rapidly progressive alzheimer's disease: A multicenter update. J. Alzheimer's Dis. 30, 751–756.

Schmidt, M., Sachse, C., Richter, W., Xu, C., Fändrich, M., and Grigorieff, N. (2009). Comparison of Alzheimer Aβ(1-40) and Aβ(1-42) amyloid fibrils reveals similar protofilament structures. Proc. Natl. Acad. Sci. U. S. A. 106, 19813–19818.

Schmidt, M., Rohou, A., Lasker, K., Yadav, J.K., Schiene-Fischer, C., Fändrich, M., Grigorieff, N., and Petsko, G.A. (2015). Peptide dimer structure in an Aβ(1-42) fibril visualized with cryo-EM. Proc. Natl. Acad. Sci. U. S. A. 112, 11858–11863.

Schützmann, M.P., Hasecke, F., Bachmann, S., Zielinski, M., Hänsch, S., Schröder, G.F., Zempel, H., and Hoyer, W. (2021). Endo-lysosomal Aβ concentration and pH trigger formation of Aβ oligomers that potently induce Tau missorting. Nat. Commun. 12, 1–14.

Scuderi, C., Facchinetti, R., Steardo, L., and Valenza, M. (2020). Neuroinflammation in Alzheimer's Disease: Friend or Foe? FASEB J. 34, 1–1.

Seaks, C.E., and Wilcock, D.M. (2020). Infectious hypothesis of Alzheimer disease. PLOS Pathog. 16, e1008596.

Selkoe, D.J. (2001). Alzheimer's Disease: Genes , Proteins , and Therapy. Perspective 81, 741–767.

Selkoe, D.J. (2008). Soluble oligomers of the amyloid β-protein impair synaptic plasticity and behavior. Behav. Brain Res. 192, 106–113.

Selkoe, D.J., and Hardy, J. (2016). The amyloid hypothesis of Alzheimer's disease at 25 years. EMBO Mol. Med. 1–14.

Sender, R., Fuchs, S., and Milo, R. (2016). Are We Really Vastly Outnumbered? Revisiting the Ratio of Bacterial to Host Cells in Humans. Cell 164, 337–340.

Sergeeva, A. V., and Galkin, A.P. (2020). Functional amyloids of eukaryotes: criteria, classification, and biological significance. Curr. Genet. 66, 849–866.

Serrano-Pozo, A., Frosch, M.P., Masliah, E., and Hyman, B.T. (2011). Neuropathological alterations in Alzheimer disease. Cold Spring Harb. Perspect. Med. 1.

Serrano-Pozo, A., Das, S., and Hyman, B.T. (2021). APOE and Alzheimer's disease: advances in genetics, pathophysiology, and therapeutic approaches. Lancet Neurol. 20, 68–80.

Shahidehpour, R.K., Higdon, R.E., Crawford, N.G., Neltner, J.H., Ighodaro, E.T., Patel, E., Price, D., Nelson, P.T., and Bachstetter, A.D. (2021). Dystrophic microglia are associated with neurodegenerative disease and not healthy aging in the human brain. Neurobiol. Aging 99, 19–27.

Shahnawaz, M., and Soto, C. (2012). Microcin Amyloid Fibrils A Are Reservoir of Toxic Oligomeric Species. J. Biol. Chem. 287, 11665–11676.

Shahnawaz, M., Park, K.W., Mukherjee, A., Diaz-Espinoza, R., and Soto, C. (2017a). Prion-like characteristics of the bacterial protein Microcin E492. Sci. Rep. 7, 1–16.

Shahnawaz, M., Tokuda, T., Waragai, M., Mendez, N., Ishii, R., Trenkwalder, C., Mollenhauer, B., and Soto, C. (2017b). Development of a Biochemical Diagnosis of Parkinson Disease by Detection of α-Synuclein Misfolded Aggregates in Cerebrospinal Fluid. JAMA Neurol. 74, 163.

Shahnawaz, M., Mukherjee, A., Pritzkow, S., Mendez, N., Rabadia, P., Liu, X., Hu, B., Schmeichel, A., Singer, W., Wu, G., et al. (2020). Discriminating α-synuclein strains in Parkinson's disease and multiple system atrophy. Nature 578, 273–277.

Sharoar, M.G., Hu, X., Ma, X.M., Zhu, X., and Yan, R. (2019). Sequential formation of different layers of dystrophic neurites in Alzheimer's brains. Mol. Psychiatry 24, 1369–1382.

Sharon, G., Sampson, T.R., Geschwind, D.H., and Mazmanian, S.K. (2016). The Central Nervous System and the Gut Microbiome. Cell 167, 915–932.

Shewmaker, F., McGlinchey, R.P., and Wickner, R.B. (2011). Structural Insights into Functional and Pathological Amyloid. J. Biol. Chem. 286, 16533–16540.

Shi, Y., and Holtzman, D.M. (2018). Interplay between innate immunity and Alzheimer disease: APOE and TREM2 in the spotlight. Nat. Rev. Immunol. 18, 759–772.

Shi, Y., Murzin, A.G., Falcon, B., Epstein, A., Machin, J., Tempest, P., Newell, K.L., Vidal, R., Garringer, H.J., Sahara, N., et al. (2021). Cryo-EM structures of tau filaments from Alzheimer's disease with PET ligand APN-1607. Acta Neuropathol. 141, 697–708.

Sims-Robinson, C., Kim, B., Rosko, A., and Feldman, E.L. (2010). How does diabetes accelerate Alzheimer disease pathology? Nat. Rev. Neurol. 6, 551–559.

Sims, R., Hill, M., and Williams, J. (2020). The multiplex model of the genetics of Alzheimer's disease. Nat. Neurosci. 23, 311–322.

Sleutel, M., Van Den Broeck, I., Van Gerven, N., Feuillie, C., Jonckheere, W., Valotteau, C., Dufrêne, Y.F., and Remaut, H. (2017). Nucleation and growth of a bacterial functional amyloid at single-fiber resolution. Nat. Chem. Biol. 13, 902–908.

Socher, E., Sticht, H., and Horn, A.H.C. (2014). The conformational stability of nonfibrillar amyloid-β peptide oligomers critically depends on the C-terminal peptide length. ACS Chem. Neurosci. 5, 161–167.

Soscia, S.J., Kirby, J.E., Washicosky, K.J., Tucker, S.M., Ingelsson, M., Hyman, B., Burton, M.A., Goldstein, L.E., Duong, S., Tanzi, R.E., et al. (2010). The Alzheimer's Disease-Associated Amyloid β-Protein Is an Antimicrobial Peptide. PLoS One 5, e9505.

Soto, C. (2012). Transmissible proteins: Expanding the prion heresy. Cell 149, 968–977.

Soto, C., and Pritzkow, S. (2018). Protein misfolding, aggregation, and conformational strains in neurodegenerative diseases. Nat. Neurosci. 21, 1332.

Sparks Stein, P., Steffen, M.J., Smith, C., Jicha, G., Ebersole, J.L., Abner, E., and Dawson, D. (2012). Serum antibodies to periodontal pathogens are a risk factor for Alzheimer's disease. Alzheimer's Dement. 8, 196–203.

Spitzer, P., Condic, M., Herrmann, M., Oberstein, T.J., Scharin-Mehlmann, M., Gilbert, D.F., Friedrich, O., Grömer, T., Kornhuber, J., Lang, R., et al. (2016). Amyloidogenic amyloid-β-peptide variants induce microbial agglutination and exert antimicrobial activity. Sci. Rep. 6.

Srinivasan, K., Friedman, B.A., Etxeberria, A., Huntley, M.A., van der Brug, M.P., Foreman, O., Paw, J.S., Modrusan, Z., Beach, T.G., Serrano, G.E., et al. (2020). Alzheimer's Patient Microglia Exhibit Enhanced Aging and Unique Transcriptional Activation. Cell Rep. 31.

Stancu, I.C., Cremers, N., Vanrusselt, H., Couturier, J., Vanoosthuyse, A., Kessels, S., Lodder, C., Brône, B., Huaux, F., Octave, J.N., et al. (2019). Aggregated Tau activates NLRP3–ASC inflammasome exacerbating exogenously seeded and non-exogenously seeded Tau pathology in vivo. Acta Neuropathol. 137, 599–617.

Steinberg, N., Keren-Paz, A., Hou, Q., Doron, S., Yanuka-Golub, K., Olender, T., Hadar, R., Rosenberg, G., Jain, R., Cámara-Almirón, J., et al. (2020). The extracellular matrix protein TasA is a developmental cue that maintains a motile subpopulation within Bacillus subtilis biofilms. Sci. Signal. 13.

Stöhr, J., Watts, J.C., Mensinger, Z.L., Oehler, A., Grillo, S.K., DeArmond, S.J., Prusiner, S.B., and Giles, K. (2012). Purified and synthetic Alzheimer's amyloid beta (Aβ) prions. Proc. Natl. Acad. Sci. U. S. A. 109, 11025–11030.

Stöhr, J., Condello, C., Watts, J.C., Bloch, L., Oehler, A., Nick, M., DeArmond, S.J., Giles, K., DeGrado, W.F., and Prusiner, S.B. (2014). Distinct synthetic Aβ prion strains producing different amyloid deposits in bigenic mice. Proc. Natl. Acad. Sci. U. S. A. 111, 10329–10334.

Stratoulias, V., Venero, J.L., Tremblay, M.-È., and Joseph, B. (2019). Microglial subtypes: diversity within the microglial community. EMBO J. 38, e101997.

Streit, W.J., Khoshbouei, H., and Bechmann, I. (2020). Dystrophic microglia in late-onset Alzheimer's disease. Glia 68, 845–854.

van Strien, N.M., Cappaert, N.L.M., and Witter, M.P. (2009). The anatomy of memory: an interactive overview of the parahippocampal-hippocampal network. Nat. Rev. Neurosci. 10, 272–282.

De Strooper, B. (2010). Proteases and proteolysis in Alzheimer disease: a multifactorial view on the disease process. Physiol. Rev. 90, 465–494.

De Strooper, B., Vassar, R., and Golde, T. (2010). The secretases: Enzymes with therapeutic potential in Alzheimer disease. Nat. Rev. Neurol. 6, 99–107.

Suárez-Calvet, M., Karikari, T.K., Ashton, N.J., Lantero Rodríguez, J., Milà-Alomà, M., Gispert, J.D., Salvadó, G., Minguillon, C., Fauria, K., Shekari, M., et al. (2020). Novel tau biomarkers phosphorylated at T181, T217 or T231 rise in the initial stages of the preclinical Alzheimer's continuum when only subtle changes in Aβ pathology are detected. EMBO Mol. Med. 12.

Sun, J., Xu, J., Ling, Y., Wang, F., Gong, T., Yang, C., Ye, S., Ye, K., Wei, D., Song, Z., et al. (2019). Fecal microbiota transplantation alleviated Alzheimer's disease-like pathogenesis in APP/PS1 transgenic mice. Transl. Psychiatry 9, 1–13.

Swanson, M.E.V., Scotter, E.L., Smyth, L.C.D., Murray, H.C., Ryan, B., Turner, C., Faull, R.L.M., Dragunow, M., and Curtis, M.A. (2020). Identification of a dysfunctional microglial population in human Alzheimer's disease cortex using novel single-cell histology image analysis. Acta Neuropathol. Commun. 8, 1–16.

Tampi, R.R., Forester, B.P., and Agronin, M. (2021). Aducanumab: evidence from clinical trial data and controversies. Drugs Context 10, 1–9.

Tan, Y.L., Yuan, Y., and Tian, L. (2020). Microglial regional heterogeneity and its role in the brain. Mol. Psychiatry 25, 351–367.

Telling, G.C., Parchi, P., DeArmond, S.J., Cortelli, P., Montagna, P., Gabizon, R., Mastrianni, J., Lugaresi, E., Gambetti, P., and Prusiner, S.B. (1996). Evidence for the conformation of the pathologic isoform of the prion protein enciphering and propagating prion diversity. Science (80-.). 274, 2079–2082.

Tenaillon, O., Skurnik, D., Picard, B., and Denamur, E. (2010). The population genetics of commensal Escherichia coli. Nat. Rev. Microbiol. 8, 207–217.

Thal, D.R., Rüb, U., Schultz, C., Sassin, I., Ghebremedhin, E., Del Tredici, K., Braak, E., and Braak, H. (2000). Sequence of Abeta -Protein Deposition in the Human Medial Temporal Lobe. J. Neuropathol. Exp. Neurol. 59, 733–748.

Thal, D.R., Ghebremedhin, E., Rüb, U., Yamaguchi, H., Del Tredici, K., and Braak, H. (2002). Two types of sporadic cerebral amyloid angiopathy. J. Neuropathol. Exp. Neurol. 61, 282–293.

Thal, D.R., Ghebremedhin, E., Orantes, M., and Wiestler, O.D. (2003). Vascular Pathology in Alzheimer Disease: Correlation of Cerebral Amyloid Angiopathy and Arteriosclerosis/Lipohyalinosis with Cognitive Decline. J. Neuropathol. Exp. Neurol. 62, 1287–1301.

Thal, D.R., Walter, J., Saido, T.C., and Fändrich, M. (2015). Neuropathology and biochemistry of Aβ and its aggregates in Alzheimer's disease. Acta Neuropathol. 129, 167–182.

Tomic, J.L., Pensalfini, A., Head, E., and Glabe, C.G. (2009). Soluble fibrillar oligomer levels are elevated in Alzheimer's disease brain and correlate with cognitive dysfunction. Neurobiol. Dis. 35, 352–358.

Torres, L., Robinson, S.A., Kim, D.G., Yan, A., Cleland, T.A., and Bynoe, M.S. (2018). Toxoplasma gondii alters NMDAR signaling and induces signs of Alzheimer's disease in wild-type, C57BL/6 mice. J. Neuroinflammation 15, 1–19.

Townsend, M., Shankar, G.M., Mehta, T., Walsh, D.M., and Selkoe, D.J. (2006). Effects of secreted oligomers of amyloid β-protein on hippocampal synaptic plasticity: A potent role for trimers. J. Physiol. 572, 477–492.

Tran, M., and Reddy, P.H. (2021). Defective Autophagy and Mitophagy in Aging and Alzheimer's Disease. Front. Neurosci. 14.

Tseng, B.P., Green, K.N., Chan, J.L., Blurton-Jones, M., and LaFerla, F.M. (2008). Aβ inhibits the proteasome and enhances amyloid and tau accumulation. Neurobiol. Aging 29, 1607–1618.

Tsigelny, I.F., Crews, L., Desplats, P., Shaked, G.M., Sharikov, Y., Mizuno, H., Spencer, B., Rockenstein, E., Trejo, M., Platoshyn, O., et al. (2008). Mechanisms of Hybrid Oligomer Formation in the Pathogenesis of Combined Alzheimer's and Parkinson's Diseases. PLoS One 3, e3135.

Tsuchiya, K., Yagishita, S., Ikeda, K., Sano, M., Taki, K., Hashimoto, K., Watabiki, S., and Mizusawa, H. (2004). Coexistence of CJD and Alzheimer's disease: An autopsy case showing typical clinical features of CJD. Neuropathology 24, 46–55.

Tükel, Ç., Raffatellu, M., Humphries, A.D., Wilson, R.P., Andrews-Polymenis, H.L., Gull, T., Figueiredo, J.F., Wong, M.H., Michelsen, K.S., Akçelik, M., et al. (2005). CsgA is a pathogen-associated molecular pattern of Salmonella enterica serotype Typhimurium that is recognized by Toll-like receptor 2. Mol. Microbiol. 58, 289–304.

Tükel, Ç., Wilson, R.P., Nishimori, J.H., Pezeshki, M., Chromy, B.A., and Bäumler, A.J. (2009). Responses to Amyloids of Microbial and Host Origin Are Mediated through Toll-like Receptor 2. Cell Host Microbe 6, 45–53.

Tükel, Ç., Nishimori, J.H., Wilson, R.P., Winter, M.G., Keestra, A.M., Van Putten, J.P.M., and Bäumler, A.J. (2010). Toll-like receptors 1 and 2 cooperatively mediate immune responses to curli, a common amyloid from enterobacterial biofilms. Cell. Microbiol. 12, 1495–1505.

Turnbaugh, P.J., Ley, R.E., Hamady, M., Fraser-Liggett, C.M., Knight, R., and Gordon, J.I. (2007). The Human Microbiome Project. Nature 449, 804–810.

Twohig, D., and Nielsen, H.M. (2019). α-synuclein in the pathophysiology of Alzheimer's disease. Mol. Neurodegener. 14.

Tycko, R. (2014). Physical and structural basis for polymorphism in amyloid fibrils. Protein Sci. 23, 1528–1539.

Tycko, R. (2015). Amyloid Polymorphism: Structural Basis and Neurobiological Relevance. Neuron 86, 632–645.

Ubeda, C., Djukovic, A., and Isaac, S. (2017). Roles of the intestinal microbiota in pathogen protection. Clin. Transl. Immunol. 6, e128.

Ulland, T.K., and Colonna, M. (2018). TREM2 — a key player in microglial biology and Alzheimer disease. Nat. Rev. Neurol. 14, 667–675.

References

Ulrich, J.D., Finn, M.B., Wang, Y., Shen, A., Mahan, T.E., Jiang, H., Stewart, F.R., Piccio, L., Colonna, M., and Holtzman, D.M. (2014). Altered microglial response to Aβ plaques in APPPS1-21 mice heterozygous for TREM2. Mol. Neurodegener. 9, 1–9.

Unger, M.M., Spiegel, J., Dillmann, K.U., Grundmann, D., Philippeit, H., Bürmann, J., Faßbender, K., Schwiertz, A., and Schäfer, K.H. (2016). Short chain fatty acids and gut microbiota differ between patients with Parkinson's disease and age-matched controls. Park. Relat. Disord. 32, 66–72.

Vaneyck, J., Segers-Nolten, I., Broersen, K., and Claessens, M.M.A.E. (2021). Cross-seeding of alpha-synuclein aggregation by amyloid fibrils of food proteins. J. Biol. Chem. 296.

Vaquer-Alicea, J., and Diamond, M.I. (2019). Propagation of Protein Aggregation in Neurodegenerative Diseases. Annu. Rev. Biochem. 88, 785–810.

Vassar, R. (2013). ADAM10 prodomain mutations cause late-onset alzheimer's disease: Not just the latest FAD. Neuron 80, 250–253.

Venegas, C., and Heneka, M.T. (2017). Danger-associated molecular patterns in Alzheimer's disease. J. Leukoc. Biol. 101, 87–98.

Venegas, C., Kumar, S., Franklin, B.S., Dierkes, T., Brinkschulte, R., Tejera, D., Vieira-Saecker, A., Schwartz, S., Santarelli, F., Kummer, M.P., et al. (2017). Microglia-derived ASC specks crossseed amyloid-β in Alzheimer's disease. Nature 552, 355–361.

Vitek, M.P., Bhattacharya, K., Glendening, J.M., Stopa, E., Vlassara, H., Bucala, R., Manogue, K., and Cerami, A. (1994). Advanced glycation end products contribute to amyloidosis in Alzheimer disease. Proc. Natl. Acad. Sci. U. S. A. 91, 4766–4770.

Vogel, J.W., Young, A.L., Oxtoby, N.P., Smith, R., Ossenkoppele, R., Strandberg, O.T., La Joie, R., Aksman, L.M., Grothe, M.J., Iturria-Medina, Y., et al. (2021). Four distinct trajectories of tau deposition identified in Alzheimer's disease. Nat. Med. 27, 871–881.

Vogt, N.M., Kerby, R.L., Dill-McFarland, K.A., Harding, S.J., Merluzzi, A.P., Johnson, S.C., Carlsson, C.M., Asthana, S., Zetterberg, H., Blennow, K., et al. (2017). Gut microbiome alterations in Alzheimer's disease. Sci. Rep. 7, 1–11.

Vuong, H.E., Yano, J.M., Fung, T.C., and Hsiao, E.Y. (2017). The Microbiome and Host Behavior. Annu. Rev. Neurosci. 40, 21–49.

Walsh, D.M., Klyubin, I., Fadeeva, J. V., Cullen, W.K., Anwyl, R., Wolfe, M.S., Rowan, M.J., and Selkoe, D.J. (2002). Naturally secreted oligomers of amyloid β protein potently inhibit hippocampal long-term potentiation in vivo. Nature 416, 535–539.

Wälti, M.A., Ravotti, F., Arai, H., Glabe, C.G., Wall, J.S., Böckmann, A., Güntert, P., Meier, B.H., and Riek, R. (2016). Atomic-resolution structure of a disease-relevant Aβ(1-42) amyloid fibril. Proc. Natl. Acad. Sci. U. S. A. 113, E4976–E4984.

Wang, W.Y., Tan, M.S., Yu, J.T., and Tan, L. (2015). Role of pro-inflammatory cytokines released from microglia in Alzheimer's disease. Ann. Transl. Med. 3, 7–7.

Wang, X., Smith, D.R., Jones, J.W., and Chapman, M.R. (2006). In Vitro Polymerization of a Functional Escherichia coli Amyloid Protein. J. Biol. Chem. 282, 3713–3719.

Wang, Y., Ulland, T.K., Ulrich, J.D., Song, W., Tzaferis, J.A., Hole, J.T., Yuan, P., Mahan, T.E., Shi, Y., Gilfillan, S., et al. (2016). TREM2-mediated early microglial response limits diffusion and toxicity of amyloid plaques. J. Exp. Med. 213, 667–675.

Watt, B., Van Niel, G., Raposo, G., and Marks, M.S. (2013). PMEL: A pigment cell-specific model for functional amyloid formation. Pigment Cell Melanoma Res. 26, 300–315.

Watts, J.C., Condello, C., Stöhr, J., Oehler, A., Lee, J., DeArmond, S.J., Lannfelt, L., Ingelsson, M., Giles, K., and Prusiner, S.B. (2014). Serial propagation of distinct strains of Aβ prions from Alzheimer's disease patients. Proc. Natl. Acad. Sci. U. S. A. 111, 10323–10328.

Webster, S.J., Bachstetter, A.D., Nelson, P.T., Schmitt, F.A., and Van Eldik, L.J. (2014). Using mice to model Alzheimer's dementia: an overview of the clinical disease and the preclinical behavioral changes in 10 mouse models. Front. Genet. 5, 1–23.

White, M.R., Kandel, R., Tripathi, S., Condon, D., Qi, L., Taubenberger, J., and Hartshorn, K.L. (2014). Alzheimer's associated β-Amyloid protein inhibits influenza a virus and modulates viral interactions with phagocytes. PLoS One 9, 1227–1241.

Wiersma, V.I., Hoozemans, J.J.M., and Scheper, W. (2020). Untangling the origin and function of granulovacuolar degeneration bodies in neurodegenerative proteinopathies. Acta Neuropathol. Commun. 8, 1–21.

Wightman, D.P., Jansen, I.E., Savage, J.E., Shadrin, A.A., Bahrami, S., Holland, D., Rongve, A., Børte, S., Winsvold, B.S., Drange, O.K., et al. (2021). A genome-wide association study with 1,126,563 individuals identifies new risk loci for Alzheimer's disease. Nat. Genet. 53, 1276–1282.

Wildburger, N.C., Esparza, T.J., Leduc, R.D., Fellers, R.T., Thomas, P.M., Cairns, N.J., Kelleher, N.L., Bateman, R.J., and Brody, D.L. (2017). Diversity of Amyloid-beta Proteoforms in the Alzheimer's Disease Brain. Sci. Rep. 7, 1–9.

Willem, M., Tahirovic, S., Busche, M.A., Ovsepian, S. V., Chafai, M., Kootar, S., Hornburg, D., Evans, L.D.B., Moore, S., Daria, A., et al. (2015). η-Secretase processing of APP inhibits neuronal activity in the hippocampus. Nature 526, 443–447.

Wittnam, J.L., Portelius, E., Zetterberg, H., Gustavsson, M.K., Schilling, S., Koch, B., Demuth, H.U., Blennow, K., Wirths, O., and Bayer, T.A. (2012). Pyroglutamate amyloid β(aβ) aggravates behavioral deficits in transgenic amyloid mouse model for Alzheimer disease. J. Biol. Chem. 287, 8154–8162.

de Wolf, F., Ghanbari, M., Licher, S., McRae-McKee, K., Gras, L., Weverling, G.J., Wermeling, P., Sedaghat, S., Kamran Ikram, M., Waziry, R., et al. (2020). Plasma tau, neurofilament light chain and amyloid-b levels and risk of dementia; a population-based cohort study. Brain 143, 1220–1232.

Wong, K.Y., Roy, J., Fung, M.L., Heng, B.C., Zhang, C., and Lim, L.W. (2020). Relationships between mitochondrial dysfunction and neurotransmission failure in Alzheimer's disease. Aging Dis. 11, 1291–1316.

Wu, Y., Du, S., Johnson, J.L., Tung, H.-Y., Landers, C.T., Liu, Y., Seman, B.G., Wheeler, R.T., Costa-Mattioli, M., Kheradmand, F., et al. (2019). Microglia and amyloid precursor protein coordinate control of transient Candida cerebritis with memory deficits. Nat. Commun. 2019 101 10, 1–15.

Xiao, Y., Ma, B., McElheny, D., Parthasarathy, S., Long, F., Hoshi, M., Nussinov, R., and Ishii, Y. (2015). Aβ (1-42) fibril structure illuminates self-recognition and replication of amyloid in Alzheimer's disease. Nat. Struct. Mol. Biol. 22, 499–505.

Yamada, M., Hamaguchi, T., and Sakai, K. (2019). Acquired cerebral amyloid angiopathy: An emerging concept. In Progress in Molecular Biology and Translational Science, (Prog Mol Biol Transl Sci), pp. 85–95.

Yan, J., Fu, X., Ge, F., Zhang, B., Yao, J., Zhang, H., Qian, J., Tomozawa, H., Naiki, H., Sawashita, J., et al. (2007). Cross-seeding and cross-competition in mouse apolipoprotein A-II amyloid fibrils and protein A amyloid fibrils. Am. J. Pathol. 171, 172–180.

Yang, T., Li, S., Xu, H., Walsh, D.M., and Selkoe, D.J. (2017). Large soluble oligomers of amyloid β-protein from alzheimer brain are far less neuroactive than the smaller oligomers to which they dissociate. J. Neurosci. 37, 152–163.

Yuan, P., Condello, C., Keene, C.D., Wang, Y., Bird, T.D., Paul, S.M., Luo, W., Colonna, M., Baddeley, D., and Grutzendler, J. (2016). TREM2 Haplodeficiency in Mice and Humans Impairs the Microglia Barrier Function Leading to Decreased Amyloid Compaction and Severe Axonal Dystrophy. Neuron 90, 724–739.

Zeng, M.Y., Cisalpino, D., Varadarajan, S., Hellman, J., Warren, H.S., Cascalho, M., Inohara, N., and Núñez, G. (2016). Gut Microbiota-Induced Immunoglobulin G Controls Systemic Infection by Symbiotic Bacteria and Pathogens. Immunity 44, 647–658.

Zetterberg, H., and Bendlin, B.B. (2021). Biomarkers for Alzheimer's disease—preparing for a new era of disease-modifying therapies. Mol. Psychiatry 26, 296–308.

Zetterberg, H., and Blennow, K. (2021). Moving fluid biomarkers for Alzheimer's disease from research tools to routine clinical diagnostics. Mol. Neurodegener. 16, 1–7.

Zetterberg, H., and Schott, J.M. (2019). Biomarkers for Alzheimer's disease beyond amyloid and tau. Nat. Med. 25, 201–203.

Zhan, X., Stamova, B., Jin, L.W., Decarli, C., Phinney, B., and Sharp, F.R. (2016). Gram-negative bacterial molecules associate with Alzheimer disease pathology. Neurology 87, 2324–2332.

Zhan, X., Stamova, B., and Sharp, F.R. (2018). Lipopolysaccharide associates with amyloid plaques, neurons and oligodendrocytes in Alzheimer's disease brain: A review. Front. Aging Neurosci. 10, 1–14.

Zhang, B., Lin, L., and Wu, S. (2021a). A Review of Brain Atrophy Subtypes Definition and Analysis for Alzheimer's Disease Heterogeneity Studies. J. Alzheimer's Dis. 80, 1339–1352.

Zhang, P.F., Hu, H., Tan, L., and Yu, J.T. (2021b). Microglia Biomarkers in Alzheimer's Disease. Mol. Neurobiol. 58, 3388–3404.

Zhang, R., Hu, X., Khant, H., Ludtke, S.J., Chiu, W., Schmid, M.F., Frieden, C., and Lee, J.M. (2009). Interprotofilament interactions between alzheimer's aβ 1-42 peptides in amyloid fibrils revealed by cryoEM. Proc. Natl. Acad. Sci. U. S. A. 106, 4653–4658.

Zhao, J., Bi, W., Xiao, S., Lan, X., Cheng, X., Zhang, J., Lu, D., Wei, W., Wang, Y., Li, H., et al. (2019). Neuroinflammation induced by lipopolysaccharide causes cognitive impairment in mice. Sci. Rep. 9, 1–12.

Zhao, J., Liu, X., Xia, W., Zhang, Y., and Wang, C. (2020). Targeting Amyloidogenic Processing of APP in Alzheimer's Disease. Front. Mol. Neurosci. 13.

Zhao, R., Hu, W., Tsai, J., Li, W., and Gan, W.B. (2017). Microglia limit the expansion of β-amyloid plaques in a mouse model of Alzheimer's disease. Mol. Neurodegener. 12.

Zhou, Y., Smith, D.R., Hufnagel, D.A., and Chapman, M.R. (2013). Experimental manipulation of the microbial functional amyloid called curli. Methods Mol. Biol. 966, 53–75.

Zhou, Y., Xu, J., Hou, Y., Leverenz, J.B., Kallianpur, A., Mehra, R., Liu, Y., Yu, H., Pieper, A.A., Jehi, L., et al. (2021). Network medicine links SARS-CoV-2/COVID-19 infection to brain microvascular injury and neuroinflammation in dementia-like cognitive impairment. Alzheimer's Res. Ther. 13, 1–19.

Zhu, W., Gregory, J.C., Org, E., Buffa, J.A., Gupta, N., Wang, Z., Li, L., Fu, X., Wu, Y., Mehrabian, M., et al. (2016). Gut Microbial Metabolite TMAO Enhances Platelet Hyperreactivity and Thrombosis Risk. Cell 165, 111–124.

Zimbone, S., Monaco, I., Gianì, F., Pandini, G., Copani, A.G., Giuffrida, M.L., and Rizzarelli, E. (2018). Amyloid Beta monomers regulate cyclic adenosine monophosphate response element binding protein functions by activating type-1 insulin-like growth factor receptors in neuronal cells. Aging Cell 17.

World Alzheimer Report 2021: Journey through the diagnosis of dementia.

(2020). 2020 Alzheimer's disease facts and figures. Alzheimer's Dement. 16, 391–460.

8. Annexes

ANNEX 1

Gomez-Gutierrez R, Morales R. *The prion-like phenomenon in Alzheimer's disease: evidence of pathology transmission in humans.* ***PLoS Pathogens*** 2020. *16(10): e1009004.* DOI: 10.1371/journal.ppat.1009004.

PLOS PATHOGENS

PEARLS

The prion-like phenomenon in Alzheimer's disease: Evidence of pathology transmission in humans

Ruben Gomez-Gutierrez[1,2,3], **Rodrigo Morales**[1,4]*

1 Department of Neurology, McGovern Medical School, The University of Texas Health Science Center at Houston, Houston, Texas, United States of America, **2** Department of Cell Biology, Genetics and Physiology, Faculty of Sciences, University of Malaga, Malaga, Spain, **3** Department of Neuroscience, Baylor College of Medicine, Houston, Texas, United States of America, **4** Centro Integrativo de Biología y Química Aplicada (CIBQA), Universidad Bernardo O'Higgins, Santiago, Chile

* Rodrigo.MoralesLoyola@uth.tmc.edu

Citation: Gomez-Gutierrez R, Morales R (2020) The prion-like phenomenon in Alzheimer's disease: Evidence of pathology transmission in humans. PLoS Pathog 16(10): e1009004. https://doi.org/10.1371/journal.ppat.1009004

Editor: Sabine Gilch, University of Calgary, CANADA

Published: October 29, 2020

Funding: Research reported in this publication was supported by the National Institute on Aging of the National Institutes of Health under Award Numbers R56AG061878 and 1RF1AG059321, and grant AARGD-18-566576 from the Alzheimer's Association, to RM. The funders had no role in study design, data collection and analysis, decision to publish, or preparation of the manuscript.

Competing interests: The authors have declared that no competing interests exist.

Prion propagation: A common mechanism among neurodegenerative proteinopathies

Most neurodegenerative diseases, such as Alzheimer's disease (AD), Parkinson's disease (PD), Huntington's disease (HD), and prion diseases, share common pathogenic features. These include the presence of misfolded protein deposits and progressive neuronal loss in specific areas of the brain. Notably, the misfolded proteins involved in these diseases (prions, amyloid-β (Aβ), tau, and α-synuclein) share common structural, biological, and biochemical features, as well as similar mechanisms of aggregation and self-propagation. The infectious prion protein (PrP^{Sc}) was the first disease-causing "proteinaceous infectious agent" ever described [1]. PrP^{Sc} has the ability to "transmit" its disease-associated conformation to normally folded prion proteins (PrP^{C}). In turn, PrP^{Sc} can transfer its disease-causing information at different biological levels, including cell to cell, tissue to tissue, or between individuals. PrP^{Sc} particles associated with Creutzfeldt–Jakob disease (CJD) are able to transmit disease by different means, including corneal and dura transplants, implantation of electrodes, administration of cadaveric-derived human growth hormone (c-hGH), and blood transfusions [2].

Due to the striking similarities between PrP^{Sc} and other disease-associated protein aggregates, it is hypothesized that all of them have the ability to be transmissible. In the case of AD, Aβ and tau have shown to self-propagate both in vitro and in vivo, further supporting that pathological hallmarks of this disease can be transmitted. Remarkably, the growing evidence suggesting human iatrogenic transmission of Aβ pathology highlights the potential issue of interindividual transmission of AD-like neuropathology. In this manuscript, we discuss protein misfolding transmission mechanisms specifically focused on Aβ and the controversial hypothesis stating that some pathological features of AD might be transmissible.

Prion-like propagation of Aβ pathology

Aβ, the peptide forming extracellular aggregates in AD brains, was described to self-propagate its misfolded conformation in vitro decades ago [3]. Further studies in a variety of platforms supported this particular property. One of them involved the intracerebral administration of AD brain extracts to young marmosets that displayed robust Aβ pathology 6 to 7 years later [4]. Taking advantage of transgenic animals mimicking some aspects of familial and sporadic AD, similar outcomes were obtained in considerable shorter times [5]. The central role of pre-

ANNEX 2

Kramm C, **Gomez-Gutierrez R**, Soto C, Telling G, Nichols T, Morales R. *In Vitro detection of Chronic Wasting Disease (CWD) prions in semen and reproductive tissues of white tailed deer bucks (Odocoileus virginianus)*. ***PLoS ONE*** 2019. *14(12): e0226560.* DOI: 10.1371/journal.pone.0226560.

PLOS ONE

RESEARCH ARTICLE

In Vitro detection of Chronic Wasting Disease (CWD) prions in semen and reproductive tissues of white tailed deer bucks *(Odocoileus virginianus)*

Carlos Kramm[1,2], Ruben Gomez-Gutierrez[1,3], Claudio Soto[1], Glenn Telling[4], Tracy Nichols[5], Rodrigo Morales[1,6]*

1 Department of Neurology, McGovern Medical School, The University of Texas Health Science Center at Houston, Houston, TX, United States of America, **2** Universidad de Los Andes, Facultad de Medicina, Las Condes, Santiago, Chile, **3** Department of Cell Biology, University of Malaga, Malaga, Spain, **4** Prion Research Center, Colorado State University, Fort Collins, CO, United States of America, **5** Veterinary Services, APHIS, United States Department of Agriculture, Fort Collins, CO, United States of America, **6** CIBQA, Universidad Bernardo OHiggins. Santiago, Chile

* Rodrigo.MoralesLoyola@uth.tmc.edu

Citation: Kramm C, Gomez-Gutierrez R, Soto C, Telling G, Nichols T, Morales R (2019) *In Vitro* detection of Chronic Wasting Disease (CWD) prions in semen and reproductive tissues of white tailed deer bucks *(Odocoileus virginianus)*. PLoS ONE 14(12): e0226560. https://doi.org/10.1371/journal.pone.0226560

Editor: Human Rezaei, INRA Centre de Jouy-en-Josas, FRANCE

Received: August 23, 2019

Accepted: November 28, 2019

Published: December 30, 2019

Data Availability Statement: All relevant data are within the manuscript and its Supporting Information files.

Funding: This work was funded by a grant from the National Institutes of Health R01AI132695 to R.M. and P01AI077774 to C.S. The content is solely the responsibility of the authors and does not necessarily represent the official views of the National Institutes of Health or The United States Department of Agriculture. The funder had no role

Abstract

Chronic Wasting Disease (CWD) is a prion disease affecting several cervid species. Among them, white-tailed deer (WTD) are of relevance due to their value in farming and game hunting. The exact events involved in CWD transmission in captive and wild animals are still unclear. An unexplored mechanism of CWD spread involves transmissions through germplasm, such as semen. Surprisingly, the presence and load of CWD prions in semen and male sexual tissues from WTD has not been explored. Here, we described the detection of CWD prions in semen and sexual tissues of WTD bucks utilizing the Protein Misfolding Cyclic Amplification (PMCA) technology. Samples were obtained *post-mortem* from farmed pre-clinical, CWD positive WTD bucks possessing polymorphisms at position 96 of the *PRNP* gene. Our results show that overall CWD detection in these samples had a sensitivity of 59.3%, with a specificity of 97.2%. The data indicate that the presence of CWD prions in male sexual organs and fluids is prevalent in late stage, pre-clinical, CWD-infected WTD (80%-100% of the animals depending on the sample type analyzed). Our findings reveal the presence of CWD prions in semen and sexual tissues of prion infected WTD bucks. Future studies will be necessary to determine whether sexual contact and/or artificial inseminations are plausible means of CWD transmission in susceptible animal species.

Introduction

Chronic Wasting Disease (CWD) is a prion disease affecting cervids including deer, elk, reindeer and moose [1–3]. CWD is unique among prionopathies as it is currently the only transmissible spongiform encephalopathy (TSE) identified in wild animals [3,4]. CWD continues to spread across North America with 26 States within the United States and 3 Canadian provinces

ANNEX 3

Gomez-Gutierrez R, Morales R. *Molecular basis of Alzheimer's Disease: New research perspectives.* ***NRC Newsletter*** 2019. *2:1-10.*

NRC newsletter

http://med.uth.edu/nrc | News & Featured Research of the Neuroscience Research Center | volume 24, number 2, Winter 2018-19

Molecular Basis of Alzheimer's Disease: New Research Perspectives

By Rodrigo Morales, Ph.D. and Ruben Gomez-Gutierrez, M.Sc

Morales

Gomez-Gutierrez

Abstract: Alzheimer's disease (AD) is the most common type of dementia among people age 65 and over. The main pathological event associated with AD is the progressive accumulation into sticky plaques of abnormally folded proteins in the brain. It is widely accepted that a pathological form of the amyloid-β (Aβ) protein initiates the AD process. Thus, the focus in several research laboratories is to detect and disrupt misfolded protein aggregates. Here, we give an overview of our recent research (and that of others) revealing similarities between the behavior of the Aβ and the prion protein, which causes "mad cow" disease and Creutzfeldt-Jakob disease, a rare human brain disorder. We believe that an understanding of the similarities between these aberrant proteins can lead to the design of new diagnostic and therapeutic strategies for AD and other brain disorders.

Alzheimer's disease (AD) is the most common cause of dementia among people age 65 and over. In people younger than 60, the prevalence of AD is less than 1 percent. According to the Alzheimer's Association's 2018 report on the disease, the prevalence in the U.S. increases exponentially with aging: 32 percent of people older than 85 are affected by AD, and by age 90, the proportion rises to 63.9 percent. The Alzheimer's Association reports that about 5.7 million people suffer from AD in the United States, and the number is projected to reach 13.8 million by the year 2050. The aging of the population, due to rises in life expectancy, makes AD one of the most severe health problems in the U.S. and other developed countries.

Continued on page 6; Morales & Gomez-Gutierrez

New Approaches to Treating Alzheimer's Disease at McGovern Medical School

By David H. Hunter, M.D. and Paul E. Schulz, M.D.

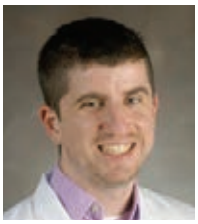

Hunter

Schulz

Abstract: Alzheimer's disease (AD), affecting 48 million people worldwide, is the most common neurodegenerative cause of memory loss. With the development of new imaging techniques, our ability to diagnose it has improved dramatically in the last few years. The new diagnostic tools have also unexpectedly taught us that the processes underlying AD begin decades before the first symptom appears. There is currently no disease-modifying treatment for Alzheimer's, but these significant breakthroughs in understanding the disease's underlying processes have led to the rational development of unique new types of medications. Here at UTHealth, basic scientists and clinicians work together and with others around the world to advance and test new treatments for this very distressing disorder. It is our hope that important new treatments will emerge in the not too distant future.

At McGovern Medical School's Memory Disorders and Dementia Clinic, we see patients with changes in their memory, thinking, emotions, and behavior. The most common cause of memory loss is Alzheimer disease (AD), but there are many other disorders that affect memory or cause dementia, including Parkinson's disease, Lewy body dementia, frontotemporal dementia, Huntington's disease, and vascular dementia. Dementia-like syndromes may also be caused by depression, sleep apnea, medications, and other medical illnesses. To determine the cause of a person's symptoms, a thorough

Continued on page 8; Hunter & Schulz

UTHealth | Neuroscience Research Center
The University of Texas Health Science Center at Houston